



2024

Synthesis of Hydroxycinnamate Derivatives and Characterization of Bioactivity as Radical Scavengers and α -Glucosidase Inhibitors

Cate Simmermaker
University of the Pacific

Follow this and additional works at: https://scholarlycommons.pacific.edu/uop_etds

 Part of the [Chemistry Commons](#)

Recommended Citation

Simmermaker, Cate. (2024). *Synthesis of Hydroxycinnamate Derivatives and Characterization of Bioactivity as Radical Scavengers and α -Glucosidase Inhibitors*. University of the Pacific, Dissertation. https://scholarlycommons.pacific.edu/uop_etds/4259

This Dissertation is brought to you for free and open access by the University Libraries at Scholarly Commons. It has been accepted for inclusion in University of the Pacific Theses and Dissertations by an authorized administrator of Scholarly Commons. For more information, please contact mgibney@pacific.edu.

Synthesis of Hydroxycinnamate Derivatives and Characterization of Bioactivity as
Radical Scavengers and α -Glucosidase Inhibitors

By

Cate Simmermaker

A Dissertation Submitted to the

Graduate School

In Partial Fulfillment of the

Requirements for the Degree of

DOCTOR OF PHILOSOPHY

Thomas J. Long School of Pharmacy and Health Sciences
Pharmaceutical and Chemical Sciences

University of the Pacific
Stockton, California

2023

Synthesis of Hydroxycinnamate Derivatives and Characterization of Bioactivity as
Radical Scavengers and α -Glucosidase Inhibitors

By

Cate Simmermaker

APPROVED BY:

Dissertation Advisor: Andreas Franz, Ph.D.

Committee Member: Liang Xue, Ph.D.

Committee Member: Skylar Carlson, Ph.D.

Committee Member: Caroline Chu, Ph.D.

Committee Member and Department Chair: Jerry Tsai, Ph.D.

Department Chair: Jianhua Ren, Ph.D.

Synthesis of Hydroxycinnamate Derivatives and Characterization of Bioactivity as
Radical Scavengers and α -Glucosidase Inhibitors

Copyright 2023

By

Cate Simmermaker

Acknowledgments

Many thanks to Dr. Andreas Franz, who gave support, patience, and flexibility in unconventional times. Thank you to my committee and University of the Pacific, Department of Chemistry. I acknowledge the efforts of this program to encourage students to prepare for and pursue career opportunities. This facilitation installed many mentors in my path helping me to expand my expectations. To those mentors, it is your encouragement and support that made those new expectations a reality. And to Nick and Maeve, thanks for putting up with me.

Synthesis of Hydroxycinnamate Derivatives and Characterization of Bioactivity as Radical Scavengers and α -Glucosidase Inhibitors

Abstract

By Cate Simmermaker

University of the Pacific
2023

Hydroxycinnamic acids (HCAs), a class of polyphenols commonly found in regularly consumed fruits and vegetables, have been investigated for efficacy as radical scavengers and glycosidase inhibitors. These compounds could mitigate the negative health effects of free radicals in oxidative stress diseases including neurodegeneration, cancer and diabetes. The HCAs investigated were caffeic acid (**1**), *p*-coumaric acid (**2**), ferulic acid (**3**), and sinapic acid (**4**). The compounds were derivatized with synthetically prepared amino acid esters through a four-step synthesis including protective acetylation, chlorination of the carboxylic acid, amidation, and subsequent deprotection of all applied protecting groups. The inclusion of diverse derivative groups allowed for the investigation of structure activity relationships through radical scavenging and enzyme inhibition assays. An assay with 2,2-diphenyl-1-picrylhydrazyl (DPPH) revealed the effect of the phenolic structure and capacity of the most active portion of the compound, but also the nature of the reaction through constant tracking, as opposed to only final capacity. Stabilization of the HCA's radical structure by aromatic substituents was found to be most important. However, structural modification of HCAs with various amino acids affected the initial rate of reaction based on the carbon chain length between the amide and amino acid carboxylic acid and the number of carboxylic acids present on the amino acid

residue. Following previous investigations of α -amylase inhibition by similar compounds, our study showed a ranked inhibition ability of **2 \approx 1>3>4**. The derivatized HCAs created for this study have been analyzed for protein-ligand interaction via the molecular docking program AutoDock Vina, Saturation-Transfer Difference (STD)-NMR, intrinsic fluorescence quenching and a robust starch-iodine microwell plate inhibition assay. Additional characterization of the protein-ligand interaction points to π - π stacking as the major contributor, similar to previously tested polyphenols, and a mechanism different from positive control inhibitors.

Table of Contents

List of Tables.....	11
List of Figures.....	12
List of Schemes.....	15
List of Abbreviations	16
Chapter 1. Introduction.....	18
Statement of the Problem	18
Research Questions	18
Chapter 2. Review of Related Literature	19
2.1 Polyphenols	19
2.1.1 Prevalence of Polyphenols in Natural Sources	20
2.1.2 Biological Activity of Polyphenols.....	22
2.1.3 Recent Use in Response to COVID-19.....	24
2.2 Free Radicals	24
2.3 Antioxidants	25
2.3.1 Radical Scavenging by Polyphenols.....	27
2.3.2 2,2-Diphenyl-1-picrylhydrazyl (DPPH) Assay.....	29
2.4 Starch Hydrolyzing Enzymes.....	31
2.4.1 Starch	31
2.4.2 Diabetes.....	32
2.4.3 Role of α -Amylase in the Digestion of Starch.....	34
2.4.3.1 Structure of α -Amylase.....	34

2.4.3.2 Mechanism of α -Amylase.....	35
2.4.3.3 Polyphenols as α -Amylase Inhibitors	36
Chapter 3: Results and Discussion	38
3.1 Hydroxycinnamic Acid Derivative Synthesis and Optimization	38
3.1.1 Amidation of HCAs with Amino Acids	42
3.1.2 Synthesis of Protected Amino Acids for Amidation	45
3.1.3 Synthesis of Alternative Phenol Protecting Groups.....	45
3.2 DPPH Assay	47
3.2.1 Time Point Analysis vs Full Capacity Measurement	48
3.2.2 Hydroxycinnamic Acids Radical Scavenging Capacity	51
3.2.3 HCA Derivatives Radical Scavenging Capacity	59
3.2.3.1 Acetylated HCAs	59
3.2.3.2 Esters of HCAs.....	60
3.2.3.3 Bis-aryl Anhydrides	61
3.2.3.4 HCA Amino Acid Derivatives.....	64
3.2.3.4.1 T ₁ Reaction Time Analysis.....	69
3.3 α -Amylase Inhibition Assay	72
3.3.1 Enzyme Assay Development	72
3.3.2 HCAs and α -Amylase Inhibition	78
3.3.2.1 HCA Derivatives	79
3.3.2.2 <i>p</i> -Coumaric Acid Inhibition Analysis	81
3.4 STD-NMR Analysis of α -Amylase and Selected Compounds.....	83
3.5 Fluorescence Analysis of Small Molecule Interaction	90

3.6 Molecular Docking of Ligands with α -Amylase	95
3.7 Native MS	101
3.7.1 Bovine Serum Albumin (BSA)	102
3.7.2 Carbonic Anhydrase	109
3.7.3 α -Glucosidase	113
Chapter 4: Conclusion	116
Chapter 5: Experimental	118
5.1 Synthesis	118
5.1.1 General Procedure: Acetylation	118
5.1.2 General Procedure: Chlorination	120
5.1.3 General Procedure: Amidation	123
5.1.4 General Procedure: Deprotection	140
5.1.5 Fischer Esterification	164
5.1.6 HCA Anhydride	159
5.1.7 Alternative Protecting Groups	160
5.1.8 General Procedure: Amino Acid Esterification	164
5.2 DPPH Assay	166
5.3 Protein-Ligand Interaction Characterization	167
5.3.1 α -Amylase Inhibition Assay	167
5.3.2 NMR and STD-NMR	168
5.3.3 Intrinsic Fluorescence Quenching	168
5.3.4 Molecular docking	169
5.3.5 Native MS – Model Proteins	169

References.....	171
Appendix	177
A. Selected ^1H NMR Spectra	177
B. Selected ^{13}C NMR Spectra.....	182
C. Selected 2D NMR.....	187
D. Selected STD-NMR Spectra.....	192
E. Selected MS Data.....	195

List of Tables

Table

1.	DPPH IC ₅₀ Values of HCAs	58
2.	DPPH IC ₅₀ Values of HCA Amide Derivatives	67
3.	α -Amylase Inhibition IC ₅₀ Values of HCAs and Derivatives	80
4.	STD-NMR Results of the HCAs	86
5.	IC ₅₀ Values of HCAs as α -Amylase Inhibitors and Fluorescence Emission at 10 μ L Addition of HCA for Comparison	92

List of Figures

Figure

1.	The Generic Structure of Phenolic Acid Class Components, Hydroxybenzoic Acids (left) and Hydroxycinnamic Acids (right)	20
2.	Structure of Resveratrol	23
3.	Antioxidant Quenching of Free Radicals Through Stabilization	26
4.	DPPH, Stable Free Radical Structure, and Product from Reaction with Effective Radical Scavenger.....	30
5.	Maltose and Isomaltose Structures Displaying the Different Linkages, for Maltose α -(1,4) and Isomaltose α -(1,6)	32
6.	α -Amylase Binding Subsites and Point of Hydrolysis (Black Arrow)	35
7.	Hydrolysis Mechanism of α -Amylase upon Amylose	36
8.	Caftaric Acid	40
9.	HAT and SET Mechanisms for Phenol	48
10.	Reduction of the Free Radical Scaffold DPPH as Confirmed by Mass Shift After Interaction with Compound 1	50
11.	Hydroxycinnamic Acids: Caffeic Acid (1), <i>p</i> -Coumaric Acid (2), Ferulic Acid (3), Sinapic Acid (4).....	51
12.	DPPH Radical Scavenging Assay Results of HCAs (15 mM) Over 10 Minutes	53
13.	Catechol Resonance Contributors in the Radical Hybrid	54
14.	Caffeic Acid Resonance Contributors	56
15.	HCA Products of Acetylation Protection.....	59
16.	The Resulting Derivatives of the Esterification of Caffeic Acid (1), Methyl (22a), Ethyl (22b), Propyl (22c)	61

17.	(a) Bis-Aryl Anhydrides. 21a : R = OMe, R1 = OMe, 21b : R = OMe, R1 = H, 21c : R = H, R1 = H. (b) The Kinetic Analysis Comparing the DPPH Radical Scavenging Capacity of HCAs to the Synthetic Anhydride Counterparts	63
18.	Amino Acids Used for Amidation Step with Acid Chloride.....	65
19.	HCA Derivatives Scavenging Profiles at 50 μ M	69
20.	Pseudo-Ring Formation Proposed for Possible Enhance Stabilization of Radical Via Radical Scavenger Compound.....	70
21.	Comparison of Synthetic Amino Acid Derivatives and the Speed of Reaction with DPPH at Initial Time Point Interval Between HCAs 1 , 3 , and 4	71
22.	Amylose Chain Helical Structure	72
23.	Absorption Response of Various Starch Concentrations Without the Inclusion of Enzymes or Inhibitors (chart) and Related Visual Appearance of the Charge Transfer Complex (picture)	74
24.	Normalized Absorption Response to Increasing α -Amylase Concentration in Method Development of Assay	76
25.	Acarbose, Positive Control Compound, Enzyme Assay Results, [blank] Contains No Acarbose Resulting in No Inhibition of the Enzyme and [0] has No Enzyme with Maximum Absorption.....	77
26.	<i>p</i> -Coumaric Derivatives Used Synthesized for Point Analysis of the HCA Structure.....	82
27.	STD-NMR Spectra for (top to bottom) Caffeic Acid (1), 18a , and <i>p</i> -Coumaric Acid (2).....	89
28.	Fluorescence Quenching of α -Amylase by 2 (top), 1 (bottom)), $\Delta E = h\nu$	93
29.	Lack of Fluorescence Quenching in α -Amylase with Acarbose Inhibition	94
30.	Compound 2 (top) and Compound 1 (bottom) Positioned in the Binding Pocket of α -Amylase with the Residues Showing Hydrogen Bonding Highlighted in Blue and Others within Proximity in Gray	97

31.	18a (top) and 18c (bottom) Compoutationally Docked in the Binding Site of α -Amylase with Residues Making Hydrogen Bonds in Blue and Residues in Proximity in Gray Including Active Site Residues	100
32.	(Top) The Primary Charge States for the Native BSA, (Bottom) The Denatured Protein as a Result of 30% MeCN Addition into the Solvent System	105
33.	UNIDEC Deconvolution of BSA	106
34.	BSA-Sinapic Acid Complex.....	107
35.	Deconvoluted Complexes Overlayed with the Four HCA Ligands, Each Complex Deconvolution is Color Coded	108
36.	Carbonic Anhydrase Charge Envelope (zoomed out) and +11 Charge (zoomed in)	110
37.	(Top to Bottom) Carbonic Anhydrase, Non-Complexed (pink), Carbonic Anhydrase-Caffeic Acid (blue), Carbonic Anhydrase-Coumaric Acid (black), Carbonic Anhydrase-Ferulic Acid (orange), Carbonic Anhydrase-Sinapic Acid (red)	111
38.	Carbonic Anhydrase Complexed with Small Molecules (from top to bottom) Control, Caffeic Acid, p-Coumaric Acid, Ferulic Acid, and Sinapic Acid at 50 CE	113
39.	α -Glucosidase Charge Envelope	114
40.	UNIDEC Deconvolution of α -Glucosidase	115

List of Schemes

Scheme

1. Full Four-Step Synthesis of Amidation of HCA with Protected Amino Acids: (a) Ac_2O , DMAP, Py, 0 °C; (b) COCl_2 , DMF, Toluene, -5°C to rt; (c) $\text{R}_2\text{-NH}_2$, Et_3N , DCM; (d) NaOH, 1:1 H_2O : MeOH 39
2. Protection Scheme Utilizing TBDMS Groups for the Phenols of Caffeic Acid and Carboxylic Acid and Subsequent Selective Deprotection of the Modifier on the Carboxylic Acid 41
3. Acetylation Scheme for Protection of the Phenol of HCAs (Example Used Caffeic Acid **1** to Compound **5**)..... 42
4. Chlorination Scheme for Synthesis of the Acid Chloride of the Carboxylic Acid of HCAs (Example Used Compound **5** to Compound **9**) 43
5. Amidation Scheme for Synthesis of the Amidated HCA (Example Used Compound **9** to Compound **13a**) 44
6. Deprotection Scheme for Synthesis of the Deprotected Amidated HCA (Examples Used Compound **13a** to Compound **17a**) 44
7. Amino Acid Methylation Synthetic Scheme..... 45
8. Ethylcarbonate Phenol Protection Synthetic Scheme 46
9. Acetonide Protecting Group Synthesis 46
10. Fischer Esterification Scheme, Caffeic Acid Methyl Ester (**22a**) 60
11. Knoevenagel Condensation Reaction Scheme Producing p-Methoxy Coumaric Acid Derivative for Analysis of Effect of Phenol Modification of α -Amylase Inhibitory Ability..... 83

List of Abbreviations

Ac ₂ O	acetic anhydride
BDE	bond dissociation energy
BSA	Bovine Serum Albumin
CDI	carbonyldiimidazole
COCl ₂	oxalyl chloride
DCC	dicyclohexyl carbodiimide
DCM	dichloromethane
DMAP	dimethylamino pyridine
DMSO	dimethyl sulfoxide
DNSA	3,5-Dinitrosalicylic acid
DPPH	2,2-diphenyl-1-picrylhydrazyl
ESI	electrospray ionization
Et ₃ N	triethylamine
GLUT	glucose transporter
HAT	hydrogen atom transfer
HCA	hydroxycinnamic acid
HCl	hydrochloric acid
IC ₅₀	half maximal inhibitory concentration
IP	ionization potential
K ₂ CO ₃	potassium carbonate
LiOH	lithium hydroxide

MeCN	methyl cyanide (acetonitrile)
MeOH	methanol
MS	mass spectrometry
NMR	Nuclear Magnetic Resonance
NOE	nuclear Overhauser effect
Py	pyridine
ROS	reactive oxygen species
SET	single electron transfer
STD	Saturation Transfer Difference
TBAF	tetra-n-butylammonium fluoride
TBDMSCl	tert-butyldimethylsilyl chloride
T2D	Type 2 Diabetes
TLC	thin layer chromatography

CHAPTER 1: INTRODUCTION

Statement of the Problem

Polyphenols are abundant in commonly consumed materials and supplemented heavily in foods and beverages, often including claims of bioactivity. Understanding the activity and functionality of various polyphenolic classes can inform the investigation of naturally occurring forms and derivatives as supplements and drug candidates.

Research Questions

What is the relative radical scavenging potential of four common hydroxycinnamic acids and the impact of synthetic derivatization on activity? Hydroxycinnamic acids have shown inhibitory potential of enzymes important to the hydrolysis of complex sugars to smaller subunits. What is the relative ability of hydroxycinnamic acids, and derivatives, on the inhibition of glucosidases and how should this inhibition be evaluated?

CHAPTER 2: REVIEW OF RELATED LITERATURE

2.1 Polyphenols

Polyphenols are a large class of molecules that contain over 10,000 individual compounds (Brglez Mojzer, Knez Hrnčič, Škerget, Knez, & Bren, 2016). There are six primary classes of polyphenols (flavonoids, phenolic acids, lignans, stilbenes, other polyphenols, and non-phenolic metabolites) and thirty-one more subclasses (Neveu et al., 2010). The most simplified breakdown of this family is phenolic acids, flavonoids, and non-flavonoids; the phenolic acids class consists of two subclasses hydroxybenzoic acids and hydroxycinnamic acids (HCAs) (El Gharras, 2009). The most basic generic structure of these classes includes a substituted phenol, the substituent groups are often other hydroxy groups or methoxy groups. Hydroxybenzoic acids include a single carboxylic acid substituent, while HCAs include an alkene linkage between the aromatic group and carboxylic acid (Figure 1).

The extraction and investigation of HCAs, as well as other polyphenols, have been shown in high concentrations in commonly consumed food and bioavailability in plasma and cell analysis. HCAs, additionally, offer a variety of proven biologically active functionalities associated with many positive health effects.

Herein, we will describe the investigation of four common HCAs as free radical scavengers and inhibitors of polysaccharide hydrolyzing enzymes. This study of bioactivity is supported through the synthetic derivatization of the basic HCAs to further understand the structure activity relationship of this class of polyphenols. Further,

unique methods were developed and optimized for addressing the interaction between HCAs and macromolecular complexes.

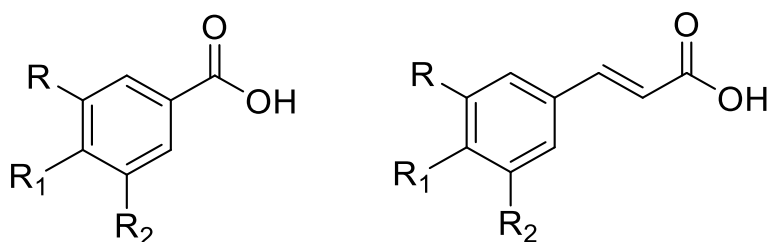


Figure 1. *The Generic Structure of Phenolic Acid Class Components, Hydroxybenzoic Acids (Left) and Hydroxycinnamic Acids (Right).*

At the most basic level these compounds are abundant and available through common food and supplements. The significance of these compounds is relevant in many applications ranging from cosmetics to medicine. This requires thorough elucidation of structure and function prior to application.

2.1.1 Prevalence of Polyphenols in Natural Sources

Considerable concentrations of polyphenols have been detected in a variety of foods. HCAs have been shown to be the predominant components in the phenolic acid concentrations of fruits. The compounds most commonly found are caffeic acid (**1**), *p*-coumaric acid (**2**), ferulic acid (**3**) and sinapic acid (**4**) (El Gharras, 2009). The foods that contain HCAs include blueberry, cherry, kiwi, plum, apples, pear, chicory, artichoke, potato, flour, cider, and coffee; the concentrations range from 50 to 2200 mg/L (Manach, Scalbert, Morand, Rémésy, & Jiménez, 2004). Caffeic acid is the most predominant in fruits, while ferulic acid is most abundant in cereal grains (Lempereur,

Rouau, & Abecassis, 1997). The variety and abundance in common foods indicates that this class of compounds are easily acquired and consumed by most people.

Grape juice and wine are also a concentrated source of HCAs in the average diet. The phenolic content of different wines has a strong impact on the profile and quality of the beverage. Investigations of phenolic compounds have revealed possible bioactivity, have allowed fingerprinting of individual varieties, and have aided in improving manufacturing techniques, storage and growing conditions. The skin of the grape is the primary location for HCAs in the wine making process. A point of differentiation between white and red wines is the time the juice spends in contact with the skin, affecting the extraction of those compounds to the final product. In an example of this, the predominant HCAs were found in three common varieties, Stanušina, Vranec, and Cabernet Sauvignon. The HCAs include *p*-coumaric acid, caftaric acid, coutaric acid, caffeic acid and fertaric acid ranging from 2 to 500 mg/L (Ivanova-Petropulos, Durakova, Ricci, Parpinello, & Versari, 2016). The primary and secondary metabolites of these polyphenols go through changes during consumption because of common processes of methylation, sulfation and glucuronidation (Manach et al., 2004). Due to the various natural derivative structures associated with the available HCAs the quantitation and understanding of the concentration differences in foods and supplements are important to the downstream biological activity associated with these starting compounds.

2.1.2 Biological Activity of Polyphenols

The biological activity of different classes of polyphenols has been linked to diseases related to inflammation, cancer, cardiovascular health, diabetes, obesity, and neurodegenerative conditions (Cory, Passarelli, Szeto, Tamez, & Mattei, 2018).

The popularization of polyphenols benefiting health outcomes originates from the *French Paradox*, a term coined in the 1980's referencing the considerably similar rates of coronary heart disease in France and other populations despite the increased consumption of cholesterol and saturated fats in the European region (Renaud & de Lorgeril, 1992). Original research presented the epidemiological correlation to the increased consumption of wine and alcohol as a causality to the decrease in coronary heart disease. This paradoxical assumption has come under further speculation due to possible under sampling of the study and the inability to control for confounding factors. The mechanistic effects of the components of wine (alcohol, polyphenols, sulfates, sugars, among others) need to be identified and directly associated with the factors that contribute to the health benefits; changes in high density lipoprotein (HDL) and low-density lipoprotein (LDL), triglyceride and fibrinogen concentrations, homeostasis, blood pressure, etc., processes lacking from the initial publication. A heavily investigated compound, resulting from this paradox, is resveratrol (Figure 2). First identified in grape vines in 1976, this compound has been shown to have chemoprotective abilities, anti-inflammatory mechanisms, antioxidant potential and antimicrobial actions (Langcake & Pryce, 1976).

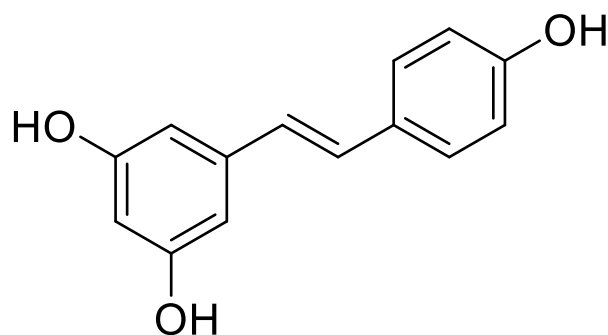


Figure 2. *Structure of Resveratrol.*

Like the popularized resveratrol, other compounds have also become subject to further characterization. Exploration of the small molecules in the polyphenol family have revealed possible bioactivity of different classes and plausible therapeutic and supplemental use.

HCAAs are shown to mirror some of the activities associated with the thoroughly investigated resveratrol in anti-inflammatory, antioxidant, and antimicrobial abilities (Taofiq, González-Paramás, Barreiro, & Ferreira, 2017). For example, caffeic acid has been shown to increase the susceptibility of pathogenic microorganisms by damaging cell membranes, inducing leakage of intracellular components of bacteria, and scavenging NO and modulating iNOS (Luís, Silva, Sousa, Duarte, & Domingues, 2014). *p*-Coumaric acid can disrupt bacteria through increasing cell membrane permeability, affect DNA replication through intercalation, inhibit LDL oxidation through oral administration, and decrease inflammation associated with rheumatoid arthritis (Lou et al., 2012). Ferulic acid has shown inhibition for lipid peroxidation, anti-inflammatory ability through inhibition of TNF- α and IL-6, and *S. aureus* and *L. monocytogenes* biofilm prevention (Graf, 1992). Sinapic acid has been shown to operate as a possible NorA

efflux pump inhibitor and suppress NLRP3 inflammasome activation (Singh, Coopoosamy, Gumedde, & Sabiu, 2022).

2.1.3 Recent Use in Response to COVID-19

In addition to these described bioactivities, in response to the COVID-19 pandemic, this class has been investigated as therapeutic and preventative medicine to SARS Cov-2. Preliminary research was completed on the ability of caffeic acid derivatives to bind and modulate the virus, as well as the ability of sinapic acid to inhibit viral replication through targeting of the envelope protein (Adem et al., 2021; Orfali et al., 2021). The polyphenols are consistently bioavailable from balanced diets and can bind and interact with macromolecules in a variety of situations. Structure-activity studies can reveal the impact that HCAs have on broader health conditions.

2.2 Free Radicals

Free radicals are molecular species that contain an unpaired electron. These species are often short lived, highly reactive, and greatly abundant biologically and in nature. A simplistic example of a free radical would be hydrogen (Halliwell, 1994). Biological free radicals are essential to normal functions, important to initiating processes for cell proliferation and regulation, the control of inflammation, and maintenance of tissue damage (Schieber & Chandel, 2014). However, when that level of free radicals is not maintained oxidative damage can occur. This damage presents itself commonly as lipid peroxidation, oxidative DNA damage, and protein oxidation. Lipid peroxidation is described by the common radical chain reaction where lipids, as part of polyunsaturated fatty acids, are attacked and oxidized by the radical, initiating the chain reaction. Through this, the reactive constituent O₂ is added to produce the

peroxyl radical which proceeds the propagation step, creating more peroxyl radicals, making the subsequent termination more difficult (Nimse & Pal, 2015).

The common culprits for this reactivity *in vivo* are referred to as reactive oxygen species (ROS), hydroxyl radical ($\text{OH}\cdot$), nitric oxide ($\text{NO}\cdot$), superoxide ($\text{O}_2\cdot^-$), hydrogen peroxide H_2O_2 (Halliwell, 1994). Free radicals are created endogenously and exogenously. Exogenous sources of free radicals are pollution, tobacco smoke, and UV radiation, among others (Phaniendra, Jestadi, & Periyasamy, 2015). The continuous evolution of society has provided more opportunity of introduction of these free radicals into the daily lives of humans on both macro and micro scales. Free radicals do not exist without control mechanisms, and it is the role of antioxidants to maintain the balance of free radicals. The diseases linked to imbalance in biological ROS concentration are diabetes, neurodegenerative diseases, cancer, arthritis, asthma, and cardiovascular disease. All the aforementioned diseases are at the center of contemporary medical research and receive large sums of money and resources to find a cure. As opposed to curing the disease after full symptoms have developed, it would be desirable to prevent onset of disease in the first place. Regulating the abundance of ROS in the human body to stay within biologically healthy norms with the help of polyphenols and specifically HCA derivatives might benefit general wellbeing.

2.3 Antioxidants

Antioxidants exist in various forms, with various mechanisms of protection. The chemical reaction principle by which antioxidants stabilize aggressive radicals into less reactive radicals is shown in Figure 3. In general, antioxidants can donate electrons

breaking the radical chain reaction and become oxidized themselves in a stable state that may eventually allow for regeneration and further antioxidative potential.

Antioxidants are classified into natural and synthetic antioxidants. Examples of biological antioxidants are enzymes such as glutathione reductase, superoxide dismutases and catalase, and small molecules such as glutathione and uric acid. Antioxidants that are consumed through foods and other manners include Vitamin A, Vitamin E, Vitamin C, carotenoids, lipoic acid and phenolic acids (Nimse & Pal, 2015). These antioxidants have different modes of action. While some protect cellular membranes, proteins, DNA, RNA, and lipids, others repair, and others seek to consolidate the free radicals through scavenging.

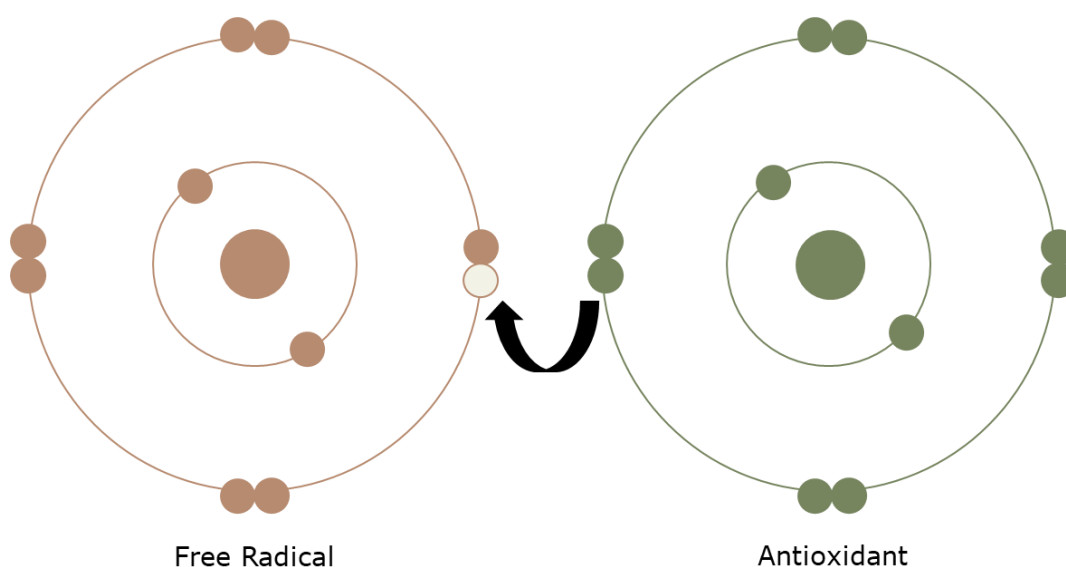


Figure 3. *Antioxidant Quenching of Free Radicals Through Stabilization.*

2.3.1 Radical Scavenging by Polyphenols

Quantifying the radical scavenging potential of small and large molecules allows for a generalized statement regarding their antioxidant potential in the human body. The information gathered, and with it the predictive value for successful ROS regulation in the human body, is highly dependent on the manner of analysis. The ability of the small molecule to scavenge radicals is often associated with three primary factors: resonance, hybridization, and electronegativity of substituents.

First, electronic resonance increases chemical stability of a radical. Therefore, if an unstable, aggressive radical transfers the unpaired electron to a different chemical structure that results in extensive electronic resonance, the damaging potential of the radical is decreased. It is not always a reasonable goal of the antioxidant to quench the unstable radical but to mitigate its destructive reactivity. Second, hybridization and the increasing s-character of the orbital can decrease stability, where a sp^3 carbon with an unpaired electron is most stable because of reduced electron affinity of the orbital, the free radical is held further from the nucleus. In comparison, a sp hybridized carbon holds the orbital closer to the nucleus and the unpaired electron is less stable. Lastly, increasing electronegativity of neighboring groups decreases the radical's stability, this is because as the orbital is held closer the greater electronegativity means more electron affinity and instability. All these factors contribute to the ability of the small molecules relative to others to scavenge radicals.

Radical scavengers operate by two main mechanisms: hydrogen atom transfer (HAT), single electron transfer (SET), or a combination of the two (Liang & Kitts, 2014). HAT includes a single step of displacement of a proton and electron, with the proton

being removed from the antioxidant molecule, this mechanism is highly dependent on the bond dissociation energy (BDE) of the antioxidant. BDE describes the bond strength between two atoms, for example the BDE of benzene C-H bonds is 112.9 kcal/mol where the phenol O-H bond is around 88.5 kcal/mol. The lower the BDE the greater ability to release the hydrogen and quench the radical (Mulder et al., 2005). SET is driven by ionization potential (IP), which is the required energy to remove an electron from an atom, here the antioxidant gives an electron to the radical. The two primary methods are not completely distinguishable according to antioxidant molecular structure and may act simultaneously (Wright, Johnson, & DiLabio, 2001).

Phenols are often investigated for antioxidant capacity and are an important functional group as some of the most effective preventative radical scavengers. Vitamin E (α -tocopherol) is one of the most crucial of these preventative scavengers (Halliwell, 1994). The structure's ability to scavenge other radicals is supported by the methyl substituents on benzene, which make resonant stabilization of an unpaired electron in the π -system particularly advantageous. Vitamin E proves even more formative by the ability to be regenerated through interaction with Vitamin C, ascorbic acid (Burton & Ingold, 1986). Some other classes of phenols that are explored include flavonoids (Tsimogiannis & Oreopoulou, 2006; Zeng et al., 2020), theaflavin (Chen & Ho, 1995), catechins (He, Xu, Yang, & Wang, 2018), and curcumin (Niu et al., 2012). The phenolic structure displayed in all these investigated compounds quenches radicals through both HAT and SET mechanisms through adequate IP and BDE, which stabilizes the new radical. The ability is reliant on the structure to rearrange to an adequately stable constitution for "trapping" (Wright et al., 2001). This radical scavenging characteristic

can be measured through various assays, most commonly, 2,2-diphenyl-1-picrylhydrazyl (DPPH), 2,2'-azino-bis(3-ethylbenzothiazoline-6-sulfonic acid) (ABTS), ferric ion reducing power (FRAP), and oxygen radical absorbance capacity (ORAC) (Liang & Kitts, 2014).

2.3.2 2,2-Diphenyl-1-picrylhydrazyl (DPPH) Assay

Originally developed by Blois (1958), the DPPH assay utilizes a stable free radical, 2,2-diphenyl-1-picrylhydrazyl, that can accept protons or electrons but not be easily oxidized (Blois, 1958). The delocalization of the free radical amongst the structure allows for existence without dimerization (Kedare & Singh, 2011). Due to this molecular conjugation the substance maintains a purple color, however upon reduction there is a color change to yellow (Figure 4). The tracking of the absorption near 520 nm and subsequent loss upon reaction with active radical scavenging compounds gives insight into the relative ability of those compounds to function as antioxidants. DPPH can react in both a HAT or SET manner and can be used for multi-component natural product extractions while being robust and inexpensive. Measurements can be conducted in two general ways. First, determination of full scavenging capacity after exhaustion of reaction with the ligand. Second, analysis of the time-dependent kinetics of the reaction to glean information on the mechanism (Xie & Schaich, 2014). In this context, UV-Vis analysis is convenient because it is cheap and sensitive.

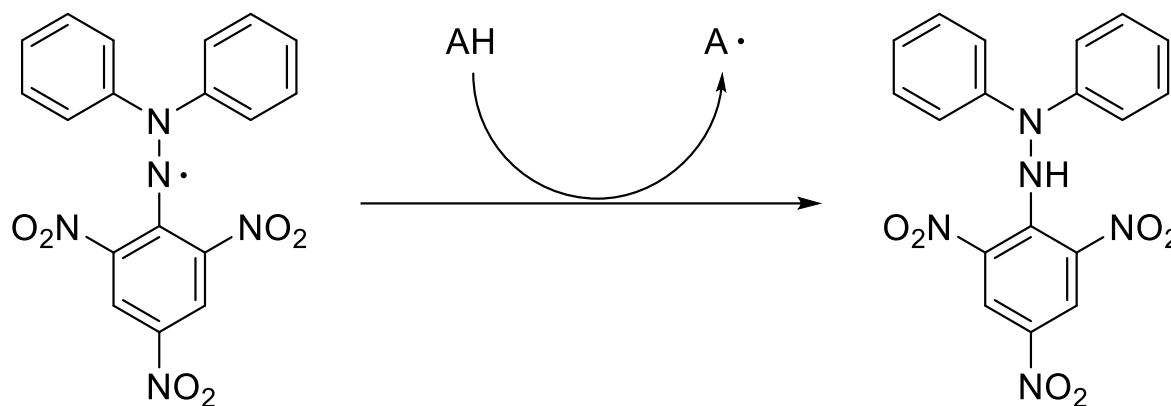


Figure 4. *DPPH, Stable Free Radical Structure, and Product from Reaction with Effective Radical Scavenger.*

DPPH assays can be completed in cuvettes, microwell plates or by HPLC, but is most effective when considering the ability of a single compound as opposed to more complex mixtures. Further, the resulting structure from reaction of the DPPH with small molecules analyzed by $^1\text{H-NMR}$ can give insight to the mechanism and effective change to the antioxidant. The UV-Vis assay does include limitations in quantitation and comparative results as the nature of the compounds being evaluated are important. Like-for-like comparison of compounds with vastly different structures and mechanisms should not be done with a single assay as the results can be misleading. Similar structures can be effectively compared through the assay. Compounds can additionally be analyzed by the speed at which reduction of DPPH occurs. Compounds reacting in the first 30 seconds are considered rapid while less reactive compounds completing reductive interaction in the first 2 minutes (Sánchez-Moreno, Larrauri, & Saura-Calixto, 1998). The least reactive compounds can take up to 5 minutes to complete interaction.

Due to this fast interaction, many studies utilize a 10-minute reaction time to measure full capacity.

2.4 Starch Hydrolyzing Enzymes

2.4.1 Starch

Starch is an essential polymeric material made up of multiple sugar residues. The consumption and digestion of starch is required to produce energy in the body. The organization of glucose molecules into polymers that make up starch are most often combined in an α -1,4 or α -1,6 manner, amylose, or amylopectin (Figure 5). The mode of polymerization determines the structure and resulting pathway for degradation of the structures. Amylopectin is made up of both α -1,4 and α -1,6 linkages giving it a branched structure, where the α -1,4 segments give a linear helix formation branched by the α -1,6 glycosidic linkages after linear sections of around 30 subunits (Dona, Pagès, & Kuchel, 2010). The branched nature of the amylopectin results in polymers that contain more glucose molecules, relative to amylose, and leads to a less dense molecule with greater solubility. Amylose is made up of primarily α -1,4 linkages, these linkages lead to a left-handed helix formation on chains of many thousands of monomers.

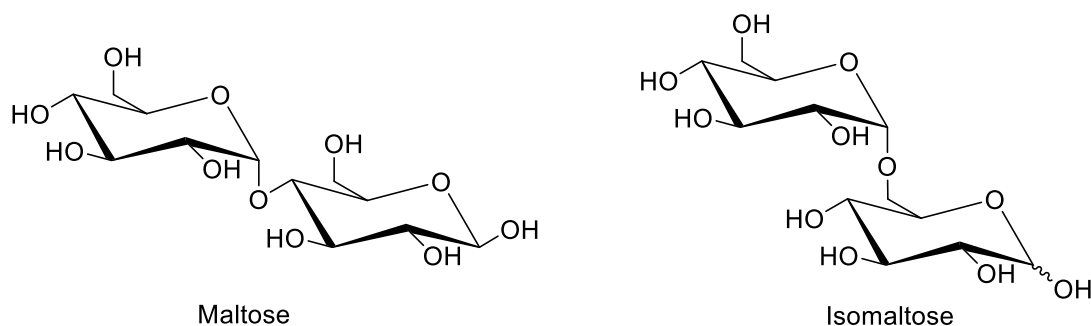


Figure 5. *Maltose and Isomaltose Structures Displaying the Different Linkages, for Maltose α -(1,4) and Isomaltose α -(1,6).*

Biologically, the relevance of starch conversion to glucose is most important as a source of energy. Animals use the glucose monomer to be processed in the cytoplasm and mitochondria to afford energy retained in ATP or glycogen. Additionally, carbohydrates can be essential to determining the function of proteins and lipids. The digestion of starches into glucose monomers is carried out by multiple enzymes. Breakdown begins immediately upon consumption by salivary amylase and then further in the intestines by pancreatic amylase. Maltose subunits are produced from amylose which is again further digested by glucosidase to glucose monomers.

2.4.2 Diabetes

The pancreas plays a significant role in the digestion of carbohydrates as the location of the primary acting amylase and the supply of insulin and glucagon. Insulin increases glycogen synthesis reducing blood glucose levels and glucagon decreases glycogen synthesis and storage, increasing blood glucose levels. The functions of this process are tightly associated with Type I (T1D) and Type II diabetes (T2D). The cells in the pancreas responsible for the production and release of insulin are β -cells. In T1D

those β -cells are destroyed through an autoimmune response (Katsarou et al., 2017). T2D is often the result of concurrent issues including poor insulin production and insulin resistance. The results of these circumstances are postprandial blood glucose elevation, over the course of the disease the impact of this situation can further worsen the ability to manage it through additional impairment of β -cells (Edelman, 1998).

The complications associated with T2D include vision impairment, diabetic neuropathy, diabetic nephropathy, and perioperative complications. Medications used to treat and manage this condition target various points in the process including slowing the production of glucose by the liver, stimulating insulin production by the β -cells, causing excess glucose to be excreted and blocking the breakdown of starches through inhibition of hydrolysis enzymes (Blair, 2016). The compounds associated with the last of those targets listed include acarbose, miglitol, and voglibose (Barrett & Udani, 2011; Walton, Sherif, Noy, & Alberti, 1979).

The incidence of diabetes in the United States is high, with an estimated 11.3% of the population having the disease in 2019. It is the eighth-leading cause of death and was further highlighted during the COVID-19 pandemic as an underlying risk factor for severe disease. In 2019, there were 1.4 million new cases of diabetes diagnosed in adults, which is 5.9 in every 1000 (CDC, 2022).

The understanding and management of T2D is a widespread issue. Greater information about the techniques that many people can access could assist in the mitigation of worsening side effects, as well as proactive care for early management.

2.4.3 Role of α -Amylase in the Digestion of Starch

α -Amylase (α -1,4-glucan-4-glucanohydrolase, E.C. 3.2.1.1) is the enzyme responsible for the breakdown of amylose strands and is present in both the saliva and pancreas. Upon consumption of starch, the enzyme acts immediately in the saliva to begin the cleavage of oligosaccharides into smaller subunits, these subunits are further processed in the pancreas where they pass through the brush border of the small intestine, then further degraded to the monomer by α -glucosidase (E.C. 3.2.1.20) and transported to the bloodstream via glucose transporter (GLUT) (Brayer et al., 2000).

Due to this role in the breakdown of starches and ultimately the production of glucose and post prandial blood glucose elevation, α -amylase inhibitors have been identified as possible therapeutic targets of control.

2.4.3.1 Structure of α -Amylase. The enzyme contains an active site located on domain A, an $(\alpha/\beta)_8$ -barrel, in a deep pocket with five sites for glucose binding and the catalytic site exists between subsites 3 and 4 (Figure 6) (Brzozowski & Davies, 1997; Gilles, Astier, Marchis-Mouren, Cambillau, & Payan, 1996). The primary active site residues that exist here are Asp197, Glu233 and Asp300 and a chloride binding site. It has been shown that chloride is required for the activation of the enzyme in an allosteric manner, although the substitution of other monovalent anions is possible for activation (Levitzki & Steer, 1974). In addition to the essential catalytic triad, available hydrophobic stacking with aromatic residues also proves to be important in binding including the repeated tryptophan residues Trp203 and Trp388, along with Tyr62 (Qian, Haser, & Payan, 1995). The limiting factor of the substrate is not greater size but rather decreased size. This is reasonable considering the stage that the substrate exists in

during first modification. The requirement for the substrate to be five subunits or larger was verified through kinetic evaluation. Additionally, the larger dextrin also showed hydrolysis at multiple bonds with maltopentaose producing maltose and maltotriose confirming the subsite hydrolysis location (Seigner, Prodanov, & Marchis-Mouren, 1987).

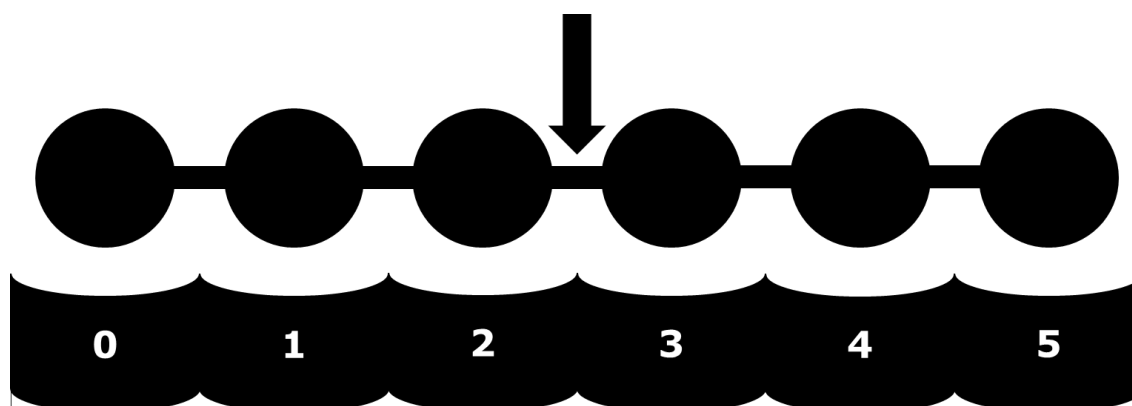


Figure 6. *α -Amylase Binding Subsites and Point of Hydrolysis (Black Arrow).*

Due to the deep pocket of the active site and the size of the substrate there is a requirement to a change in the oligosaccharide profile resulting in a kink in the sugar chain. This change of direction is affected by the modified glycosidic bond torsion angle and distortion of the sugar ring to half-chair (Brzozowski & Davies, 1997).

2.4.3.2 Mechanism of α -Amylase. The mechanism associated with the hydrolysis of the substrate is first driven by nucleophilic attack of the C1 by aspartic acid in the active site, then hydrolysis of the bond by the water molecule between the nucleophilic oxygen and C1 (Figure 7).

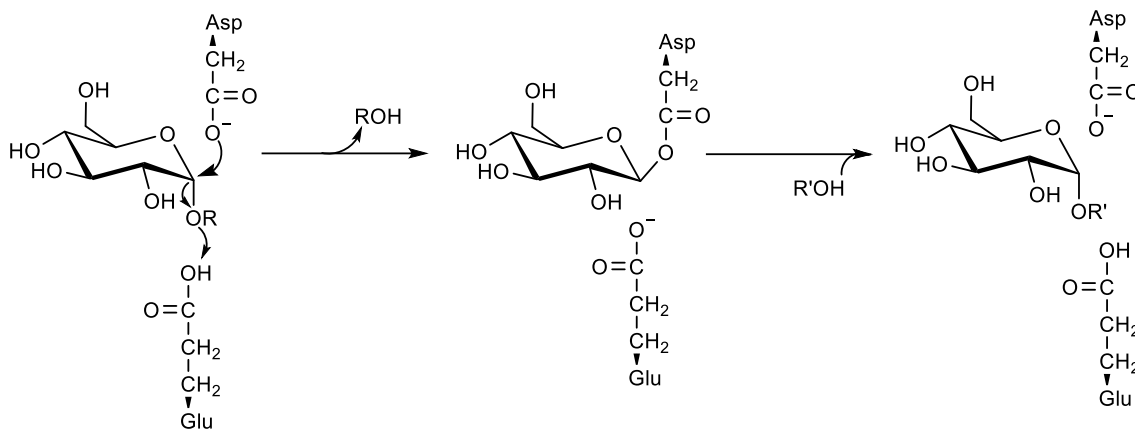


Figure 7. *Hydrolysis Mechanism of α -Amylase upon Amylose.*

The mechanism of inhibition of compounds for α -amylase is dependent on the structure. Where compounds that are substrate imitators, like acarbose, may interact with subsites similarly to the substrate, various families have different mechanisms of inhibition relying upon essential points of available interaction.

2.4.3.3 Polyphenols as α -Amylase Inhibitors. The large polyphenol class, and diverse families, have been investigated for their ability to inhibit α -amylase. The dependence on different segments of the compounds from groupings proves to be varied. Some of the common classes investigated are flavonoids, phenolic acids, flavans, stilbenes, lignans, and anthocyanins (Sun, Warren, & Gidley, 2019).

Flavonoids are characterized by a primary scaffold of two phenyl rings connected through an oxygen heterocyclic ring with a carbonyl substituent. Substitution at the rings diversifies this family of compounds and has a strong effect on the ability of the compounds to inhibit α -amylase. Hydroxyl substituents to the scaffold are shown to enhance the ability of the compound for inhibition while reduction in conjugation and rigidity of the scaffold leads to decreased inhibition ability (Lo Piparo et al., 2008).

Glycosylation substituents did not afford the same advantage as hydroxyl substituents, reducing inhibition, as seen in the comparison of quercetin and rutin (H. Cao & Chen, 2012; Li et al., 2009; Proença et al., 2019; Wang et al., 2022).

Flavans consist of structures similar to that of flavonoids, lacking the carbonyl on the heterocyclic ring. This class is often found with a galloyl moiety such as epicatechin gallate (ECG), epigallocatechin (EGC) and epigallocatechin gallate (EGCG). Counter to the effects of the glycosylation in flavonoids the galloyl moiety adds to the inhibition potential of flavans (J. Cao et al., 2020; Sun, Warren, Netzel, & Gidley, 2016).

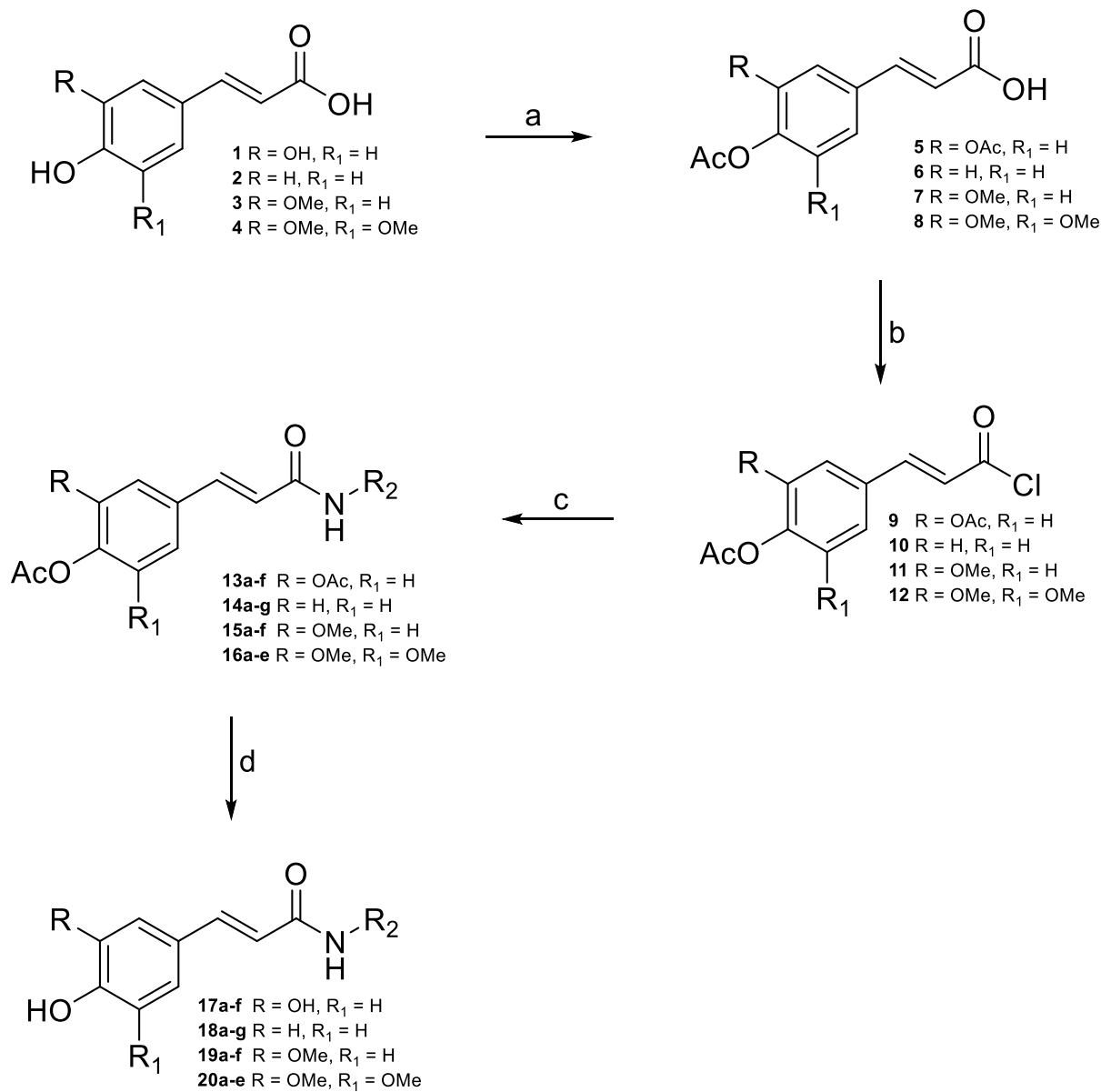
Diverse classes of polyphenols are enhanced and diminished differently by the synthetic inclusion of substituents and additions of various functional groups, which elucidates the mechanism of inhibition.

CHAPTER 3: RESULTS AND DISCUSSION

3.1 Hydroxycinnamic Acid Derivative Synthesis and Optimization

The modification of polyphenols has been explored extensively, leading to many verified methods of derivation. Polyphenols of various types, as discussed previously (2.1), can influence many important biological processes including fundamental aspects of oxidative stress disorders, the effective mechanisms associated with degenerative diseases, and other multi factorial conditions through indirect endogenous defenses and modification of cellular signaling pathways (Han, Shen, & Lou, 2007). The primary scaffolds of polyphenols are readily available from nature and have resulted in many interesting investigations.

Our investigations focused on various synthetic pathways and protecting groups to optimize the synthesis and prepare a library of compounds for subsequent biochemical studies. The class of compounds constructed were HCAs primarily derivatized with amino acids to generate libraries of carboxamides. The starting materials used were compounds **1**, **2**, **3**, and **4** (Scheme 1).



Scheme 1. Full Four-Step Synthesis of Amidation of HCA with Protected Amino Acids:

(a) Ac₂O, DMAP, Py, 0 °C; (b) COCl₂, DMF, Toluene, -5 °C to rt; (c) R₂-NH₂, Et₃N, DCM; (d) NaOH, 1:1 H₂O: MeOH.

Initially, the structure of caftaric acid (Figure 8) was considered as a scaffold for derivatization (Chagas, Lourenço, Monteiro, Ferreira, & Ferreira, 2017). The ester linkage to the tartaric acid modality extending from the caffeic acid core encouraged a coupling agent for combination of the tartaric acid portion at the hydroxy to the carboxylic acid of caffeic acid, that would require a stable protecting group on the reactive hydroxyl groups of the phenol.

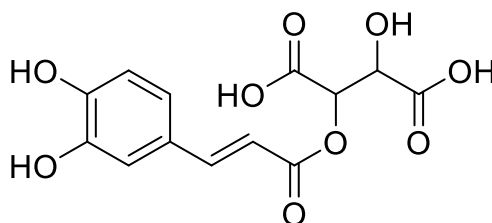
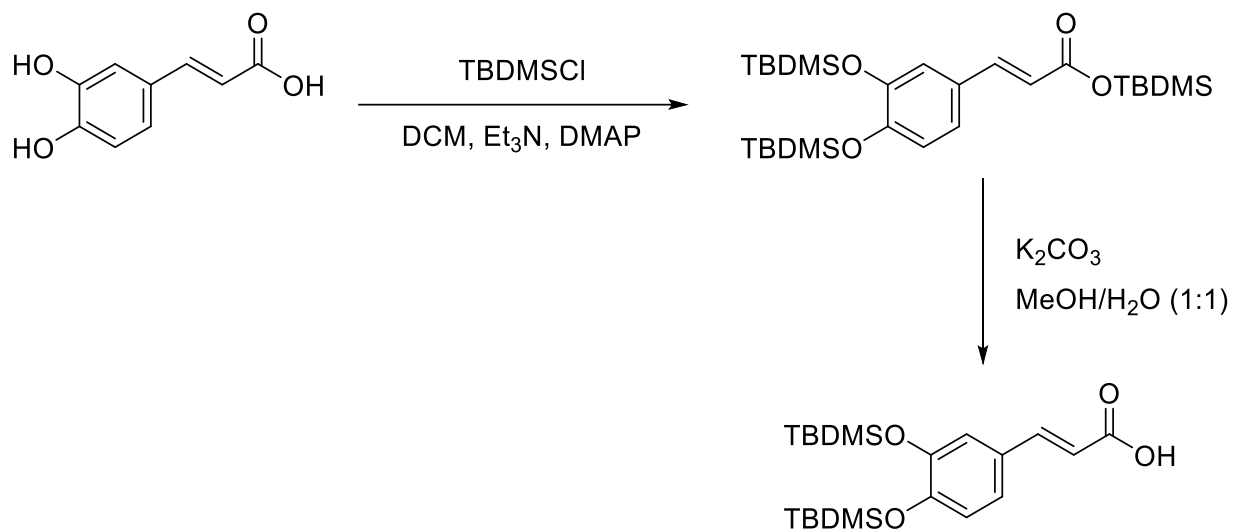


Figure 8. *Caftaric Acid.*

The protection was first completed with *tert*-butyldimethylsilyl chloride (TBDMSCl) in DCM with Et₃N and DMAP, both the phenols and the carboxylic acid functional groups were protected. To allow for availability of the carboxylic acid hydroxyl, it was selectively deprotected by K₂CO₃ in MeOH:H₂O 1:1 mixture (Scheme 2). The protected caffeic acid analogue was then coupled (dicyclohexylcarbodiimide) DCC in DCM containing a catalytic quantity of (*N,N*-dimethylaminopyridine) DMAP with dimethyl tartrate. The inconvenience of the DCC coupling agent is the byproduct of dicyclohexylurea. Dicyclohexylurea is readily soluble in a variety of solvents, aqueous and organic, making it difficult to completely remove.



Scheme 2. *Protection Scheme Utilizing TBDMS Groups for the Phenols of Caffeic Acid and Carboxylic Acid and Subsequent Selective Deprotection of the Modifier on the Carboxylic Acid.*

The use of *N,N*-carbonyldiimidazole (CDI), a related coupling agent, reduces this issue and works more ubiquitously for the synthesis of esters and amides. TBDMS protection groups and the methyl groups on the tartaric acid portion were removed with TBAF and LiOH.

An improved alternative to the initially proposed pathway presented itself via acetylation. It allowed direct protection of the phenolic hydroxyl groups without the need to deprotect the carboxylic acid before amidation. Acetylation protection of the phenols lent well to the eventual proposed route of carboxamides. The synthesis allowed for a mild deprotection scheme which efficiently deprotected at all positions simplifying the number of synthetic steps. Alternative routes of protection, such as methylation, were

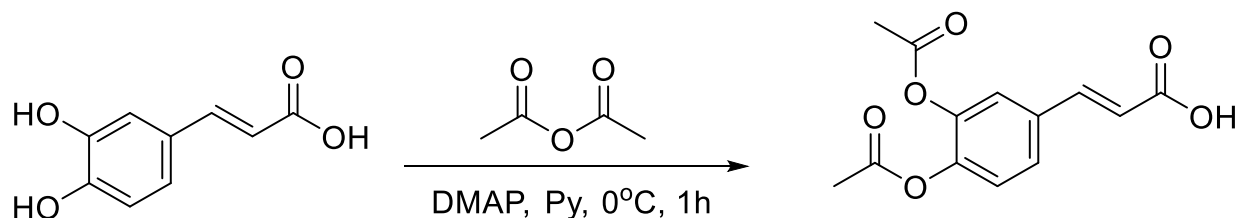
used at both the carboxylic acid and *p*-hydroxy substituent to resolve different structure activity relationship queries and the roles that these two locations play.

We developed a simplified process for the amidation of various polyphenolic starting materials.

3.1.1 Amidation of HCAs with Amino Acids

The route pursued for the synthesis of HCA-amino acid amide conjugates was a four-step process including acetylation of the phenolic region of the HCA, chlorination of the carboxylic acid to enhance reactivity, amidation of the acid chloride with methyl or ethyl ester protected amino acids, and finally the concurrent phenol and amino acid deprotection.

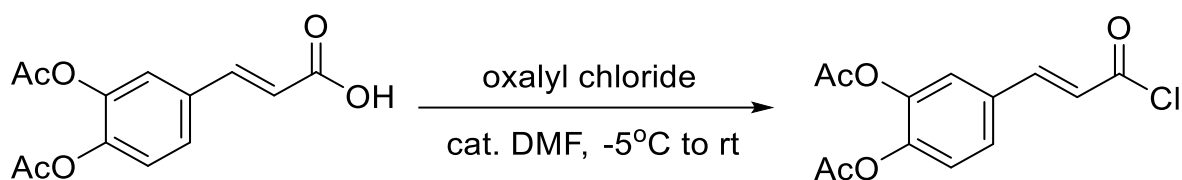
The interest in utilizing amino acids as the structurally diverse amide region stemmed from historical interest in the groups as efficient prooxidants, biological relevance, readily available starting materials, and controlled functional group variability around a consistent amine and carboxylic acid backbone.



Scheme 3. *Acetylation Scheme for Protection of the Phenol of HCAs (Example Used Caffeic Acid **1** to Compound **5**).*

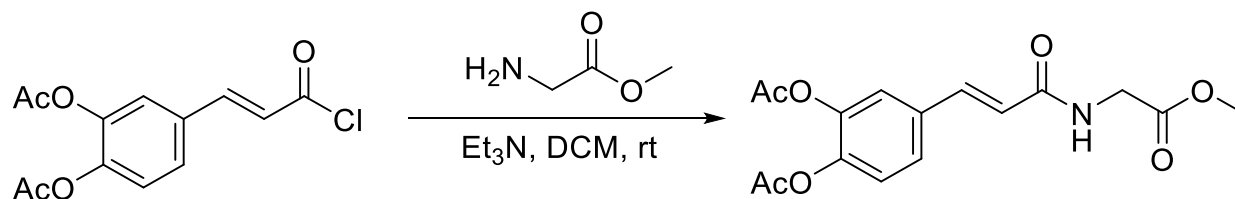
The first synthetic protection of the phenol was accomplished through acetylation with acetic anhydride as the acetylating reagent, DMAP as the recyclable

organocatalyst and basic organic solvent pyridine (Scheme 3) (Scriven, 1983). The selective acetylation of the phenol over the carboxylic acid is a result of innate functional group pKa. The acid dissociation constant (pKa) of the phenol is greater than that of the carboxylic acid, because of this the phenol is able to react with the acetic anhydride to be acetylated while the electrophilic carboxylic acid will not.



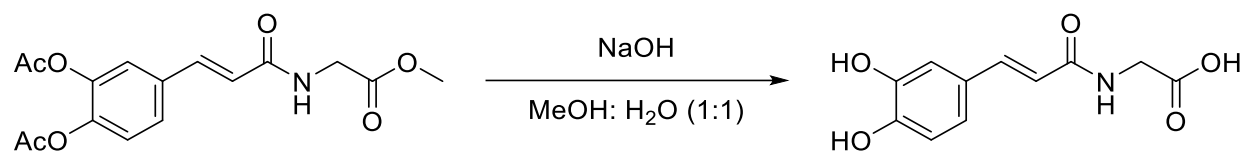
Scheme 4. Chlorination Scheme for Synthesis of the Acid Chloride of the Carboxylic Acid of HCAs (Example Used Compound **5** to Compound **9**).

Although the carboxylic acid alone could react with the amine by dehydration, those reaction conditions are typically harsh and cause formation of side-products. However, with acid chloride for example, the extremely efficient chloride leaving group addresses the issue of slow reaction while removing the chance of byproducts as with some reagents such as dicyclohexyl carbodiimide, DCC. Oxalyl chloride (COCl_2) and catalytic DMF in toluene was used to convert the carboxylic acid of the previously acetylated HCA to an acid chloride (Scheme 4) (Adams & Ulich, 1920). Conversion of a carboxylic acid to an acid chloride can be completed via numerous conditions and methods. A related alternative to the use of COCl_2 is the more common SOCl_2 , which is also readily available in most organic synthesis labs but more hazardous.



Scheme 5. *Amidation Scheme for Synthesis of the Amidated HCA (Example Used Compound **9** to Compound **13a**).*

Amino acid methyl esters were used for the synthesis of acetylated HCA amides via addition-elimination. Conditions of this synthetic step included a mixture of the reactants along with Et_3N and DCM at $0\text{ }^\circ\text{C}$ (Scheme 5). Successful synthesis required optimization at the point of reagent addition order. The base catalyst and amino acid methyl ester were dissolved in DCM and the acid chloride solution in DCM was added dropwise.



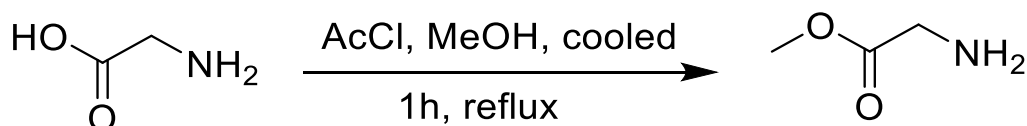
Scheme 6. *Deprotection Scheme for Synthesis of the Deprotected Amidated HCA (Examples Used Compound **13a** to Compound **17a**).*

For deprotection of the amino acid methyl ester and the acetylated phenolic groups, simple base catalyzed deprotection was employed. In a mixture of $\text{MeOH}:\text{H}_2\text{O}$, 1:1, sodium hydroxide was added and stirred at room temperature. The results of this hydrolysis were carboxylate salt and alcohol, which needed to be acidified to the

carboxylic acid (Scheme 6) (Ren et al., 2015). The base catalysis employs an irreversible mechanism and is complete after 1 hour without additional heat at high yield.

3.1.2 Synthesis of Protected Amino Acids for Amidation

Protection of the carboxylic acid portion of the amino acid was achieved by methylation. This method allowed for the amine to stay available for amidation with the acid chloride of the HCAs **9-12**, while the carboxylic acid remained protected with reduced chance of significant byproducts. Some protected amino acids were available commercially and purchased, including *O*-*tert*-butyl-L-serine methyl ester and β -alanine ethyl ester, which were used in the amidation step without any modification. The methyl ester and ethyl ester amino acids purchased were similarly deprotected by the deprotection step.

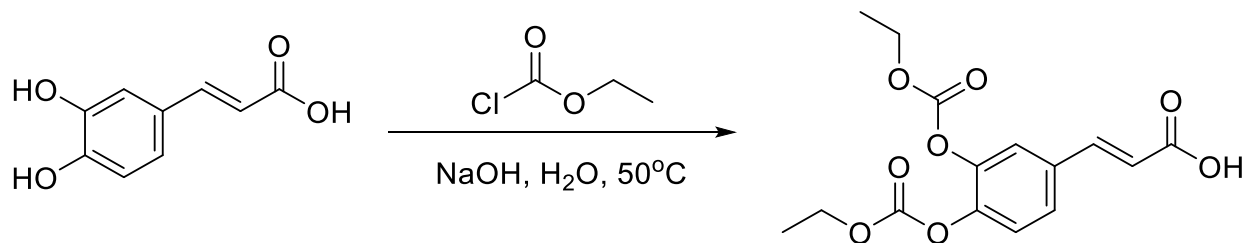


Scheme 7. *Amino Acid Methylation Synthetic Scheme.*

Most amino acids were methylated utilizing acetyl chloride, although aspartic acid methylation was completed more successfully via SOCl_2 and MeOH (Scheme 7).

3.1.3 Synthesis of Alternative Phenol Protecting Groups

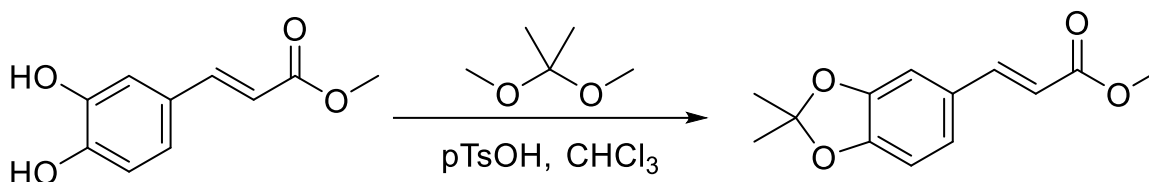
Further, more methods of phenol protection were investigated for preparation of alternative HCA derivatives. We found both advantages and disadvantages to all protecting groups regarding the synthesis and subsequent analysis.



Scheme 8. *Ethylcarbonate Phenol Protection Synthetic Scheme.*

Here, ethylcarbonate derivatives of caffeic acid, while leaving the carboxylic acid portion of the compound unencumbered for reaction (Scheme 8). With a lower yield (25%) compared to that of the highly efficient acetylation, this method was not pursued further in the synthetic scheme.

The acetonide derivative is an option specifically for the catechol portion of caffeic acid.



Scheme 9. *Acetonide Protecting Group Synthesis.*

A disadvantage of this route is that it required an additional preparation step through protection of the carboxylic acid via Fischer esterification prior to reaction with 2,2-dimethoxypropane (Scheme 9). Nevertheless, this reaction proceeded in high yield (85%) but required deprotection of the methyl ester for further reaction at the carboxylic acid with LiOH in the end.

The synthesis of a variety of scaffolds through various methods afforded a small library of compounds with structural diversity at the phenol and the carboxylic acid giving unique comparisons to address the structure activity relationships of the synthesized derivatives of HCAs. The four-step acetylation, chlorination, amidation and deprotection method was used for all of the HCA-amino acid derivatives and the Fischer esterification route was used for all methylation of the carboxylic acid for HCAs. The exploration of alternative synthetic methods helped to find an optimized scheme.

3.2 DPPH Assay

As DPPH allows both HAT and SET mechanisms, covered previously (section 2.3.2), the test is not limited to specific classes of compounds. However, as polyphenols have been shown to engage radicals in both HAT and SET mechanisms this assay allows for convenient establishment of full capacity potential, the point at which the added antioxidant has been fully depleted and will no longer scavenge free radicals without regeneration (Figure 9). The direct comparison of differing compound classes with the DPPH assay can prove complicated and ineffective. However, comparison within the same compound class, especially the HCAs, can be done effectively.

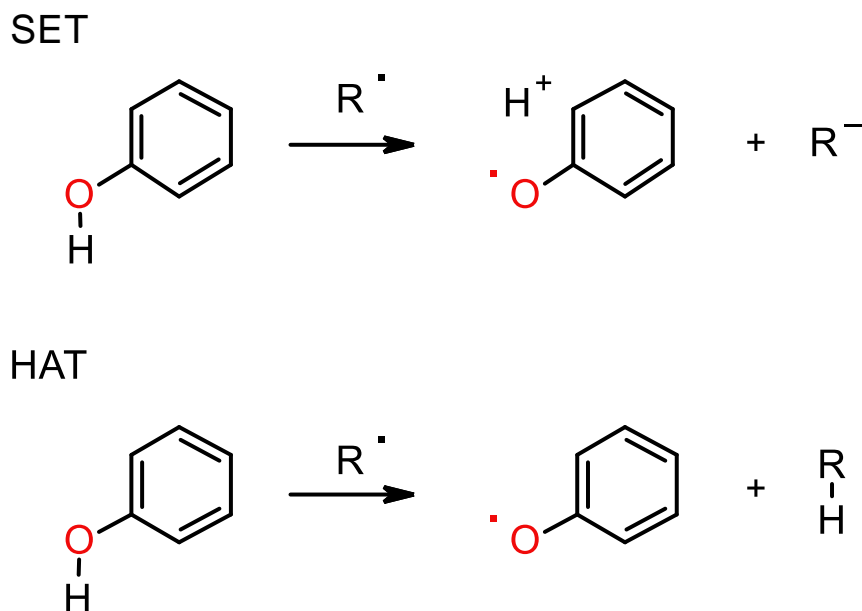


Figure 9. *HAT and SET Mechanisms for Phenol.*

There are two critical points to consider when using the DPPH analysis method and those are solvent effects and steric hinderance. Both have significant effects on the results of the analysis (Shojaee, Moeenfarid, & Farhoosh, 2022). Based on previous testing with similar compounds and comparative analysis an alcohol solvent was chosen. This added to the lifetime of the DPPH radical for more consistent results over multiple experiments, while also improving the solubility of both the DPPH radical and compounds being assessed for scavenging. Different solvents were evaluated, and methanol was determined to be the best regarding compound solubilities, reaction rates, and minimal uncontrolled radical reduction.

3.2.1 Time Point Analysis vs Full Capacity Measurement

Most radical scavenging assays with DPPH only consider full scavenging capacity which is reached after around 10 minutes. More modern evaluations take

kinetic data into consideration from tracking of the radical presence over the course of the testing period. Initially, we evaluated all compounds for up to 45 minutes. However, no changes were detected after 10 minutes in each case, and therefore, we considered all reactions complete after 10 minutes. Unlike other studies, time points were taken starting at 0 s and every minute thereafter. Compounds could then be compared for speed and efficiency at different segments of the overall reaction along with evaluation of full scavenging capacity. DPPH reduction via reaction with an active ligand was confirmed by analysis Direct Analysis in Real Time (DART) on a JEOL AccuTOF-DART mass spectrometer (Figure 10). The reduced structure of DPPH changed by a single mass unit confirming the addition of a hydrogen to the original free radical structure.

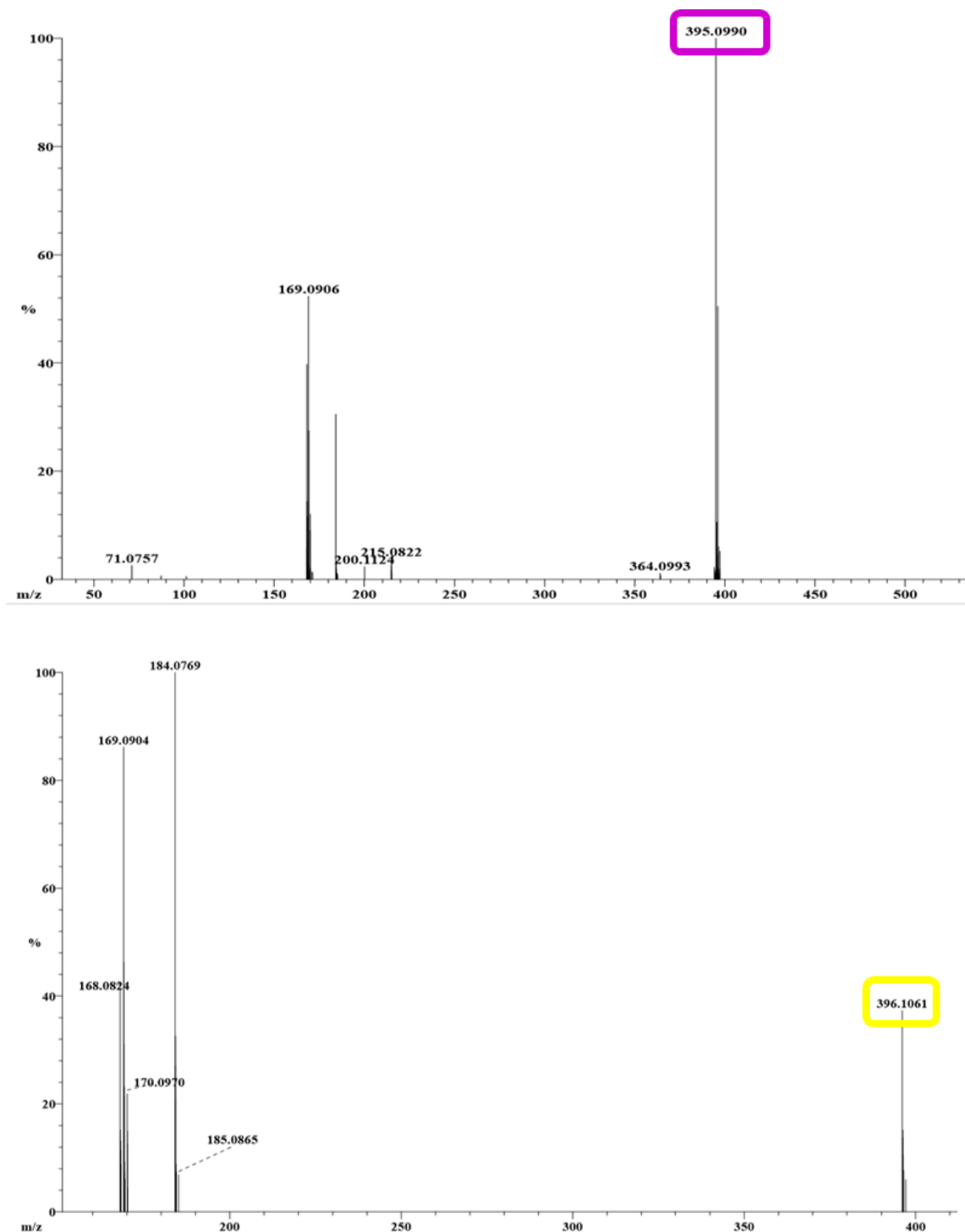


Figure 10. *Reduction of the Free Radical Scaffold DPPH as Confirmed by Mass Shift After Interaction with Compound 1.*

The shift of one mass unit can be seen before and after reaction with a radical scavenging small molecule, in this case compound **1**.

3.2.2 Hydroxycinnamic Acids Radical Scavenging Capacity

The HCAs tested have a consistent *p*-hydroxy functional group with an α,β -unsaturated carboxylic acid substituent (Figure 11). Variation in the scaffolds comes from the additional substituents on the aromatic ring. Caffeic acid (**1**) presents an additional hydroxyl group (catechol), *p*-coumaric acid (**2**) includes no additional substituents, ferulic acid (**3**) contains a single methoxy group ortho to the hydroxy, and sinapic acid (**4**) has two methoxy substituents surrounding the *p*-hydroxy.

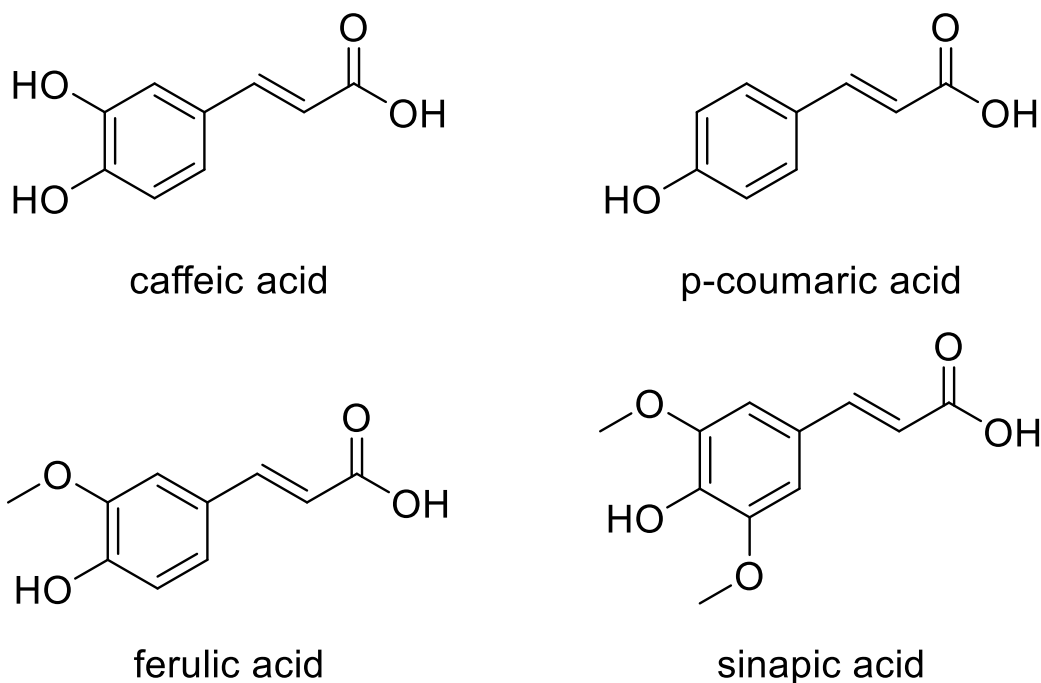


Figure 11. *Hydroxycinnamic Acids: Caffeic Acid (1), p-Coumaric Acid (2), Ferulic Acid (3), Sinapic Acid (4).*

The impacts of these additional substituents are significant in changing the ability of the generic *p*-coumaric acid (**2**) by more than 10-fold in some cases. The ranking of these compounds is consistent with those evaluated in other studies **1** (IC₅₀ 15.6 mM) > **4** (IC₅₀ 19.1 mM) > **3** (IC₅₀ 58.5 mM) >> **2** (IC₅₀ > 200 mM). The total capacity, as defined above by the IC₅₀ value, is not the only variation observed by the interaction of HCAs with DPPH. The kinetics of scavenging vary as well (Figure 12).

Compounds **4** and **2** present fast initial scavenging of free radicals followed by an asymptotic maximum, while compounds **1** and **3** show a rapid but more gradual increase in radical scavenging over 6 minutes followed by a later asymptotic maximum. Although, this initial interaction is not a diagnostic of the overall capacity, as the top scoring HCAs vary in curve profile, it may inform the mechanism of radical scavenging of the small molecule. Compound **1** has the greatest radical scavenging potential via stabilization through the neighboring hydroxy substituent on the benzene, followed by compound **4** with two surrounding methoxy substituents for stabilization, then compound **3** with the single additional methoxy substituent, and finally compound **2** with no substituent stabilization around the *p*-hydroxy.

The ranking of the HCAs is directly related to their structures and linked to their ability to be effective radical scavengers.

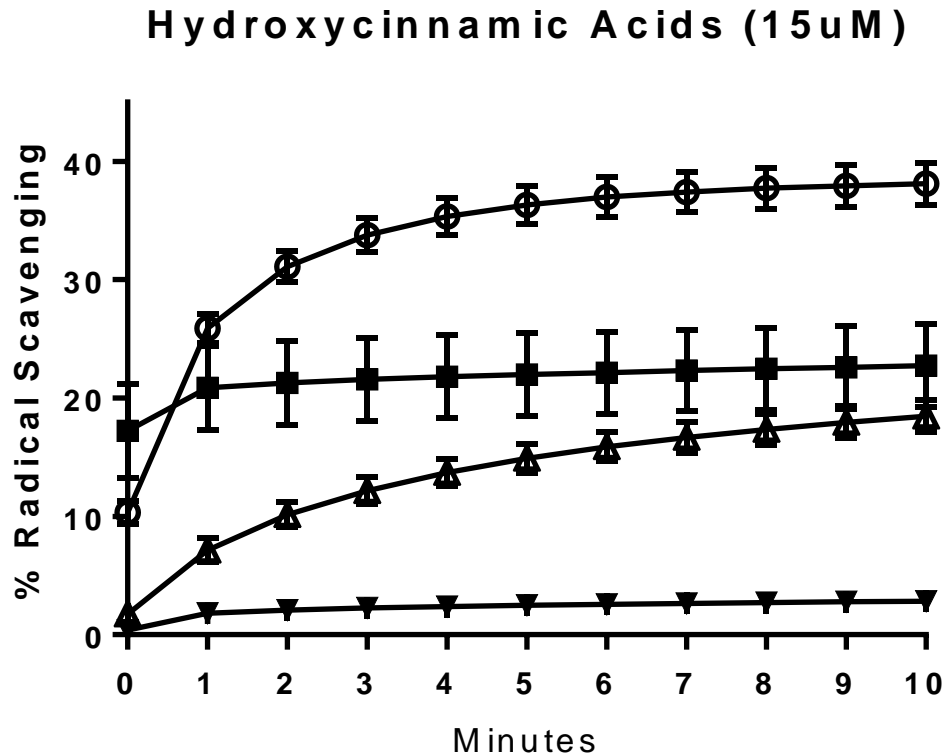


Figure 12. *DPPH Radical Scavenging Assay Results of HCAs (15 mM) Over 10 Minutes. Caffeic Acid (1) [open circle], Sinapic Acid (4) [black square], Ferulic Acid (3) [open triangle] and p-Coumaric Acid (2) [black triangle].*

Important aspects of a phenols ability to scavenge and support radicals comes from the factors explained previously, (2.3.1), resonance, hybridization, and electronegativity. Specific to the HCAs, there are multiple points of scavenging activity. The phenol can donate a hydrogen and support the radical through resonance. When this is a catechol the unpaired electron is stabilized by more resonance contributors as compared to the single *p*-substituent (Figure 13).

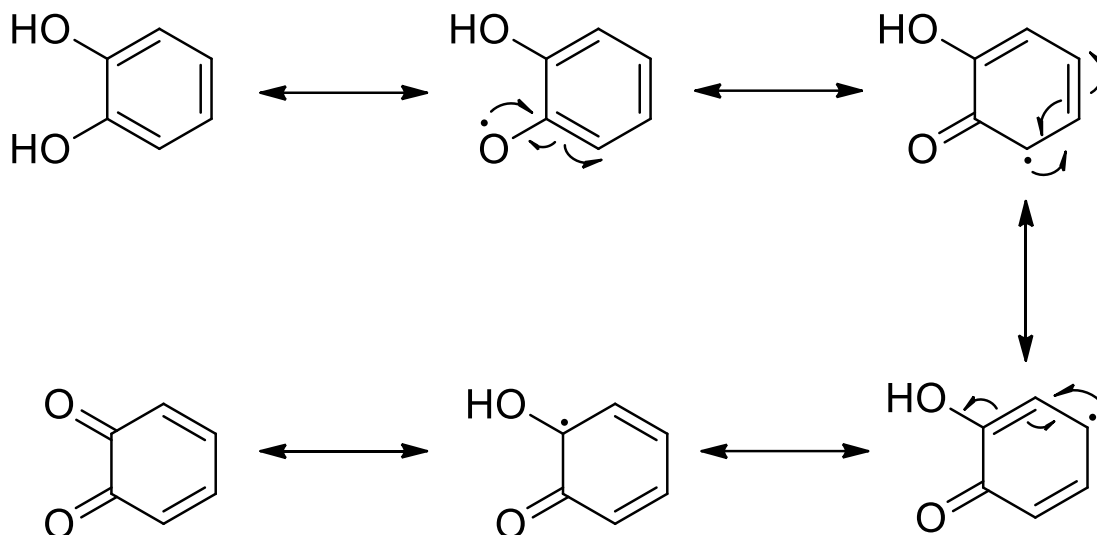


Figure 13. *Catechol Resonance Contributors in the Radical Hybrid.*

The four contributing resonance structures associated with the catechol radical stabilization, together with two points of oxidation as opposed to one, made it the most efficient of the small molecules tested.

Additional substituents at the position para to the phenol did not improve the capacity of the scavenger as promotion from phenol to catechol did. However, the conjugated acrylic functional group can theoretically extend the resonance capacity of the HCAs (Figure 14). Upon interaction with free radicals, **1** proceeds to an o-quinone through semi-quinone formation with the ability to donate two hydrogens doubling the capacity of compounds like **2**, **3**, and **4**. However, the acrylic functional group that is consistent throughout the HCAs does allow an alternative mode of extending the radical resonance. As seen in Figure 14, the addition of the substituent to the catechol formation from Figure 13 expands the resonance formations to nine, from four. The

extension of resonance is a vital part of the ability of antioxidants and further “trapping” of the radicals.

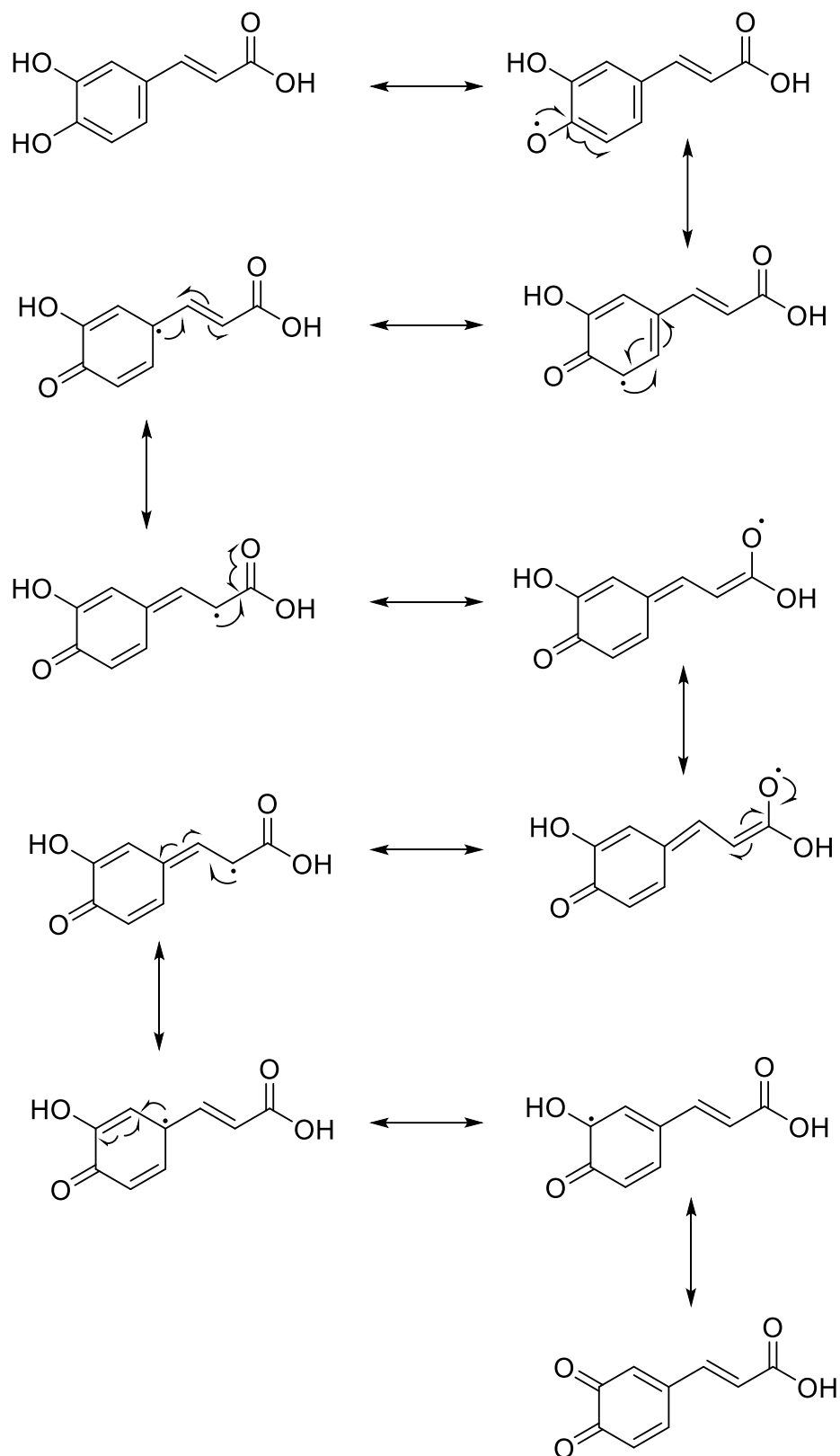
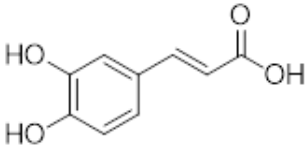
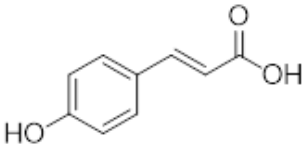
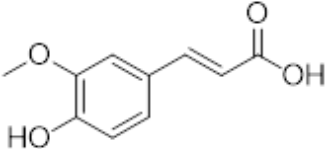
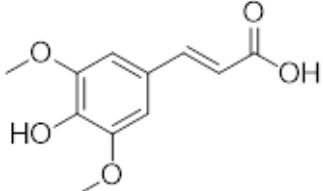


Figure 14. *Caffeic Acid Resonance Contributors.*

While amplification of the scavenging potential of **1** is due to the multiple donating locations, the enhancement of **3** and **4** from that of **2** is based on radical stabilization by surrounding substituents, similar to caffeic acid above.

The enhancement by the additional OH of **1** is lost in **4**, but the resulting radical is support by two methoxy substituents, the radical of **3** is less supported than that of **4** as it contains only a single methoxy substituent and finally, **2** relies upon only the aromatic ring (Table 1). This ordering and difference in scavenging capacity conveys the structural importance of surrounding substituents as the capacity among **2**, **3**, and **4** are identical.

Table 1.*DPPH IC₅₀ values of HCAs.*

ID	R	R ₁	R ₂	DPPH Radical Scavenging IC ₅₀ (μ M)
Caffeic acid (1) 	H	OH	COOH	15.66
<p><i>p</i>-Coumaric acid (2)</p> 	H	H	COOH	>200
Ferulic acid (3) 	H	OCH ₃	COOH	58.53
Sinapic acid (4) 	OCH ₃	OCH ₃	COOH	19.05

Through BDE calculations the *p*-hydroxyl group is the most likely location of hydrogen donation (Urbaniak, Molski, & Szlag, 2012). Further understanding of the impact of this functional group as well as the available carboxylic acid was pursued by the synthesis of derivatives described in the following section.

3.2.3 HCA Derivatives Radical Scavenging Capacity

3.2.3.1 Acetylated HCAs. With the protected product from the full four-step synthesis (Figure 15), analysis of the radical scavenging capacity of the HCAs without the activity of the *p*-hydroxy can be evaluated. The results of these compounds in the scavenging of the DPPH radical showed no activity, at the highest tested concentration 200 mM. Without the *p*-hydroxy group, or in the case of **1** the dihydroxy motif, there was no way for this class to effectively scavenge radicals.

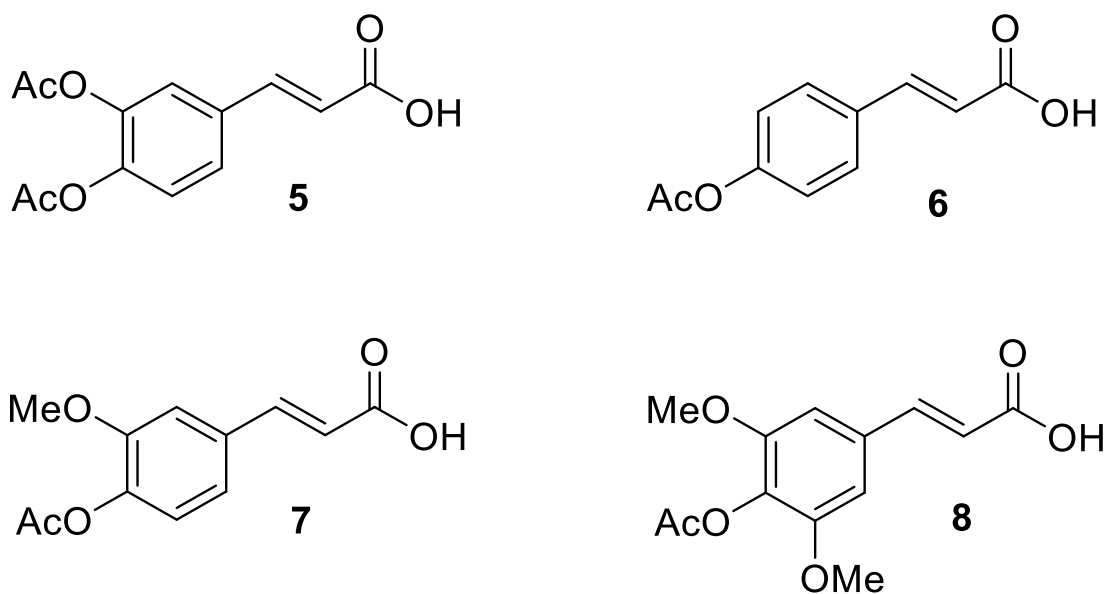
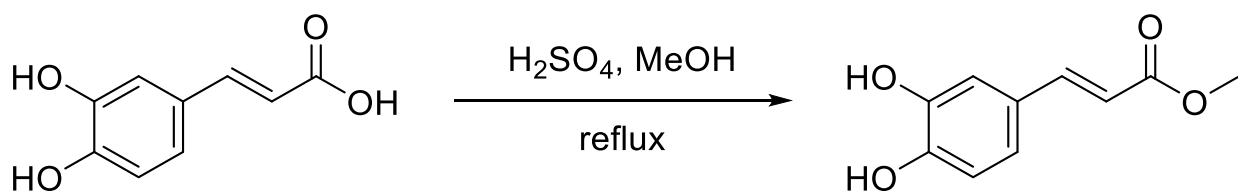


Figure 15. HCA Products of Acetylation Protection.

By assigning primary activity to the phenols, the conclusion was that the carboxylic acid functional group shows no detectable ability to scavenge DPPH radicals. To further support this hypothesis the **1** scaffold was protected at the COOH functional group through Fischer esterification.

3.2.3.2 Esters of HCAs. The esterification of HCAs should not have an impact on scavenging. If a variation occurred nonetheless, it may be due to a mechanistic feature different than that of direct hydrogen donation. These modifications to the scaffolds will begin to inform important aspects of the DPPH assay and driving factors, including the roles of solvent interaction with the scavenging small molecules and the impact of steric hinderance because of including larger substituents.



Scheme 10. Fischer Esterification Scheme, Caffeic Acid Methyl Ester (**22a**).

The caffeic acid derivatives synthesized included a methyl, ethyl, and propyl substituent to investigate the impact of chain length, if any (Figure 16).

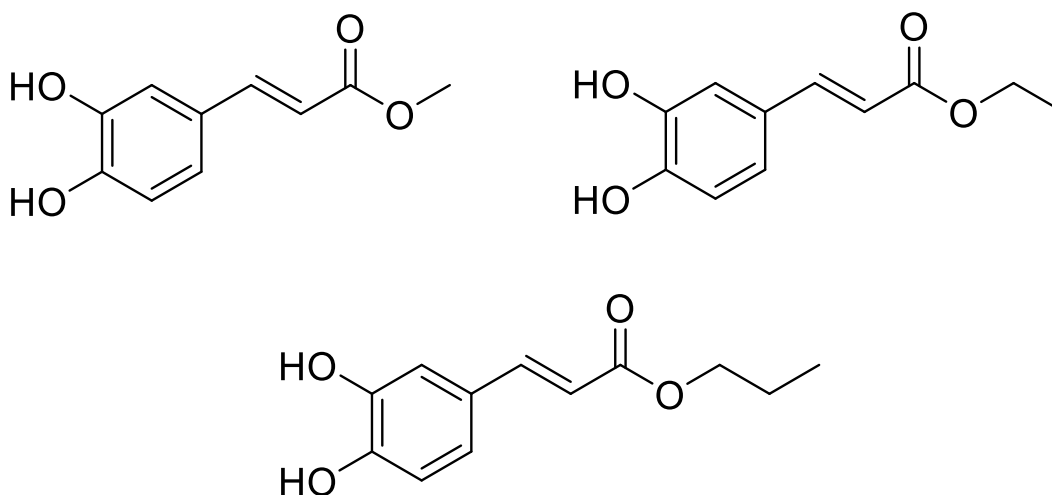


Figure 16. *The Resulting Derivatives of the Esterification of Caffeic Acid (1), Methyl (22a), Ethyl (22b), Propyl (22c).*

Results of the analysis show modest enhancement to the total scavenging potential of the new derivatives. The small enhancement exemplifies the two major factors in DPPH scavenging. First, the addition of small alkyl chains at the carboxylic acid did not increase the size of the compounds enough to cause increased steric hinderance and decrease scavenging power. Secondly, esterification decreased polarity and the extent of solvation, which was a rationale for better interaction between the radical scavenger and DPPH molecules.

3.2.3.3 Bis-aryl Anhydrides. Identification of the primary reactive region of the polyphenol allowed further interrogation of the ability to modify the total capacity of the subunit. This could be effectively doubled by duplicating the hydroxyl group. The carboxylic acid portion of the HCAs allows for efficient combination via an anhydride or diamide functional group connection to a bis-anhydride or imide. The impact of applying a compound with two active hydroxyls does enhance the total antioxidant capacity of

the compound. As an example of the overall trend, the synthesized compound **21c**, which contains two connected *p*-hydroxy substituted benzenes linked via an anhydride showed total capacity of 9% compared to the original single **2**, which leveled out under 5% when tested at a concentration of 15 mM. The capacity of the bis-aryl substituents may not exactly double due to additional steric hindrance as well as the possible inability of the compound to simultaneously reduce two free radicals. An advantage of the bis-aryl compound is that it maintains the potential for radical scavenging beyond a single antioxidative action. The profile of the time point reduction curve does not change from original HCA to anhydride derivative as shown in Figure 17.

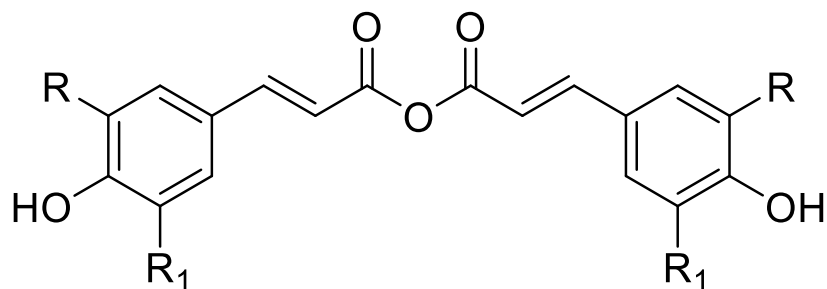
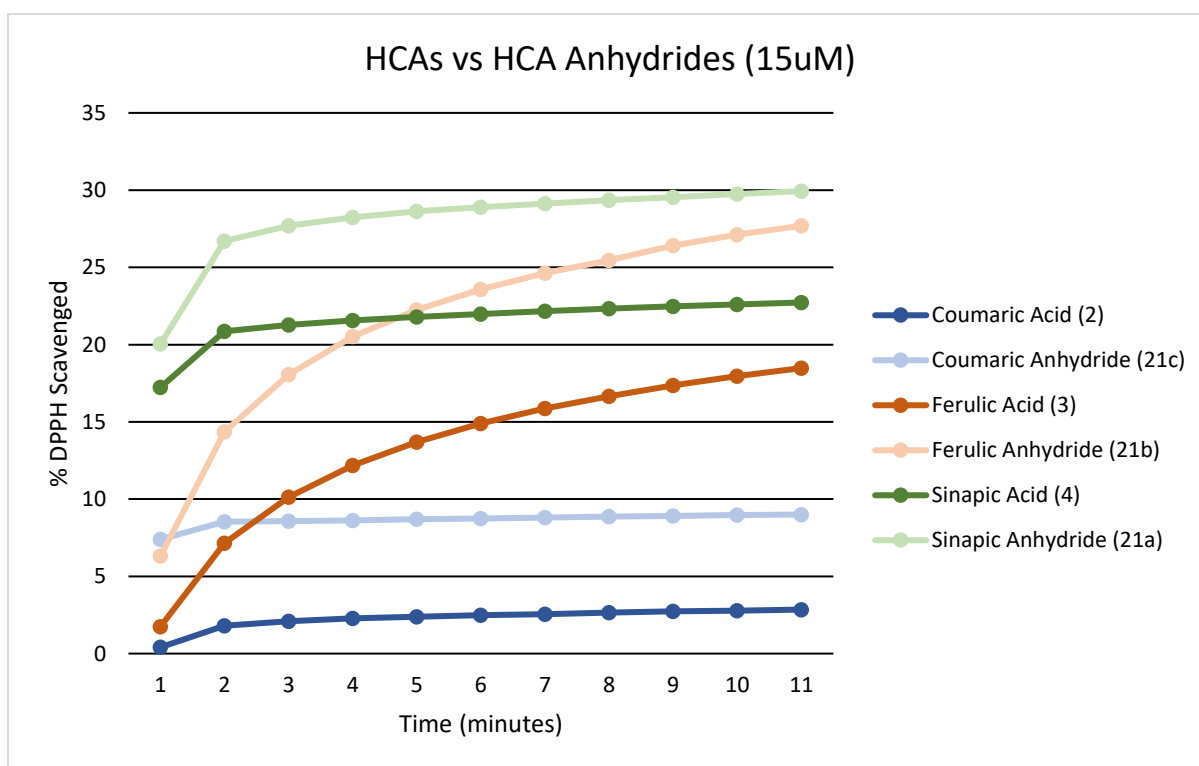
a**b**

Figure 17. (a) *Bis-Aryl Anhydrides*. **21a**: $R = \text{OMe}$, $R_1 = \text{OMe}$, **21b**: $R = \text{OMe}$, $R_1 = \text{H}$, **21c**: $R = \text{H}$, $R_1 = \text{H}$. (b) *The Kinetic Analysis Comparing the DPPH Radical Scavenging Capacity of HCAs to the Synthetic Anhydride Counterparts.*

The addition of a competing or complimentary scavenging group could allow for increased overall potential. For example, amino acids have been shown to support

radical scavenging through prooxidant capacity or reactivation of the primary antioxidant. To understand the role of the amino acids, each amino acid was tested without any modification. All tested amino acids show no lone scavenging ability via the DPPH assay.

3.2.3.4 HCA Amino Acid Derivatives. Protection of the carboxylic acids on the amino acids was completed by one-pot methylation via an S_N2 reaction creating an alkyl halide intermediate in MeOH. These methylated amino acids were converted to the amide (Figure 18).

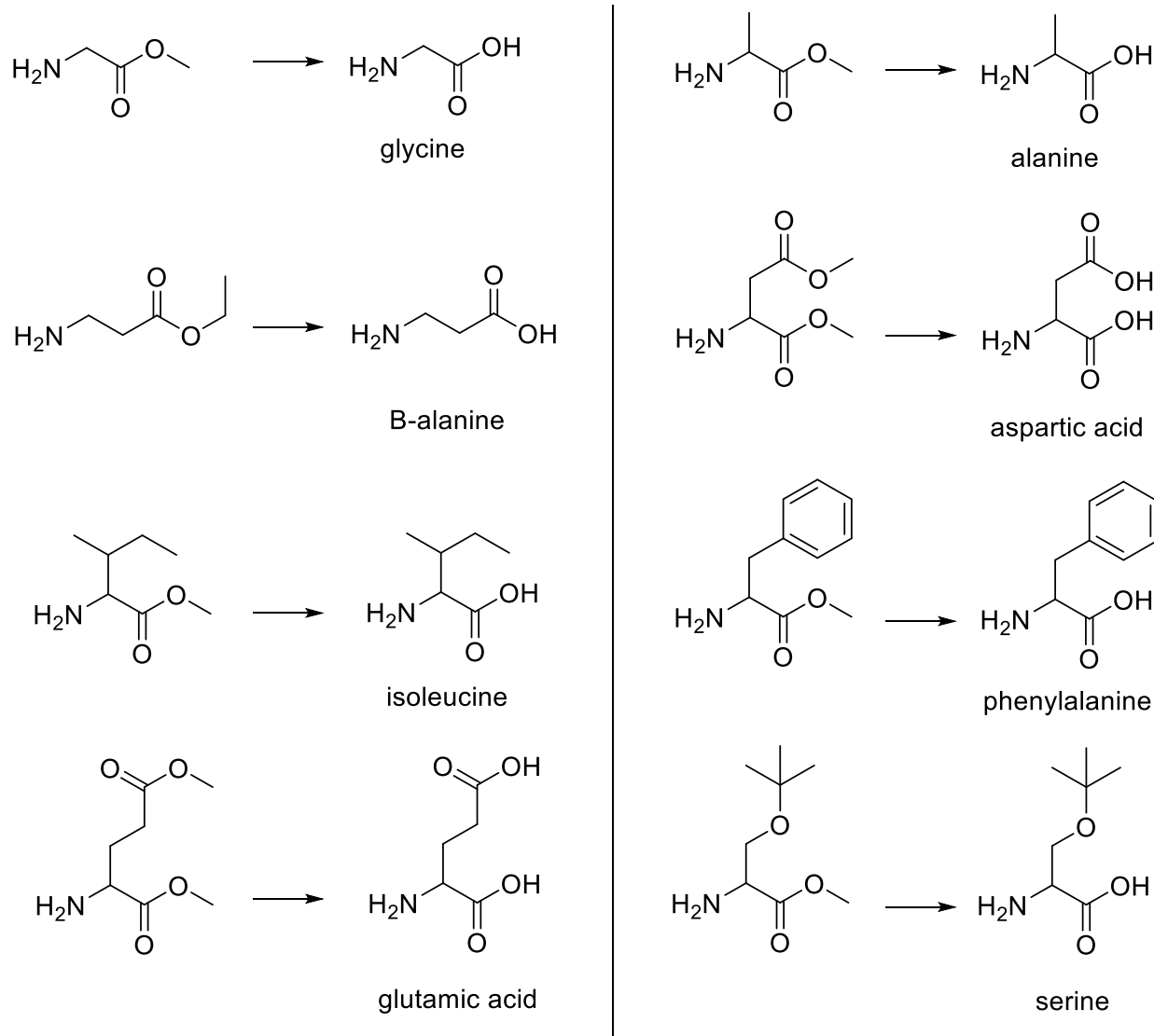
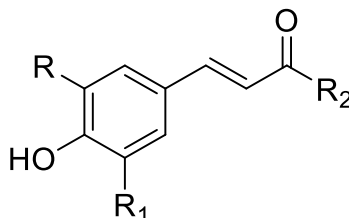


Figure 18. *Amino Acids Used for Amidation Step with Acid Chloride.*

In comparison to that of the backbone structure (caffeic acid), the amino acid addition would maintain the carboxylic acid but also include an additional functional group. Of those chosen, glycine, alanine, isoleucine and β -alanine add carbon chain length to the structure or alkyl additions, aspartic acid and glutamic acid vary the backbone by including an additional carboxylic acid group, phenylalanine includes an

additional aromatic region, and serine-*t*-Bu adds a bulky *tert*-butoxy group. These differences can inform the impact of chain length, size, polarity and other characteristics on the radical scavenging properties of the compounds.

Table 2.*DPPH IC₅₀ Values of HCA Amide Derivatives.*

ID	R	R ₁	R ₂	DPPH Radical Scavenging IC ₅₀ (μM)
17a	OH	H	-Gly	15.85
17b	OH	H	-Ala	14.08
17c	OH	H	-Ile	16.43
17d	OH	H	-Phe	17.54
17e	OH	H	-Ser-tBu	21.07
17f	OH	H	-Asp	19.94
18a	H	H	-Gly	>200
18b	H	H	-Ala	>200
18c	H	H	-Phe	>200
18d	H	H	-Ser-tBu	>200
18e	H	H	-Asp	>200
19a	OCH ₃	H	-Gly	>50
19b	OCH ₃	H	-Ala	24.64
19c	OCH ₃	H	-Phe	56.70
19d	OCH ₃	H	-Ser-tBu	46.22
19e	OCH ₃	H	-Asp	100.42
20a	OCH ₃	OCH ₃	-Gly	16.45
20b	OCH ₃	OCH ₃	-Ala	91.33
20c	OCH ₃	OCH ₃	-Ile	16.26
20d	OCH ₃	OCH ₃	-Ser-tBu	65.60
20e	OCH ₃	OCH ₃	-Asp	>50

A trend among the IC₅₀ values was the ability of smaller substituents to scavenge more efficiently, which was consistent with an original observation of steric hinderance preventing the antioxidant from closely encountering the radical. Additions such as aspartic acid, which has two free carboxylic acids, increasing steric hinderance, and phenylalanine which has a bulky aromatic region and serine-*t*-Bu with the large *tert*-butyl region, consistently show larger IC₅₀ values.

The general profile of the curves does not vary significantly among the derivatives (Figure 19). While there may be changes to the overall stability of the radical once quenched by the antioxidant, the initial interaction with the radical and through the phenol region remained consistent.

The results obtained from the *p*-coumaric amide (**18a-f**) are not shown in Figure 19 where even high concentrations had only very minor scavenging activity. Overall, despite the addition of prooxidant amino acids, derivatives of *p*-coumaric acid did not engage in distinguishable radical scavenging activity.

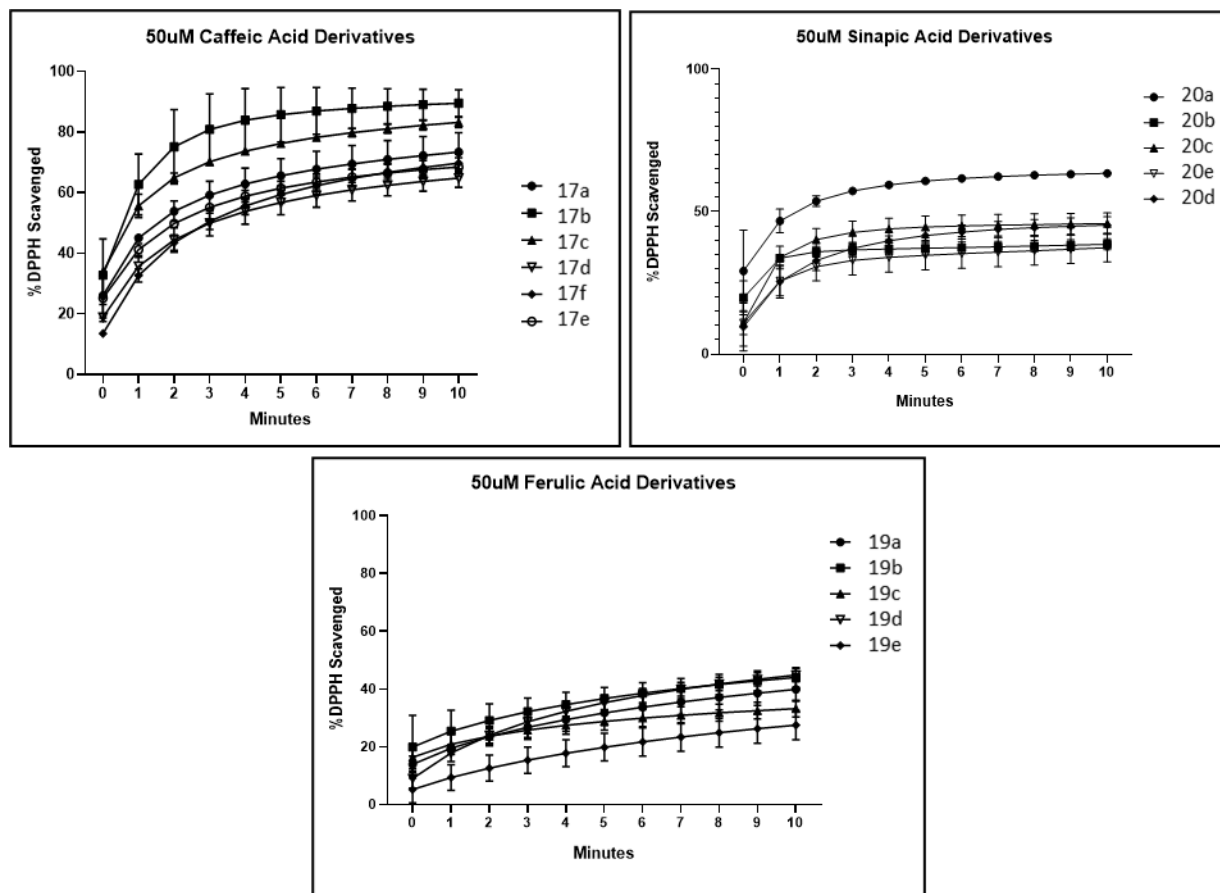


Figure 19. HCA Derivatives Scavenging Profiles at 50 μM.

The kinetic profile of all derivatives was only minimally affected by the nature of the amino acid.

3.2.3.4.1 T_1 Reaction Time Analysis. Change in DPPH scavenged over the course of the reaction allowed for further understanding of interactions between compounds and free radicals. Initial findings showed a decrease in initial rate of reaction (T_1) with increased carboxylic acid groups present, seen with the aspartic acid derivatives of **1**, **3**, and **4** (Figure 2). Derivatives for glutamic acid **20f** and β-alanine **20g** with sinapic acid were analyzed by the same method at a single concentration for comparison. The decrease in activity for compounds with two carboxylic acid groups

was observed again but there was also a notable decrease between **20g** and **20a** and between **20f** and **20e**. The variable between these derivatives is the increase in chain length at the derivative portion of the molecule (Figure 18).

Resonance is an essential characteristic of a radical scavenger to stabilize an unpaired electron. Initially, the addition of the amino acid was proposed to create stability through the formation of a pseudo-ring, stabilizing the radical when present at the carbonyl oxygen of the derivative HCA through interaction of the carboxylic acid group on the amino acid portion of the compound (Figure 20).

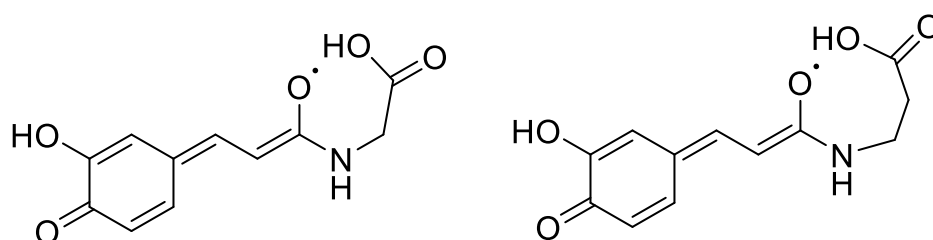


Figure 20. *Pseudo-Ring Formation Proposed for Possible Enhance Stabilization of Radical Via Radical Scavenger Compound.*

Alternatively, the primary aspect of radical scavenging reduction, specific to the DPPH assay, could be more reliant upon steric hinderance. As the derivatives were built up with bulkier additions to the HCAs it became increasingly difficult for the small molecules to encounter the DPPH radical, in an effective position. This could be a primary determinant of the development in T_1 as observed. Bulkier amino acids used for derivatization resulted in less DPPH scavenged at early time points during analysis (Figure 21).

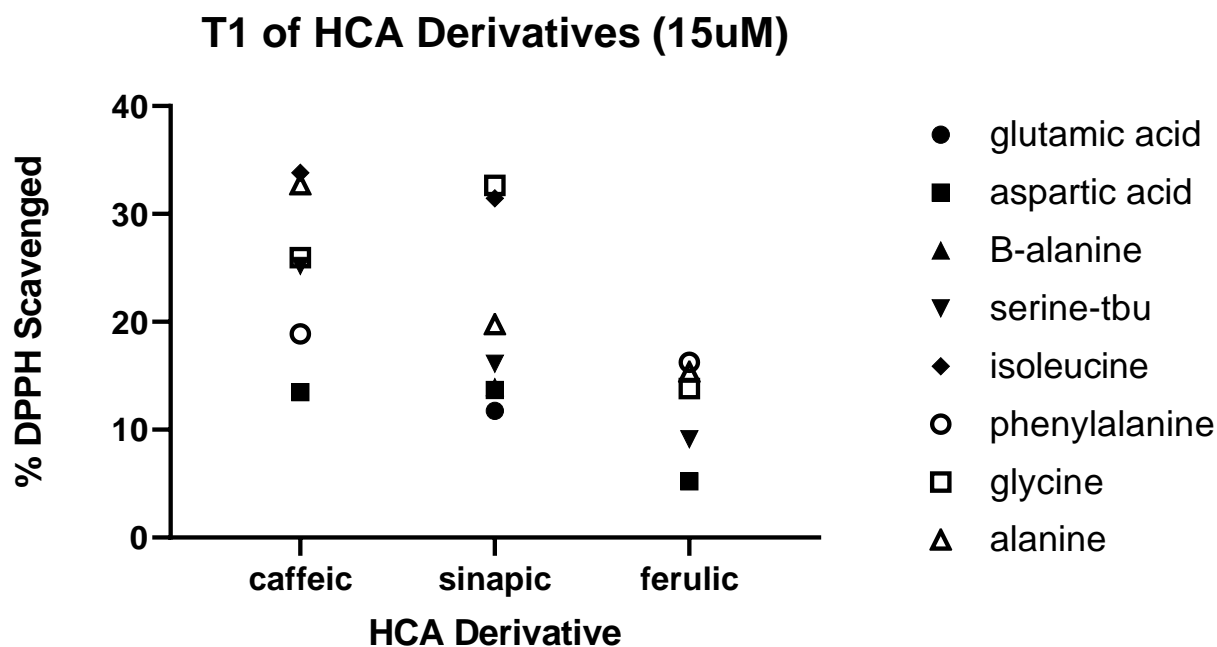


Figure 21. Comparison of Synthetic Amino Acid Derivatives and the Speed of Reaction with DPPH at Initial Time Point Interval Between HCAs **1**, **3**, and **4**.

The structural addition of the amino acid did not enhance the total capacity of the compound, as detected with the DPPH assay. The derivative addition showed modification of the initial rate of reaction observed for **1**, **3**, and **4**, however, general ability to scavenge radicals was influenced primarily by the hydroxy and methoxy arrangement on the aromatic ring. We observed increased scavenging for **1** through additional hydroxyl groups increasing stabilization and the enhanced ability to donate hydrogen atoms, or stability through substituents exemplified by the difference between **4** and **3**. In the absence of those stabilizing substituents, the capacity of the single hydroxyl was substantially reduced as observed with **2**.

The most effective radical scavenger is **1**, caffeic acid. The origin of hydrogen donation and reactivity is phenol. The carboxylic acid functional group does not play a significant role in free radical scavenging as determined by the DPPH assay. The primary factors associated with scavenging potential of HCAs are radical stability as a function of surrounding substituents to the phenol and steric hinderance. The carboxylic acid group of this class offers a reasonable location for synthetic derivatization. The synthetic group that most effectively enhanced the scavenging capacity of this class of compounds, that was tested, was the combination of two HCAs combined through an anhydride.

3.3 α -Amylase Inhibition Assay

3.3.1 Enzyme Assay Development

The use of KI/I₂ indicator for starch concentration measurements is reliant on creation of a charge transfer complex between the -helices of α -(1,4) glycosidic linkages in glucose homopolymer (amylose, “starch”) and the I₃⁻ indicator (Figure 22).

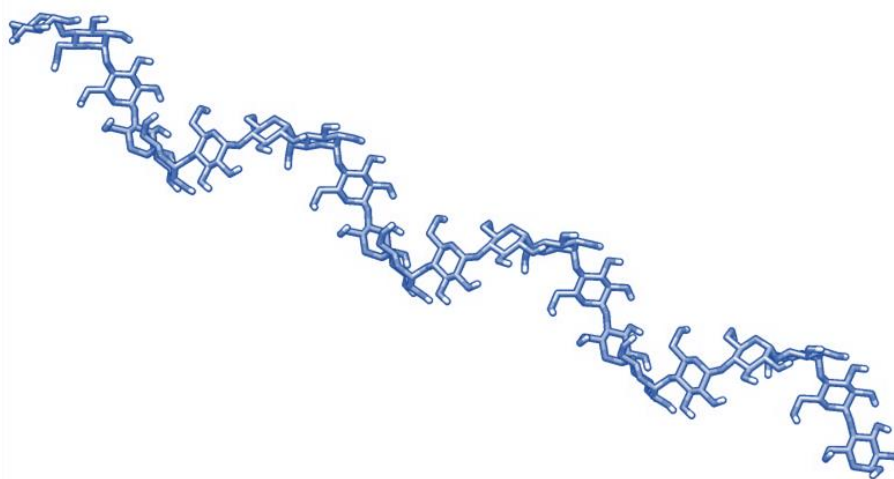


Figure 22. *Amylose Chain Helical Structure.*

I_3^- and amylose create charge transfer complexes with various points of maximum absorption based on the amylose chain length. Chains greater than 40 subunits in length show a blue color, which becomes red or orange between 10 and 40 subunits and no visible color below 10 (Bailey & Whelan, 1961; Moulay, 2013). Tracking reduction of absorption at 580 nm can simply quantify the amount of remaining α -(1,4) amylose chains.

Amylose is the specific substrate of α -amylase and is broken down via hydrolysis to simpler subunits. Reliance upon the helical amylose structure, α -(1,4) linkages, can be confirmed through the testing of other sugar substrates. Glucose, the substrate monomer, maltose, an α -(1,4) disaccharide, and dextran, a polysaccharide consisting of primarily α -(1,6) glycosidic linkages thus not forming a helical structure, were tested with the same procedures as amylose. While strong absorption at 580 nm related to the amylose/ I_3^- charge transfer complex can be seen with the addition of indicator, no absorption is observed for the maltose, glucose, or dextran substrates (Figure 23). This confirms that there is no signal interference related to these byproducts or other related enzymatic products and substrate contaminants.

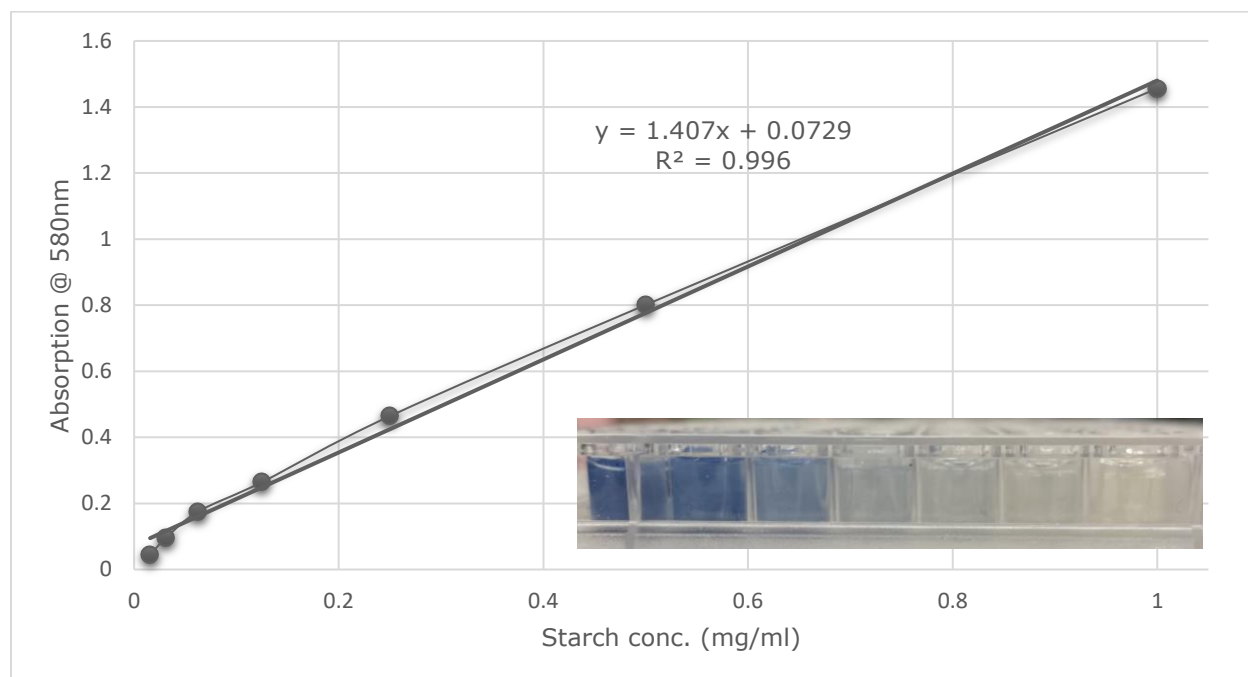


Figure 23. *Absorption Response of Various Starch Concentrations Without the Inclusion of Enzymes or Inhibitors (chart) and Related Visual Appearance of the Charge Transfer Complex (picture).*

Optimization of the assay was determined through analysis of various conditions derived from previous sources of similar assays more commonly associated with α -amylase activity, as opposed to inhibition (Fuwa, 1954; Oliveira, Pinheiro, Fonseca, Cabrita, & Maia, 2019; Visvanathan et al., 2020; Xiao, Storms, & Tsang, 2006). Tested conditions included incubation times of 5 minutes, 15 minutes, 30 minutes, and 45 minutes and incubation temperatures of 24 °C, 38 °C, and 54 °C. Selection of conditions was based on the maximum enzyme activity tracked by lack of absorption at 580 nm, showing little to no creation of charge transfer complexes (Figure 23). The starch to enzyme ratio was then optimized to identify ideal test conditions that would

fully exhibit the inhibition of the enzyme at various levels (Figure 24). Another point of optimization was the order of addition of the different assay components. It has been shown that incubation between the starch and ligands before introduction of the enzyme can influence the outcome of the assay (Aleixandre, Gil, Sineiro, & Rosell, 2022).

These experimental conditions were investigated, and no variation was seen with our assay independent of the order that the substrate, ligand, and enzyme were combined in the well plate. The optimized protocol that was used included the preparation of porcine pancreas α -amylase in 10 mM phosphate buffer at 0.25 mg/ml, potato starch was preparation at 0.5 mg/ml, inhibitors preparation in 20% methanol, and the dissolution of I_2 at 5 mM. The assay was carried out by adding prepared standards and stocks for starch (100 mL), ligand (40 mL), and then α -amylase (100 mL) followed by incubation at 37°C for 15 min followed by 1 M HCl (20 mL) and iodine solution (40 mL). This methodology would be carried out for all of the tested small molecules in triplicate.

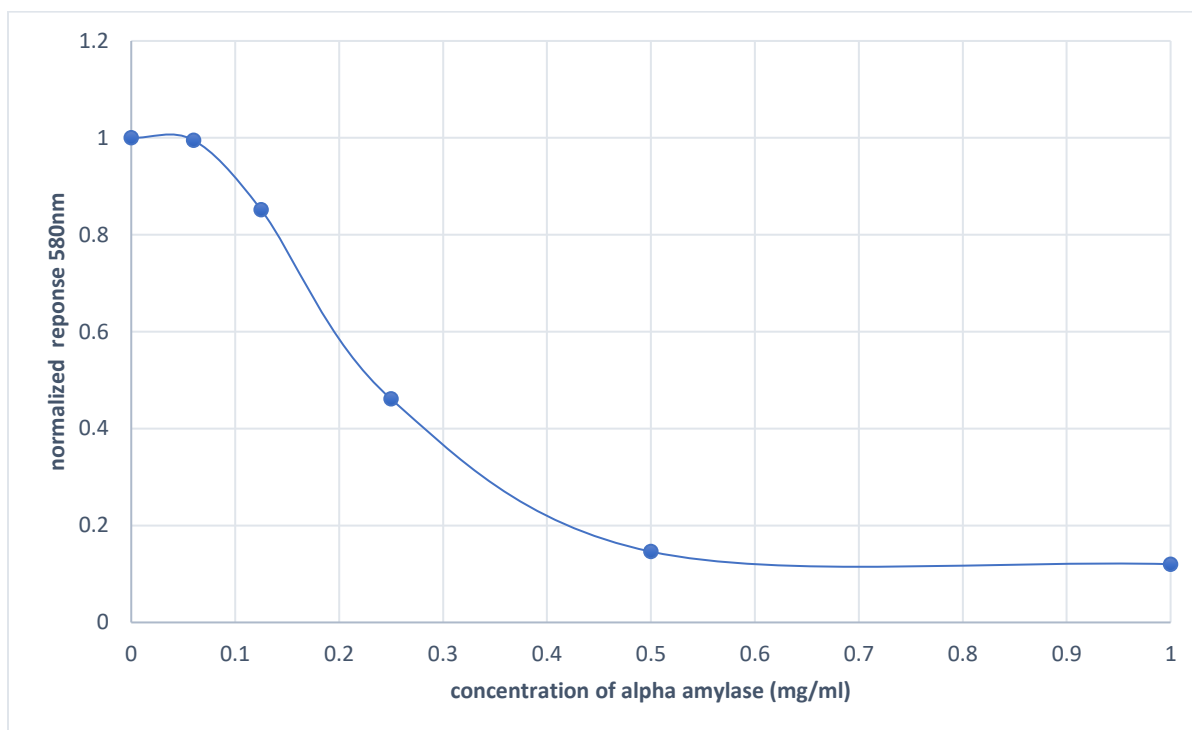


Figure 24. *Normalized Absorption Response to Increasing α -Amylase Concentration in Method Development of Assay.*

This was further validated using the known inhibitor, Acarbose (Figure 25). Acarbose is a pseudotetrasaccharide that acts as a carbohydrate with a point of flexibility between the first and second glucose. The nitrogen in this location allows for greater binding affinity (AG, 1994). The pseudocarbohydrate nature of the inhibitor allows for almost natural binding of the substrate in the pocket, however, the similar subunits also make the compound subject to structural modification (Gilles et al., 1996). Tested in a biological environment it has been shown that Acarbose undergoes change by transglycosylation resulting in a longer chain which can be an even more efficient inhibitor (Brzozowski & Davies, 1997). The greater assimilation to the long chain substrates enhances the ability of the ligand to inhibit the enzyme.

Acarbose Inhibition of alpha-Amylase

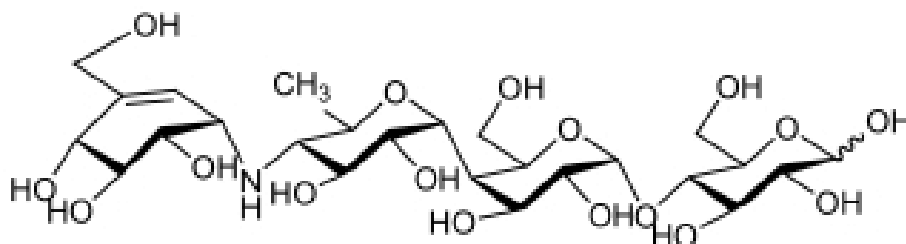
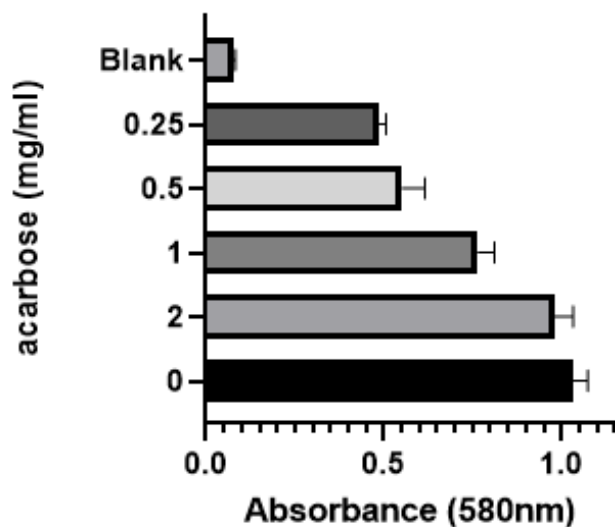


Figure 25. *Acarbose, Positive Control Compound, Enzyme Assay Results, [blank] Contains No Acarbose Resulting in No Inhibition of the Enzyme and [0] has No Enzyme with Maximum Absorption.*

There are various spectroscopic methods of inhibition estimations for α -amylase available. Other assays include a reducing sugar method, which indicates the amount of sugars available for reduction as a result of hydrolysis, of these the most common DNSA (3,5-dinitrosalicylic acid) method requires many steps and high heat; an enzymatic method utilizing the interaction of hydrolysis product with glucose oxidase,

similar to a blood glucose level determination; chromogenic methods which rely upon the hydrolysis of a chromogen from a substrate that achieves a fluorescent or optical signal; and turbidimetric methods which measures remaining turbidity caused by the starch concentration (Visvanathan et al., 2020). The benefit of our robust method bridges the negative and positive aspects of the above methods. The cost of analysis is low, the number of steps in the assay is lower than others, minimal heating is required, and movement of the assay to a 96-well plate from start to finish, reaction and analysis, reduces the chances for experimental error. The assay was prepared and run on multiple days, by more than one person, and in replicate showing consistent results, thus providing a robust protocol.

3.3.2 HCAs and α -Amylase Inhibition

The investigation of polyphenols, including the HCAs, is generally completed in complex mixtures as the result of food or natural product extractions. The complete comparison of the HCA with a single assay method in neat standards gives further understanding to the interactions that exist between polyphenols and α -amylase.

Different from radical scavenging efficiency, the pattern of inhibitory action was not dependent on the substituents on the phenol. Utilizing the starch iodide assay the inhibitory ability of HCAs on α -amylase was ranked as **2** (IC_{50} 3.17 mg/ml) > **1** (IC_{50} 3.48 mg/ml) > **3** (IC_{50} 4.337 mg/ml) > **4** (IC_{50} 5.547 mg/ml). The most inactive radical scavenger was the most effective inhibitor of α -amylase. Steric hinderance likely has a different effect for this scenario, additional bulk around the *p*-phenol hinders the most effective fit of the inhibitor into the binding pocket or active site of the enzyme. Counter to the pattern of additional bulk **1** has similar inhibitory potential to that of **2**. These

patterns inform the possible driving forces behind the protein-ligand interactions and eventual inhibition of α -amylase. These may include non-covalent interactions such as van der Waals contacts, ions pairs, hydrogen bonds, dipole and stacking interactions (Du et al., 2016). Despite the bulk of an additional phenol the benefit of another effective hydrogen bonding location may overcome the steric hinderance issue.

3.3.2.1 HCA Derivatives. Carboxamide derivatives originally synthesized for the evaluation of radical scavenging potential were investigated for the ability to inhibit α -amylase. Methyl esters in the HCA family had been investigated primarily for inhibition of the complimentary sugar processing enzyme, α -glucosidase (Chochkova et al., 2017). Derivatives of compound 2 were the best inhibitors, regardless of the functional group added at the derivative site.

Table 3. *α -Amylase Inhibition IC₅₀ Values of HCAs and Derivatives.*

ID	R	R ₁	R ₂	α -Amylase Inhibition IC ₅₀ (mg/ml)
17a	OH	H	-Gly	> 6
17d	OH	H	-Phe	> 6
17e	OH	H	-Ser-tBu	3.64
18a	H	H	-Gly	3.60
18b	H	H	-Ala	5.31
18c	H	H	-Phe	> 6
18d	H	H	-Ser-tBu	> 6
18f	H	H	- β Ala	> 6
18g	H	H	-NHCH ₂ CH ₂ NHCOU	3.06
19a	OCH ₃	H	-Gly	5.84
19c	OCH ₃	H	-Phe	> 6
19f	OCH ₃	H	- β Ala	> 6
Caffeic acid 1	H	OH	COOH	3.48
<i>p</i> -Coumaric acid 2	H	H	COOH	3.17
Ferulic acid 3	H	OCH ₃	COOH	4.34
Sinapic acid 4	OCH ₃	OCH ₃	COOH	5.58
Acarbose	-	-	-	0.68

The inclusion of phenylalanine derivatives allows for the evaluation of additional aromatic regions, beyond the scaffold HCA structure. The addition of phenylalanine did not enhance the inhibitory potential of any of the HCAs. One derivative allowed for effective enhancement of the inhibitory ability of the HCA, this was the bis-aryl diamine. Compound **18g** (IC₅₀ 3.057 mg/ml), which presents two directions of a primary binding mode for **2**, increased the inhibitory ability, where the addition of β -alanine to the *p*-coumaric acid scaffold (**18f**) showed a decrease in the inhibitory action. The derivatives of greatest capacity compared to the primary scaffold included **18a** (IC₅₀ 3.604 mg/ml) and **18b** (IC₅₀ 5.313 mg/ml), which had the ability to minimally modify measured inhibition in comparison to **2**. This factor encouraged further investigation of the role of the aromatic region of the HCAs through point-change analysis of the most effect inhibitor.

3.3.2.2 p-Coumaric Acid Inhibition Analysis. Compound **2** was the most effective HCA inhibitor tested, further analysis of the essential binding functionalities of the structure was completed by synthetically modifying single points of the structure (Figure 26).

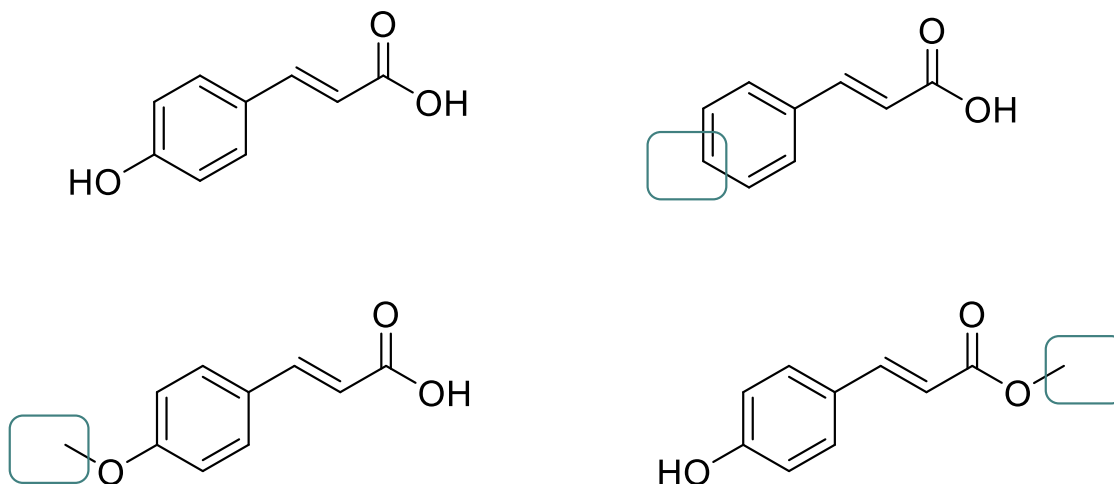
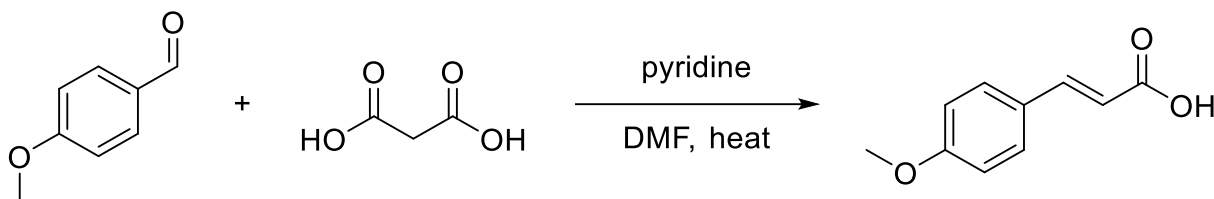


Figure 26. *p*-Coumaric (2) Derivatives Used Synthesized for Point Analysis of the HCA Structure.

The cinnamic acid derivative *trans*-cinnamic acid is naturally occurring (Figure 26, top right). The structure has the same backbone as the tested HCAs without the phenol substituent. Possible reliance upon the hydroxy substituent on the aromatic portion of **2** was examined through assay testing. *trans*-Cinnamic acid (IC_{50} 3.259 mg/ml), without the phenolic substituent, showed minimal loss in inhibitory ability. Apparently, the aromatic core was essential for binding but not the hydroxyl group. The methyl ester derivative was synthesized by the Fischer esterification technique described above and did not have any adverse effect (IC_{50} 3.309 mg/ml), whereas the methylated phenol obtained through a Knoevenagel condensation reaction (Scheme 11) negatively affected the inhibitory ability.



Scheme 11. *Knoevenagel Condensation Reaction Scheme Producing p-Methoxy Coumaric Acid Derivative for Analysis of Effect of Phenol Modification of α -Amylase Inhibitory Ability.*

The reduction in inhibition as a result of protection of the phenol trends with the primary HCA ranking that showed bulk around the phenol may decrease inhibition and the minimal variation of inhibition between the methyl ester and **2** informs the importance of the phenol region in the active site as opposed to the COOH region of the tested compounds. Although inhibition may not rely on the presence of the para-phenol, the available binding location may be supportive of overall interaction. Further investigation of the mode of binding and the essential characteristics of the possible inhibitors can be accomplished through various methods including STD-NMR to view the binding epitope, fluorescence spectroscopy to consider the role of π - π stacking in the protein-ligand interaction and molecular docking to further visualize and help to inform the results of the assay, STD-NMR, and fluorescence results.

3.4 STD-NMR Analysis of α -Amylase and Selected Compounds

Nuclear Magnetic Resonance (NMR) spectroscopy affords a diverse portfolio of methods to evaluate chemical structure, conformation and interaction with solvents, other compounds, and macromolecules. The analysis of specific interactions between macromolecules and ligands can be achieved through ¹H line broadening, relaxation

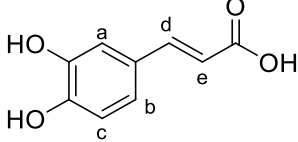
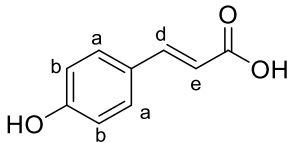
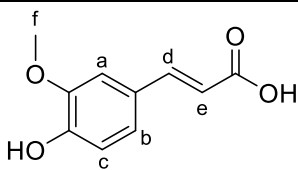
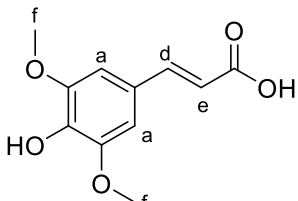
time change, chemical shift perturbations, paramagnetic ligand tagging, transferred NOE, inter-ligand NOE, saturation transfer difference (STD), water-LOGSY, and DOSY experiments, among others (Maity, Gundampati, & Suresh Kumar, 2019). STD-NMR is a technique useful in observing which ligands in a mixture interact with available protein. A single ligand with well-separated discernable ^1H signals permits identification of specific binding epitopes, i.e. which part of the ligand interacts with the host molecule. If successful, STD-NMR is observable through ligand-based signals enhanced by the nuclear Overhauser effect (NOE). NOE refers to the change of signal intensity due to polarization transfer from a perturbed resonance, that has been selectively irradiated, to another resonance that is physically nearby in space (Aue, Bartholdi, & Ernst, 1976). NOE is utilized in STD-NMR by perturbing the signal of the macromolecule thereby enhancing the signal of ligands selectively interacting with the macromolecule. The basis of the experiment relies upon subtracted spectra from two different scenarios. One spectrum results from the protein being selectively saturated (on-resonance) and the other recorded without selective saturation of the protein (off-resonance). With this, the difference spectrum displays only signals that result from magnetization transfer from the protein to the ligand (Viegas, Manso, Nobrega, & Cabrita, 2011). Reliance upon weak-binding ligands could lead to false negatives when investigating a mixture of compounds for ligand-protein association. Weak-ligand binding is required for the creation of the difference spectrum because it records signal not from the ligands interacting, but from the ligands that have interacted and then dissociated. If dissociation does not occur due to irreversible binding, saturation of the proton signals is not observed, despite strong and selective interaction. Further, establishing a binding

epitope from the relative saturation of protons more strongly associated to the protein spatially becomes possible. Binding epitope, in this context, refers to a mapped assessment of binding behavior of specific protons of available ligands to the saturated protein. In many cases, a general low-resolution geometry of the ligand inside the binding pocket can be inferred. Protons with the largest difference signals experienced greater magnetization transfer and were closer to the irradiated macromolecule. Protons can then be scored in a relative percent scale to qualitatively establish the binding mode of the ligand with the macromolecule. STD-NMR has been shown to be an effective indicator of α -amylase and polyphenolic interactions, sometimes including the use of X-ray diffraction (XRD) to corroborate the results (Sun, Wang, & Miao, 2020).

As proof of concept, a well-known interaction was first tested to confirm that STD-NMR analysis was successfully being carried out with confidence. Bovine serum albumin (BSA) was used in interaction with tryptophan utilizing standard parameters and the JEOL pulse sequence “sat_transfer_difference”. Results were consistent with that of previously published work, exhibiting strong interaction between BSA and the ligand at the aromatic region with weaker interaction at the amine and carboxylic acid portion of tryptophan (Appendices: Selected STD-NMR Spectra).

The HCAs STD-NMR results with α -amylase mirrored the results of the assay, **2 > 1 > 3 > 4**. The interactions for the primary HCAs can be seen in Table 4. Here the proton signals are scored based on the results in the difference spectrum divided by the integration associated with the pure compound spectrum and multiplied by 100 for a percentage comparison.

Table 4.*STD-NMR Results of the HCAs.*

 <p>Caffeic acid (1)</p>				
Proton Assignment	Chemical Shift	¹ H Integration	STD Integration	%
A	6.99	1	0.57	57
B	6.7	1	0.77	77
C	6.9	1	0.21	21
D	7.38	1	1	100
E	6.1	1	0.20	20
 <p>p-Coumaric acid (2)</p>				
Proton Assignment	Chemical Shift	¹ H Integration	STD Integration	%
A	6.726	2	2	100
B	7.460	2	1.04	50
D	7.375	1	1	100
E	6.181	1	0.25	25
 <p>Ferulic acid (3)</p>				
Proton Assignment	Chemical Shift	¹ H Integration	STD Integration	%
A	7.1	1	0.19	19
B	6.7	1	0.74	74
C	6.95	1	0.18	18
D	7.4	1	1	100
E	6.2	1	0.26	26
F	3.65	3	0.75	25
 <p>Sinapic acid (4)</p>				
Proton Assignment	Chemical Shift	¹ H Integration	STD Integration	%
A	6.8	2	0.93	47
D	7.4	1	1	100
E	6.2	1	0.39	39
F	3.65	6	2.28	38

The difference spectra for compounds **1** and **2** can be seen in Figure 27. The qualitative binding epitope shown by the results of the STD-NMR reveal two primary points of interaction. The interaction of the aromatic region with the protein is strong (proton *a* being the closest) and is unaffected by additional substituents in compound **2**. Compound **1** with the catechol moiety has non symmetric interactions of the protons adjacent to the OH substituents and a change of the primary interactions on the aromatic ring to proton *b*, which like **2** is non-adjacent to the phenol. Compounds **3** and **4** show a similar pattern, but with less effective interaction of the aromatic protons, associated with the additional methoxy substituents. Interestingly, the methoxy groups did not show strong interaction.

Despite the reduction of interaction with the aromatic protons, the pattern of interactions between other common protons were similar, implying a similar mode of binding. The most novel aspect of the STD-NMR results presented here is the interaction at proton *d*. A consistent primary point of interaction amongst the HCAs is the vinylic α -hydrogen to the aromatic ring, from there, interaction decreases to the aromatic hydrogens and then the β -hydrogen. The alkene linkage between the aromatic region and the carboxylic acid region proves important in the overall interaction. If the unsaturation itself or the specific length of the carbon chain was the critical feature for binding was not clear. Circumstantial evidence for the possible significance of the planarity and rigidity of the alkene was gathered from the newly synthesized phenylalanine derivatives. Although not an exact comparison due to the amide linkage, the phenylalanine derivatives have an aromatic region separated by an alkane chain from a terminal carboxylic acid. The phenylalanine derivative of HCAs did

not have significant inhibitory ability or match that of the *trans*-cinnamic acid. Therefore, the presence of an alkene linkage between the aromatic portion of the compound and the carboxylic acid may be a key factor to the binding of the HCAs and derivatives. Upon further testing of amino acid derivatives of HCAs, we discovered a change in binding geometry. A compound such as **18a** with a relatively efficient inhibitory ability shows a completely different binding epitope with decreased STD-signal at vinylic proton *d* across the double bond from the carboxamide (Figure 27). Instead, we observed an increase at the second vinylic proton *e* right next to the carboxamide along with significant enhancement at the methylene protons of the glycine moiety. On the other end of the structure, the aromatic interaction changed from *a* protons to *b* protons. This implied stronger interaction between the α -amylase binding site and the amino acid portion of the compound at the expense of interaction with the phenol portion.

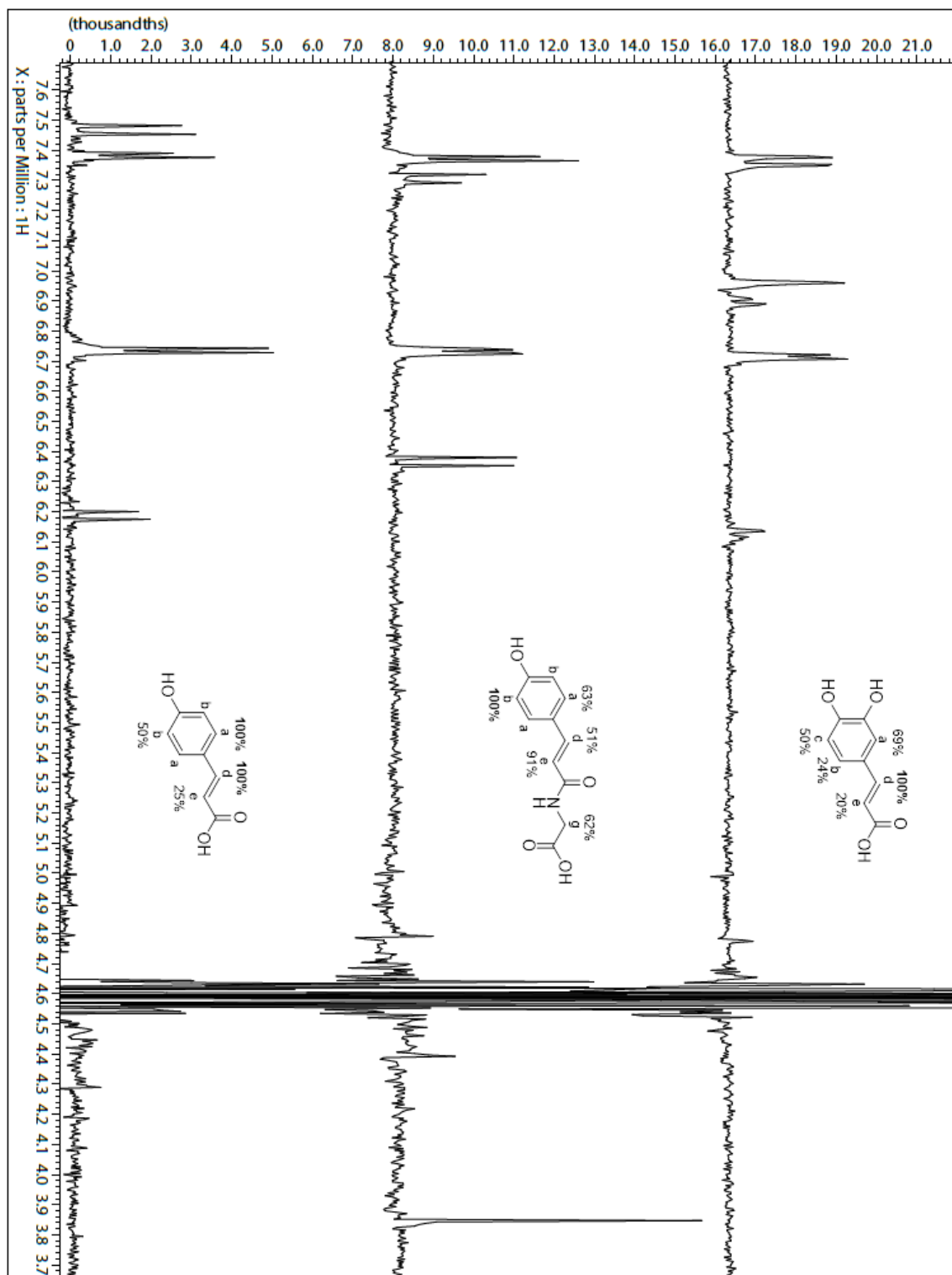


Figure 27. STD-NMR Spectra for (top to bottom) Caffeic Acid (1), **18a**, and p-Coumaric Acid (2).

Modified interaction of the aromatic region was consistent in the testing of small molecules that had lesser inhibitory value such as **18f**. The larger β -alanine derivative showed increased interaction at the amino acid but less interaction with the phenol, comparatively. These results are rooted in the assumption that efficiency of magnetization transfer is equivalent for all protons, which may not be strictly valid and could result in error.

Underlying structural principles that determine the strength of binding to α -amylase may also be factors in the inhibitory interaction of HCAs and hydroxybenzoic acids with α -amylase. The former class of compounds contain all similar functional groups apart from the alkene linkage between the carboxylic acid and the phenol.

3.5 Fluorescence Analysis of α -Amylase and Small Molecule Interaction

Fluorescence spectrophotometry is the detection of emitted radiation absorbed at a wavelength larger than that of the specific excitation radiation. The emission energy is lower than that of the absorbed energy because the electron moves to the lowest vibrational energy state before emission (Lakowicz, 1999). Compounds with the ability to fluoresce generally exhibit aromatic groups with low-energy $\pi \rightarrow \pi^*$ transitions, impacted by alkane, oxygen, nitro and halogen substituents, or rigidity. Fluorescence can be affected by pH for aromatic groups with substituents that are either acidic or basic (Skoog, 2007). The majority of fluorophores are classified in the small molecule category, however there are protein fluorophores that can be used in the same way. Targeting fluorescence information for the analysis of ligand-protein interaction can occur in multiple scenarios. Fluorophore quenching and Foerster resonance energy transfer (FRET) are the most common. A specific quenching technique often used for

binding assays with proteins relies upon the intrinsic fluorescence of aromatic amino acid residues, often tryptophan. As small molecules or other proteins interact with tryptophan in the protein structure, the changed environment can diminish or completely quench the emission signal of the tryptophan (Möller & Denicola, 2002). Additional information about the binding mode becomes available when the location of the tryptophan residue can inform enzyme inhibition or the ability of the protein to transport a small molecule. The fluorescence of tryptophan is quenched through external π - π interactions when a ligand is present. If the ligand is an inhibitor of the protein more information can be gathered through inhibition assays.

The impact of the π - π interactions on the overall interaction of the HCA derivatives and α -amylase was investigated through the tracking of intrinsic aromatic fluorescence quenching. A proof-of-concept experiment was developed based on the well-known interaction between bovine serum albumin (BSA) and HCAs (Jin et al., 2012). Here, the original HCAs were tested to confirm their concentration-dependent ability to quench the aromatic fluorescence signal from the BSA protein, **1 > 2 > 3 > 4**.

Table 5.

IC₅₀ Values of HCAs as α -Amylase Inhibitors and Fluorescence Emission at 10 μ g/mL

Addition of HCA for Comparison at $I_{\text{emission}} = 360$ nm, $\Delta E = h\nu$.

Compound	IC ₅₀ (μ M)	Fluorescence Intensity [emission intensity]
Caffeic acid (1)	3.48	414.15
<i>p</i> -Coumaric acid (2)	3.17	428.77
Ferulic acid (3)	4.34	551.92
Sinapic acid (4)	5.58	579.43

The aromatic residues present in the active site of α -amylase include Trp58, Trp59 and Tyr62. Emission spectra were acquired between 300 and 450 nm with a $I_{\text{emission}} = 360$ nm for α -amylase with HCAs and Acarbose at $I_{\text{ex}} = 280$ nm. The intensity of the emission spectra was decreased upon the addition of increasing concentrations of the HCAs in the order **1 \approx 2 > 3 > 4**, consistent with the measurements in the inhibition assay. The HCAs were tested at 6 different concentrations with α -amylase representing the unmodified blank measurement (Figure 28). The 10 μ g/mL addition of the different ligands gives direct comparison to quenching capacity to other ligands (Table 5). The decreased fluorescence signal is associated with the increased quenching by interaction with the ligand.

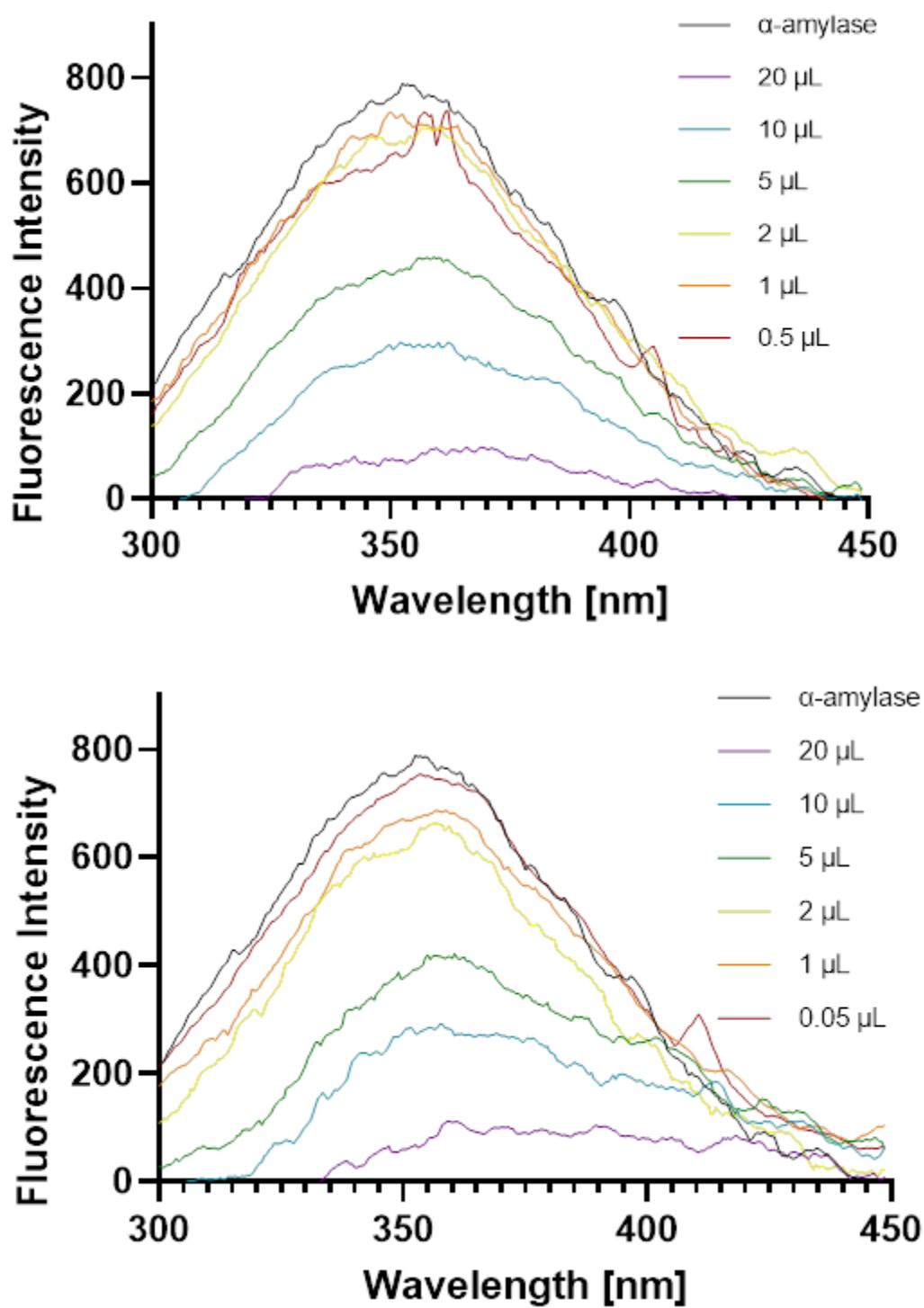


Figure 28. Fluorescence Quenching of α -Amylase by **2** (top), **1** (bottom), $\Delta E = h\nu$.

The interaction between HCAs and α -amylase showed modification of intrinsic tryptophan fluorescence. Modification of tryptophan fluorescence may point to π - π stacking as a driving factor in the inhibition of starch hydrolysis through binding, in the binding pocket, adjacent to the active site. Acarbose showed a lack of quenching despite strong inhibition with and without addition of substrate to the sample, which could be simply hypothesized based on the lack of aromatic rings in the known inhibitor (Figure 29).

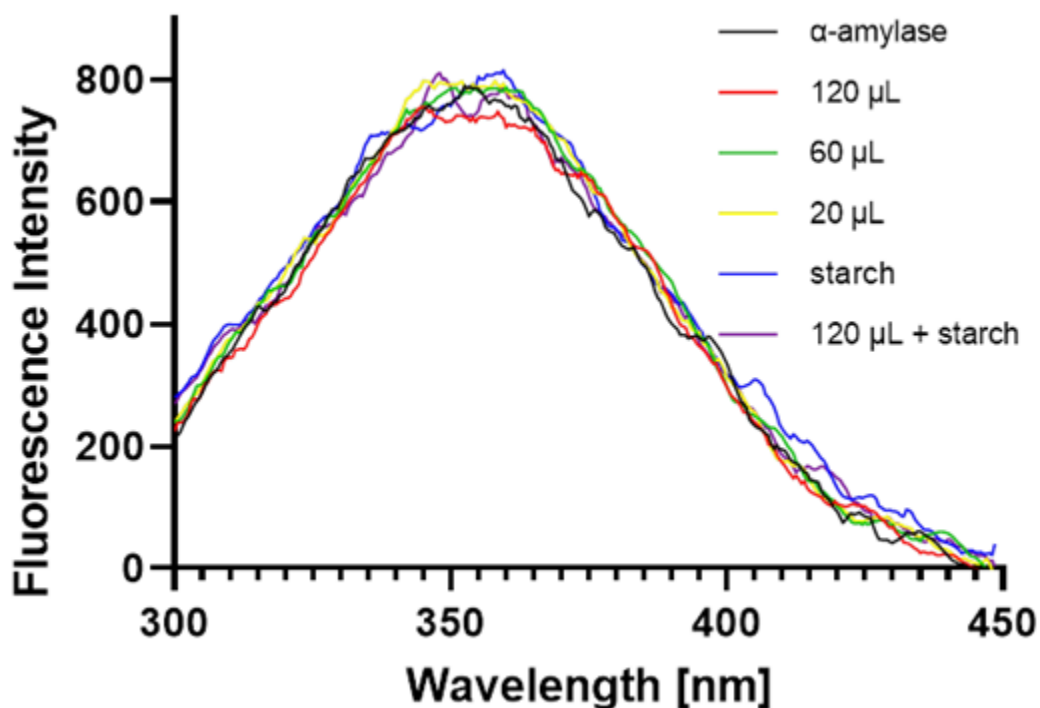


Figure 29. *Lack of Fluorescence Quenching in α -Amylase with Acarbose Inhibition.*

The use of Acarbose in the fluorescence quenching assay also operates as a control. The reduced fluorescence is related to specific interaction of the small molecules with the protein, as opposed to the result of a general mixture.

The results from enzyme inhibition assays, binding epitope investigation, and fluorescence quenching results inform the possible overall interaction. Furthermore, the use of computational molecular docking can combine these pieces of information in a visual representation of binding.

3.6 Molecular Docking of Ligands with α -Amylase

Computational methods for the interactions of ligands and macromolecules (drug discovery) continue to become more popular and developed. The use of molecular docking in drug discovery appears in virtual screening, high throughput screening, pharmacophore modeling, and quantitative structure activity relationship (Meng, Zhang, Mezei, & Cui, 2011). Molecular docking for the analysis of interaction between ligands and macromolecules allows for investigation of forces on a level difficult to attain in a wet lab setting. Molecular docking results at the atomic level can further inform the experiments carried out in the laboratory. There is assumed error in the results of molecular docking experiments. The simulations are predictive and dependent on the sampling algorithm used. Results described are generally used to understand the results of other assays, in this case enzyme inhibition, STD-NMR, and fluorescence. Sampling algorithms include matching algorithms, incremental construction, multiple copy simultaneous search, genetic algorithms, molecular dynamics, and Monte Carlo. Molecular docking also provides scoring functions to classify better or worse ligands, which is critical for successful drug discovery. The basis of the scoring is based on the

estimated binding affinity, and the three classes for scoring are force-field-based, empirical and knowledge-based (Meng et al., 2011).

Autodock Vina, is an open-source program that builds upon the previously developed AutoDock 4 (Trott & Olson, 2010). The programming suite is tailored to those without expert computational knowledge (Forli et al., 2016). The sampling function employed is Lamarckian Genetic Algorithm and scoring function, United-Atom. The limitation of this technique revolves around the approximations that are taken for quick analysis and ease of use, one often highlighted is the rigidity of the macromolecule. Utilizing receptor files that have been associated with ligands there is a consideration that it is in the form or function strongly associated with natural binding, but there are assumptions through use of this structure. In this dissertation, molecular docking was used to understand the results of other screening methods described above, not standing alone. There is only discussion of agreement or disagreement of these outcomes.

The binding pocket of α -amylase is broad and contains acidic residues at the active site required for substrate hydrolysis Asp197, Glu233, Asp300 and Asp96 (Gilles et al., 1996). The interruption of active site binding interaction through blocking by non-covalent ligand binding was found essential to deter the hydrolysis of the starch substrate. It has been shown that polyphenols may interact with the enzyme at the binding site containing the above residues (Lo Piparo et al., 2008; Martinez-Gonzalez, Díaz-Sánchez Á, de la Rosa, Bustos-Jaimes, & Alvarez-Parrilla, 2019). Molecular docking was used to observe plausible binding conformations for the small molecule inhibitors.

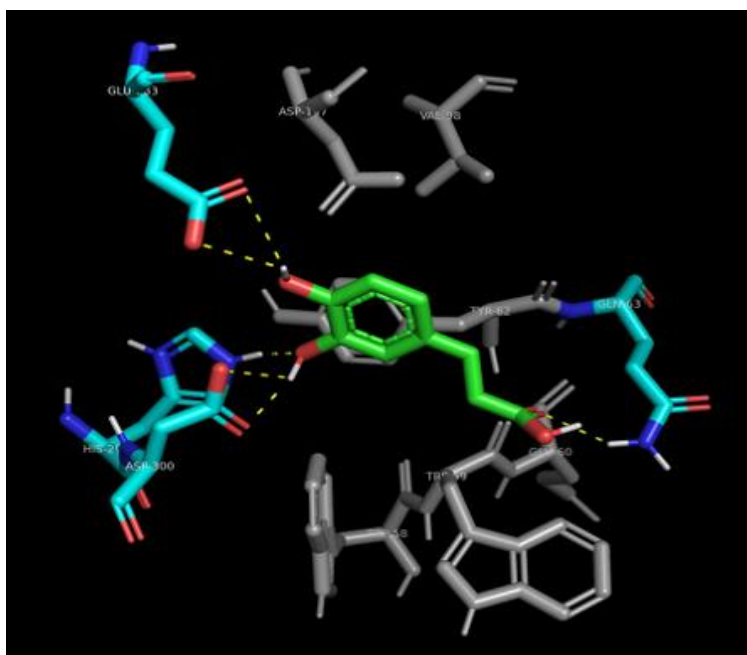


Figure 30. *Compound 2 (top) and Compound 1 (bottom) Positioned in the Binding Pocket of α -Amylase with the Residues Showing Hydrogen Bonding Highlighted in Blue and Others within Proximity in Gray.*

Compound **2** (-6.5 kcal/mol) showed the greatest ability for π - π stacking interaction with Tyr62 residue situated in the substrate binding cleft, other available aromatic residues in the vicinity that may contribute to the stability in binding include Trp58 and Trp59. This interaction was consistent with the ligand-protein fluorescence assay described above, the greater interaction leading to less fluorescence emission from the intrinsic aromatic residues. In the molecular docking results, there were also strong hydrogen bonds formed (Figure 30). For **2**, the phenolic region bonded to His299, which sat in the center of the catalytic residues Asp300, Asp97, Glu233, and Asp197, while the carboxylic acid region of the scaffold interacted with Gln63.

The dihydroxy moiety of **1** allowed for additional hydrogen bonds to form between the enzyme and inhibitor. The phenolic region bonded directly to Asp300, His299 and Glu233 while the carboxylic acid maintained its binding to Gln63, like **2** (Figure 30). The general binding configuration between the two most efficient inhibitors, as shown in the starch-iodide assay, remains the same and the inclusion of an additional hydroxy substituent does not largely modify the interaction. More intricately, the formation of additional hydrogen bonds with the catechol region could be cause for the deterioration of the π - π stacking interactions in the cleft. Despite a larger dipole moment for catechol (**1**) as opposed to (**2**), the difference in interaction was minor as detected by the most efficient computational binding formation between compound **1** and compound **2**. This was consistent with only minor differences shown in the enzyme inhibition assay, in fluorescence quenching, and also in the more informative STD-NMR results. The position of the vinylic α -hydrogen to the aromatic ring remains strongly associated with the surface of the macromolecule.

The close interaction of this particular position does not have a direct impact on binding but may rather be a result of efficient positioning of the aromatic portion of the small molecule. The reduced proton interaction of some HCA derivatives through binding epitope studies confirmed the less effective interaction for these small molecules with the binding site. As stronger interactions occurred with the larger derivative regions, the aromatic region was bonded less strongly, which decreased the inhibitory efficiency of the compounds.

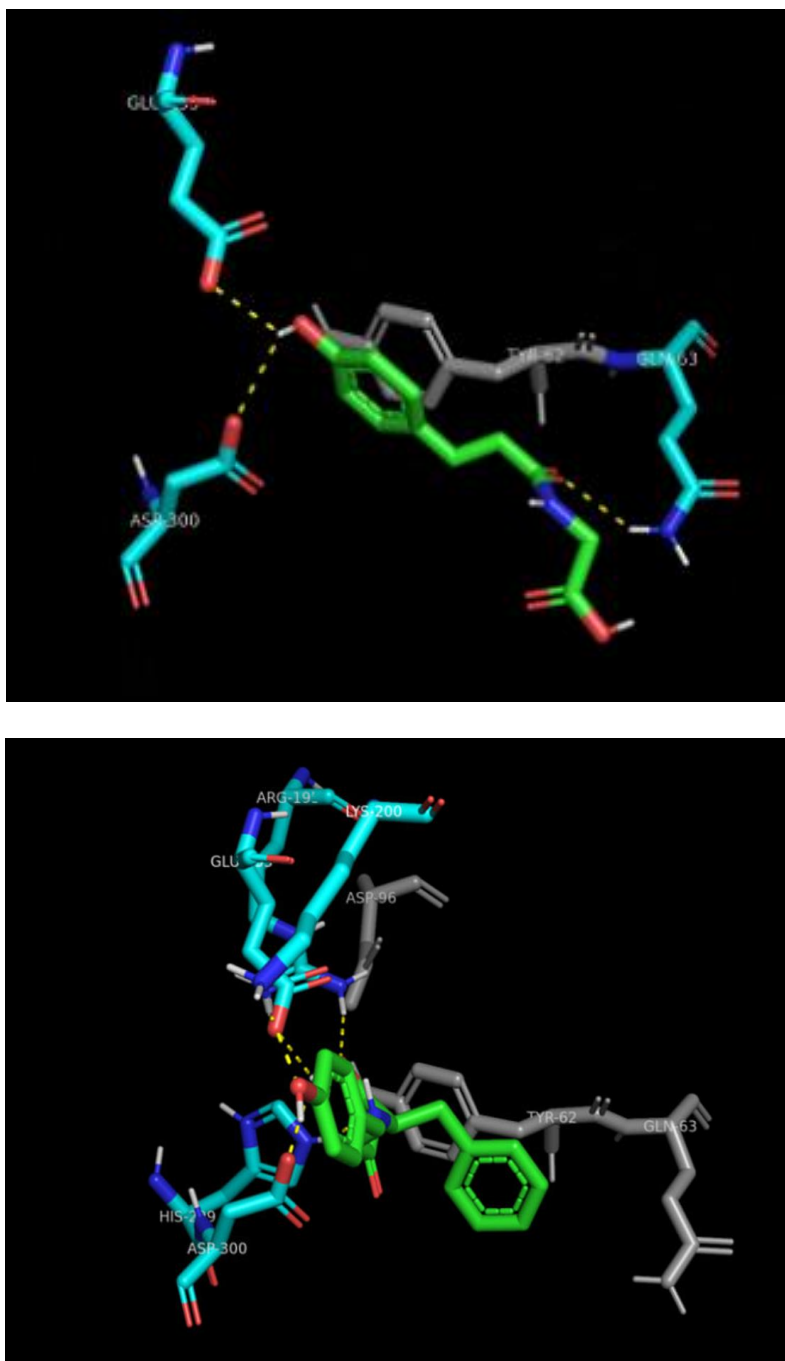


Figure 31. *18a* (top) and *18c* (bottom) Computationally Docked in the Binding Site of α -Amylase with Residues Making Hydrogen Bonds in Blue and Residues in Proximity in Gray Including Active Site Residues.

Amidation of the primary scaffolds modified the binding as seen in the STD-NMR and enzyme assays. The aromatic region's ability for unmodified interaction, exemplified by **18a** (-6.2 kcal/mol), which had slight inhibitory inactivation compared to **2**, created additional hydrogen bonds with Asp300, Glu233 and Gln63 but decreased efficient π - π interaction (Figure 31).

The addition of phenylalanine at the amidated portion (**18c**) modified binding completely. The derivative slipped up the broad binding pocket moving the phenol away from the active site. Hydrogen bonding interactions were still seen with residues Asp300, Glu233 and Asp96, however, the π - π interaction is fully disrupted with the phenylalanine aromatic region being closer to the active site than that of the phenol. These results were also consistent with the notion that the alkene substituent to the aromatic portion of the HCAs was important to inhibition and interaction.

The results of the binding studies agreed with the STD-NMR analysis. It was clear that the α -hydrogen to the aromatic ring is in proximity of the cleft in various binding positions with the greatest interaction existing at the phenolic moiety compared to the carboxylic acid portion, non-dependent of the innate aromatic substituents.

3.7 Native MS

An advantage of high resolution and high range mass spectrometry is the ability to monitor reactions or interaction-based changes to ligands and macromolecules. Native mass spectrometry, in this case, was used to characterize the non-covalent complexes created by the addition and incubation of ligands to macromolecules. Characterization of protein-ligand complexes offers functional information regarding metabolism of small molecules, interfering interactions, and unintended binding (Leney

& Heck, 2017). Use of ESI-MS can reveal protein-ligand interaction with increased resolution and sensitivity not always possible with other methods. Bovine serum albumin (BSA) has been shown to bind to the phenyl ring substituents of hydroxycinnamic acids (HCA) using fluorescence and NMR spectroscopy (Jin et al., 2012). BSA-ligand interactions with bisphenol derivatives tracked by ESI-MS show results consistent with fluorescence quenching data (Luo, Li, Fang, & Wang, 2016). Here, HCA complexes of BSA were characterized under native MS conditions. Additionally, the HCAs were also investigated for non-covalent complexing with carbonic anhydrase. Hydroxycinnamic acids, specifically *p*-coumaric acid (**2**) and ferulic acid (**3**) and known sulfonamides have been successfully detected as inhibitors of carbonic anhydrase (Sarıkaya, Gülçin, & Supuran, 2010; Zoppi, Nocentini, Supuran, Pratesi, & Messori, 2020). These two experiments were used as proof-of-concept for the possible evaluation of glycosidases with small molecule inhibitors and method development.

3.7.1 Bovine Serum Albumin (BSA)

Multiple aspects of method development were required for successful analysis of non-covalent interactions in ESI-MS, first, instrumentation. The analysis of large molecules was done using LC/Q-TOF instrumentation with an AJS-ESI ion source. The benefits of utilizing a time-of-flight mass analyzer include the ability to analyze a wide mass range with a nearly constant resolution over the acquired range, but the limitation is inefficient desolvation of ions; however advancements continue to improve on these issues (Tamara, den Boer, & Heck, 2022). The chromatographic technique used was size exclusion chromatography (SEC). This method cleans up the sample under near

biological conditions. SEC columns allow for efficient desalting while maintaining aqueous conditions and fractionation through size-based separation. With SEC, small molecules passage in the column is slowed by diffusion through pores while large molecules are able to move more quickly through the column, resulting in separation of small and large molecules. The solvent system selected for the native analysis was 100 mM ammonium acetate at pH 7 and was kept at an isocratic gradient with a flow rate of 0.4 ml/min. Optimized source parameters can be found in section 5.3.5

Bovine serum albumin is a protein that has taken on many tasks in physiology, as well as in laboratory practices. Serum albumin is largely available in the blood, having very specific functions important to daily life such transportation of water-insoluble fatty acids, steroids, and metal ions (Peters, 1995). The ability of serum albumin to bind very specifically directs the above functions, however, a key feature of serum albumin is not specificity but rather its ubiquitous nature. This establishes an alternative set of functions including the transportation of exogenous compounds, removal of toxins, and activity as a free radical scavenger offering mitigation to reactive oxygen species. BSA is often used as a laboratory standard and an important addition to enzyme assays for stability. Due to the likelihood that a drug or supplement would encounter serum albumins it is often used for investigation of off target interaction in the body (Curry, 2009). The first report of the BSA primary structure was resolved by J.R. Brown in 1975 and revised in 1990 by Hirayama at 583 amino acids in length made up of 21 tyrosine residues, 2 tryptophan residues and at pH 5-7 it contains 17 intrachain disulfide bridges and 1 sulfhydryl group with an average molecular weight of 66430.3 Da (Brown J, 1975; Hirayama, Akashi, Furuya, & Fukuhara, 1990). The albumin

sequences are characterized by disulfide double loops with triplet repeats. It has three homologous domains (I, II and III) and six subdomains (Ia, Ib, IIa, IIb, IIIa, IIIb) with an estimated α -helix composition of 54% and β -sheet composition of 18%. Homology between the structure of BSA and HSA makes the protein an adequate initial template for interaction investigation.

Initial method development revolved around seeing the native protein envelope of BSA. The protein samples were prepared in 10 mM ammonium phosphate buffer and the standard solution was prepared at 1 mg/ml. Standard dilutions were injected with the previously described. The primary charge states observed were between +18 and +12. These charge states resulted in m/z signals between 3700 and 5500 (Figure 32).

The reliance upon aqueous buffers for analysis of the native structure was obvious upon addition of only 30 % acetonitrile (MeCN) into the isocratic solvent system, resulting in denaturing of the protein (Figure 32). Denaturation of the protein does not affect the amino acid composition of the protein but rather the charge distribution and capacity for proper folding. In native conditions the protein generally carries fewer charges due to the limited physical space available as a product of folded protein structure. The denatured solutions produce highly charged ions as a result of non-covalent bond disruption and protein unfolding. While there may be overlap in charge states in both denatured and native conditions, the gap resulting from the unfolding can be substantial.

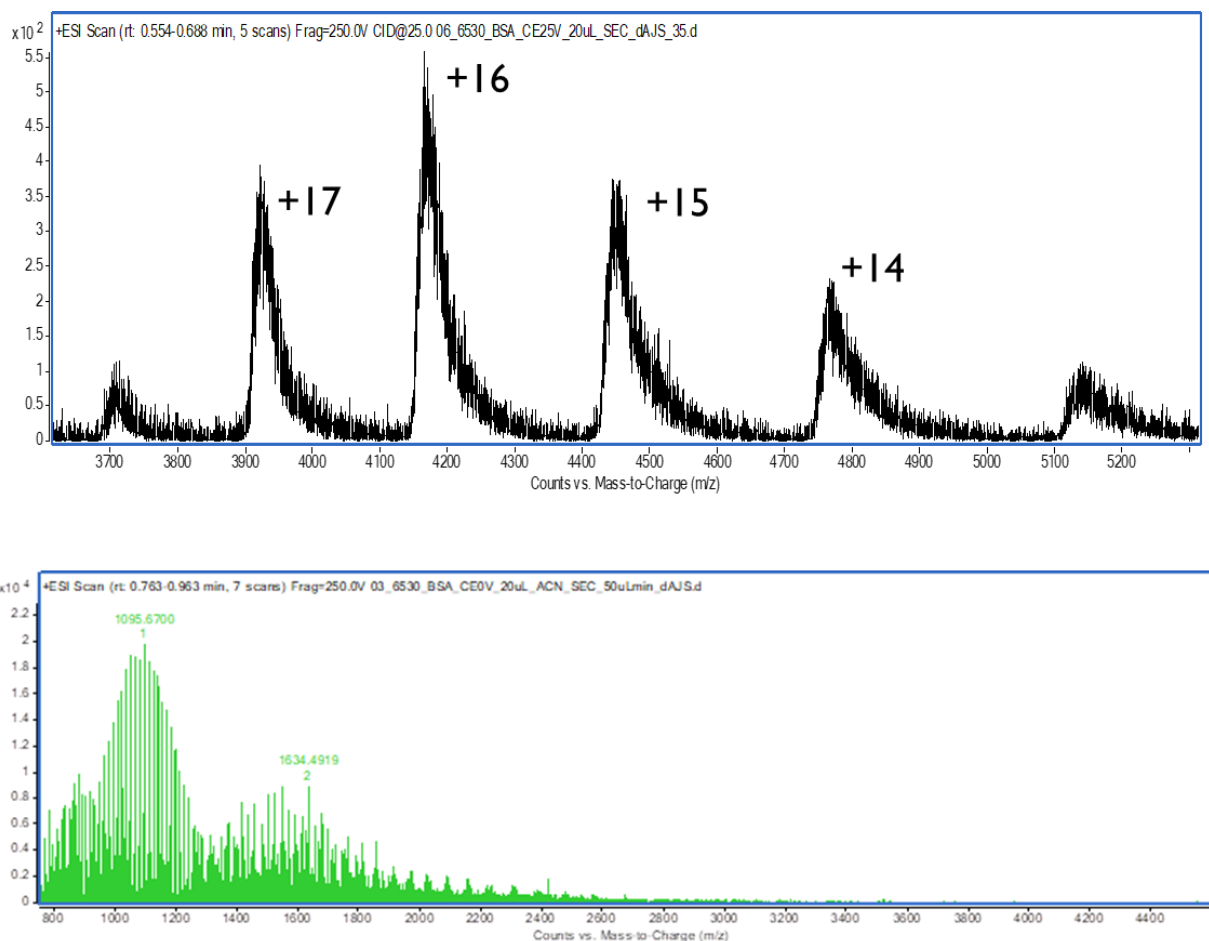


Figure 32. (Top) The Primary Charge States for the Native BSA, (Bottom) The Denatured Protein as a Result of 30% MeCN Addition into the Solvent System.

Deconvolution is the calculation of the neutral molecular weight from the charged protein envelope. The deconvolution software UNIDEC from the Marty Lab was used to determine the molecular weight of BSA at 66,740 Da (Figure 33) (Marty et al., 2015).

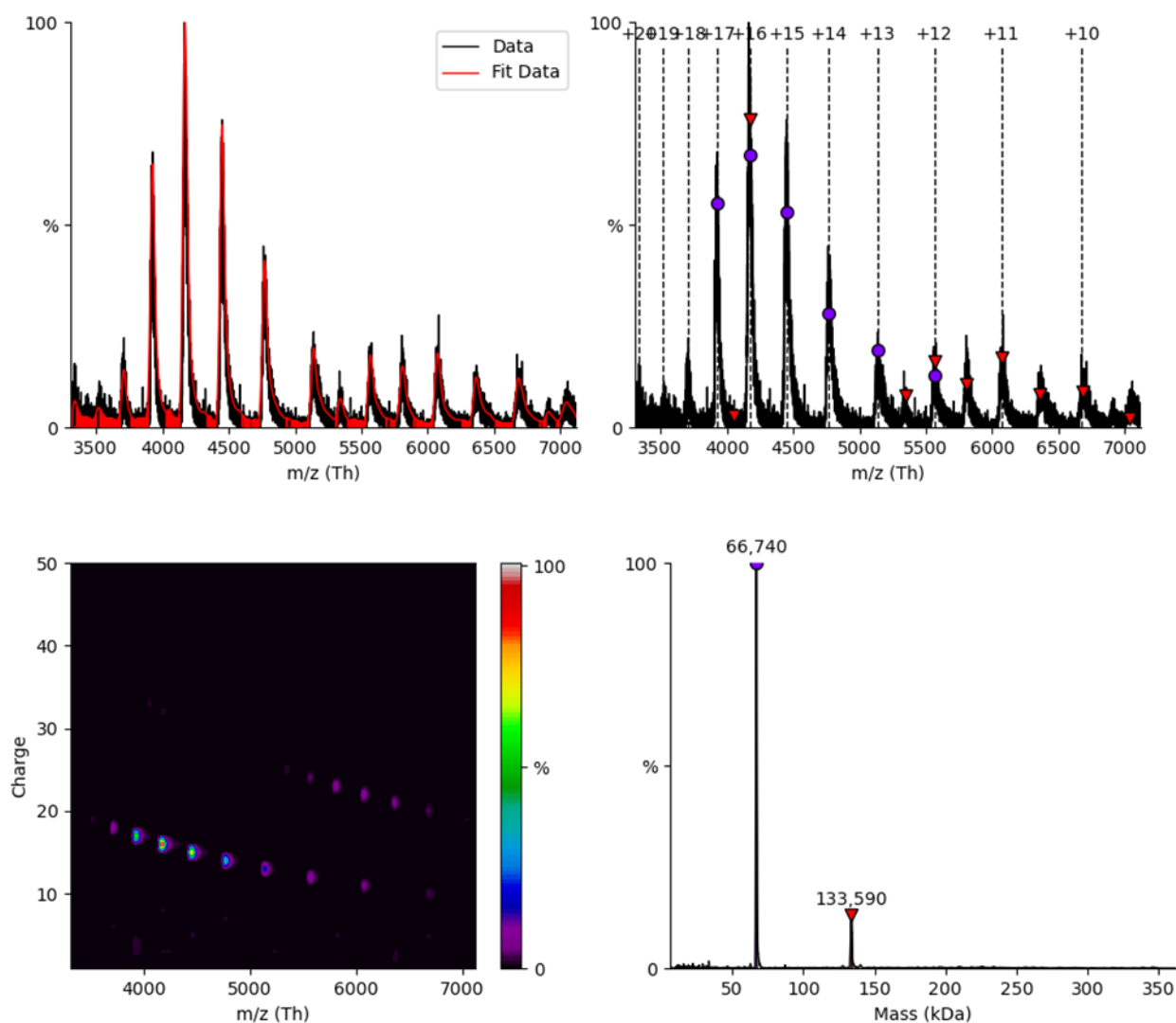


Figure 33. *UNIDEC Deconvolution of BSA.*

Complexes were created through incubation of BSA with ligands. The ligands were originally prepared in MeOH and then diluted with buffer to 5 mg/ml, however, the introduction of organic solvent increased denaturation of the protein. The sample preparation was optimized by diluting the ligands in ammonium bicarbonate buffer and then lightly mixing and incubating at 37 °C for 30 minutes. This optimization allowed preparation of samples with excess ligand while also reducing protein unfolding by

including organic solvent. The resulting complexes associated can be seen in Figure 34 and 35. The LC/Q-TOF used is equipped with reference mass solution, this solution is constantly added during sample introduction in order to act as internal reference mass for mass correction.

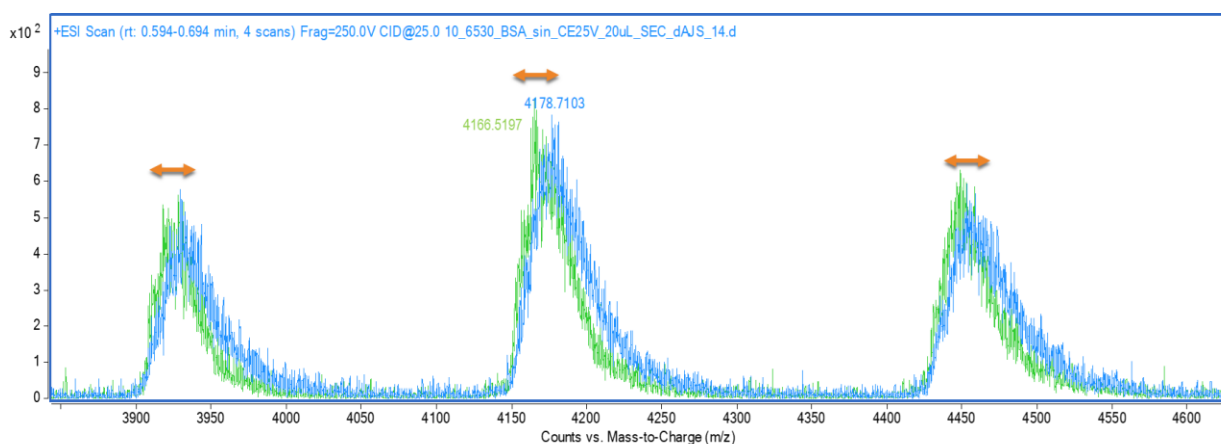


Figure 34. *BSA-Sinapic Acid Complex.*

The combination of BSA with caffeic acid (**1**) and sinapic acid (**4**) resulted in a mass shift of the charge envelope (Figure 35). The nature of the charge envelope of BSA makes it difficult to discern the shift exactly. The overlays of all complex mixtures show also that the size difference created by the non-covalent complexes with small molecules and large macromolecules creates a shift for the more efficient binders of BSA, while no shift is seen for compounds like that of ferulic acid (**3**) and *p*-coumaric acid (**2**) (Figure 35).

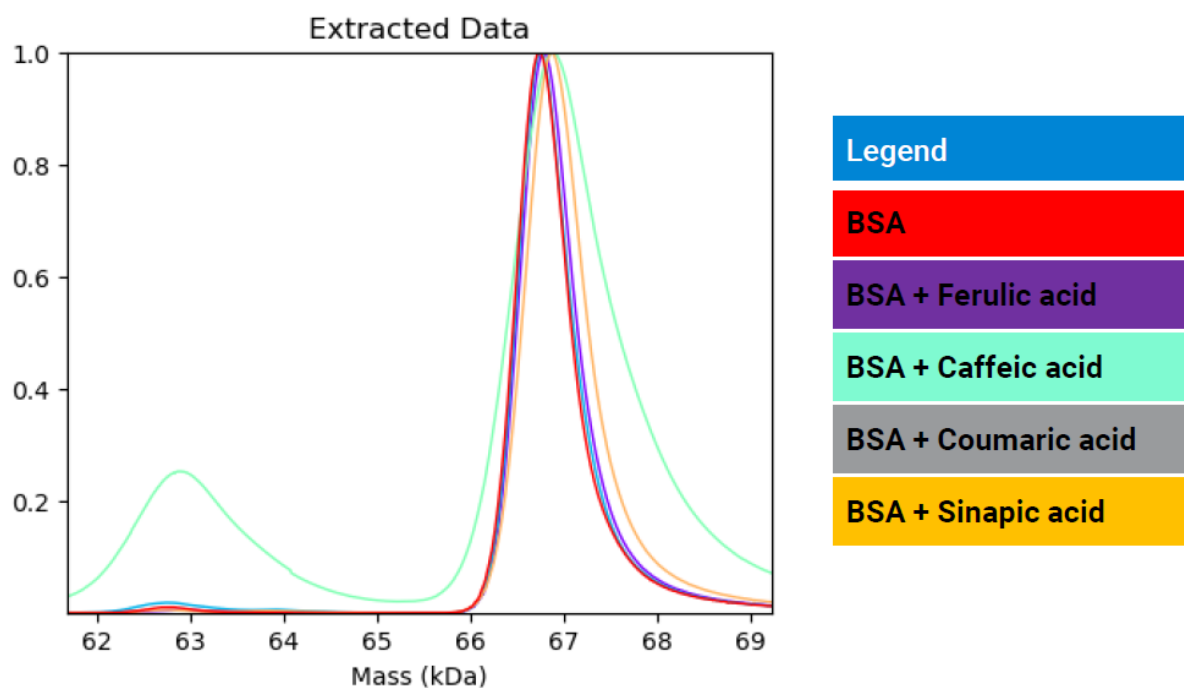


Figure 35. *Deconvoluted Complexes Overlaid with the Four HCA Ligands, Each Complex Deconvolution is Color Coded.*

The technique of native ESI-MS in the analysis of non-covalent ligand-macromolecule complexes presents numerous advantages to other more traditional techniques. This analysis requires no labeling, is sensitive, reproducible and consumes only a small amount of sample in analysis. While method development was found complicated by multiple factors initially, optimization of solvent, sample preparation, and ion source conditions resulted in a robust protocol.

To improve the ability to monitor macromolecules and HCA ligands, specifically, a macromolecule with two alternative characteristics was pursued. Firstly, a larger shift between a smaller protein and the ligand could reveal protein binding more clearly. Second, a more defined protein envelope signal would allow for clearer deconvolution.

3.7.2 Carbonic Anhydrase

Carbonic anhydrase is a 29 kDa molecular weight enzyme responsible for the catalysis of the interconversion of carbon dioxide and water to carbonic acid and bicarbonate. The sample preparation from the BSA assay was repeated for carbonic anhydrase, the difference in data acquisition methods was the use of an SEC guard column. With carbonic anhydrase a union was placed in the position of the column, a flow injection method. The protein envelope of carbonic anhydrase can be seen in Figure 36, with the most intense charges from +10 to +14, with +11 being the most abundant. The signals are thinner, by nature of the protein structure, and the primary charge is smaller by way of the protein size. These characteristics combine to allow for easier detection, and clearer deconvolution, of the possible non-covalent complexes. In the development of the experiment, we reviewed literature evidence that there may be interaction between the HCAs and the enzyme. Coumarin derivatives have been shown to induce an inhibition of carbonic anhydrase through hydrolysis to 2-hydroxycinnamic acid and capsaicin, the active component of chili peppers, has also been identified as having inhibitory capacity (Arabaci, Gulcin, & Alwasel, 2014; Petreni et al., 2021).

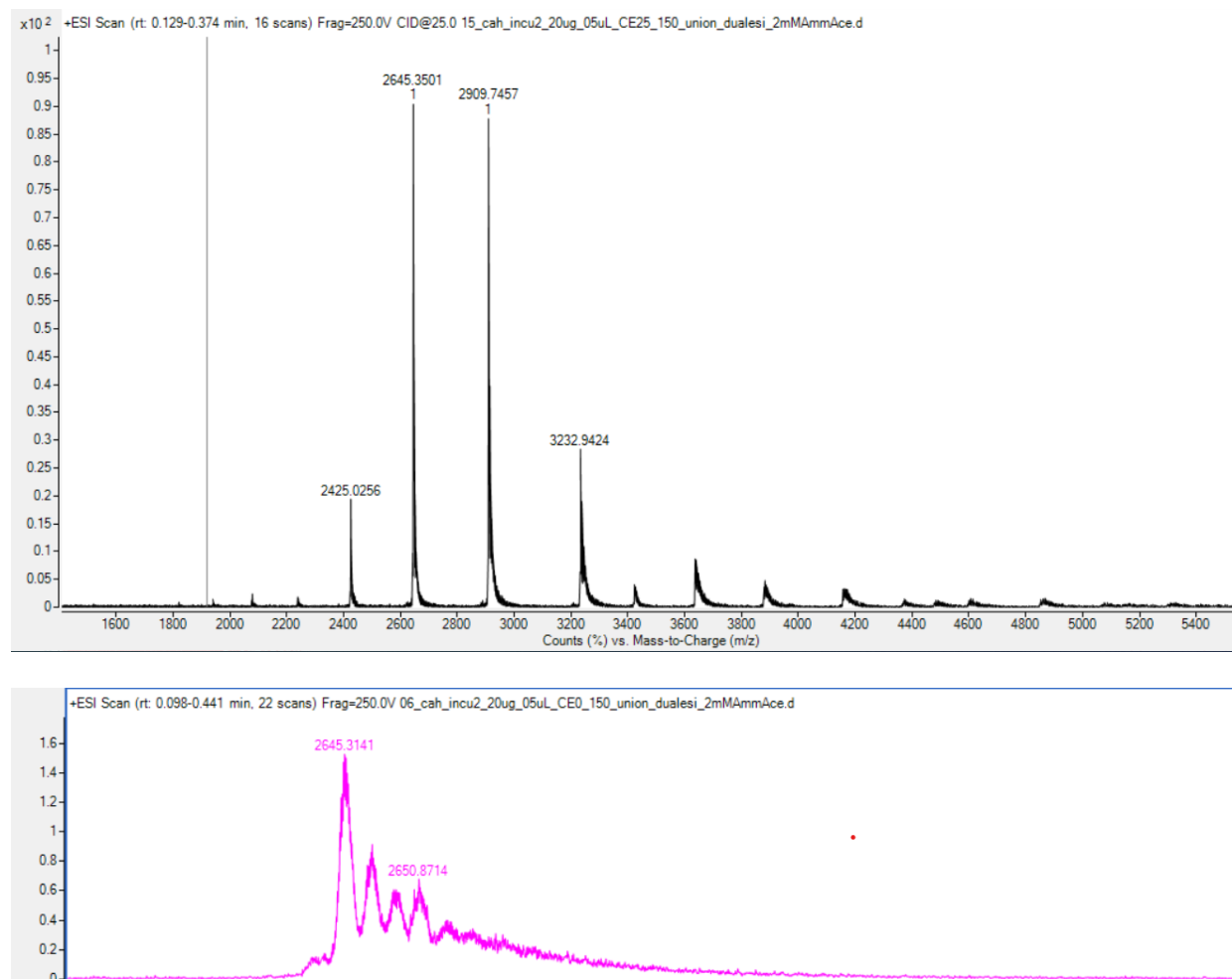


Figure 36. *Carbonic Anhydrase Charge Envelope (zoomed out) and +11 Charge (zoomed in).*

These and other studies have shown the interaction of HCA like structures with carbonic anhydrase. Upon incubation with the prepared ligands in 100:1 mixtures, the samples were immediately loaded and run. For carbonic anhydrase there were multiple complexes created with the non-complexed enzyme remaining (Figure 37).

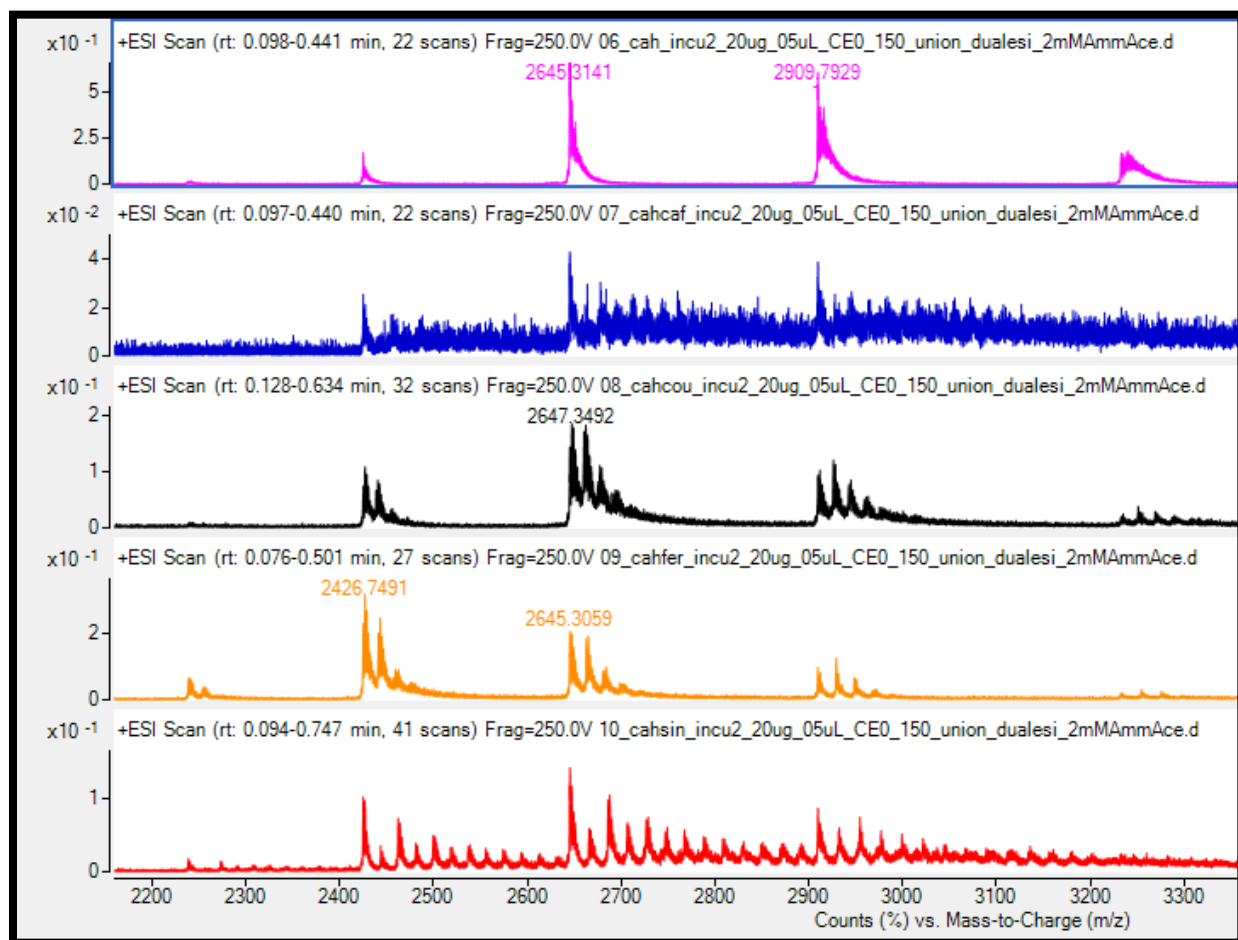


Figure 37. (Top to Bottom) Carbonic Anhydrase, Non-Complexed (pink), Carbonic Anhydrase-Caffeic Acid (blue), Carbonic Anhydrase-Coumaric Acid (black), Carbonic Anhydrase-Ferulic Acid (orange), Carbonic Anhydrase-Sinapic Acid (red).

We observed binding of multiple ligands. Ferulic acid (**3**) and *p*-coumaric acid (**2**) show signals for 1, 2 and 3 ligands binding while also maintaining the free enzyme, while sinapic acid shows the ability to complex more than 3 ligands. This experiment was expanded over a wider window of time to analyze the possible change of complexing over the course of 6 hours but there was no meaningful change. The analysis was initially completed at a collision energy (CE) of 0 V, allowing for the most

efficient conditions for non-covalent complexes to exist. The CE can be strategically modified to start to compare binding efficiency of the ligands. The complexes were tested at 0, 25, 50 and 75 V CE, always also running the non-complexed enzyme in the same conditions for comparison.

Comparing the ability of the complex to remain intact upon addition of collision energy allows a relative estimation of binding efficacy of the small molecule to the macromolecule. Thus, the more collision energy required to disrupt the non-covalent complex the greater the interaction between the two parts. Without standards this estimation of binding efficiency is qualitative and relative between the tested compounds. An example of the CE addition is shown in Figure 38. Here, with a CE of 50 used the only complex remaining is that of sinapic acid (**4**). At this collision energy, all other complexes dissociated completely, and the remaining signal was that of the protein alone.

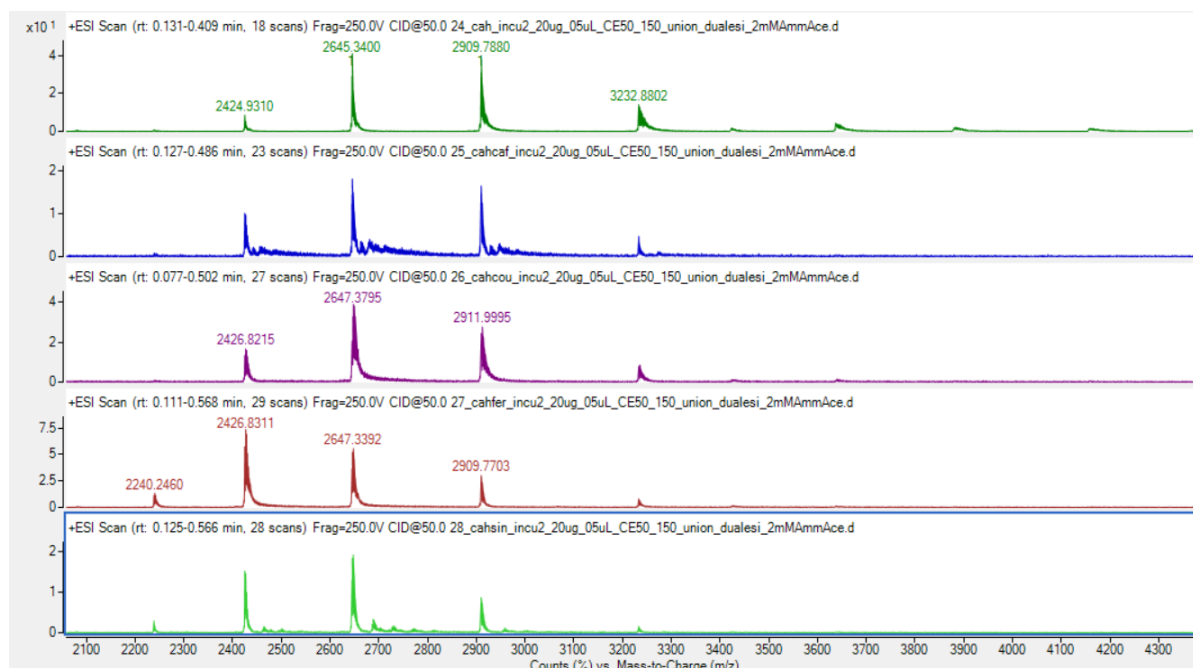


Figure 38. *Carbonic Anhydrase Complexed with Small Molecules (from top to bottom) Control, Caffeic Acid, p-Coumaric Acid, Ferulic Acid, and Sinapic Acid at 50 CE.*

Increased CE showed minimal effect on the abundance of protonated native protein itself. In fact, low levels of CE have been used frequently as a declustering technique as the folded protonated protein often still contains non-covalent small molecules. Although useful in declustering, use of collision energy needs to be heavily optimized to avoid unfolding, especially in non-covalent complexing studies to maintain the identifiable shift in MW caused by the ligand.

3.7.3 α -Glucosidase

The use of native complexing with BSA and carbonic anhydrase is proof of concept for future studies. Most effectively, the investigation of glucosidase enzymes and the complexes associated with the addition of possible inhibitors may enhance the efficiency and information gathered from screening. Consideration of these two

different native macromolecule complexes lends itself to the method development for other macromolecules.

α -Glucosidase is a 60 - 80 kDa MW macromolecule depending on the source and is highly glycosylated. This size, similar to that of BSA, could lean the same difficulties associated with analysis. Although the glycosylation, could give a detailed envelope similar to that of carbonic anhydrase, further highlighting the importance of protein specific method optimization for the analysis of non-covalent complexes via native ESI-MS.

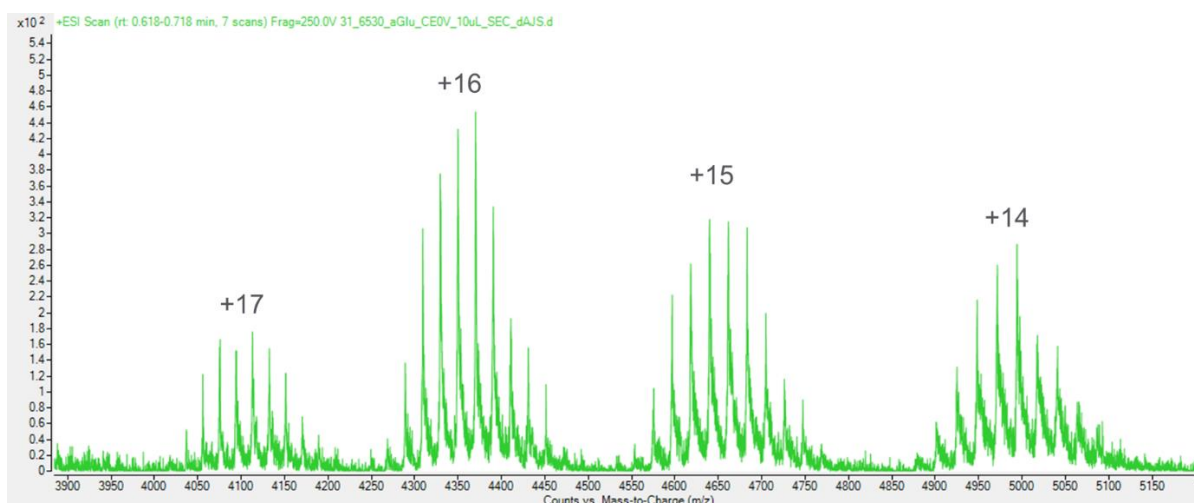


Figure 39. *α -Glucosidase Charge Envelope.*

Shown in Figure 39, the charge envelope with a primary charge state of +16 presents a quite different profile from that of BSA, more similar to the carbonic anhydrase. There are highly resolved peaks within each charge state related to the glycosylation of the protein. In Figure 40, further information can be gathered from deconvolution of the charge envelope, showing a MW of 69.9 kDa.

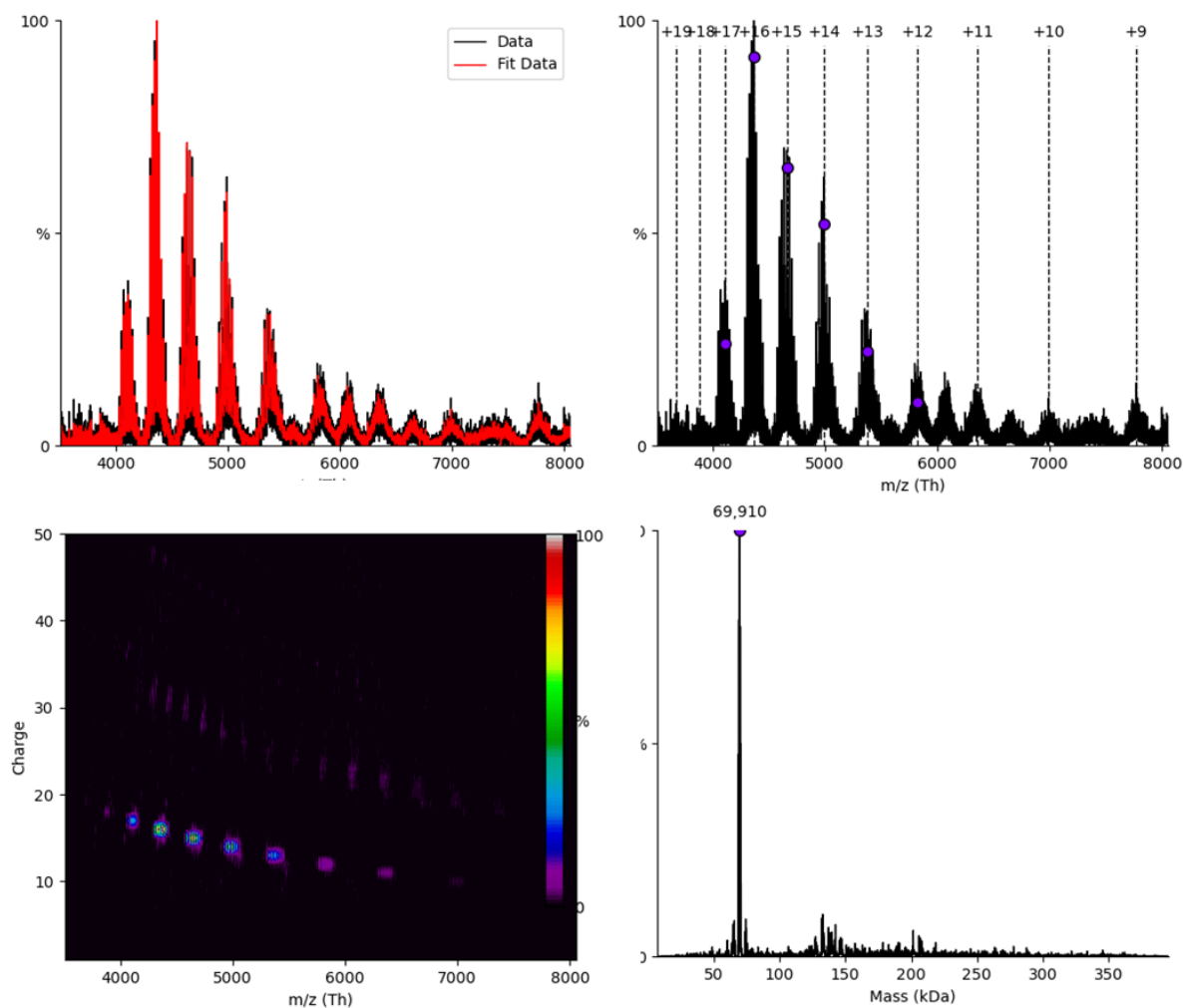


Figure 40. *UNIDEC Deconvolution of α -Glucosidase.*

. The detection of the native enzyme bodes well for the development of the small molecule assay. The conditions shown as successful for BSA and carbonic anhydrase did not produce a ligand-protein complex that had been seen with the alternative macromolecules. This could be a result of the analysis or sample preparation methods and need to be further explored to resolve and create a successful assay.

CHAPTER 4: CONCLUSION

In this study the hydroxycinnamic acids class of polyphenols, and synthetically prepared derivatives were evaluated for effectiveness as free radical scavengers and glucosidase inhibitors. The HCAs ranked **2 > 4 > 3 > 1** in radical scavenging ability, the use of the DPPH assay allowed for various radical scavenging mechanisms and comparison within a structural family of compounds resulting in effective direct comparison. Using a four-step synthetic method, the HCAs were derivatized to include amino acids at the carboxylic acid portion. The amino acid addition on HCA compound class did not enhance the ability of the small molecules to scavenge radicals. The derivatization highlighted solvent effects and steric hindrance as determining factors in the evaluation of radical scavenging via the DPPH assay. Linking two HCA molecules via an anhydride produced a small molecule that was more effective at scavenging free radicals compared to the HCA starting material. Overall, the effectiveness of the HCA to scavenge molecules was predominantly determined by the substituents present on the phenol. The catechol was the most effective scavenger followed by phenols supported by surrounding methoxy groups, and most ineffective a phenol without neighboring substituents.

HCAs were evaluated as α -amylase inhibitors in a 96-well plate starch-iodide assay to reduce experimental error and lead to more accurate results. The assay resulted in ranking of HCAs with inhibitory ability as **1 \approx 2 > 3 > 4**. Direct comparison of these HCAs using the same assay allowed for true ranking. The results of the assay were investigated and supported using alternative evaluations including STD-NMR for

binding epitope, fluorescence quenching assay for π - π interactions, and computational docking. Testing of derivatized HCAs as inhibitors yielded a *p*-coumaric acid diamine derivative (**18g**) which showed better efficacy as an inhibitor compared to the primary HCA. The fluorescence quenching assay informed the importance of π - π stacking in the interaction of polyphenols with the binding region of α -amylase. STD-NMR offered information on the effectiveness of various regions, apart from the phenol, in the inhibitory interaction.

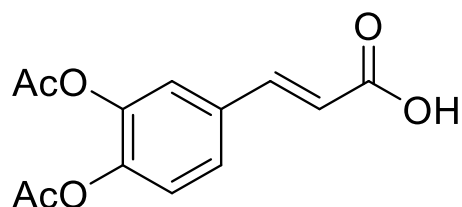
HCAs can easily generate effective derivatives, and the ubiquitous and abundant nature makes this class an attractive target for more investigation. More phenolic features improve radical scavenging efficiency. Structural improvement upon the enzyme inhibitors to enhance protein binding could possibly come from a pseudo-carbohydrate like structure that mimics the natural ligand. Further, the use of even more sensitive assays and evaluation of enzyme kinetics may further the understanding of this interaction. There have been alternative enzyme targets identified with this class of compounds which could increase understanding of off-target biological effects, as well as evaluate alternative routes for reducing the hydrolysis of polysaccharides to the monomer.

CHAPTER 5: EXPERIMENTAL

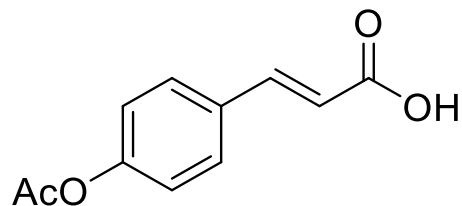
5.1 Synthesis

5.1.1 General Procedure: Acetylation

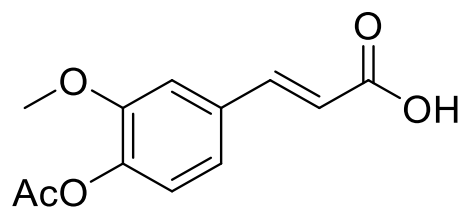
HCA (**1-4**) (0.555 mmol, 1.00 eq) was dissolved in pyridine (0.6 mL) and treated with DMAP (0.014 mmol, 0.03 eq) and acetic anhydride (1.388 mmol, 2.50 eq) at 0°C and stirred for 4 hours. After, the crude reaction mixture was poured over ice and acidified to pH 2 with 1 M HCl. The aqueous layer was extracted with EtOAc (3 x 10 mL) and dried over Na₂SO₄. Solvents were then removed under reduced pressure and recrystallized in H₂O/EtOH.

3-(3,4-Diacetoxyphenyl)prop-2-enoic acid (5)

Compound (**5**) was prepared according to the general procedure after workup the compound was obtained in 75% yield as an off white powdery solid (400 mg). ¹H NMR (d-DMSO, 600MHz): δ 2.25 (s, 3H), 2.26 (s, 3H) 6.50 (d, 1H, *J* = 16.1 Hz), 7.28 (d, 1H, *J* = 8.4 Hz), 7.54 (d, 1H, *J* = 16.1 Hz), 7.60 (dd, 1H, *J* = 2.1, 8.4 Hz), 7.63(s, 1H, *J* = 2.1 Hz). ¹³C NMR (d-DMSO, 150MHz): 20.8, 20.9, 119.0, 120.8, 123.5, 124.6, 127.3, 133.6, 142.7, 143.8, 167.9, 168.6, 168.7.

3-(4-Acetoxyphenyl)prop-2-enoic acid (6)

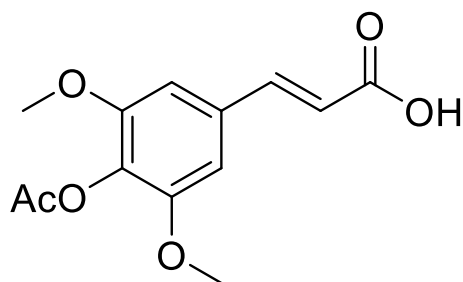
Compound (6) was prepared according to the general procedure after workup the compound was obtained in 90% yield as an off-white solid (284 mg). ^1H NMR (d-DMSO, 600MHz): δ 2.25 (s, 3H), 6.48 (d, 1H, J = 16.1 Hz), 7.14 (d, 2H, J = 8.6 Hz), 7.56 (d, 1H, J = 16.1 Hz), 7.71 (d, 2H, J = 8.6 Hz). ^{13}C NMR (d-DMSO, 150MHz): 21.4, 119.8, 122.9, 129.9, 132.5, 143.5, 152.4, 168.1, 169.6.

3-(4-Acetoxy-3-methoxy-phenyl)prop-2-enoic acid (7)

Compound (7) was prepared according to the general procedure after workup the compound was obtained in 80% yield as a white powder solid (480 mg). ^1H NMR (d-DMSO, 600MHz): δ 2.22 (s, 3H), 3.792 (s, 3H), 6.55 (d, 1H, J = 16.0Hz), 7.08 (dd, 1H, J = 2.1, 8.2 Hz), 7.23 (d, 1H, J = 8.2 Hz), 7.45 (d, 1H, J = 2.1 Hz), 7.55 (d, 1H, J = 16.0 Hz).

^{13}C NMR (d-DMSO, 150MHz): δ 20.9, 56.5, 112.4, 120.1, 121.9, 123.7, 133.8, 141.3, 143.9, 151.7, 168.1, 168.9.

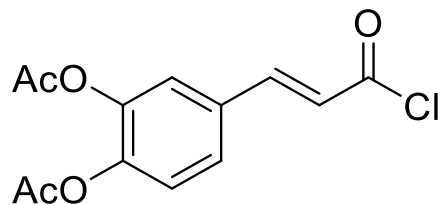
3-(4-Acetoxy-3,5-dimethoxy-phenyl)prop-2-enoic acid (8)



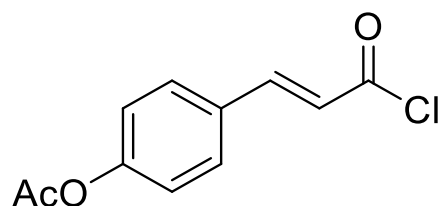
Compound (8) was prepared according to the general procedure after workup the compound was obtained in 90% yield as a yellow powdery solid (158 mg). ^1H NMR (d-DMSO, 600MHz): δ 2.22 (s, 3H), 3.77 (s, 3H), 6.59 (d, 1H, $J = 14.9$ Hz), 7.08 (s, 2H), 7.53 (d, 1H, $J = 16.0$ Hz). ^{13}C NMR (d-DMSO, 150MHz): δ 20.7, 56.7, 105.7, 120.2, 129.9, 133.2, 144.3, 152.5, 168.1, 168.5.

5.1.2 General Procedure: Chlorination

Acetylated HCA (**5-8**) (1.892 mmol, 1.00 eq) was dissolved in toluene (10.5 mL) with DMF (6 drops) and treated with oxalyl chloride (3.974 mmol, 2.1 eq) while stirring at -5°C . The reaction was removed from ice bath after 15 minutes and proceeded for 4h at room temperature. The reaction mixture was concentrated under reduced pressure. HCA acid chloride (**9-12**) was pushed forward without further purification.

[2-Acetoxy-4-[(E)-3-chloro-3-oxo-prop-1-enyl]phenyl] acetate (9)

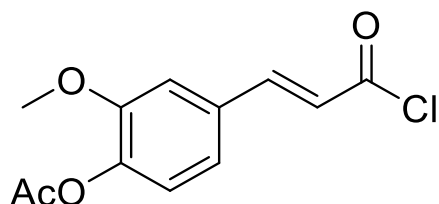
Compound (9) was prepared according to the general procedure after workup the compound was obtained in 99% yield as a light yellow solid (500 mg). ^1H NMR (d-DMSO, 600MHz): δ 2.25 (s, 3H), 2.25 (s, 3H), 6.50 (d, 1H, J = 16.0 Hz), 7.28 (d, 1H, J = 8.3 Hz), 7.53 (d, 1H, J = 16.0 Hz), 7.60 (dd, 1H, J = 2.1, 8.5 Hz), 7.63 (d, 1H, J = 2.1 Hz). ^{13}C NMR (d-DMSO, 150MHz): 20.9, 20.9, 120.9, 123.5, 124.6, 127.3, 133.7, 142.7, 142.9, 143.8, 167.9, 168.7, 168.8.

[4-[(E)-3-Chloro-3-oxo-prop-1-enyl]phenyl] acetate (10)

Compound (10) was prepared according to the general procedure after workup the compound was obtained in 99% yield as an off-white solid (100 mg). ^1H NMR (d-DMSO, 600MHz): δ 2.23 (s, 3H), 6.48 (d, 1H, J = 16.0 Hz), 7.13 (d, 1H, J = 8.6 Hz), 7.54 (d, 1H,

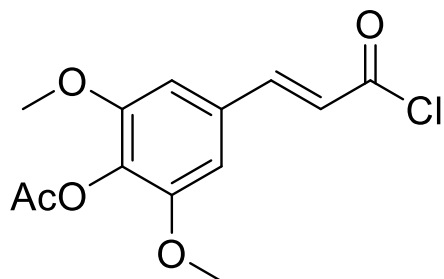
$J = 16.0$ Hz), 7.69 (d, 2H, $J = 8.6$ Hz). ^{13}C NMR (d-DMSO, 150MHz): 21.4, 119.8, 122.9, 129.9, 132.4, 143.4, 152.3, 168.0, 169.6.

[4-[(E)-3-Chloro-3-oxo-prop-1-enyl]-2-methoxy-phenyl] acetate (11)



Compound (11) was prepared according to the general procedure after workup the compound was obtained in 99% yield as a yellow solid (107 mg). ^1H NMR (d-DMSO, 600MHz): δ 2.24 (s, 3H), 3.80 (s, 3H), 6.57 (d, 1H, $J = 16.0$ Hz), 7.10 (d, 1H, $J = 8.1$ Hz), 7.24 (dd, 1H, $J = 2.0, 8.2$ Hz), 7.46 (d, 1H, $J = 2.0$ Hz), 7.56 (d, 1H, $J = 16.0$ Hz). ^{13}C NMR (d-DMSO, 150MHz): δ 20.9, 56.5, 112.4, 120.1, 121.9, 123.7, 133.8, 141.3, 143.9, 151.7, 168.1, 168.9.

(E)-4-(3-Chloro-3-oxoprop-1-en-1-yl)-2,6-dimethoxyphenyl acetate (12)

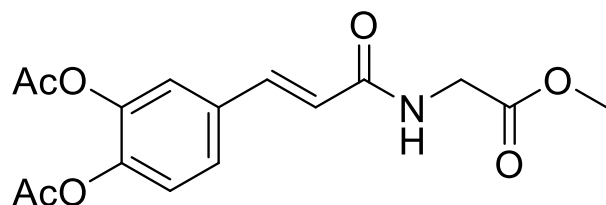


Compound (12) was prepared according to the general procedure after workup the compound was obtained in 99% yield as a light orange powdery solid (117 mg). ^1H NMR (d-DMSO, 600MHz): δ 2.22 (s, 3H), 3.76 (s, 6H), 6.60 (d, 1H, $J = 16.0$ Hz), 7.07 (s, 2H), 7.53 (d, 1H, $J = 16.0$ Hz). ^{13}C NMR (d-DMSO, 150MHz): δ 20.7, 56.7, 105.7, 120.3, 129.9, 133.2, 144.3, 152.5, 168.1, 168.5.

5.1.3 General Procedure: Amidation

Amino acid methyl ester (0.354 mmol, 2.00 eq) and Et_3N (6 drops) was dissolved in DCM (2 mL), the solution of **(9-12)** dissolved in DCM (2 mL) was added dropwise at room temperature and allowed to stir for 30 minutes to 1 hour, progress was tracked by TLC. The mixture was diluted to 20 mL with EtOAc was washed with brine (1 x 10 mL), 1M HCl (1x 10 mL), brine (1 x 10 mL), and NaHCO_3 (1 x 10 mL) then dried over Na_2SO_4 . Solvent removed under reduced pressure.

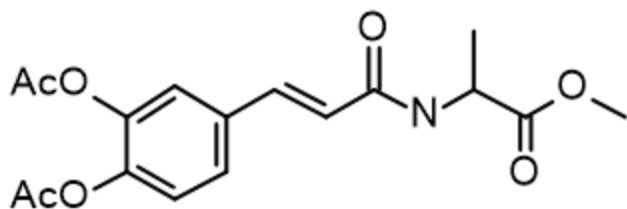
Methyl 2-[[*(E)*-3-(3,4-diacetoxyphenyl)prop-2-enoyl]amino]acetate (13a)



Compound (13a) was prepared according to the general procedure after workup the compound was obtained in 47% yield as an off-white solid (50 mg). ^1H NMR (d-DMSO, 600MHz): δ 2.25 (s, 3H), 2.26 (s, 3H), 3.61 (s, 3H), 3.95 (d, 2H, $J = 5.9$ Hz), 6.66 (d, 1H, $J = 15.9$ Hz), 7.29 (d, 1H, $J = 8.3$ Hz), 7.41 (d, 1H, $J = 15.8$ Hz), 7.49 (m, 2H), 8.52

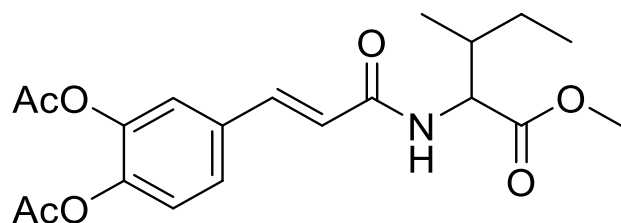
(t, 1H, $J = 5.9$ Hz). ^{13}C NMR (d-DMSO, 150MHz): δ 20.9, 41.3, 52.3, 123.0, 124.7, 126.6, 138.4, 142.8, 143.3, 165.7, 168.7, 168.8, 170.9.

Methyl 2-[[*(E)*-3-(3,4-diacetoxyphenyl)prop-2-enoyl]amino]propanoate (13b)



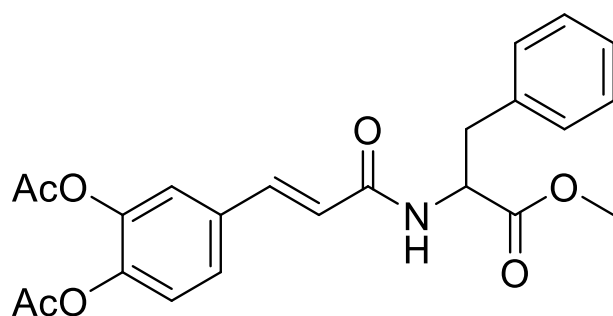
Compound (13b) was prepared according to the general procedure after workup the compound was obtained in 62% yield as a yellow solid (190 mg). ^1H NMR (d-DMSO, 600MHz): δ 1.30 (d, 3H, $J = 6.9$ Hz), 2.26 (s, 3H), 2.26 (s, 3H), 3.61 (s, 3H), 4.36 (q, 1H, $J = 6.9$ Hz), 6.63 (d, 1H, $J = 15.8$ Hz), 7.29 (d, 1H, $J = 8.3$ Hz), 7.40 (d, 1H, $J = 15.8$ Hz), 7.46 (d, 1H, $J = 2.1$ Hz), 7.48 (dd, 1H, $J = 1.4, 8.3$ Hz), 8.54 (d, 1H, $J = 6.87$). ^{13}C NMR (d-DMSO, 150MHz): δ 17.6, 20.9, 48.3, 52.5, 123.0, 124.7, 126.4, 134.2, 138.3, 142.8, 143.3, 168.7, 170.2, 173.6.

Methyl 2-[[*(E)*-3-(3,4-diacetoxyphenyl)prop-2-enoyl]amino]-3-methyl-pentanoate (13c)



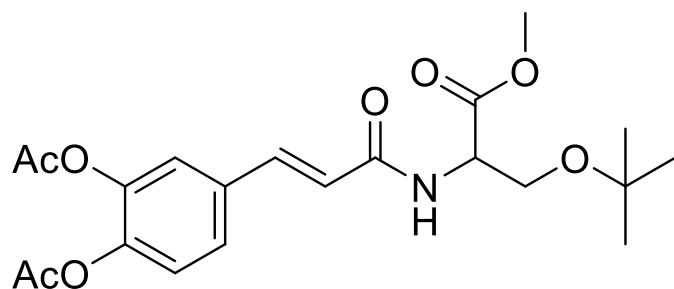
Compound (13c) was prepared according to the general procedure after workup the compound was obtained in 16% yield as a white solid (22 mg). ^1H NMR (d-DMSO, 600MHz): δ 0.82 (m, 6H), 1.37 (m, 2H), 1.78 (m, 1H), 2.24 (s, 3H), 2.25 (s, 3H), 3.60 (s, 3H), 4.30 (d, 1H, $J = 6.4$), 6.76 (d, 1H, $J = 15.8$), 7.28 (d, 1H, $J = 8.3$), 7.37 (d, 1H, $J = 15.8$ Hz), 7.45 (d, 1H, $J = 2.0$), 7.47 (dd, 1H, $J = 2.1$, 8.4 Hz), 8.42 (d, 1H, $J = 8.2$ Hz). ^{13}C NMR (d-DMSO, 150MHz): δ 11.7, 16.0, 20.9, 25.4, 37.0, 52.2, 57.1, 122.9, 123.3, 124.7, 126.4, 134.3, 138.2, 142.9, 143.3, 165.4, 168.7, 172.6.

Methyl 2-[[*(E)*-3-(3,4-diacetoxyphenyl)prop-2-enoyl]amino]-3-phenyl-propanoate (13d)



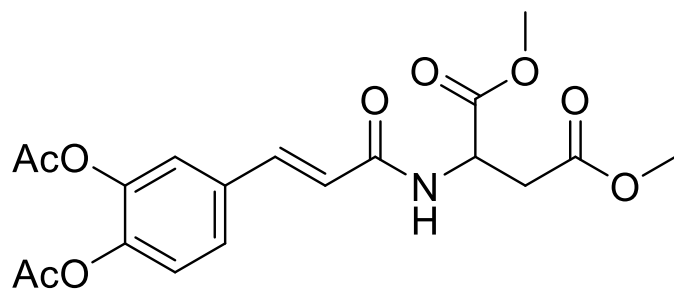
Compound (13d) was prepared according to the general procedure after workup the compound was obtained in 63% yield as a light yellow solid (111 mg). ^1H NMR (d-DMSO, 600MHz): δ 2.25 (s, 3H), 2.26 (s, 3H), 2.93 (m, 1H), 3.05 (m, 1H), 3.59 (s, 3H), 4.57 (m, 1H), 6.63 (d, 1H, $J = 15.8$), 7.16 - 7.28 (m, 6H), 7.34 (d, 1H, $J = 15.8$ Hz), 7.45 (d, 1H, $J = 2.0$), 7.46 (dd, 1H, $J = 2.1$, 8.4 Hz), 8.56 (d, 1H, $J = 7.7$ Hz). ^{13}C NMR (d-DMSO, 150MHz): δ 20.9, 37.3, 52.5, 54.3, 122.9, 124.7, 126.5, 127.1, 128.8, 129.6, 134.1, 137.7, 138.4, 139.2, 142.8, 143.3, 165.2, 168.7, 172.6.

Methyl 2-[[*(E)*-3-(3,4-diacetoxyphenyl)prop-2-enoyl]amino]-3-phenyl-propanoate (13e)



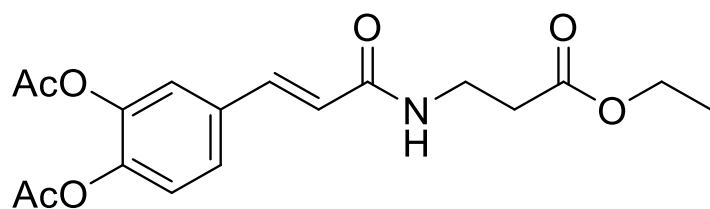
Compound (13e) was prepared according to the general procedure after workup the compound was obtained in 91% yield as a light yellow solid (68 mg). ^1H NMR (d-DMSO, 600MHz): δ 1.09 (s, 9H), 2.26 (s, 3H), 2.27 (s, 3H), 3.52 (q, 1H, J = 4.1, 9.5 Hz), 3.62 (s, 3H), 3.67 (q, 1H, J = 4.8, 9.5 Hz), 4.56 (q, 1H, J = 4.2 Hz), 6.87 (d, 1H, J = 15.8 Hz), 7.29 (d, 1H, J = 8.3 Hz), 7.40 (d, 1H, J = 15.8 Hz), 7.46 (d, 1H, J = 2.0), 7.48 (dd, 1H, J = 2.0, 8.4 Hz), 8.33 (d, 1H, J = 8.0 Hz). ^{13}C NMR (d-DMSO, 150MHz): δ 20.9, 20.9, 27.6, 52.5, 53.6, 62.2, 73.6, 122.9, 123.3, 124.7, 126.5, 134.3, 138.3, 142.8, 143.3, 165.3, 168.7, 168.8, 171.3.

Dimethyl 2-[[*(E)*-3-(3,4-diacetoxyphenyl)prop-2-enoyl]amino] butanedioate (13f)

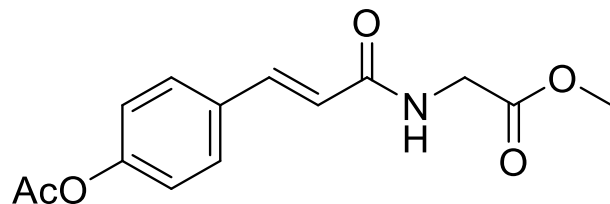


Compound (13f) was prepared according to the general procedure after workup the compound was obtained in 30% yield as a yellow oil (91 mg). ^1H NMR (d-DMSO, 600MHz): δ 2.25 (s, 3H), 2.26 (s, 3H), 2.77 (dd, 1H, $J = 7.1, 16.6$ Hz), 2.84 (dd, 1H, $J = 5.8, 16.6$ Hz), 3.58 (s, 3H), 3.61 (s, 3H), 4.73 (q, 1H, $J = 6.2, 7.2$ Hz), 6.66 (d, 1H, $J = 15.8$ Hz), 7.28 (d, 1H, $J = 8.3$ Hz), 7.40 (d, 1H, $J = 15.7$ Hz), 7.47 (d, 1H, $J = 2.0$ Hz), 7.49 (dd, 1H, $J = 2.2, 8.3$ Hz), 8.62 (d, 1H, $J = 7.9$ Hz). ^{13}C NMR (d-DMSO, 150MHz): δ 20.8, 36.2, 49.2, 52.3, 52.8, 122.9, 123.0, 124.7, 126.5, 137.7, 138.6, 142.8, 143.4, 165.1, 168.8, 171.0, 171.7.

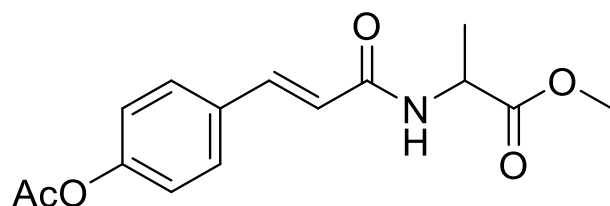
Ethyl 3-[[*(E)*-3-(3,4-diacetoxyphenyl)prop-2-enoyl]amino] propanoate (13g)



Compound (13g) was prepared according to the general procedure after workup the compound was obtained in 30% yield as an off-white solid (25 mg). ^1H NMR (d-DMSO, 600MHz): δ 1.15 (t, 3H, $J = 7.6$ Hz), 2.25 (s, 3H), 2.26 (s, 3H), 2.48 (t, 2H, $J = 6.9$ Hz), 3.37 (q, 2H, $J = 6.9$ Hz), 4.04 (q, 2H, $J = 7.6$ Hz), 6.57 (d, 1H, $J = 15.8$ Hz), 7.27 (d, 1H, $J = 8.3$ Hz), 7.37 (d, 1H, $J = 15.8$ Hz), 7.44 (d, 2H, $J = 2.1$ Hz), 7.46 (dd, 1H, $J = 2.1, 8.3$ Hz), 8.52 (t, 1H, $J = 5.5$ Hz). ^{13}C NMR (d-DMSO, 150MHz): δ 14.6, 20.9, 34.4, 35.5, 60.5, 122.8, 123.7, 124.7, 126.4, 134.3, 137.6, 142.8, 143.2, 165.3, 168.7, 171.9.

Methyl 2-[[*(E)*-3-(4-acetoxyphenyl)prop-2-enoyl]amino]acetate (14a)

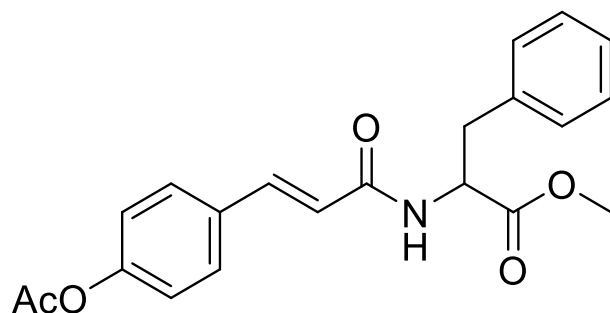
Compound (14a) was prepared according to the general procedure after workup the compound was obtained in 15% yield as an off-white solid (10 mg). ^1H NMR (d-DMSO, 600MHz): δ 2.24 (s, 3H), 3.62 (s, 3H), 3.94 (d, 1H, $J = 5.9$ Hz), 6.66 (d, 1H, $J = 15.8$ Hz), 7.15 (s, 2H), 7.42 (d, 1H, $J = 15.8$ Hz), 7.60 (d, 2H, $J = 8.5$ Hz), 8.57 (t, 1H). ^{13}C NMR (d-DMSO, 150MHz): 21.4, 32.0, 41.3, 52.3, 122.0, 123.0, 129.3, 132.9, 139., 151.9, 165.9, 170.9, 172.5.

Methyl 2-[[*(E)*-3-(4-acetoxyphenyl)prop-2-enoyl]amino]propanoate (14b)

Compound (14b) was prepared according to the general procedure after workup the compound was obtained in 75% yield as a white solid (95 mg). ^1H NMR (d-DMSO, 600MHz): δ 2.24 (s, 3H), 2.47 (s, 3H), 3.37 (q, 1H, $J = 6.3$ Hz), 6.55 (d, 1H, $J = 15.8$ Hz), 7.13 (d, 2H, $J = 8.5$ Hz), 7.38 (d, 1H, $J = 15.8$ Hz), 7.56 (d, 2H, $J = 8.5$ Hz), 8.19 (s, 1H).

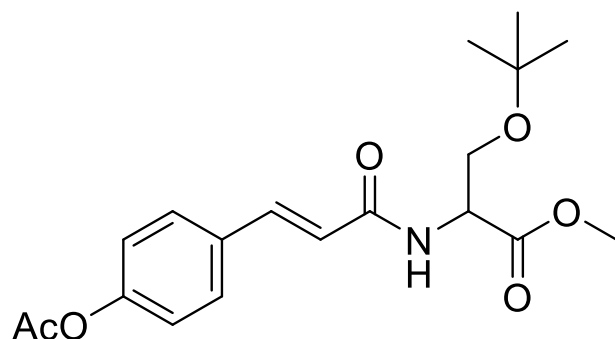
^{13}C NMR (d-DMSO, 150MHz): 21.4, 34.2, 35.4, 52.0, 122.9, 123.0, 129.2, 133.1, 138.3, 151.8, 165.5, 169.6, 172.3.

Methyl 2-[[*(E)*-3-(4-acetoxyphenyl)prop-2-enoyl]amino]-3-phenyl-propanoate (14c)



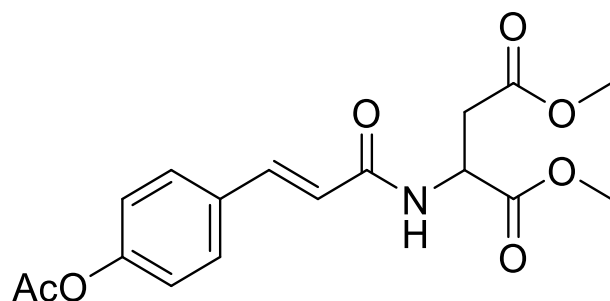
Compound (14c) was prepared according to the general procedure after workup the compound was obtained in 83% yield as an off-white solid (100 mg). ^1H NMR (d-DMSO, 600MHz): δ 2.26 (s, 3H), 2.95 (dd, 1H, J = 4.6, 9.3 Hz), 3.08 (dd, 1H, J = 5.5, 8.3 Hz), 3.61 (s, 3H), 4.6 (qd, 1H, J = 1.5, 2.4, 5.4 Hz), 6.63 (d, 1H, J = 15.8 Hz), 7.16 (d, 2H, J = 8.6 Hz), 7.24 (m, 5H), 7.38 (d, 1H, J = 15.8 Hz), 7.58 (d, 2H, J = 8.6 Hz), 8.56 (d, 1H, J = 7.7 Hz). ^{13}C NMR (d-DMSO, 150MHz): 20.8, 51.9, 53.8, 121.4, 122.4, 126.6, 128.7, 129.0, 132.3, 137.1, 138.6, 151.3, 164.9, 169.0, 172.0.

Methyl 2-[[*(E)*-3-(4-acetoxyphenyl)prop-2-enoyl]amino]-3-*tert*-butoxy-propanoate (14d)



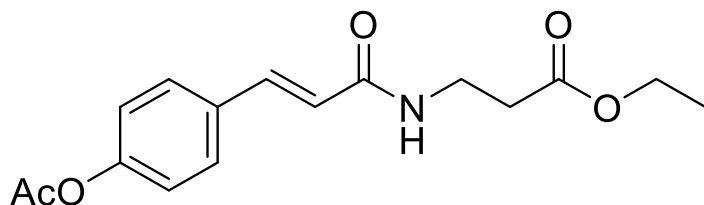
Compound (14d) was prepared according to the general procedure after workup the compound was obtained in 92% yield as an off-white solid (111 mg). ^1H NMR (d-DMSO, 600MHz): δ 1.09 (s, 9H), 2.25 (s, 3H), 3.52 (q, 1H, J = 4.6, 9.3 Hz), 3.62 (s, 3H), 3.67 (q, 1H, J = 4.9, 9.5 Hz), 6.85 (d, 1H, J = 15.8 Hz), 7.15 (d, 2H, J = 8.7 Hz), 7.41 (d, 1H, J = 15.8 Hz), 7.58 (d, 2H, J = 8.6 Hz), 8.32 (d, 1H, J = 8.0 Hz). ^{13}C NMR (d-DMSO, 150MHz): 21.4, 27.7, 52.5, 53.6, 62.2, 73.6, 122.3, 122.9, 129.3, 133.1, 139.0, 151.8, 165.5, 169.6, 171.3.

Dimethyl 2-[[*(E)*-3-(4-acetoxyphenyl)prop-2-enoyl]amino]butanedioate (14e)



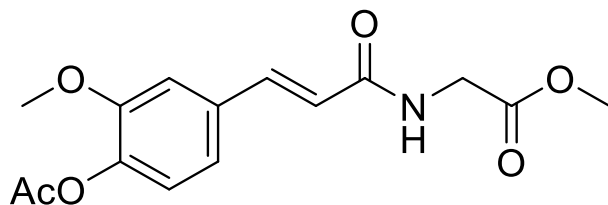
Compound (14e) was prepared according to the general procedure after workup the compound was obtained in 62% yield as a white solid (71 mg). ^1H NMR (d-DMSO, 600MHz): δ 2.26 (s, 3H), 2.82 (dq, 2H, J = 5.8, 16.6 Hz), 3.61 (s, 3H), 3.63 (s, 3H), 4.76 (q, 1H, J = 6.0 Hz), 6.68 (d, 1H, J = 15.8 Hz), 7.17 (d, 2H, J = 8.7 Hz), 7.44 (d, 1H, J = 15.8 Hz), 7.61 (d, 2H, J = 8.7 Hz), 8.60 (d, 1H, J = 8.0 Hz). ^{13}C NMR (d-DMSO, 150MHz): 20.9, 35.7, 48.6, 51.7, 52.2, 121.3, 122.4, 128.8, 132.3, 138.8, 151.4, 164.8, 169.1, 170.5, 171.1.

Ethyl 3-[[*(E)*-3-(4-acetoxyphenyl)prop-2-enoyl]amino]propanoate (14f)



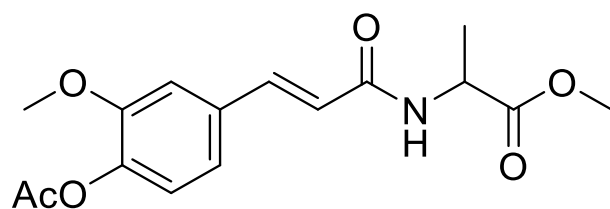
Compound (14f) was prepared according to the general procedure after workup the compound was obtained in 81% yield as a white solid (113 mg). Pushed forward without further characterization.

Methyl 2-[[*(E)*-3-(4-acetoxy-3-methoxy-phenyl)prop-2-enoyl]amino]acetate (15a)



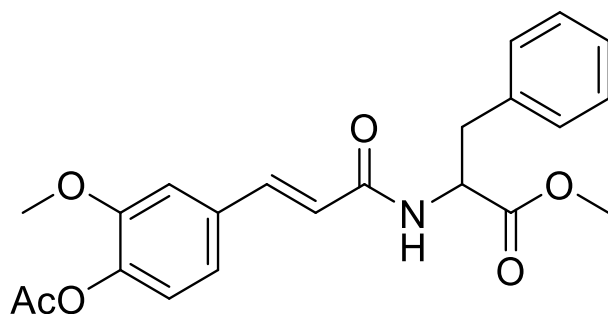
Compound (15a) was prepared according to the general procedure after workup the compound was obtained in 60% yield as an off-white solid (18 mg). ^1H NMR (d-DMSO, 600MHz): δ 2.23 (s, 3H), 3.62 (s, 3H), 3.79 (s, 3H), 3.95 (d, 2H, $J = 6.0$ Hz), 6.69 (d, 1H, $J = 16.0$ Hz), 7.10 (d, 1H, $J = 8.1$ Hz), 7.15 (dd, 1H, $J = 1.4, 8.2$ Hz), 7.32 (d, 1H, $J = 1.5$ Hz), 7.42 (d, 1H, $J = 15.8$ Hz), 8.47 (t, 1H, $J = 5.8$ Hz). ^{13}C NMR (d-DMSO, 150MHz): δ 20.9, 41.3, 52.3, 56.4, 112.2, 120.7, 122.3, 123.8, 134.3, 139.4, 140.8, 151.6, 165.9, 169.0, 170.9.

Methyl 2-[[*(E)*-3-(4-acetoxy-3-methoxy-phenyl)prop-2-enoyl]amino]propanoate (15b)



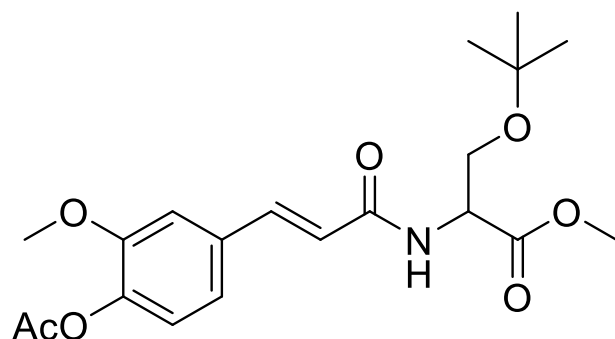
Compound (15b) was prepared according to the general procedure after workup the compound was obtained in 68% yield as a white solid (22 mg). ^1H NMR (d-DMSO, 600MHz): δ 1.30 (d, 3H, $J = 7.2$ Hz), 2.23 (s, 3H), 3.61 (s, 3H), 3.79 (s, 3H), 4.37 (q, 1H, $J = 7.2$ Hz), 6.65 (d, 1H, $J = 15.8$ Hz), 7.01 (d, 1H, $J = 8.1$ Hz), 7.14 (dd, 1H, $J = 1.8, 8.2$ Hz), 7.30 (d, 1H, $J = 1.7$ Hz), 7.40 (d, 1H, $J = 15.8$ Hz), 8.49 (d, 1H, $J = 7.1$ Hz). ^{13}C NMR (d-DMSO, 150MHz): δ 17.6, 20.9, 48.3, 52.5, 56.3, 112.1, 120.7, 122.3, 123.8, 134.3, 139.3, 140.8, 151.6, 165.2, 169.0, 173.7.

Methyl 2-[[*(E)*-3-(4-acetoxy-3-methoxy-phenyl)prop-2-enoyl]amino]-3-phenylpropanoate (15c)



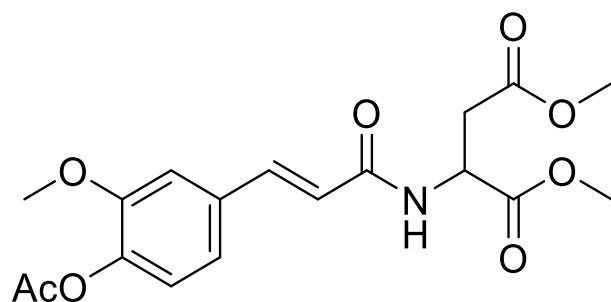
Compound (15c) was prepared according to the general procedure after workup the compound was obtained in 76% yield as an off-white solid (60 mg). ^1H NMR (d-DMSO, 600MHz): δ 2.23 (s, 3H), 2.94 (dd, 1H, $J = 9.3, 13.9$ Hz), 3.06 (dd, 1H, $J = 5.4, 13.9$ Hz), 3.60 (s, 3H), 3.78 (s, 3H), 4.59 (q, 1H, $J = 5.5$ Hz), 6.65 (d, 1H, $J = 15.8$ Hz), 7.10 (d, 1H, $J = 8.2$ Hz), 7.12 (dd, 1H, $J = 1.6, 8.2$ Hz), 7.23 (m, 5H), 7.28 (d, 1H, $J = 1.6$ Hz), 7.36 (d, 1H, $J = 15.8$ Hz), 8.52 (d, 1H, $J = 7.7$ Hz). ^{13}C NMR (d-DMSO, 150MHz): δ 20.9, 37.3, 52.5, 54.3, 56.3, 112.0, 120.8, 122.2, 123.8, 127.1, 128.8, 129.6, 134.2, 137.7, 139.5, 140.8, 151.6, 165.4, 169.0, 172.6.

Methyl 2-[[*(E)*-3-(4-acetoxy-3-methoxy-phenyl)prop-2-enoyl]amino]-3-tert-butoxy-propanoate (15d)



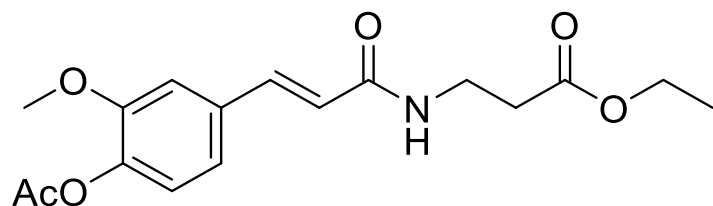
Compound (15d) was prepared according to the general procedure after workup the compound was obtained in 67% yield as a light yellow solid (26 mg). ^1H NMR (d-DMSO, 600MHz): δ 1.09 (s, 9H), 2.23 (s, 3H), 3.52 (dd, 1H, J = 4.2 Hz), 3.62 (s, 3H), 3.67 (dd, 1H, J = 4.7 Hz), 3.79 (s, 3H), 4.56 (q, 1H, J = 4.4 Hz), 6.88 (d, 1H, J = 15.8 Hz), 7.10 (d, 1H, J = 8.2 Hz), 7.14 (dd, 1H, J = 1.8, 8.2 Hz), 7.31 (d, 1H, J = 1.7 Hz), 7.40 (d, 1H, J = 15.8 Hz), 8.26 (d, 1H, J = 8.0 Hz). ^{13}C NMR (d-DMSO, 150MHz): δ 20.9, 27.7, 52.5, 53.6, 56.3, 62.2, 73.6, 112.0, 120.8, 122.5, 123.8, 134.4, 139.3, 140.8, 151.6, 165.5, 169.0, 171.3.

Dimethyl 2-[[*(E)*-3-(4-acetoxy-3-methoxy-phenyl)prop-2-enoyl]amino]butanedioate (15e)



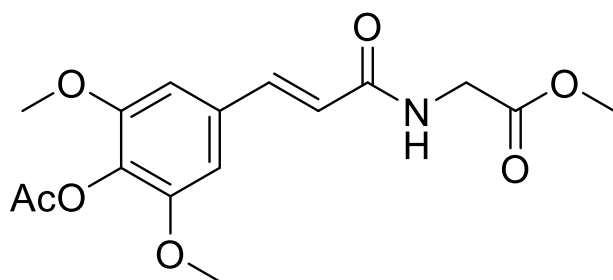
Compound (15e) was prepared according to the general procedure after workup the compound was obtained in 71% yield as an off-white solid (58 mg). ^1H NMR (d-DMSO, 600MHz): δ 2.23 (s, 3H), 2.77 (dd, 1H, $J = 7.1, 16.6$ Hz), 2.84 (dd, 1H, $J = 6.3, 17.1$ Hz), 3.60 (s, 3H), 3.62 (s, 3H), 3.79 (s, 3H), 6.68 (d, 1H, $J = 15.8$ Hz), 7.10 (d, 1H, $J = 8.1$ Hz), 7.14 (dd, 1H, $J = 1.6, 8.1$ Hz), 7.31 (d, 1H, $J = 1.6$ Hz), 7.41 (d, 1H, $J = 15.8$ Hz), 8.54 (d, 1H, $J = 8.0$ Hz). ^{13}C NMR (d-DMSO, 150MHz): δ 20.9, 36.2, 49.2, 52.2, 52.8, 56.3, 112.0, 120.9, 122.2, 123.8, 134.2, 139.7, 140.9, 151.6, 165.3, 169.0, 171.0, 171.7.

Ethyl 3-[[*(E)*-3-(4-acetoxy-3-methoxy-phenyl)prop-2-enoyl]amino]propanoate (15f)



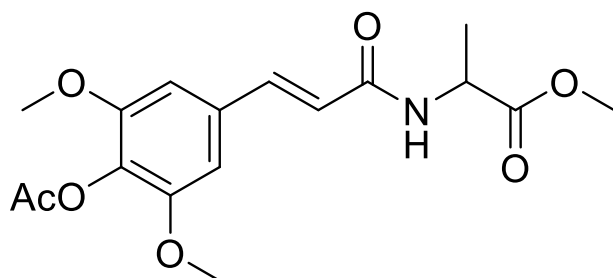
Compound (15f) was prepared according to the general procedure after workup the compound was obtained in 90% yield as a yellow solid (90 mg). Pushed forward without further characterization.

Methyl 2-[[*(E)*-3-(4-acetoxy-3,5-dimethoxy-phenyl)prop-2-enoyl]amino]acetate (16a)



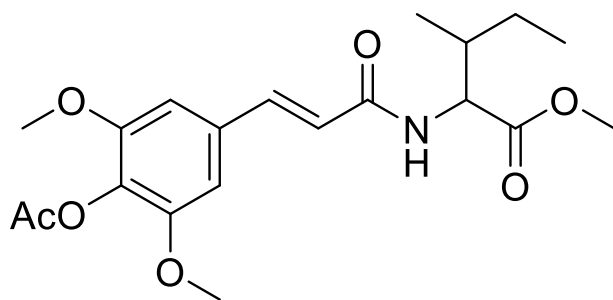
Compound (16a) was prepared according to the general procedure after workup the compound was obtained in 57% yield as a light yellow solid (17 mg). ^1H NMR (d-DMSO, 600MHz): δ 2.22 (s, 3H), 3.62 (s, 3H), 3.77 (s, 6H), 3.95 (d, 2H, $J = 5.9$ Hz), 6.72 (d, 1H, $J = 15.7$ Hz), 6.96 (s, 2H), 7.40 (d, 1H, $J = 15.81$ Hz), 8.45 (t, 1H, $J = 5.8$ Hz). ^{13}C NMR (d-DMSO, 150MHz): δ 20.7, 41.4, 52.3, 56.6, 105.0, 122.4, 129.5, 133.7, 139.8, 152.5, 165.9, 168.5, 170.9.

Methyl 2-[[*(E)*-3-(4-acetoxy-3,5-dimethoxy-phenyl)prop-2-enoyl]amino]propanoate (16b)



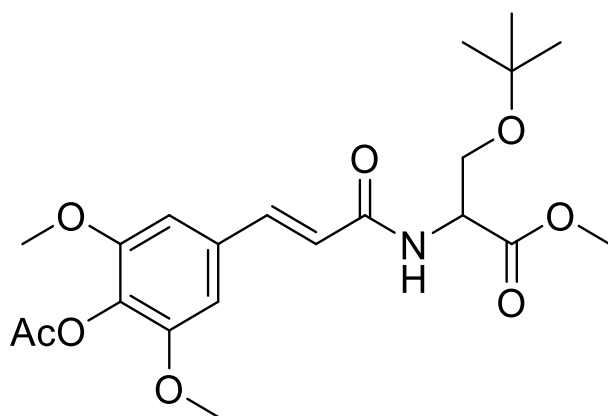
Compound (16b) was prepared according to the general procedure after workup the compound was obtained in 66% yield as an off-white solid (20 mg). ^1H NMR (d-DMSO, 600MHz): δ 1.30 (d, 3H, $J = 7.2$ Hz), 2.22 (s, 3H), 3.61 (s, 3H), 3.77 (s, 6H), 4.37 (q, 2H, $J = 7.2$ Hz), 6.67 (d, 1H, $J = 15.7$ Hz), 6.95 (s, 2H), 7.39 (d, 1H, $J = 15.8$ Hz), 8.48 (d, 1H, $J = 7.0$ Hz). ^{13}C NMR (d-DMSO, 150MHz): δ 17.6, 20.7, 48.3, 52.5, 56.6, 105.9, 122.5, 129.5, 133.7, 139.7, 152.5, 165.2, 168.6, 173.6.

Methyl 2-[[*(E)*-3-(4-acetoxy-3,5-dimethoxy-phenyl)prop-2-enoyl]amino]-3-methylpentanoate (16c)

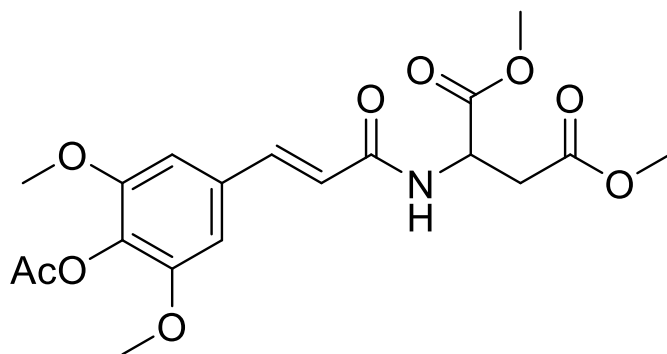


Compound (16c) was prepared according to the general procedure after workup the compound was obtained in 38% yield as an off-white solid (26 mg). ^1H NMR (d-DMSO, 600MHz): δ 0.84 (m, 6H), 1.19 (m, 1H), 1.39 (m, 3H), 1.79 (m, 1H), 2.22 (s, 3H), 3.62 (s, 3H), 3.77 (s, 6H), 4.36 (dd, 2H, $J = 6.4, 8.1$ Hz), 6.81 (d, 1H, $J = 15.8$ Hz), 6.94 (s, 2H), 7.38 (d, 1H, $J = 15.7$ Hz), 8.34 (d, 1H, $J = 8.1$ Hz). ^{13}C NMR (d-DMSO, 150MHz): δ 11.7, 16.0, 20.7, 25.4, 37.0, 52.2, 56.5, 57.1, 104.8, 129.4, 133.8, 139.7, 152.5, 165.6, 168.6, 170.0.

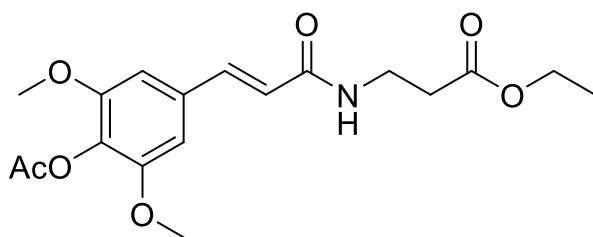
Methyl 2-(3-(4-acetoxy-3,5-dimethoxyphenyl)acrylamido)-3-(tert-butoxy)propanoate (16d)



Compound (16d) was prepared according to the general procedure after workup the compound was obtained in 50% yield as a yellow solid (120 mg). ^1H NMR (d-DMSO, 600MHz): δ 1.09 (s, 9H), 2.22 (s, 3H), 3.52 (m, 1H), 3.62 (s, 3H), 3.68 (m, 1H), 3.77 (s, 6H), 4.57 (q, 1H, $J = 4.3$ Hz), 6.91 (d, 1H, $J = 15.7$ Hz), 6.96 (s, 2H), 7.39 (d, 1H, $J = 15.7$ Hz), 8.24 (d, 1H, $J = 8.0$ Hz). ^{13}C NMR (d-DMSO, 150MHz): δ 20.7, 27.7, 52.5, 53.6, 56.5, 62.2, 73.6, 104.9, 122.7, 129.5, 133.8, 139.7, 152.5, 165.4, 168.6, 171.3.

Dimethyl 2-(3-(4-acetoxy-3,5-dimethoxyphenyl)acrylamido) succinate (16e)

Compound (16e) was prepared according to the general procedure after workup the compound was obtained in 25% yield as a yellow solid (15 mg). ^1H NMR (d-DMSO, 600MHz): δ 2.22 (s, 3H), 2.81 (qd, 2H, J = 5.6, 16.6 Hz), 3.59 (s, 3H), 3.76 (s, 6H), 4.75 (q, 1H, J = 7.2 Hz), 6.72 (d, 1H, J = 15.7 Hz), 6.96 (s, 2H), 7.40 (d, 1H, J = 15.7 Hz), 8.55 (d, 1H, J = 7.9 Hz). ^{13}C NMR (d-DMSO, 150MHz): δ 20.7, 36.2, 49.2, 52.3, 56.6, 104.9, 122.4, 129.5, 133.6, 140.0, 152.5, 165.3, 168.6, 171.0, 171.7.

Ethyl-3-(3-(4-acetoxy-3,5-dimethoxyphenyl)acrylamido)propanoate (16f)

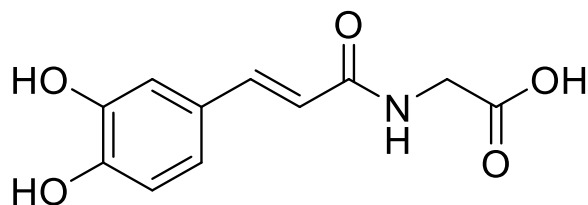
Compound (16f) was prepared according to the general procedure after workup the compound was obtained in 25% yield as a yellow solid (15 mg). ^1H NMR (d-DMSO, 600MHz): δ 2.22 (s, 3H), 2.81 (qd, 2H, J = 5.6, 16.6 Hz), 3.59 (s, 3H), 3.76 (s, 6H), 4.75 (q, 1H, J = 7.2 Hz), 6.72 (d, 1H, J = 15.7 Hz), 6.96 (s, 2H), 7.40 (d, 1H, J = 15.7 Hz), 8.55

(d, 1H, $J = 7.9$ Hz). ^{13}C NMR (d-DMSO, 150MHz): δ 20.7, 36.2, 49.2, 52.3, 56.6, 104.9, 122.4, 129.5, 133.6, 140.0, 152.5, 165.3, 168.6, 171.0, 171.7.

5.1.4 General Procedure: Deprotection

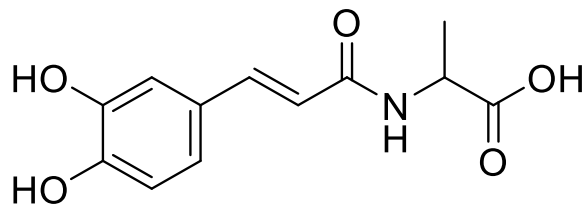
In deprotection, **(13-16)** (0.149 mmol, 1.00 eq) was dissolved in MeOH:H₂O (1:1) (1.5 mL) and treated with NaOH (0.447 mmol, 3.00 eq) and stirred for 15 minutes at room temperature and then concentrated to half volume. The mixture was acidified with HCl (1 M) to pH 3 and extracted with EtOAc (2 x 10 mL) the extracts were combined and dried over Na₂SO₄, then concentrated **(17-20)**.

2-[[*(E)*-3-(3,4-Dihydroxyphenyl)prop-2-enoyl]amino]acetic acid (17a)



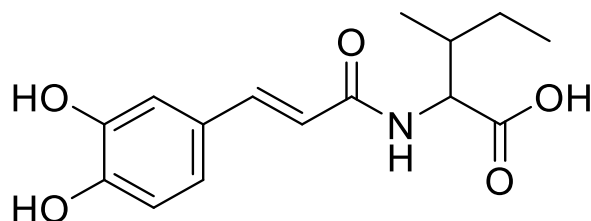
Compound (17a) was prepared according to the general procedure after workup the compound was obtained in 90% yield as an off-white solid (32 mg). ^1H NMR (d-DMSO, 600MHz): δ 3.81 (d, 2H), 6.37 (d, 1H), 6.72 (d, 1H) 6.82 (dd, 1H), 6.93 (d, 1H), 7.22 (d, 1H). ^{13}C NMR (d-DMSO, 150MHz): δ 114.3, 116.3, 118.4, 121.1, 126.8, 140.2, 146.1, 147.9, 166.3, 170.9. HRMS: C₁₁H₁₁NO₅ [M+H]_{cal} m/z 238.071; [M+H]_{exp} m/z 238.0681.

2-[[*(E)*-3-(3,4-Dihydroxyphenyl)prop-2-enoyl]amino]propanoic acid (17b)



Compound (17b) was prepared according to the general procedure after workup the compound was obtained in 71% yield as a light yellow solid (15 mg). ^1H NMR (d-DMSO, 600MHz): δ 1.27 (d, 3H, $J = 7.3$ Hz), 4.27 (q, 1H, $J = 7.3$ Hz), 6.37 (d, 1H, $J = 15.0$ Hz), 6.71 (d, 1H, $J = 8.0$ Hz) 6.80 (dd, 1H, $J = 8.0$ Hz), 6.91 (s, 1H), 7.20 (d, 1H, $J = 16.7$ Hz). ^{13}C NMR (d-DMSO, 150MHz): δ 17.9, 48.1, 114.3, 116.3, 118.5, 125.4, 140.2, 143.3, 143.5, 165.7, 170.9. HRMS: $\text{C}_{12}\text{H}_{13}\text{NO}_5$ $[\text{M}+\text{H}]_{\text{cal}} m/z$ 252.0866; $[\text{M}+\text{H}]_{\text{exp}} m/z$ 252.0779.

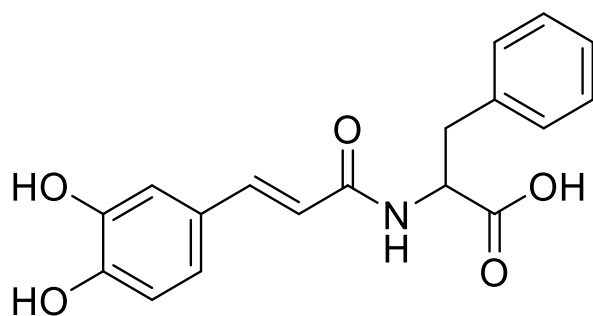
2-[[*(E)*-3-(3,4-Dihydroxyphenyl)prop-2-enoyl]amino]-3-methyl-pentanoic acid (17c)



Compound (17c) was prepared according to the general procedure after workup the compound was obtained in 98% yield as an off-white solid (20 mg). ^1H NMR (d-DMSO, 600MHz): δ 0.94 (dd, 3H, $J = 2.1, 5.3$ Hz), 1.25 (t, 3H, $J = 7.1$ Hz), 1.46 (m, 2H),

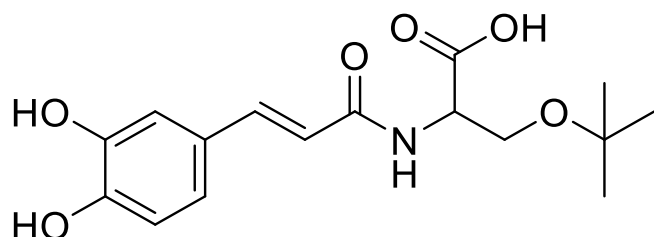
1.94 (m, 1H), 3.76 (s, 3H) 4.72 (q, 1H, $J = 5.1$ Hz), 6.26 (d, 1H, $J = 15.5$ Hz), 6.96 (dd, 1H, $J = 1.8, 8.3$ Hz), 7.05 (d, 1H, $J = 1.8$ Hz), 7.50 (d, 1H, $J = 15.5$ Hz). HRMS: $C_{15}H_{19}NO_5$ $[M+H]_{cal} m/z 294.1336$; $[M+H]_{exp} m/z 294.1334$.

2-[[*(E)*-3-(3,4-Dihydroxyphenyl)prop-2-enoyl]amino]-3-phenyl-propanoic acid (17d)



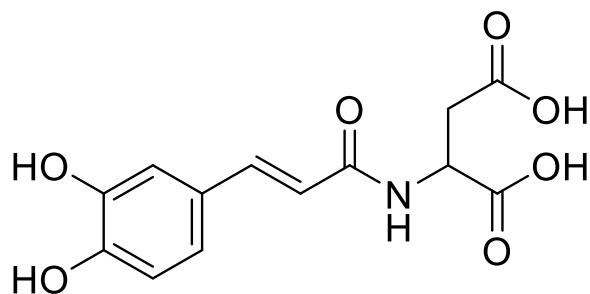
Compound (17d) was prepared according to the general procedure after workup the compound was obtained in 90% yield as a light orange solid (40 mg). 1H NMR (d-DMSO, 600MHz): δ 2.87 (dd, 1H, $J = 9.7, 14.0$ Hz), 3.07 (m, 1H), 4.50 (m, 1H), 6.35 (d, 1H, $J = 15.7$ Hz), 6.70 (d, 1H, $J = 8.2$ Hz), 6.78 (dd, 1H, $J = 2.0, 8.2$ Hz), 6.89 (d, 1H, $J = 2.1$), 7.15 (d, 1H, $J = 15.5$ Hz), 7.21-7.25 (m, 6H), 8.28 (d, 1H, $J = 8.1$ Hz). HRMS: $C_{18}H_{17}NO_5$ $[M+H]_{cal} m/z 328.1179$; $[M+H]_{exp} m/z 328.1148$.

3-tert-Butoxy-2-[[*(E)*-3-(3,4-dihydroxyphenyl)prop-2-enoyl]amino] propanoic acid (17e)



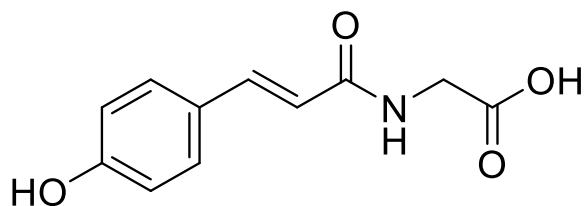
Compound (17e) was prepared according to the general procedure after workup the compound was obtained in 99% yield as an off-white solid (41 mg). ^1H NMR (d-DMSO, 600MHz): δ 1.09 (s, 9H), 3.50 (dd, 1H, $J = 4.0, 9.4$ Hz), 3.64 (dd, 1H, $J = 4.8, 9.4$ Hz), 4.45 (q, 1H, $J = 4.0$ Hz), 6.59 (d, 1H, $J = 15.6$ Hz), 6.71 (d, 1H, $J = 8.1$ Hz), 6.81 (dd, 1H, $J = 2.0, 8.3$ Hz), 6.93 (d, 1H, $J = 2.0$), 7.20 (d, 1H, $J = 15.6$ Hz), 8.06 (d, 1H, $J = 8.1$ Hz). ^{13}C NMR (d-DMSO, 150MHz): δ 27.7, 53.4, 62.4, 73.4, 114.5, 116.2, 118.8, 121.1, 126.9, 140.2, 146.1, 165.9, 172.4. HRMS: $\text{C}_{16}\text{H}_{21}\text{NO}_6$ $[\text{M}+\text{H}]_{\text{cal}}$ m/z 324.1442; $[\text{M}+\text{H}]_{\text{exp}}$ m/z 324.1488.

2-[[*(E)*-3-(3,4-Dihydroxyphenyl)prop-2-enoyl]amino]butanedioic acid (17f)



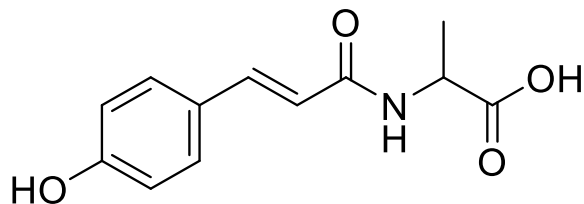
Compound (17f) was prepared according to the general procedure after workup the compound was obtained in 87% yield as a white solid (20 mg). ^1H NMR (d-DMSO, 600MHz): δ 2.60 (dd, 1H, $J = 7.3, 16.6$ Hz), 2.70 (dd, 1H, $J = 5.5, 16.6$ Hz), 4.60 (q, 1H, $J = 7.3$ Hz), 6.39 (d, 1H, $J = 15.7$ Hz), 6.71 (d, 1H, $J = 8.0$ Hz) 6.81 (dd, 1H, $J = 2.0, 8.3$ Hz), 6.92 (d, 1H, $J = 2.0$ Hz), 7.21 (d, 1H, $J = 15.7$ Hz), 8.29 (d, 1H, $J = 7.90$). ^{13}C NMR (d-DMSO, 150MHz): δ 36.7, 49.2, 116.2, 118.5, 121.1, 121.2, 129.7, 140.4, 144.4, 146.1, 172.4, 172.6, 173.1. HRMS: $\text{C}_{13}\text{H}_{13}\text{NO}_7$ $[\text{M}+\text{H}]_{\text{cal}} m/z$ 296.0765; $[\text{M}+\text{H}]_{\text{exp}} m/z$ 296.0805.

2-[[*(E)*-3-(4-Hydroxyphenyl)prop-2-enoyl]amino]acetic acid (18a)



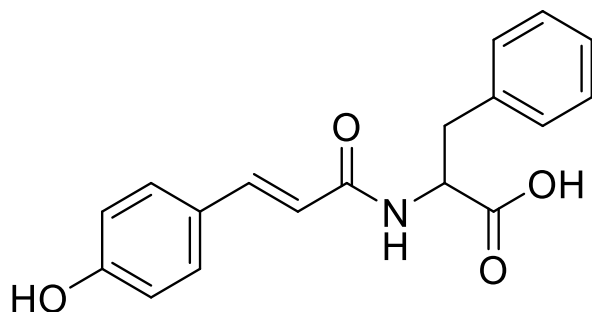
Compound (18a) was prepared according to the general procedure after workup the compound was obtained in 50% yield as a white solid (40 mg). ^1H NMR (d-DMSO, 600MHz): δ 3.84 (d, 2H, $J = 5.9$ Hz), 6.47 (d, 1H, $J = 15.7$ Hz), 6.77 (d, 2H, $J = 8.6$ Hz), 7.32 (d, 1H, $J = 8.6$ Hz), 8.27 (t, 1H). ^{13}C NMR (d-DMSO, 150MHz): 40.8, 115.8, 118.1, 129.3, 139.3, 159.1, 165.7, 167.6, 171.4. HRMS: $\text{C}_{11}\text{H}_{11}\text{NO}_4$ $[\text{M}+\text{H}]_{\text{cal}} m/z$ 222.0761; $[\text{M}+\text{H}]_{\text{exp}} m/z$ 222.0689.

2-[[*(E)*-3-(4-Hydroxyphenyl)prop-2-enoyl]amino]propanoic acid (18b)



Compound (18b) was prepared according to the general procedure after workup the compound was obtained in 83% yield as a white solid (60 mg). HRMS: C₁₂H₁₁NO₄ [M+H]_{cal} *m/z* 236.0917; [M+H]_{exp} *m/z* 236.0789.

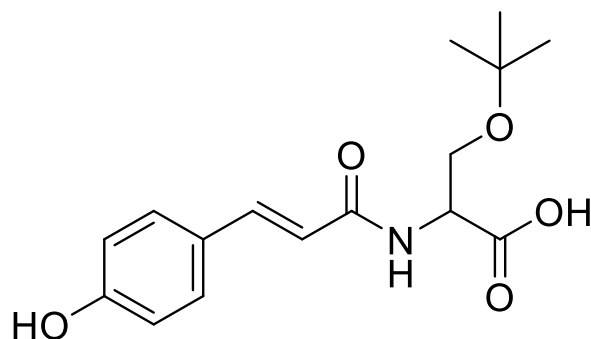
2-[[*(E)*-3-(4-Hydroxyphenyl)prop-2-enoyl]amino]-3-phenyl-propanoic acid (18c)



Compound (18c) was prepared according to the general procedure after workup the compound was obtained in 96% yield as an off-white solid (80 mg). ¹H NMR (d-DMSO, 600MHz): δ 2.85 (dd, 1H, *J* = 9.5, 13.9 Hz), 3.08 (dd, 1H, *J* = 4.8, 13.9 Hz), 4.53 (m, 1H), 6.45 (d, 1H, *J* = 15.8 Hz), 6.76 (d, 1H, *J* = 8.7 Hz), 7.18 (m, 1H), 7.24 (m, 5H), 7.36 (d, 2H, *J* = 8.7 Hz), 8.26 (d, 1H, *J* = 8.1 Hz). ¹³C NMR (d-DMSO, 150MHz): 37.4,

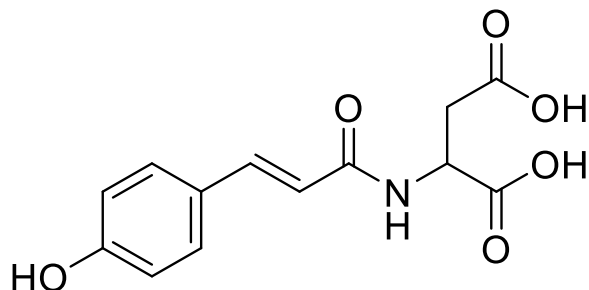
54.1, 116.3, 118.6, 126.3, 128.7, 129.6, 129.8, 138.2, 139.9, 159.5, 165.9, 173.7. HRMS: $C_{18}H_{17}NO_4$ $[M+H]_{cal}$ m/z 312.123; $[M+H]_{exp}$ m/z 312.1251.

3-tert-Butoxy-2-[[*(E)*-3-(4-hydroxyphenyl)prop-2-enoyl]amino]propanoic acid (18d)



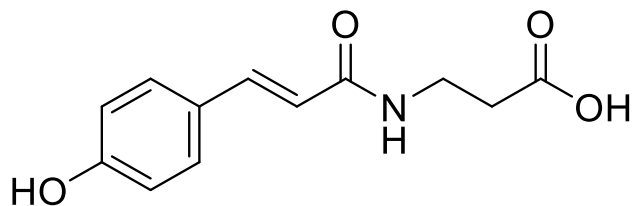
Compound (18d) was prepared according to the general procedure after workup the compound was obtained in 97% yield as a yellow solid (90 mg). 1H NMR (d-DMSO, 600MHz): δ 1.09 (s, 9H), 3.50 (q, 1H, J = 4.1, 9.4 Hz), 3.65 (q, 1H, J = 4.7, 9.4 Hz), 4.46 (q, 1H, J = 4.3, 8.4 Hz), 6.67 (d, 1H, J = 15.8 Hz), 6.76 (d, 2H, J = 8.7 Hz), 7.29 (d, 1H, J = 15.8 Hz), 7.37 (d, 2H, J = 8.6 Hz), 8.00 (d, 1H, J = 8.2 Hz). ^{13}C NMR (d-DMSO, 150MHz): 27.7, 53.4, 62.4, 73.4, 116.3, 118.9, 126.5, 129.8, 139.8, 159.4, 165.9, 172.4. HRMS: $C_{16}H_{21}NO_5$ $[M+H]_{cal}$ m/z 308.1492; $[M+H]_{exp}$ m/z 308.1542.

2-[[*(E)*-3-(4-Hydroxyphenyl)prop-2-enoyl]amino]butanedioic acid (18e)



Compound (18e) was prepared according to the general procedure after workup the compound was obtained in 85% yield as a light yellow solid (40 mg). ^1H NMR (d-DMSO, 600MHz): δ 2.26 (s, 3H), 2.82 (dq, 2H, $J = 5.8, 16.6$ Hz), 3.61 (s, 3H), 3.63 (s, 3H), 4.76 (q, 1H, $J = 6.0$ Hz), 6.68 (d, 1H, $J = 15.8$ Hz), 7.17 (d, 2H, $J = 8.7$ Hz), 7.44 (d, 1H, $J = 15.8$ Hz), 7.61 (d, 2H, $J = 8.7$ Hz), 8.60 (d, 1H, $J = 8.0$ Hz). ^{13}C NMR (d-DMSO, 150MHz): 20.9, 35.7, 48.6, 51.7, 52.2, 121.3, 122.4, 128.8, 132.3, 138.8, 151.4, 164.8, 169.1, 170.5, 171.1. HRMS: $\text{C}_{13}\text{H}_{13}\text{NO}_6$ $[\text{M}+\text{H}]_{\text{cal}} m/z$ 280.0816; $[\text{M}+\text{H}]_{\text{exp}} m/z$ 280.0832.

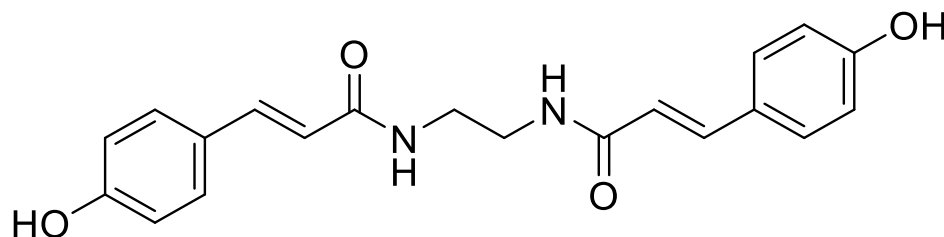
3-[[*(E)*-3-(4-Hydroxyphenyl)prop-2-enoyl]amino]propanoic acid (18f)



Compound (18f) was prepared according to the general procedure after workup the compound was obtained in 99% yield as a light yellow solid (100 mg). ^1H NMR (d-

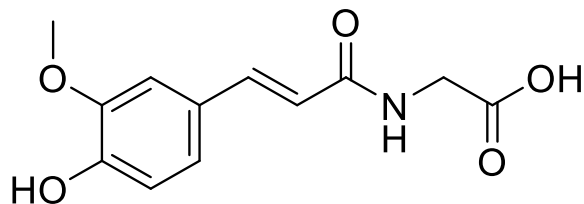
DMSO, 600MHz): δ 2.40 (t, 2H, J = 6.5 Hz), 3.33 (q, 2H, J = 6.7 Hz), 6.40 (d, 1H, J = 15.8 Hz), 6.75 (d, 2H, J = 8.4 Hz), 7.27 (d, 1H, J = 15.7 Hz), 7.34 (d, 2H, J = 8.4 Hz), 8.03 (t, 1H, J = 5.1 Hz). ^{13}C NMR (d-DMSO, 150MHz): δ 34.6, 35.5, 116.3, 119.1, 126.4, 129.7, 139.3, 159.4, 166.0, 173.5. HRMS: $\text{C}_{12}\text{H}_{13}\text{NO}_4$ $[\text{M}+\text{H}]_{\text{cal}}$ m/z 236.0917; $[\text{M}+\text{H}]_{\text{exp}}$ m/z 236.0780.

***(E)*-3-(4-Hydroxyphenyl)-N-[2-[[*(E)*-3-(4-hydroxyphenyl)prop-2-enoyl]amino]ethyl]prop-2-enamide (18g)**



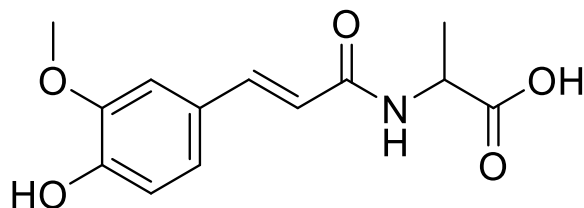
Compound (18g) was prepared according to the general procedure after workup the compound was obtained in 84% yield as a white solid (10 mg). ^1H NMR (d-DMSO, 600MHz): δ 3.25 (t, 4H), 6.38 (d, 2H, J = 15.6 Hz), 6.77 (d, 4H, J = 7.1 Hz), 7.32 (d, 2H, J = 15.7 Hz), 7.38 (d, 4H, J = 7.1 Hz), 8.09 (s, 2H), 9.83 (s, 2H). ^{13}C NMR (d-DMSO, 150MHz): δ 40.2, 115.7, 115.9, 128.0, 129.2, 139.7, 139.9, 157.7, 188.3. HRMS: $\text{C}_{20}\text{H}_{20}\text{N}_2\text{O}_4$ $[\text{M}+\text{H}]_{\text{cal}}$ m/z 353.1496; $[\text{M}+\text{H}]_{\text{exp}}$ m/z 353.1527.

2-[[*(E)*-3-(4-Hydroxy-3-methoxy-phenyl)prop-2-enoyl]amino]acetic acid (19a)



Compound (19a) was prepared according to the general procedure after workup the compound was obtained in 70% yield as a light yellow solid (14 mg). ^1H NMR (d-DMSO, 600MHz): δ 3.77 (s, 3H), 3.82 (d, 2H, J = 5.8 Hz), 6.50 (d, 1H, J = 15.7 Hz), 6.76 (d, 1H, J = 8.1 Hz), 6.97 (dd, 1H, J = 2.0, 8.1 Hz), 7.11 (d, 1H, J = 1.9 Hz), 7.31 (d, 1H, J = 15.7 Hz), 8.19 (t, 1H, J = 5.8 Hz). ^{13}C NMR (d-DMSO, 150MHz): δ 41.4, 56.1, 111.4, 116.2, 118.9, 122.1, 126.8, 140.1, 148.4, 148.9, 166.2, 171.9. HRMS: $\text{C}_{12}\text{H}_{13}\text{NO}_5$ $[\text{M}+\text{H}]_{\text{cal}} m/z$ 252.0866; $[\text{M}+\text{H}]_{\text{exp}} m/z$ 252.0766.

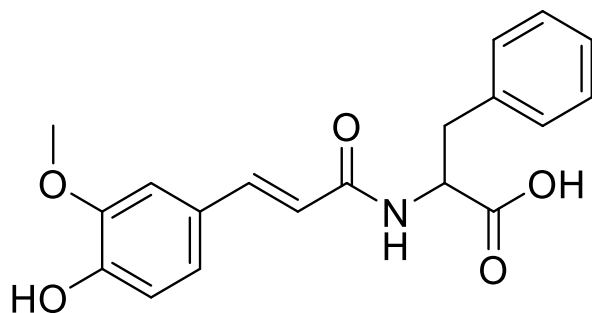
2-[[*(E)*-3-(4-Hydroxy-3-methoxy-phenyl)prop-2-enoyl]amino]propanoic acid (19b)



Compound (19b) was prepared according to the general procedure after workup the compound was obtained in 99% yield as an off-white solid (15 mg). ^1H NMR (d-DMSO, 600MHz): δ 1.27 (d, 3H, J = 7.3 Hz), 3.61 (s, 3H), 4.28 (q, 1H, J = 7.3 Hz), 6.49 (d, 1H, J = 15.7 Hz), 6.76 (d, 1H, J = 8.2 Hz), 6.96 (dd, 1H, J = 1.9, 8.2 Hz), 7.09 (d, 1H,

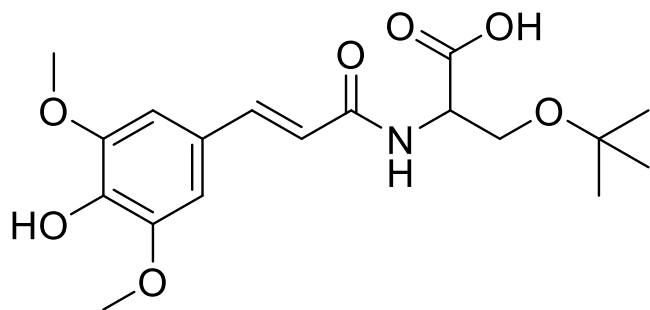
$J = 1.9$ Hz), 7.29 (d, 1H, $J = 15.7$ Hz), 8.19 (d, 1H, $J = 7.3$ Hz). ^{13}C NMR (d-DMSO, 150MHz): δ 17.9, 48.1, 56.0, 111.3, 116.2, 119.1, 122.1, 126.9, 139.9, 148.4, 148.9, 165.6, 174.8. HRMS: $\text{C}_{13}\text{H}_{15}\text{NO}_5$ $[\text{M}+\text{H}]_{\text{cal}} m/z$ 266.1023; $[\text{M}+\text{H}]_{\text{exp}} m/z$ 266.1081.

2-[[*(E)*-3-(4-Hydroxy-3-methoxy-phenyl)prop-2-enoyl]amino]-3-phenyl-propanoic acid (19c)



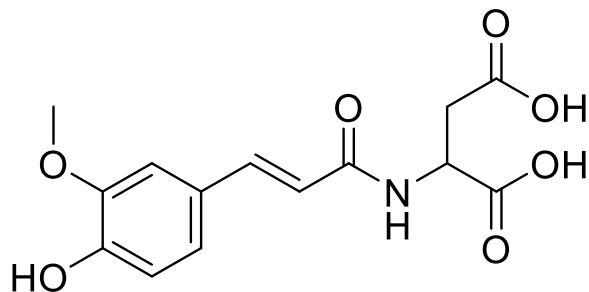
Compound (19c) was prepared according to the general procedure after workup the compound was obtained in 95% yield as an orange solid (6 mg). ^1H NMR (d-DMSO, 600MHz): δ 2.88 (dd, 1H, $J = 9.5, 13.9$ Hz), 3.08 (dd, 1H, $J = 4.8, 14.0$ Hz), 3.76 (s, 3H), 4.52 (se, 1H, $J = 4.8$ Hz), 6.48 (d, 1H, $J = 15.7$ Hz), 6.75 (d, 1H, $J = 8.1$ Hz), 6.93 (dd, 1H, $J = 1.9, 8.1$ Hz), 7.08 (d, 1H, $J = 1.9$ Hz), 7.16 (t, 1H, $J = 7.1$ Hz), 7.23 (m, 5H), 8.18 (d, 1H, $J = 8.1$ Hz). ^{13}C NMR (d-DMSO, 150MHz): δ 37.4, 54.1, 56.0, 111.2, 116.1, 118.9, 122.2, 126.8, 128.7, 129.6, 138.2, 140.1, 148.3, 148.9, 168.9, 173.7. HRMS: $\text{C}_{19}\text{H}_{19}\text{NO}_5$ $[\text{M}+\text{H}]_{\text{cal}} m/z$ 342.1336; $[\text{M}+\text{H}]_{\text{exp}} m/z$ 342.1387.

3-tert-Butoxy-2-[[*(E)*-3-(4-hydroxy-3,5-dimethoxy-phenyl)prop-2-enoyl]amino]propanoic acid (19d)



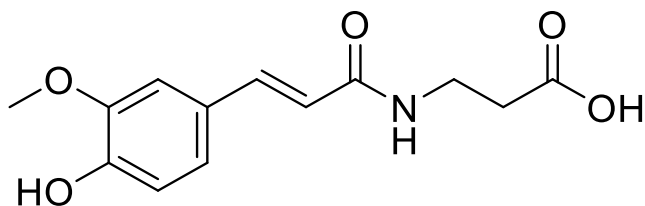
Compound (19d) was prepared according to the general procedure after workup the compound was obtained in 82% yield as an off-white solid (20 mg). ^1H NMR (d-DMSO, 600MHz): δ 1.09 (s, 9H), 3.51 (dd, 1H, $J = 3.9, 9.3$ Hz), 3.66 (dd, 1H, $J = 4.6, 9.3$ Hz), 3.78 (s, 3H), 4.46 (q, 1H, $J = 4.1$ Hz), 6.72 (d, 1H, $J = 15.7$ Hz), 6.76 (d, 1H, $J = 8.1$ Hz), 6.96 (dd, 1H, $J = 1.8, 8.1$ Hz), 7.12 (d, 1H, $J = 1.8$ Hz), 7.29 (d, 1H, $J = 15.7$ Hz), 7.92 (d, 1H, $J = 8.2$ Hz). ^{13}C NMR (d-DMSO, 150MHz): δ 27.7, 53.4, 56.0, 62.4, 73.3, 111.2, 116.1, 119.3, 122.3, 126.9, 139.9, 148.4, 148.9, 165.8, 172.4. HRMS: $\text{C}_{17}\text{H}_{23}\text{NO}_6$ $[\text{M}+\text{H}]_{\text{cal}} m/z$ 338.1598; $[\text{M}+\text{H}]_{\text{exp}} m/z$ 338.1655.

2-[[[(E)-3-(4-Hydroxy-3-methoxy-phenyl)prop-2-enoyl]amino]butanedioic acid (19e)



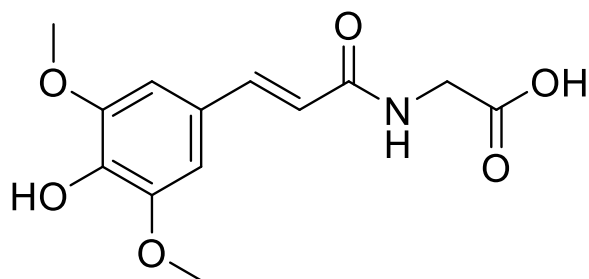
Compound (19e) was prepared according to the general procedure after workup the compound was obtained in 99% yield as an off-white solid (21 mg). ^1H NMR (d-DMSO, 600MHz): δ 2.62 (q, 1H, $J = 7.1$ Hz), 2.69 (q, 1H, $J = 5.4$ Hz), 3.77 (s, 3H), 4.62 (q, 1H, $J = 7.1$ Hz), 6.54 (d, 1H, $J = 15.7$ Hz), 6.76 (d, 1H, $J = 8.1$ Hz), 6.96 (dd, 1H, $J = 1.8, 8.1$ Hz), 7.11 (d, 1H, $J = 1.8$ Hz), 7.29 (d, 1H, $J = 15.7$ Hz), 8.19 (d, 1H, $J = 8.1$ Hz). ^{13}C NMR (d-DMSO, 150MHz): δ 36.7, 49.2, 56.0, 111.2, 116.1, 119.0, 122.3, 126.8, 140.2, 148.4, 148.9, 165.7, 172.3, 173.0. HRMS: $\text{C}_{14}\text{H}_{15}\text{NO}_7$ $[\text{M}+\text{H}]_{\text{cal}} m/z$ 310.0921; $[\text{M}+\text{H}]_{\text{exp}} m/z$ 310.0965.

3-[[[(E)-3-(4-Hydroxy-3-methoxy-phenyl)prop-2-enoyl]amino]propanoic acid (19f)



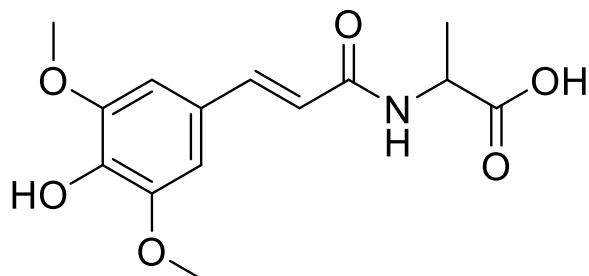
Compound (19f) was prepared according to the general procedure after workup the compound was obtained in 54% yield as an off-white solid (40 mg). ^1H NMR (d-DMSO, 600MHz): δ 2.40 (t, 2H, $J = 6.8$ Hz), 3.32 (q, 2H, $J = 6.7$ Hz), 3.76 (s, 3H), 6.42 (d, 1H, $J = 15.7$ Hz), 6.75 (d, 1H, $J = 8.1$ Hz), 6.94 (dd, 1H, $J = 1.9, 8.1$ Hz), 7.08 (d, 1H, $J = 1.9$ Hz), 7.27 (d, 1H, $J = 15.7$ Hz), 7.99 (t, 1H, $J = 5.6$ Hz). ^{13}C NMR (d-DMSO, 150MHz): δ 33.0, 33.9, 55.5, 110.8, 115.6, 121.5, 126.4, 139.0, 147.8, 148.2, 165.4, 172.9. HRMS: $\text{C}_{13}\text{H}_{15}\text{NO}_5$ $[\text{M}+\text{H}]_{\text{cal}} m/z$ 266.1023; $[\text{M}+\text{H}]_{\text{exp}} m/z$ 266.0970.

2-[[*(E)*-3-(4-Hydroxy-3,5-dimethoxy-phenyl)prop-2-enoyl]amino]acetic acid (20a)



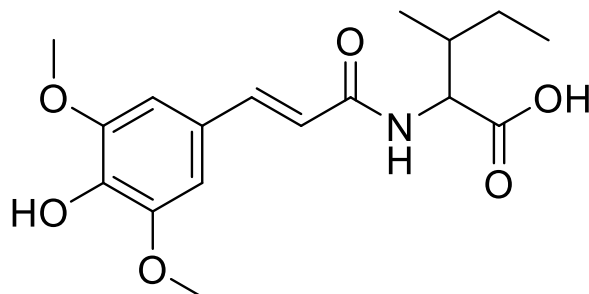
Compound (20a) was prepared according to the general procedure after workup the compound was obtained in 99% yield as an off-white solid (10 mg). ^1H NMR (d-DMSO, 600MHz): δ 3.76 (s, 6H), 3.83 (d, 2H, $J = 5.8$ Hz), 6.58 (d, 1H, $J = 15.7$ Hz), 6.84 (s, 2H), 7.31 (d, 1H, $J = 15.7$ Hz), 8.16 (t, 1H, $J = 5.8$ Hz). HRMS: $\text{C}_{13}\text{H}_{15}\text{NO}_6$ $[\text{M}+\text{H}]_{\text{cal}} m/z$ 282.0972; $[\text{M}+\text{H}]_{\text{exp}} m/z$ 282.0869.

2-[[*(E)*-3-(4-Hydroxy-3,5-dimethoxy-phenyl)prop-2-enoyl]amino]propanoic acid (20b)



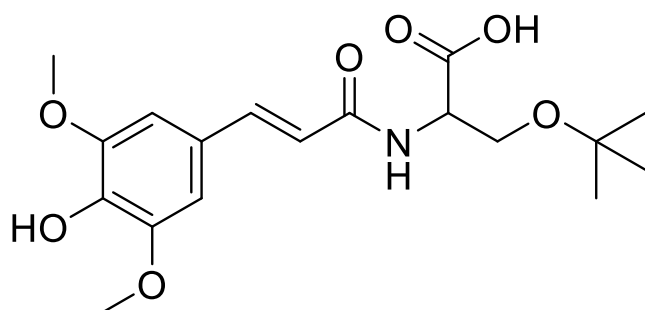
Compound (20b) was prepared according to the general procedure after workup the compound was obtained in 60% yield as a light yellow solid (27 mg). ^1H NMR (d-DMSO, 600MHz): δ 1.28 (d, 3H, $J = 7.2$ Hz), 3.76 (s, 6H), 4.28 (q, 1H, $J = 5.7$ Hz), 6.54 (d, 1H, $J = 15.0$ Hz), 6.83 (s, 2H), 7.30 (d, 1H, $J = 19.6$ Hz), 8.18 (d, 1H, $J = 6.4$ Hz). HRMS: $\text{C}_{14}\text{H}_{17}\text{NO}_6$ $[\text{M}+\text{H}]_{\text{cal}} m/z$ 296.1129; $[\text{M}+\text{H}]_{\text{exp}} m/z$ 296.1153.

2-[[*(E)*-3-(4-Hydroxy-3,5-dimethoxy-phenyl)prop-2-enoyl]amino]-3-methyl-pentanoic acid (20c)



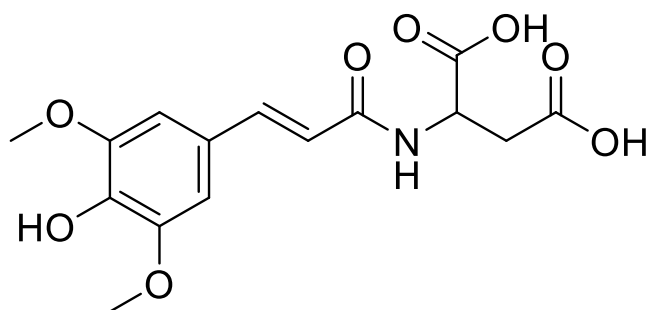
Compound (20c) was prepared according to the general procedure after workup the compound was obtained in 73% yield as a light yellow solid (16 mg). ^1H NMR (d-DMSO, 600MHz): δ 0.839 (q, 6H, $J = 7.05, 15.8$ Hz), 1.39 (m, 1H), 1.79 (m, 1H), 3.76 (s, 6H), 4.27 (dd, 2H, $J = 6.0, 8.5$ Hz), 6.68 (d, 1H, $J = 15.8$ Hz), 6.82 (s, 2H), 7.28 (d, 1H, $J = 15.6$ Hz), 8.01 (d, 1H, $J = 8.4$ Hz). HRMS: $\text{C}_{17}\text{H}_{23}\text{NO}_6$ $[\text{M}+\text{H}]_{\text{cal}}$ m/z 338.1598; $[\text{M}+\text{H}]_{\text{exp}}$ m/z 338.1488.

3-tert-Butoxy-2-[[*(E)*-3-(4-hydroxy-3,5-dimethoxy-phenyl)prop-2-enoyl]amino]propanoic acid (20d)



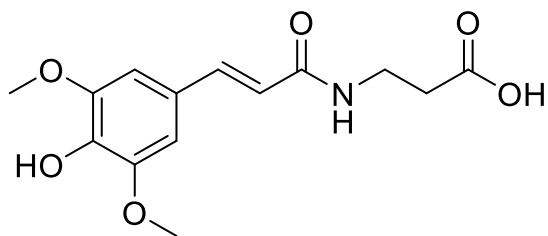
Compound (20d) was prepared according to the general procedure after workup the compound was obtained in 95% yield as an yellow solid (82 mg). ^1H NMR (d-DMSO, 600MHz): δ 1.09 (s, 9H), 3.51 (m, 1H), 3.66 (m, 1H), 3.76 (s, 6H), 4.47 (q, 1H, $J = 4.3$ Hz), 6.77 (d, 1H, $J = 15.8$ Hz), 6.85 (s, 2H), 7.29 (d, 1H, $J = 15.7$ Hz), 7.89 (d, 1H, $J = 8.1$ Hz). HRMS: $\text{C}_{18}\text{H}_{25}\text{NO}_7$ $[\text{M}+\text{H}]_{\text{cal}}$ m/z 368.1704; $[\text{M}+\text{H}]_{\text{exp}}$ m/z 368.1777.

2-[[*(E)*-3-(4-Hydroxy-3,5-dimethoxy-phenyl)prop-2-enoyl]amino]butanedioic acid (20e)



Compound (20e) was prepared according to the general procedure after workup the compound was obtained in 98% yield as a light yellow solid (20 mg). ^1H NMR (d-DMSO, 600MHz): δ 2.66 (qd, 2H, J = 5.6, 16.6 Hz), 3.76 (s, 6H), 4.61 (q, 1H, J = 6.6 Hz), 6.59 (d, 1H, J = 13.2 Hz), 6.84 (s, 2H), 7.30 (d, 1H, J = 18.4 Hz), 8.16 (d, 1H, J = 7.4 Hz). HRMS: $\text{C}_{15}\text{H}_{17}\text{NO}_8$ $[\text{M}+\text{H}]_{\text{cal}}$ m/z 340.1027; $[\text{M}+\text{H}]_{\text{exp}}$ m/z 340.1051.

3-(3-(4-Hydroxy-3,5-dimethoxyphenyl)acrylamido)propanoic acid (20f)



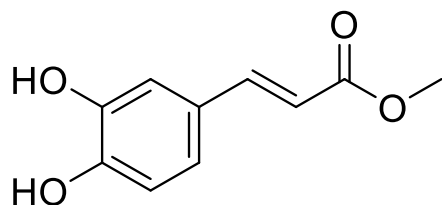
Compound (20f) was prepared according to the general procedure after workup the compound was obtained in 98% yield as a light yellow solid (20 mg). ^1H NMR (d-DMSO, 600MHz): δ 2.39 (t, 2H, J = 6.8 Hz), 2.81 (q, 2H, J = 5.9 Hz), 3.74 (s, 6H), 6.44

(d, 1H, $J = 15.7$ Hz), 6.80 (s, 2H), 7.27 (d, 1H, $J = 15.7$ Hz), 7.99 (t, 1H, $J = 7.9$ Hz). ^{13}C NMR (d-DMSO, 150MHz): δ 20.7, 36.2, 49.2, 52.3, 56.6, 104.9, 122.4, 129.5, 133.6, 140.0, 152.5, 165.3, 168.6, 171.0, 171.7.

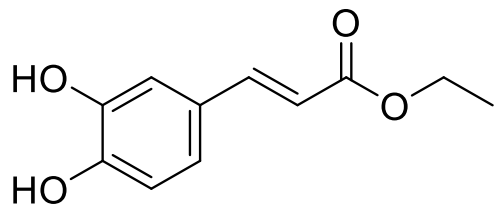
5.1.5 Fischer Esterification

HCA (**1,2**) (0.278 mmol, 1.00 eq) was dissolved in MeOH, EtOH, or PrOH (5 ml), treated with H_2SO_4 (0.902 mmol, 3.25 eq), and refluxed for 4h. The reaction mixture was then diluted with EtOAc (10 ml), washed with NaHCO_3 (2 x 5 mL) and then with H_2O (3 x 5 mL), dried over Na_2SO_4 and evaporated to obtain **22a-c** and **23**.

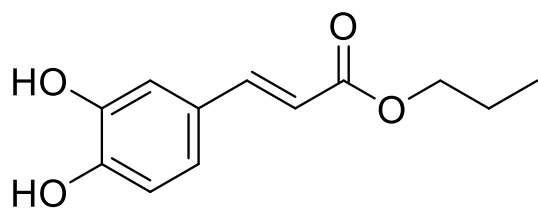
Methyl (E)-3-(3,4-dihydroxyphenyl)prop-2-enoate (22a)



Compound (22a) was prepared according to the general procedure after workup the compound was obtained in 56% yield as an off-white solid (72 mg). ^1H NMR (d-DMSO, 600MHz): δ 3.65 (s, 3H), 6.24 (d, 1H, $J = 15.9$ Hz), 6.72 (d, 1H, $J = 8.2$ Hz), 6.97 (dd, 1H, $J = 2.1, 8.2$ Hz), 7.02 (d, 1H, $J = 2.1$ Hz), 7.45 (d, 1H, $J = 15.9$ Hz). ^{13}C NMR (d-DMSO, 150MHz): 51.8, 114.2, 115.3, 116.2, 122.0, 126.0, 145.7, 146.1, 149.0, 167.6.

Ethyl (E)-3-(3,4-dihydroxyphenyl)prop-2-enoate (22b)

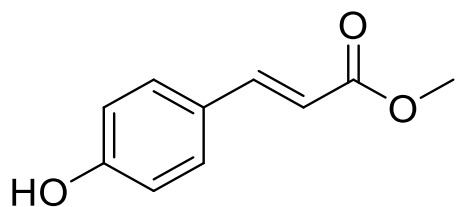
Compound (22b) was prepared according to the general procedure after workup the compound was obtained in 51% yield as a light orange solid (30 mg). ^1H NMR (d-DMSO, 600MHz): δ 1.20 (t, 3H, $J = 7.1$ Hz), 4.11 (q, 2H, $J = 7.1$ Hz), 6.22 (d, 1H, $J = 15.9$ Hz), 6.72 (d, 1H, $J = 8.1$ Hz), 6.96 (dd, 1H, $J = 1.8, 8.2$ Hz), 7.00 (d, 1H, $J = 1.9$ Hz), 7.43 (d, 1H, $J = 15.9$ Hz). ^{13}C NMR (d-DMSO, 150MHz): 14.8, 60.2, 114.5, 115.3, 116.2, 121.9, 145.6, 146.1, 167.1.

Propyl (E)-3-(3,4-dihydroxyphenyl)prop-2-enoate (22c)

Compound (22c) was prepared according to the general procedure after workup the compound was obtained in 99% yield as a yellow solid (120 mg). ^1H NMR (d-DMSO, 600MHz): δ 0.88 (t, 3H, $J = 7.4$ Hz), 1.60 (t, 2H, $J = 6.7$ Hz), 4.03 (t, 2H, $J = 6.7$ Hz), 6.23 (d, 1H, $J = 15.9$ Hz), 6.72 (d, 1H, $J = 8.2$ Hz), 6.97 (dd, 1H, $J = 2.1, 8.2$ Hz), 7.01 (d, 1H,

$J = 2.1$ Hz), 7.44 (d, 1H, $J = 15.9$ Hz). ^{13}C NMR (d-DMSO, 150MHz): 10.9, 22.2, 65.7, 114.5, 115.3, 116.2, 121.9, 126.0, 145.5, 146.1, 148.9, 167.2.

Methyl (E)-3-(4-hydroxyphenyl)prop-2-enoate (23)

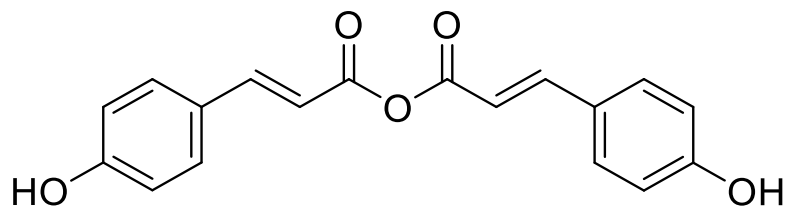


Compound (23) was prepared according to the general procedure after workup the compound was obtained in 70% yield as a white solid (350 mg). ^1H NMR (d-DMSO, 600MHz): δ 3.65 (s, 3H), 6.36 (d, 1H, $J = 16.0$ Hz), 6.76 (d, 2H, $J = 8.7$ Hz), 7.52 (m, 3H), 9.99 (s, 1H). ^{13}C NMR (d-DMSO, 150MHz): δ 51.8, 114.4, 116.3, 125.6, 130.9, 145.3, 160.4, 167.6. HRMS: $\text{C}_{10}\text{H}_{10}\text{O}_3$ $[\text{M}+\text{H}]_{\text{cal}} m/z$ 193.0733; $[\text{M}+\text{H}]_{\text{exp}} m/z$ 193.0704.

5.1.6 HCA Anhydride

HCA (**2**) (1.827 mmol, 2.00 eq) was dissolved in DCM (15 mL) and treated with 1-ethyl-3-(3-dimethylaminopropyl)carbodiimide (EDC; 0.914 mmol, 1.00 eq) at 0°C, then stirred at rt for 8 hours. THF (10 mL) was then added, and mixture was stirred overnight. The mixture was washed with water (1 x 10 mL) and brine (1 x 10 mL) then dried over Na_2SO_4 . Solvent removed under reduced pressure to obtain **21**.

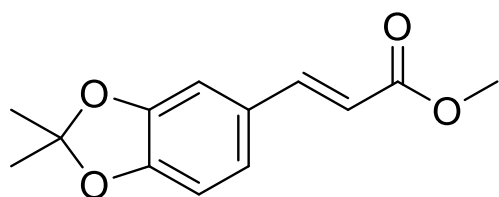
3-(4-Hydroxyphenyl)prop-2-enoyl-3-(4-hydroxyphenyl)prop-2-enoate (21)



Compound (21) was prepared according to the general procedure after workup the compound was obtained in 98% yield as a white solid (285 mg). ^1H NMR (d-DMSO, 600MHz): δ 6.53 (d, 2H, $J = 15.9$ Hz), 6.82 (m, 4H), 7.64 (m, 4H), 7.76 (d, 2H, $J = 15.9$ Hz). ^{13}C NMR (d-DMSO, 150MHz): δ 115.9, 116.3, 116.5, 130.6, 131.8, 144.7, 160.1, 168.5. HRMS: $\text{C}_{18}\text{H}_{14}\text{O}_5$ $[\text{M}+\text{H}]_{\text{cal}} m/z$ 311.0914; $[\text{M}+\text{H}]_{\text{exp}} m/z$ 311.0914.

5.1.7 Alternative Protecting Groups

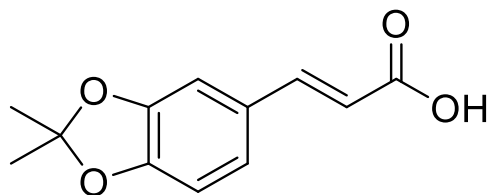
Methyl-3-(2,2-dimethyl-1,3-benzodioxol-5-yl)prop-2-enoate (24)



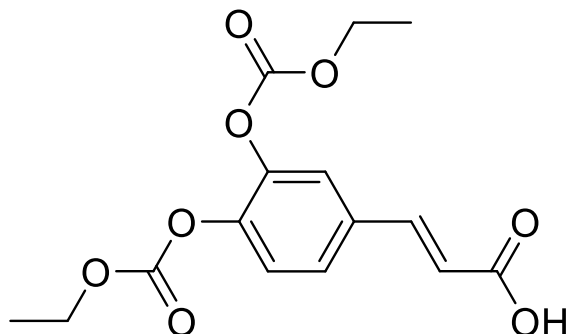
Compound (24) was prepared according to the following procedure caffeic acid methyl ester, 22a, (1.030 mmol, 1.00 eq) was added to CHCl_3 (20 ml) and stirred for 5 min at room temperature. The mixture was then treated with 2,2-dimethoxypropane (3.244 mmol, 3.15 eq) and pTsOH (0.124 mmol, 0.12 eq) and then refluxed overnight.

The mixture was evaporated under reduced pressure to an off-white solid at 85% yield (200 mg) and then pushed forward without further purification. ^1H NMR (d-DMSO, 600MHz): δ 1.64 (s, 6H), 3.68 (s, 3H), 6.47 (d, 1H, $J = 15.8$ Hz), 6.85 (d, 1H, $J = 8.3$ Hz), 7.14 (dd, 1H, $J = 1.4, 8.3$ Hz), 7.31 (d, 1H, $J = 1.4$ Hz), 7.55 (d, 1H, $J = 15.8$ Hz). ^{13}C NMR (d-DMSO, 150MHz): δ 25.5, 51.3, 106.5, 108.3, 115.2, 118.9, 124.7, 128.0, 144.6, 147.6, 149.0, 166.9.

3-(2,2-Dimethyl-1,3-benzodioxol-5-yl)prop-2-enoic acid (24a)

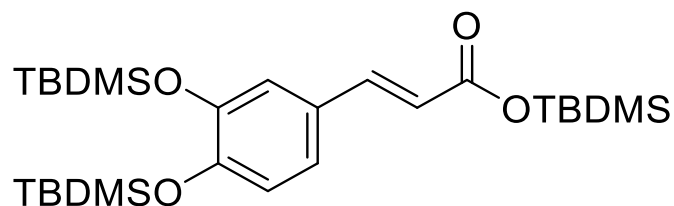


Selective deprotection of the methyl ester proceeded with the addition of the product with LiOH (90 mg) in MeOH:H₂O 1:1 (12 ml) at room temperature overnight after workup the compound was obtained in 60% yield as an orange solid (140 mg), compound (24a). ^1H NMR (d-DMSO, 600MHz): δ 1.64 (s, 6H), 6.35 (d, 1H, $J = 15.8$ Hz), 6.84 (d, 1H, $J = 8.3$ Hz), 7.10 (d, 1H, $J = 6.9$ Hz), 7.26 (s, 1H), 7.47 (d, 1H, $J = 15.8$ Hz). ^{13}C NMR (d-DMSO, 150MHz): δ 25.5, 106.5, 108.3, 116.6, 118.8, 124.3, 128.2, 144.0, 147.6, 148.7, 167.8.

3-[3,4-bis(Ethoxycarbonyloxy)phenyl]prop-2-enoic acid (25)

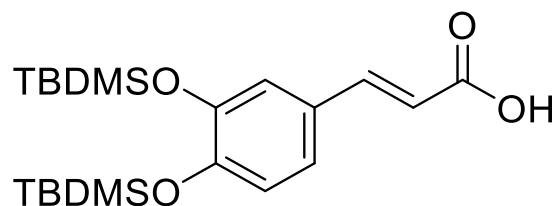
Compound (25) was prepared according to the following procedure caffeic acid (2.775 mmol, 1.00 eq) was dissolved in 1M NaOH (9 ml) and stirred in an ice bath. The mixture was treated with ethylchloroformate (5.551 mmol, 2.00 eq) dropwise, allowed to come to room temperature and stirred for 5 hours. The mixture was poured over water (75 ml) and extracted with EtOAc (20 ml x 3) and washed with H₂O (10 ml), brine (10 ml), 1M HCl (10 ml), and H₂O (10 ml). The organic was then dried with Na₂SO₄ and the solvent was removed under reduced pressure and the compound was obtained in 25% yield as a light orange solid (250 mg). ¹H NMR (d-DMSO, 600MHz): δ 1.25 (t, 6H, *J* = 7.0 Hz), 4.23 (q, 4H, *J* = 7.1 Hz), 6.55 (d, 1H, *J* = 15.9 Hz), 7.44 (d, 1H, *J* = 8.4 Hz), 7.56 (d, 1H, *J* = 15.9 Hz), 7.66 (d, 1H, *J* = 8.6 Hz), 7.80 (d, 1H, *J* = 11.0 Hz). ¹³C NMR (d-DMSO, 150MHz): δ 14.5, 65.9, 121.4, 123.2, 124.3, 127.7, 134.1, 142.4, 142.8, 143.6, 152.3, 152.4, 167.9. (Scheme 8)

[*tert*-Butyl(dimethyl)silyl] (*E*)-3-[3,4-bis[[*tert*-butyl(dimethyl)silyl]oxy]phenyl]prop-2-enoate (26)



Caffeic acid (2.775 mmol, 1.00 eq) was dissolved in DCM (14 ml) under N₂ and treated with TBDMSCl (9.714 mmol, 3.50 eq), Et₃N (18.04 mmol, 6.50 eq) and DMAP (0.278 mmol, 0.10 eq) and was stirred at room temperature for 12 hours. The product was dissolved in DCM (20 ml) and washed with 0.1 M HCl (10 ml x 5) and brine (10 ml) and then dried over Na₂SO₄ to an off white solid in 99% yield (1.43g). ¹H NMR (d-DMSO, 600MHz): δ -0.09 (s, 18H), 0.79 (s, 27H), 6.13 (d, 1H, *J* = 15.8 Hz), 6.71 (d, 1H, *J* = 8.3 Hz), 6.91 (dd, 1H, *J* = 2.1, 8.3 Hz), 6.98 (d, 1H, *J* = 2.1 Hz), 7.36 (d, 1H, *J* = 15.8 Hz).

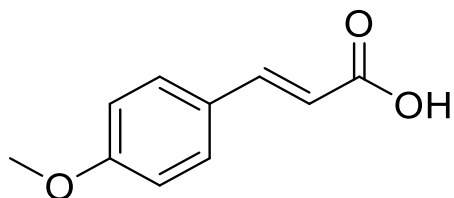
(*E*)-3-[3,4-bis[[*tert*-Butyl(dimethyl)silyl]oxy]phenyl]prop-2-enoic acid (26a)



The product was then pushed forward for selective deprotection (0.191 mmol, 1.00 eq) was dissolved in MeOH: H₂O 1:1 (3 mL) and treated with K₂CO₃ (0.191 mmol, 1.00

eq) and stirred at room temperature for 5 hours. For workup, the clear reaction mixture was added to Et₂O (15 ml) and washed with 0.1M HCl (10 ml x 4) and dried over Na₂SO₄ to a gray solid in 85% yield. ¹H NMR (d-DMSO, 600MHz): δ 0.163 (s, 12H), 0.92 (s, 18H), 6.28 (d, 1H, *J* = 15.9 Hz), 6.84 (d, 1H, *J* = 8.3 Hz), 7.10 (d, 1H, *J* = 2.1 Hz), 7.17 (dd, 1H, *J* = 2.0, 8.3 Hz), 7.46 (d, 1H, *J* = 15.9 Hz).

3-(4-Methoxyphenyl)prop-2-enoic acid (27)



Malonic acid (5.509 mmol, 3.00 eq), 4-methoxybenzaldehyde (1.836 mmol, 1.00 eq) and pyridine (6 drops) were combined in DMF (3 ml) and was refluxed at 90°C overnight. The mixture was worked up with H₂O (15 ml) and acidified to p ¹H NMR (d-DMSO, 600MHz): δ 3.76 (s, 3H), 6.34 (d, 1H, *J* = 15.9 Hz), 6.94 (dd, 2H, *J* = 1.8, 6.9 Hz), 7.51 (d, 1H, *J* = 15.9 Hz), 7.60 (dd, 2H, *J* = 1.8, 6.9 Hz). ¹³C NMR (d-DMSO, 150MHz): δ 55.9, 114.8, 114.9, 117.0, 127.3, 130.4, 144.3, 161.4, 168.4. HRMS: C₁₀H₁₀O₃ [M+H]_{cal} *m/z* 193.0733; [M+H]_{exp} *m/z* 193.0865.

5.1.8 General Procedure: Amino Acid Esterification

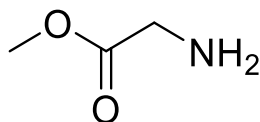
Amidation was carried out with amino acid methyl esters that had been prepared through esterification with SOCl₂ in MeOH.

Glycine (700 mg, 9.325 mmol, 1.00 eq) suspended in MeOH (62 mL) and treated with acetyl chloride (1.331 mL, 18.649 mmol, 2.00 eq) in ice bath, allowed to stir for 5

minutes and refluxed at 70°C for 2h, time differed between compounds tracked by TLC.

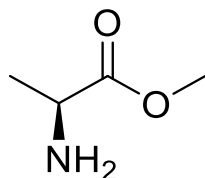
Solution concentrated under reduced pressure to white powder.

Methyl 2-aminoacetate



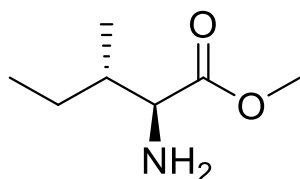
^1H NMR (d-DMSO, 600MHz): δ 3.67 (s, 3H), 3.76 (s, 1H). ^{13}C NMR (d-DMSO, 150MHz): δ 40.1, 53.4, 168.8.

Methyl (2S)-2-aminopropanoate



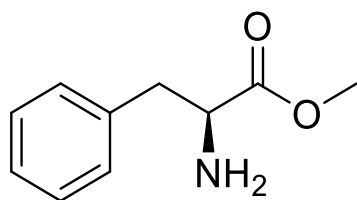
^1H NMR (d-DMSO, 600MHz): δ 2.46 (d, 3H), 2.97 (q, 2H), 3.60 (s, 3H). ^{13}C NMR (d-DMSO, 150MHz): δ 31.8, 35.1, 52.3, 171.3.

2,3-Methyl 2-amino-3-methylpentanoate



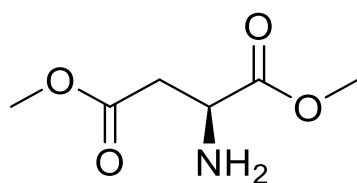
^1H NMR (d-DMSO, 600MHz): δ 1.41 (t, 3H), 1.53 (d, 3H), 1.89 (m, 2H), 2.08 (m, 1H), 3.72 (s, 3H), 4.60 (d, 1H). ^{13}C NMR (d-DMSO, 150MHz): δ 11.9, 14.8, 25.8, 36.4, 53.1, 56.6, 169.6.

(S)-Methyl 2-amino-3-phenylpropanoate



^1H NMR (d-DMSO, 600MHz): δ 3.04 (m, 1H), 3.15 (m, 1H), 3.60 (s, 3H), 4.19 (t, 1H), 7.19 (d, 2H), 7.23 (t, 1H), 7.30 (t, 2H). ^{13}C NMR (d-DMSO, 150MHz): δ 36.4, 53.2, 53.9, 127.9, 129.2, 130.0, 135.2, 169.9.

Dimethyl (2S)-2-aminobutanedioate



^1H NMR (d-DMSO, 600MHz): δ 2.95 (m, 2H), 3.61 (s, 3H), 3.69 (s, 3H), 4.31 (s, 1H).

^{13}C NMR (d-DMSO, 150MHz): δ 34.5, 48.9, 52.7, 53.6, 169.2, 170.1.

5.2 DPPH Assay

Based on an assay described previously, a methanolic DPPH solution (0.09136 mM) was prepared (Xie & Schaich, 2014). Derivative samples were prepared at multiple

concentrations (200 to 5 mM) in MeOH. DPPH solution (1 mL) was added into a micro quartz cuvette followed by the tested compound dilution (10 μ L), reaction was tracked by UV/Vis spectroscopy at 515 nm over 10 minutes. Each reaction was done in triplicate. The UV/Vis spectrophotometer used in the analysis was a Perkin Elmer Lambda 35 UV/VIS Spectrometer.

$$\text{Radical Scavenging \%} = \frac{\text{Abs of Blank} - \text{Abs of Sample}}{\text{Abs of Blank}} \times 100$$

Percent radical scavenging was calculated with Abs_{Blank} as absorbance of the DPPH unaffected by any compounds and Abs_{sample} as the observed absorbance at each time point of analysis for DPPH with the tested compound. Methanol was used as the solvent to afford effective solubility and the extend the lifetime of the radical. The assay was tracked over the course of 10 minutes at various time points allowing for an assessment of the velocity of reactivity with the ligand.

5.3 Protein-Ligand Interaction Characterization

5.3.1 α -Amylase Inhibition Assay

Based on an assay described previously, determination of α -amylase inhibition was carried out via the starch-iodine method with modifications (Xiao et al., 2006). The technique was transferred to scale appropriate for 96 microwell plate. This format made additional transfer of solutions/aliquots obsolete and minimized experimental error. Porcine pancreas α -amylase was prepared in 10 mM phosphate buffer at 0.25 mg/ml, potato starch was prepared at 0.5 mg/ml by first diluting into 5 ml of the cold buffer and then into 195 ml of boiling buffer, inhibitors were prepared in 20% methanol, KI was mixed into water followed by the addition and dissolution of I₂ at 5 mM, and 1 M HCl was prepared. The assay was carried out by adding starch (100 μ L), ligand (40 μ L), then α -

amylase (100 mL) followed by incubation at 37°C for 15 min followed by 1 M HCl (20 mL) and iodine solution (40 mL). During incubation, a microwell plate mat was used to avoid evaporation. The plate was immediately read by the plate reader (Tecan Infinite 200 Pro) at 580 nm. The assays were all completed in triplicate on multiple days with various stock solutions.

5.3.2 NMR and STD-NMR

NMR spectra were acquired on an ECA-600 JEOL NMR spectrometer at room temperature in deuterated chloroform, DMSO- d_6 and/or D₂O, using the solvent signals (7.25 ppm, 2.50 ppm, and 4.80 ppm, respectively) as the internal reference.

HCAs were prepared at 5 mM concentration and mixed with 10 μ M α -amylase in 10% DMSO- d_6 and 90% D₂O. Each HCA was prepared separately for structure determination, integration comparison, and assignment of signals. STD spectra were acquired with the “sat_transfer_difference” experiment including an on-resonance frequency of 0.9 ppm and an off-resonance frequency of -40 ppm. All spectra were acquired with a 5 ppm offset and a spectral width of 15 ppm at rt with sample spinning (15 Hz). The temperature was constant at 24 °C, and 8192 scans were collected at a resolution of 4096 datapoints and were zero-filled 4x. The relaxation delay of 3 s was long enough for complete T₁ relaxation between pulses, and the receiver gain of 50 was adequate for all samples at the concentration described above.

5.3.3 Intrinsic Fluorescence Quenching

Florescence experiments were carried out on a Perkin Elmer LS 55 Fluorescence Spectrometer. Emission spectra were recorded between 300 and 500 nm with an excitation of 280 nm used. Solutions of ligands (1 mg/ml) in 40:60 MeOH:H₂O and α -

amylase (0.5 mg/ml) in 10 mM buffer were prepared. Each sample was made to hold enzyme concentration constant with increasing amount of ligand. The final concentration of α -amylase was 0.25 mg/ml and ligands ranged from 1.25 to 10 μ g/ml.

5.3.4 Molecular docking

Ligands were drawn and loaded in ChemDraw and minimized using Chem3D. Resulting ligand conformations were analyzed for interaction utilizing AutoDock Vina 1.1.2 and AutoDock Tools 1.5.6 (Trott & Olson, 2010). The enzyme structure (PDB 1OSE) was loaded from The PDB Database (Gilles et al., 1996). The protein was opened in AutoDock Tools and prepared by removing water and adding polar hydrogens. The gridbox was centered around the present ligand and recorded. Following gridbox setup, the present ligand was removed, and the macromolecule was saved as PDBQT. The ligand was loaded, and torsions were selected to allow all available bonds to be flexible. The ligand was then saved as a PDBQT. The grid box for docking was set at 40 \times 40 \times 52 pts. A configuration file was created listing the grid box settings and generic exhaustiveness with an appropriate output file generating 9 possible formations ranked by resulting Kcal/mol. AutoDock Vina was run three times to compare top scores with default settings. Interactions and docking results were analyzed via PyMol (The PyMol Molecular Graphics System, Version 3.2.2, Schrödinger, LLC.).

5.3.5 Native MS – Model Proteins

The protein stock solution was prepared at 1 mg/ml in 10 mM ammonium phosphate buffer, ligands were prepared in ammonium bicarbonate buffer at 1 mg/ml. The protein (10 μ L) and ligands (200 μ L) were mixed lightly and then incubated for 30 minutes at 37°C. The BSA-HCA study was performed using the 6530 LC/Q-TOF mass

spectrometer (Agilent Technologies) equipped with an Agilent Jet Stream (AJS) source utilizing an Infinity II 1290 HPLC. The mobile phase was 100 mM ammonium acetate (pH 7) at a flow rate of 0.4 ml/min and injection volume of 10 μ L. The column used was an Agilent AdvanceBio SEC guard column, 4.6 x 30 mm, 1.9 μ m that was maintained at room temperature. The gradient was isocratic and run for 6 minutes. Spectra were acquired over a range of m/z 600 – 4800 in positive ion mode. The source parameters were drying gas temperature 365°C, drying gas flow 12 L min⁻¹, nebulizer gas 60 psi, sheath gas temperature, sheath gas flow 12 L min⁻¹, capillary voltage 4500 V, nozzle voltage 2000 V, and fragmentor voltage 250 V. Each experiment was repeated in triplicate. The carbonic anhydrase – HCA study was performed using the 6545XT LC/Q-TOF mass spectrometer (Agilent Technologies) the parameters above were kept the same apart from the change to a flow injection method, bypassing the desalting of the SEC column employed with the BSA experiment.

References

- Adams, R., & Ulich, L. H. (1920). The use of oxalyl chloride and bromide for producing acid chlorides, acid bromides or acid anhydrides. *Journal of the American Chemical Society*, 42(3), 599-611. doi:10.1021/ja01448a024
- Adem, Ş., Eyupoglu, V., Sarfraz, I., Rasul, A., Zahoor, A. F., Ali, M., . . . Elfiky, A. A. (2021). Caffeic acid derivatives (CAFDs) as inhibitors of SARS-CoV-2: CAFDs-based functional foods as a potential alternative approach to combat COVID-19. *Phytomedicine*, 85, 153310. doi:10.1016/j.phymed.2020.153310
- AG, H. B. B. (1994). Pharmacology of α -glucosidase inhibition. *European Journal of Clinical Investigation*, 24(S3), 3-10. doi:<https://doi.org/10.1111/j.1365-2362.1994.tb02249.x>
- Aleixandre, A., Gil, J. V., Sineiro, J., & Rosell, C. M. (2022). Understanding phenolic acids inhibition of α -amylase and α -glucosidase and influence of reaction conditions. *Food Chem*, 372, 131231. doi:10.1016/j.foodchem.2021.131231
- Arabaci, B., Gulcin, I., & Alwasel, S. (2014). Capsaicin: a potent inhibitor of carbonic anhydrase isoenzymes. *Molecules*, 19(7), 10103-10114. doi:10.3390/molecules190710103
- Aue, W. P., Bartholdi, E., & Ernst, R. R. (1976). Two-dimensional spectroscopy. Application to nuclear magnetic resonance. *Journal of Chemical Physics*, 64, 2229-2246.
- Bailey, J. M., & Whelan, W. J. (1961). Physical properties of starch. I. Relationship between iodine stain and chain length. *J Biol Chem*, 236, 969-973.
- Barrett, M. L., & Udani, J. K. (2011). A proprietary alpha-amylase inhibitor from white bean (*Phaseolus vulgaris*): A review of clinical studies on weight loss and glycemic control. *Nutrition Journal*, 10(1), 24. doi:10.1186/1475-2891-10-24
- Blair, M. (2016). Diabetes Mellitus Review. *Urologic Nursing*, 36(1), 27-36. doi:10.7257/1053-816X.2016.36.1.27
- Blois, M. S. (1958). Antioxidant Determinations by the Use of a Stable Free Radical. *Nature*, 181(4617), 1199-1200. doi:10.1038/1811199a0
- Brayer, G. D., Sidhu, G., Maurus, R., Rydberg, E. H., Braun, C., Wang, Y., . . . Withers, S. G. (2000). Subsite mapping of the human pancreatic alpha-amylase active site through structural, kinetic, and mutagenesis techniques. *Biochemistry*, 39(16), 4778-4791. doi:10.1021/bi9921182
- Brglez Mojzer, E., Knez Hrnčič, M., Škerget, M., Knez, Ž., & Bren, U. (2016). Polyphenols: Extraction Methods, Antioxidative Action, Bioavailability and Anticarcinogenic Effects. *Molecules*, 21(7). doi:10.3390/molecules21070901
- Brown J, R. (1975). Structure of Bovine serum albumin. *Federation Proceedings*, 34, 591-591.
- Brzozowski, A. M., & Davies, G. J. (1997). Structure of the *Aspergillus oryzae* α -Amylase Complexed with the Inhibitor Acarbose at 2.0 Å Resolution. *Biochemistry*, 36(36), 10837-10845. doi:10.1021/bi970539i
- Burton, G. W., & Ingold, K. U. (1986). Vitamin E: application of the principles of physical organic chemistry to the exploration of its structure and function. *Accounts of Chemical Research*, 19(7), 194-201. doi:10.1021/ar00127a001
- Cao, H., & Chen, X. (2012). Structures required of flavonoids for inhibiting digestive enzymes. *Anticancer Agents Med Chem*, 12(8), 929-939. doi:10.2174/187152012802650110
- Cao, J., Zhang, Y., Han, L., Zhang, S., Duan, X., Sun, L., & Wang, M. (2020). Number of galloyl moieties and molecular flexibility are both important in alpha-amylase inhibition by galloyl-based polyphenols. *Food & Function*, 11(5), 3838-3850. doi:10.1039/C9FO02735A
- CDC. (2022). Diabetes - Report Card. Retrieved from <https://www.cdc.gov/diabetes/library/reports/reportcard.html>

- Chagas, R., Lourenço, A. M., Monteiro, S., Ferreira, R. B., & Ferreira, L. M. (2017). Is caffeic acid, as the major metabolite present in Moscatel wine protein haze hydrolysate, involved in protein haze formation? *Food Research International*, 98, 103-109. doi:<https://doi.org/10.1016/j.foodres.2016.09.007>
- Chen, C.-W., & Ho, C.-T. (1995). Antioxidant properties of polyphenols extracted from green and black teas. *Journal of Food Lipids*, 2(1), 35-46. doi:<https://doi.org/10.1111/j.1745-4522.1995.tb00028.x>
- Chochkova, M. G., Petrova, P. P., Stoykova, B. M., Ivanova, G. I., Štícha, M., Dibó, G., & Milkova, T. S. (2017). Structure-Activity Relationships of N-Cinnamoyl and Hydroxycinnamoyl Amides on α -Glucosidase Inhibition. *Journal of Chemistry*, 2017, 6080129. doi:10.1155/2017/6080129
- Cory, H., Passarelli, S., Szeto, J., Tamez, M., & Mattei, J. (2018). The Role of Polyphenols in Human Health and Food Systems: A Mini-Review. *Frontiers in nutrition*, 5, 87-87. doi:10.3389/fnut.2018.00087
- Curry, S. (2009). Lessons from the crystallographic analysis of small molecule binding to human serum albumin. *Drug Metab Pharmacokinet*, 24(4), 342-357. doi:10.2133/dmpk.24.342
- Dona, A., Pagès, G., & Kuchel, P. (2010). Digestion of starch: In vivo and in vitro kinetic models used to characterise oligosaccharide or glucose release. *Carbohydrate Polymers*, 80, 599-617. doi:10.1016/j.carbpol.2010.01.002
- Du, K.-z., Wang, X.-z., Liu, Y., Hu, P., Utama, M. I. B., Gan, C. K., . . . Kloc, C. (2016). Weak Van der Waals Stacking, Wide-Range Band Gap, and Raman Study on Ultrathin Layers of Metal Phosphorus Trichalcogenides. *ACS Nano*, 10(2), 1738-1743. doi:10.1021/acsnano.5b05927
- Edelman, S. V. (1998). Type II diabetes mellitus. *Advances in internal medicine*, 43, 449-500. Retrieved from <http://europepmc.org/abstract/MED/9506190>
- El Gharras, H. (2009). Polyphenols: food sources, properties and applications – a review. *International Journal of Food Science & Technology*, 44(12), 2512-2518. doi:<https://doi.org/10.1111/j.1365-2621.2009.02077.x>
- Forli, S., Huey, R., Pique, M. E., Sanner, M. F., Goodsell, D. S., & Olson, A. J. (2016). Computational protein–ligand docking and virtual drug screening with the AutoDock suite. *Nature Protocols*, 11(5), 905-919. doi:10.1038/nprot.2016.051
- Fuwa, H. (1954). A new method for microdetermination of amylase activity by the use of amylose as the substrate. *The Journal of Biochemistry*, 41(5), 583-603. doi:10.1093/oxfordjournals.jbchem.a126476
- Gilles, C., Astier, J.-P., Marchis-Mouren, G., Cambillau, C., & Payan, F. (1996). Crystal Structure of Pig Pancreatic α -amylase Isoenzyme II, in Complex with the Carbohydrate Inhibitor Acarbose. *European Journal of Biochemistry*, 238(2), 561-569. doi:<https://doi.org/10.1111/j.1432-1033.1996.0561z.x>
- Graf, E. (1992). Antioxidant potential of ferulic acid. *Free Radical Biology and Medicine*, 13(4), 435-448. doi:[https://doi.org/10.1016/0891-5849\(92\)90184-I](https://doi.org/10.1016/0891-5849(92)90184-I)
- Halliwell, B. (1994). Free radicals and antioxidants: a personal view. *Nutr Rev*, 52(8 Pt 1), 253-265. doi:10.1111/j.1753-4887.1994.tb01453.x
- Han, X., Shen, T., & Lou, H. (2007). Dietary Polyphenols and Their Biological Significance. *International Journal of Molecular Sciences*, 8(9), 950-988. Retrieved from <https://www.ncbi.nlm.nih.gov/pmc/articles/PMC3871896/>
- He, J., Xu, L., Yang, L., & Wang, X. (2018). Epigallocatechin Gallate Is the Most Effective Catechin Against Antioxidant Stress via Hydrogen Peroxide and Radical Scavenging Activity. *Medical science monitor : international medical journal of experimental and clinical research*, 24, 8198-8206. doi:10.12659/MSM.911175

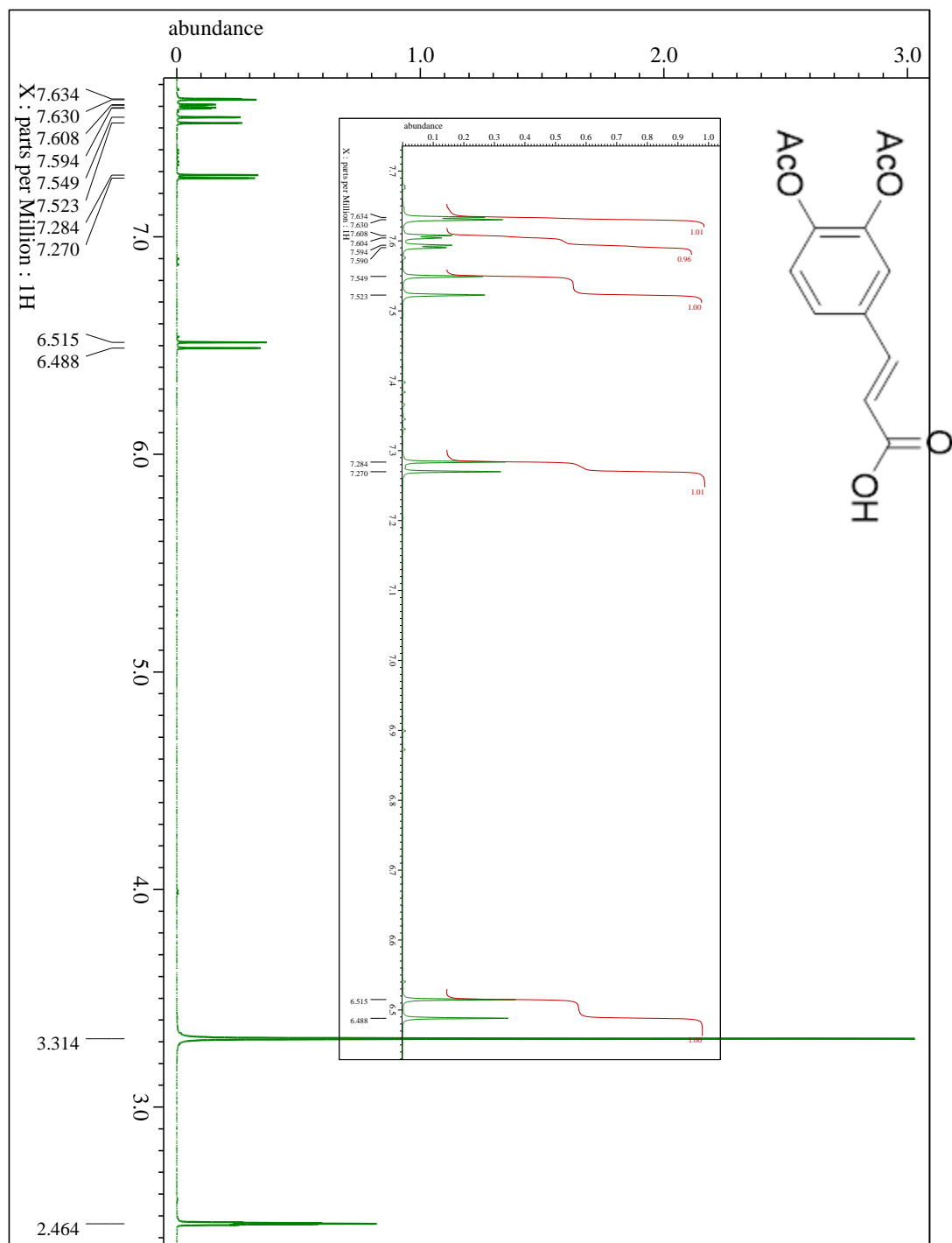
- Hirayama, K., Akashi, S., Furuya, M., & Fukuhara, K.-i. (1990). Rapid confirmation and revision of the primary structure of bovine serum albumin by ESIMS and frit-FAB LC/MS. *Biochemical and Biophysical Research Communications*, 173(2), 639-646. doi:[https://doi.org/10.1016/S0006-291X\(05\)80083-X](https://doi.org/10.1016/S0006-291X(05)80083-X)
- Ivanova-Petropulos, V., Durakova, S., Ricci, A., Parpinello, G. P., & Versari, A. (2016). Extraction and evaluation of natural occurring bioactive compounds and change in antioxidant activity during red winemaking. *J Food Sci Technol*, 53(6), 2634-2643. doi:10.1007/s13197-016-2235-7
- Jin, X. L., Wei, X., Qi, F. M., Yu, S. S., Zhou, B., & Bai, S. (2012). Characterization of hydroxycinnamic acid derivatives binding to bovine serum albumin. *Org Biomol Chem*, 10(17), 3424-3431. doi:10.1039/c2ob25237f
- Katsarou, A., Gudbjörnsdóttir, S., Rawshani, A., Dabelea, D., Bonifacio, E., Anderson, B. J., . . . Lernmark, Å. (2017). Type 1 diabetes mellitus. *Nature Reviews Disease Primers*, 3(1), 17016. doi:10.1038/nrdp.2017.16
- Kedare, S. B., & Singh, R. P. (2011). Genesis and development of DPPH method of antioxidant assay. *J Food Sci Technol*, 48(4), 412-422. doi:10.1007/s13197-011-0251-1
- Lakowicz, J. R. (1999). *Principles of fluorescence spectroscopy*. New York, NY: Kluwer Acad./Plenum Publ.
- Langcake, P., & Pryce, R. J. (1976). The production of resveratrol by *Vitis vinifera* and other members of the Vitaceae as a response to infection or injury. *Physiological Plant Pathology*, 9(1), 77-86. doi:[https://doi.org/10.1016/0048-4059\(76\)90077-1](https://doi.org/10.1016/0048-4059(76)90077-1)
- Lempereur, I., Rouau, X., & Abecassis, J. (1997). Genetic and Agronomic Variation in Arabinoxylan and Ferulic Acid Contents of Durum Wheat (*Triticum durum*L.) Grain and Its Milling Fractions. *Journal of Cereal Science*, 25(2), 103-110. doi:<https://doi.org/10.1006/jcrs.1996.0090>
- Leney, A. C., & Heck, A. J. (2017). Native Mass Spectrometry: What is in the Name? *J Am Soc Mass Spectrom*, 28(1), 5-13. doi:10.1007/s13361-016-1545-3
- Levitzki, A., & Steer, M. L. (1974). The allosteric activation of mammalian alpha-amylase by chloride. *Eur J Biochem*, 41(1), 171-180. doi:10.1111/j.1432-1033.1974.tb03257.x
- Li, Y., Gao, F., Gao, F., Shan, F., Bian, J., & Zhao, C. (2009). Study on the interaction between 3 flavonoid compounds and alpha-amylase by fluorescence spectroscopy and enzymatic kinetics. *J Food Sci*, 74(3), C199-203. doi:10.1111/j.1750-3841.2009.01080.x
- Liang, N., & Kitts, D. (2014). Antioxidant Property of Coffee Components: Assessment of Methods that Define Mechanisms of Action. *Molecules (Basel, Switzerland)*, 19, 19180-19208. doi:10.3390/molecules191119180
- Lo Piparo, E., Scheib, H., Frei, N., Williamson, G., Grigorov, M., & Chou, C. J. (2008). Flavonoids for Controlling Starch Digestion: Structural Requirements for Inhibiting Human α -Amylase. *Journal of Medicinal Chemistry*, 51(12), 3555-3561. doi:10.1021/jm800115x
- Lou, Z., Wang, H., Rao, S., Sun, J., Ma, C., & Li, J. (2012). p-Coumaric acid kills bacteria through dual damage mechanisms. *Food Control*, 25(2), 550-554. doi:<https://doi.org/10.1016/j.foodcont.2011.11.022>
- Luís, Â., Silva, F., Sousa, S., Duarte, A. P., & Domingues, F. (2014). Antistaphylococcal and biofilm inhibitory activities of gallic, caffeic, and chlorogenic acids. *Biofouling*, 30(1), 69-79. doi:10.1080/08927014.2013.845878
- Luo, H., Li, C., Fang, H., & Wang, X. (2016). Comparative study of the interactions between bisphenol analogues and serum albumins by electrospray mass spectrometry and fluorescence spectroscopy. *Rapid Communications in Mass Spectrometry*, 30(S1), 162-167. doi:<https://doi.org/10.1002/rcm.7633>

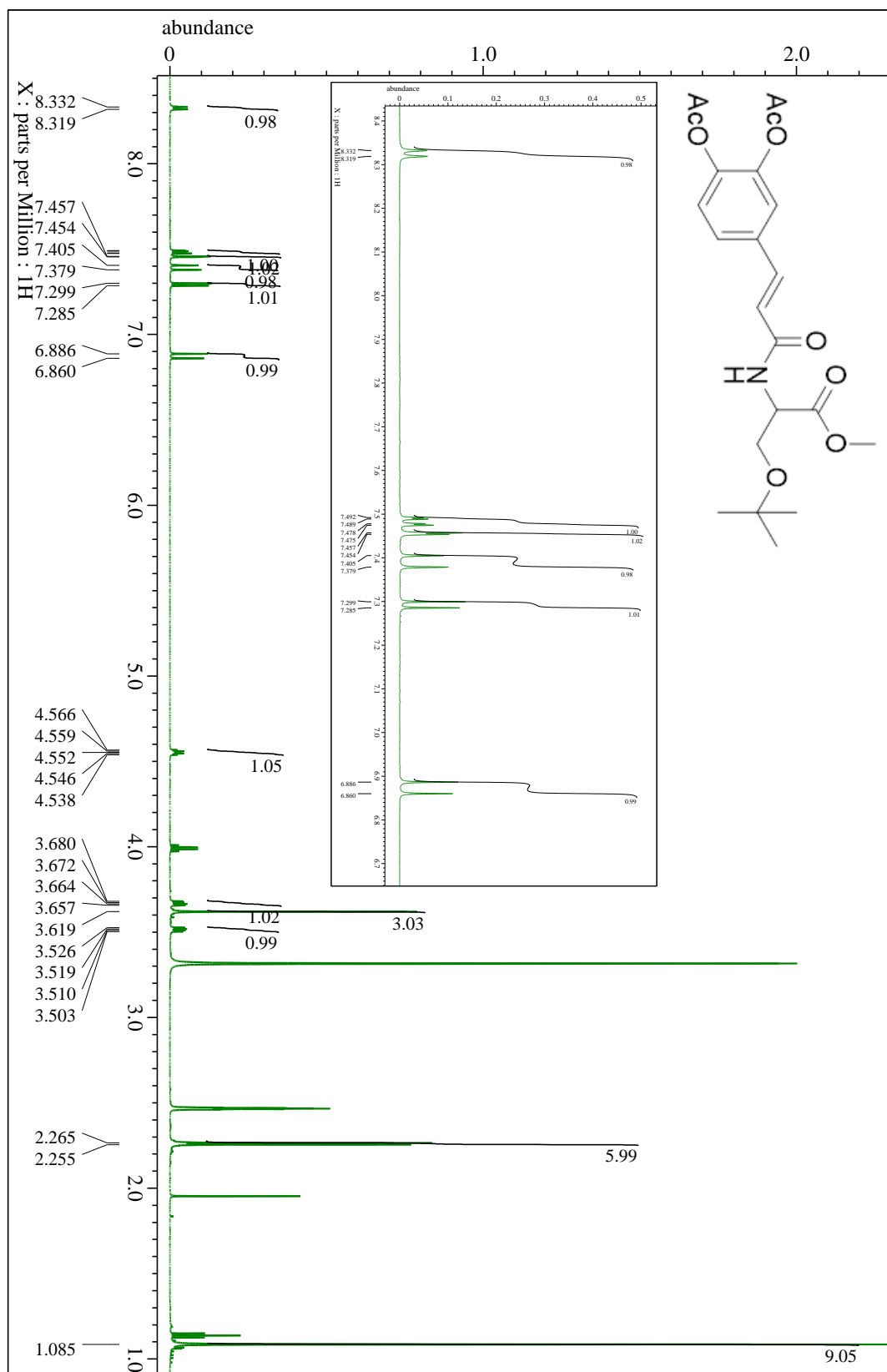
- Maity, S., Gundampati, R. K., & Suresh Kumar, T. K. (2019). NMR Methods to Characterize Protein-Ligand Interactions. *Natural Product Communications*, 14(5), 1934578X19849296. doi:10.1177/1934578x19849296
- Manach, C., Scalbert, A., Morand, C., Rémésy, C., & Jiménez, L. (2004). Polyphenols: food sources and bioavailability. *The American Journal of Clinical Nutrition*, 79(5), 727-747. doi:10.1093/ajcn/79.5.727
- Martinez-Gonzalez, A. I., Díaz-Sánchez Á, G., de la Rosa, L. A., Bustos-Jaimes, I., & Alvarez-Parrilla, E. (2019). Inhibition of α -amylase by flavonoids: Structure activity relationship (SAR). *Spectrochim Acta A Mol Biomol Spectrosc*, 206, 437-447. doi:10.1016/j.saa.2018.08.057
- Marty, M. T., Baldwin, A. J., Marklund, E. G., Hochberg, G. K. A., Benesch, J. L. P., & Robinson, C. V. (2015). Bayesian Deconvolution of Mass and Ion Mobility Spectra: From Binary Interactions to Polydisperse Ensembles. *Analytical Chemistry*, 87(8), 4370-4376. doi:10.1021/acs.analchem.5b00140
- Meng, X. Y., Zhang, H. X., Mezei, M., & Cui, M. (2011). Molecular docking: a powerful approach for structure-based drug discovery. *Curr Comput Aided Drug Des*, 7(2), 146-157. doi:10.2174/157340911795677602
- Möller, M., & Denicola, A. (2002). Study of protein-ligand binding by fluorescence. *Biochemistry and Molecular Biology Education*, 30(5), 309-312. doi:<https://doi.org/10.1002/bmb.2002.494030050089>
- Moulay, S. (2013). Molecular iodine/polymer complexes. *Journal of Polymer Engineering*, 33(5), 389-443. doi:10.1515/polyeng-2012-0122
- Mulder, P., Korth, H.-G., Pratt, D. A., DiLabio, G. A., Valgimigli, L., Pedulli, G. F., & Ingold, K. U. (2005). Critical Re-evaluation of the O–H Bond Dissociation Enthalpy in Phenol. *The Journal of Physical Chemistry A*, 109(11), 2647-2655. doi:10.1021/jp047148f
- Neveu, V., Perez-Jiménez, J., Vos, F., Crespy, V., du Chaffaut, L., Mennen, L., . . . Scalbert, A. (2010). Phenol-Explorer: an online comprehensive database on polyphenol contents in foods. *Database (Oxford)*, 2010, bap024. doi:10.1093/database/bap024
- Nimse, S. B., & Pal, D. (2015). Free radicals, natural antioxidants, and their reaction mechanisms. *RSC Advances*, 5(35), 27986-28006. doi:10.1039/C4RA13315C
- Niu, Y., Ke, D., Yang, Q., Wang, X., Chen, Z., An, X., & Shen, W. (2012). Temperature-dependent stability and DPPH scavenging activity of liposomal curcumin at pH 7.0. *Food Chemistry*, 135(3), 1377-1382. doi:<https://doi.org/10.1016/j.foodchem.2012.06.018>
- Oliveira, H. M., Pinheiro, A. Q., Fonseca, A. J. M., Cabrita, A. R. J., & Maia, M. R. G. (2019). Flexible and expeditious assay for quantitative monitoring of alpha-amylase and amyloglucosidase activities. *MethodsX*, 6, 246-258. doi:10.1016/j.mex.2019.01.007
- Orfali, R., Rateb, M. E., Hassan, H. M., Alonazi, M., Gomaa, M. R., Mahrous, N., . . . Sayed, A. M. (2021). Sinapic Acid Suppresses SARS CoV-2 Replication by Targeting Its Envelope Protein. *Antibiotics*, 10(4), 420. Retrieved from <https://www.mdpi.com/2079-6382/10/4/420>
- Peters, T. (1995). 2 - The Albumin Molecule: Its Structure and Chemical Properties. In T. Peters (Ed.), *All About Albumin* (pp. 9-II). San Diego: Academic Press.
- Petreni, A., Osman, S. M., Alasmay, F. A., Almutairi, T. M., Nocentini, A., & Supuran, C. T. (2021). Binding site comparison for coumarin inhibitors and amine/amino acid activators of human carbonic anhydrases. *Eur J Med Chem*, 226, 113875. doi:10.1016/j.ejmech.2021.113875
- Phaniendra, A., Jestadi, D. B., & Periyasamy, L. (2015). Free radicals: properties, sources, targets, and their implication in various diseases. *Indian journal of clinical biochemistry : IJCB*, 30(1), 11-26. doi:10.1007/s12291-014-0446-0

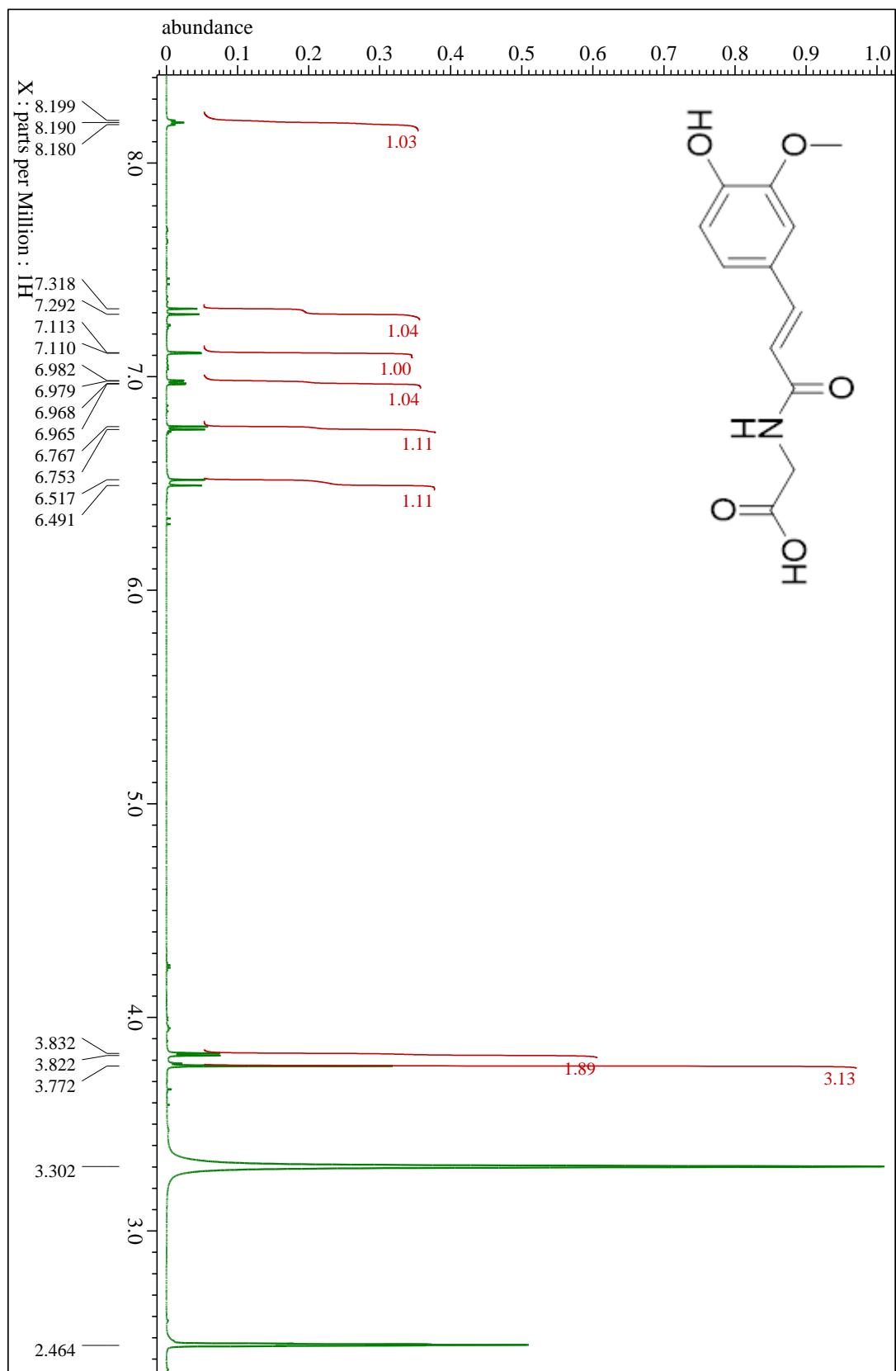
- Proença, C., Freitas, M., Ribeiro, D., Tomé, S. M., Oliveira, E. F. T., Viegas, M. F., . . . Fernandes, E. (2019). Evaluation of a flavonoids library for inhibition of pancreatic α -amylase towards a structure-activity relationship. *Journal of enzyme inhibition and medicinal chemistry*, 34(1), 577-588. doi:10.1080/14756366.2018.1558221
- Qian, M., Haser, R., & Payan, F. (1995). Carbohydrate binding sites in a pancreatic alpha-amylase-substrate complex, derived from X-ray structure analysis at 2.1 Å resolution. *Protein Sci*, 4(4), 747-755. doi:10.1002/pro.5560040414
- Ren, B., Wang, M., Liu, J., Ge, J., Zhang, X., & Dong, H. (2015). Zemplén transesterification: a name reaction that has misled us for 90 years. *Green Chemistry*, 17(3), 1390-1394. doi:10.1039/C4GC02006E
- Renaud, S., & de Lorgeril, M. (1992). Wine, alcohol, platelets, and the French paradox for coronary heart disease. *Lancet*, 339(8808), 1523-1526. doi:10.1016/0140-6736(92)91277-f
- Sánchez-Moreno, C., Larrauri, J. A., & Saura-Calixto, F. (1998). A procedure to measure the antiradical efficiency of polyphenols. *Journal of the Science of Food and Agriculture*, 76(2), 270-276. doi:[https://doi.org/10.1002/\(SICI\)1097-0010\(199802\)76:2<270::AID-JSFA945>3.0.CO;2-9](https://doi.org/10.1002/(SICI)1097-0010(199802)76:2<270::AID-JSFA945>3.0.CO;2-9)
- Sarikaya, S. B., Gülçin, I., & Supuran, C. T. (2010). Carbonic anhydrase inhibitors: Inhibition of human erythrocyte isozymes I and II with a series of phenolic acids. *Chem Biol Drug Des*, 75(5), 515-520. doi:10.1111/j.1747-0285.2010.00965.x
- Schieber, M., & Chandel, Navdeep S. (2014). ROS Function in Redox Signaling and Oxidative Stress. *Current Biology*, 24(10), R453-R462. doi:<https://doi.org/10.1016/j.cub.2014.03.034>
- Scriven, E. F. V. (1983). 4-Dialkylaminopyridines: super acylation and alkylation catalysts. *Chemical Society Reviews*, 12(2), 129-161. doi:10.1039/CS9831200129
- Seigner, C., Prodanov, E., & Marchis-Mouren, G. (1987). The determination of subsite binding energies of porcine pancreatic α -amylase by comparing hydrolytic activity towards substrates. *Biochimica et Biophysica Acta (BBA) - Protein Structure and Molecular Enzymology*, 913(2), 200-209. doi:[https://doi.org/10.1016/0167-4838\(87\)90331-1](https://doi.org/10.1016/0167-4838(87)90331-1)
- Shojaee, M. S., Moeenfar, M., & Farhoosh, R. (2022). Kinetics and stoichiometry of gallic acid and methyl gallate in scavenging DPPH radical as affected by the reaction solvent. *Scientific Reports*, 12(1), 8765. doi:10.1038/s41598-022-12803-3
- Singh, K., Cooposamy, R. M., Gumede, N. J., & Sabiu, S. (2022). Computational Insights and In Vitro Validation of Antibacterial Potential of Shikimate Pathway-Derived Phenolic Acids as NorA Efflux Pump Inhibitors. *Molecules*, 27(8). doi:10.3390/molecules27082601
- Skoog, D. A. C. S. R. H. F. J. (2007). *Principles of instrumental analysis*. Belmont, CA: Thomson Brooks/Cole.
- Sun, L., Wang, Y., & Miao, M. (2020). Inhibition of α -amylase by polyphenolic compounds: Substrate digestion, binding interactions and nutritional intervention. *Trends in Food Science & Technology*, 104, 190-207. doi:<https://doi.org/10.1016/j.tifs.2020.08.003>
- Sun, L., Warren, F., & Gidley, M. (2019). Natural products for glycaemic control: Polyphenols as inhibitors of alpha-amylase. *Trends in Food Science & Technology*, 91. doi:10.1016/j.tifs.2019.07.009
- Sun, L., Warren, F. J., Netzel, G., & Gidley, M. J. (2016). 3 or 3'-Galloyl substitution plays an important role in association of catechins and theaflavins with porcine pancreatic α -amylase: The kinetics of inhibition of α -amylase by tea polyphenols. *Journal of Functional Foods*, 26, 144-156. doi:<https://doi.org/10.1016/j.jff.2016.07.012>

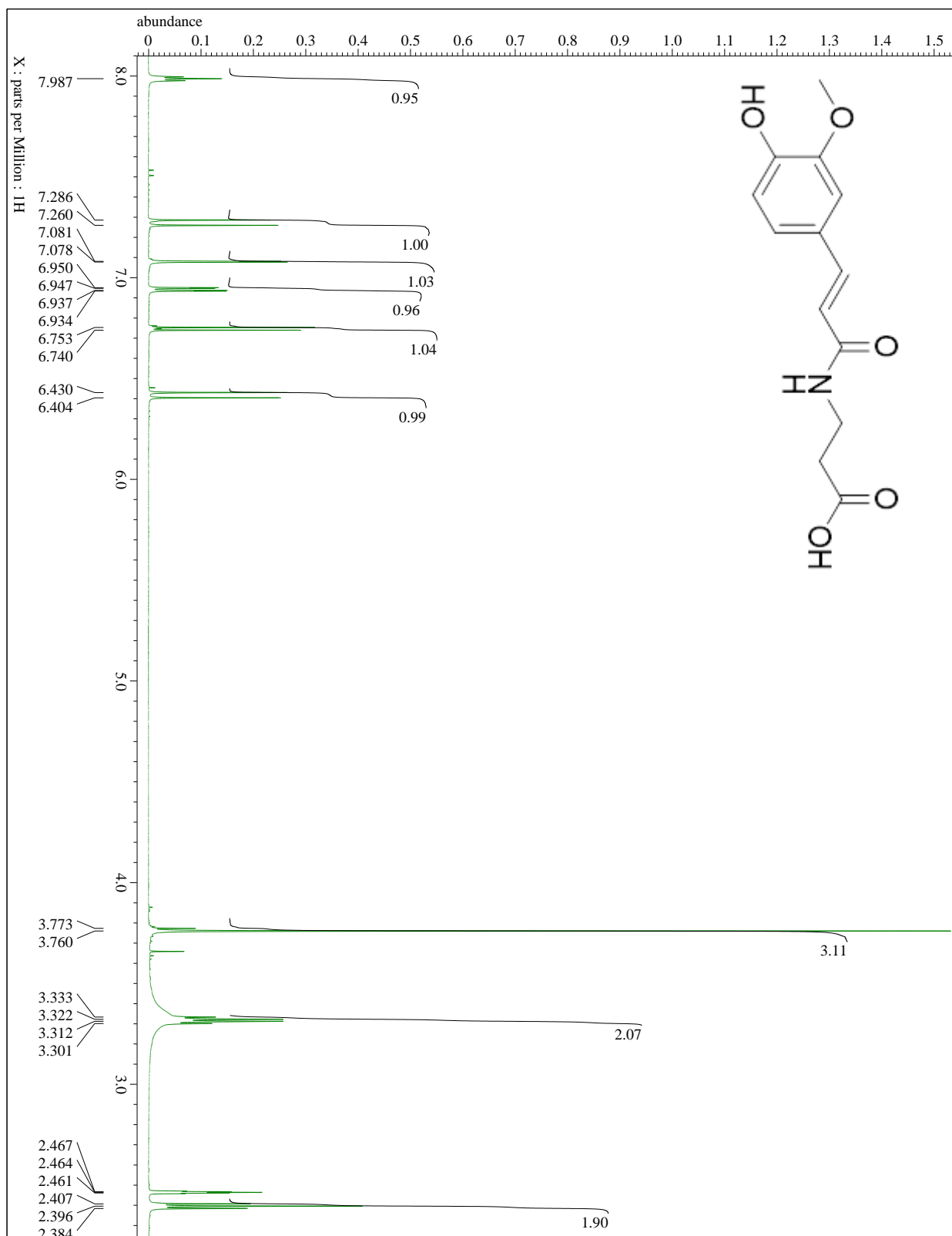
- Tamara, S., den Boer, M. A., & Heck, A. J. R. (2022). High-Resolution Native Mass Spectrometry. *Chemical Reviews*, 122(8), 7269-7326. doi:10.1021/acs.chemrev.1c00212
- Taofiq, O., González-Paramás, A. M., Barreiro, M. F., & Ferreira, I. C. F. R. (2017). Hydroxycinnamic Acids and Their Derivatives: Cosmeceutical Significance, Challenges and Future Perspectives, a Review. *Molecules (Basel, Switzerland)*, 22(2), 281. doi:10.3390/molecules22020281
- Trott, O., & Olson, A. J. (2010). AutoDock Vina: improving the speed and accuracy of docking with a new scoring function, efficient optimization, and multithreading. *J Comput Chem*, 31(2), 455-461. doi:10.1002/jcc.21334
- Tsimogiannis, D. I., & Oreopoulou, V. (2006). The contribution of flavonoid C-ring on the DPPH free radical scavenging efficiency. A kinetic approach for the 3',4'-hydroxy substituted members. *Innovative Food Science & Emerging Technologies*, 7(1), 140-146. doi:<https://doi.org/10.1016/j.ifset.2005.09.001>
- Urbaniak, A., Molski, M., & Szelag, M. (2012). Quantum-chemical Calculations of the Antioxidant Properties of trans-p-coumaric Acid and trans-sinapinic Acid. *computational methods in science and technology*, 18, 117-128.
- Viegas, A., Manso, J., Nobrega, F. L., & Cabrita, E. J. (2011). Saturation-Transfer Difference (STD) NMR: A Simple and Fast Method for Ligand Screening and Characterization of Protein Binding. *Journal of Chemical Education*, 88(7), 990-994. doi:10.1021/ed101169t
- Visvanathan, R., Qader, M., Jayathilake, C., Jayawardana, B. C., Liyanage, R., & Sivakanesan, R. (2020). Critical review on conventional spectroscopic α -amylase activity detection methods: merits, demerits, and future prospects. *Journal of the Science of Food and Agriculture*, 100(7), 2836-2847. doi:<https://doi.org/10.1002/jsfa.10315>
- Walton, R. J., Sherif, I. T., Noy, G. A., & Alberti, K. G. (1979). Improved metabolic profiles in insulin-treated diabetic patients given an alpha-glucosidehydrolase inhibitor. *Br Med J*, 1(6158), 220-221. doi:10.1136/bmj.1.6158.220
- Wang, L., Wang, L., Wang, T., Li, Z., Gao, Y., Cui, S. W., & Qiu, J. (2022). Comparison of quercetin and rutin inhibitory influence on Tartary buckwheat starch digestion in vitro and their differences in binding sites with the digestive enzyme. *Food Chemistry*, 367, 130762. doi:<https://doi.org/10.1016/j.foodchem.2021.130762>
- Wright, J. S., Johnson, E. R., & DiLabio, G. A. (2001). Predicting the Activity of Phenolic Antioxidants: Theoretical Method, Analysis of Substituent Effects, and Application to Major Families of Antioxidants. *Journal of the American Chemical Society*, 123(6), 1173-1183. doi:10.1021/ja002455u
- Xiao, Z., Storms, R., & Tsang, A. (2006). A quantitative starch-iodine method for measuring alpha-amylase and glucoamylase activities. *Anal Biochem*, 351(1), 146-148. doi:10.1016/j.ab.2006.01.036
- Xie, J., & Schaich, K. M. (2014). Re-evaluation of the 2,2-Diphenyl-1-picrylhydrazyl Free Radical (DPPH) Assay for Antioxidant Activity. *Journal of Agricultural and Food Chemistry*, 62(19), 4251-4260. doi:10.1021/jf500180u
- Zeng, Y., Song, J., Zhang, M., Wang, H., Zhang, Y., & Suo, H. (2020). Comparison of In Vitro and In Vivo Antioxidant Activities of Six Flavonoids with Similar Structures. *Antioxidants (Basel)*, 9(8). doi:10.3390/antiox9080732
- Zoppi, C., Nocentini, A., Supuran, C. T., Pratesi, A., & Messori, L. (2020). Native mass spectrometry of human carbonic anhydrase I and its inhibitor complexes. *J Biol Inorg Chem*, 25(7), 979-993. doi:10.1007/s00775-020-01818-8

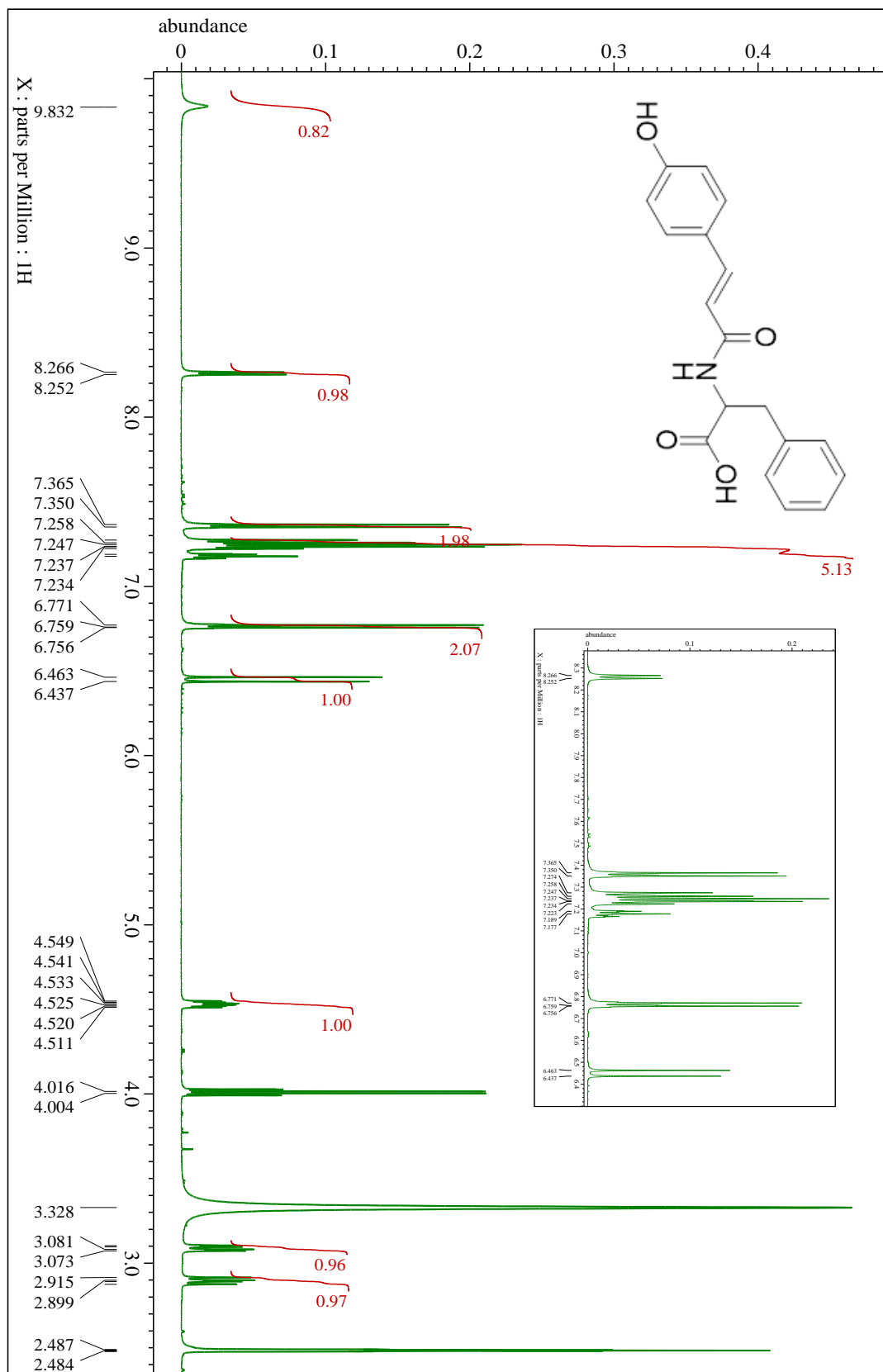
Appendix

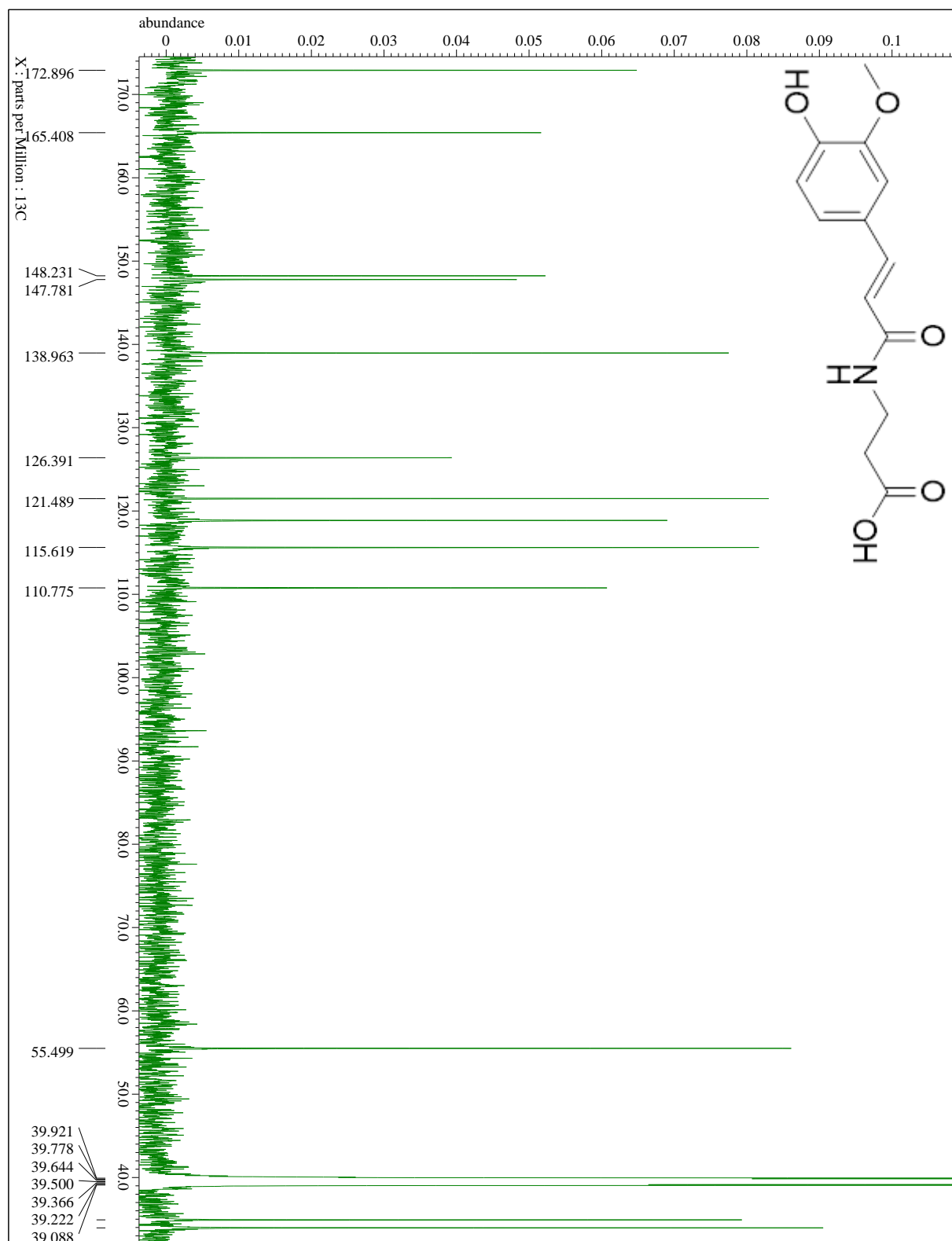
A. Selected ^1H -NMR Spectra

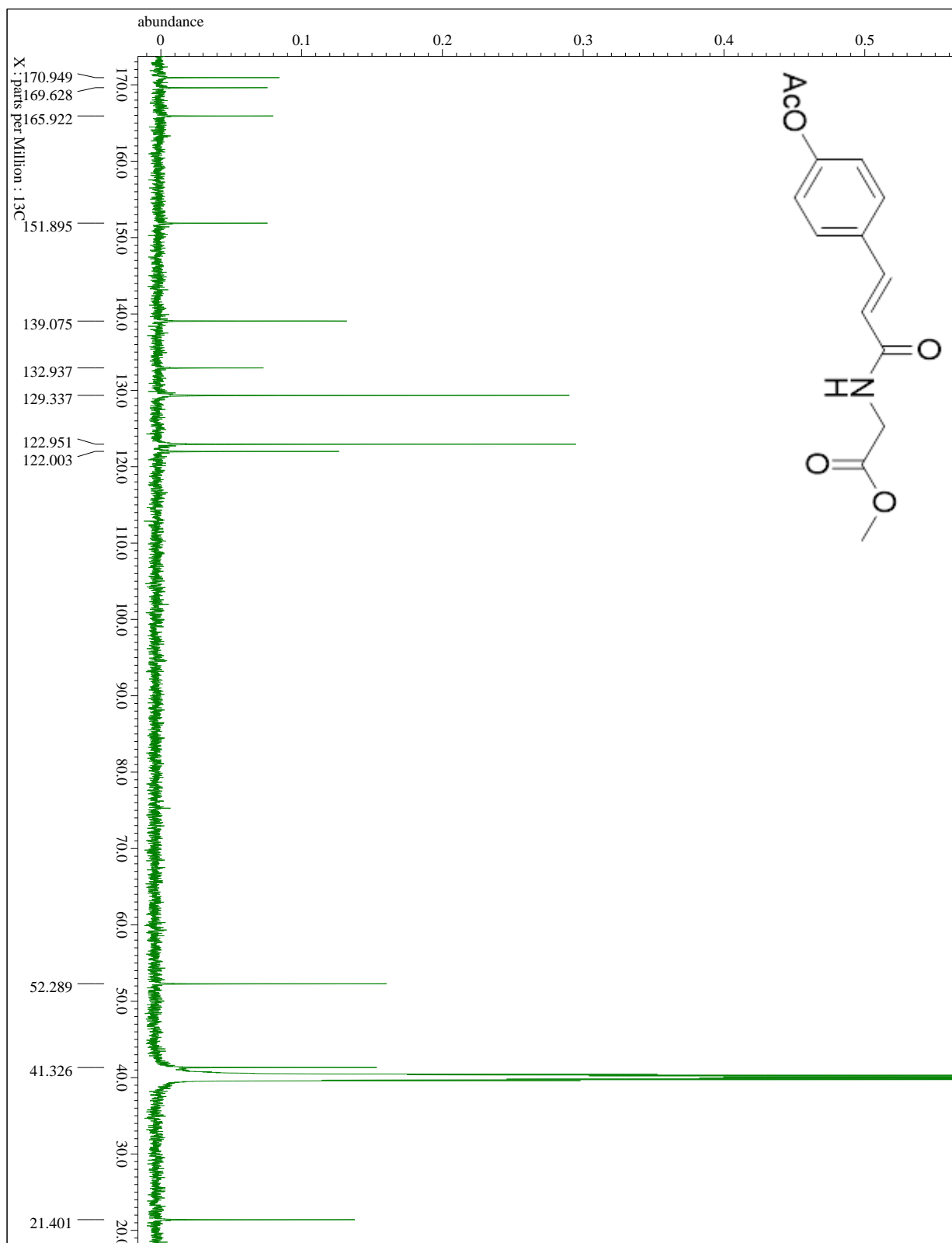


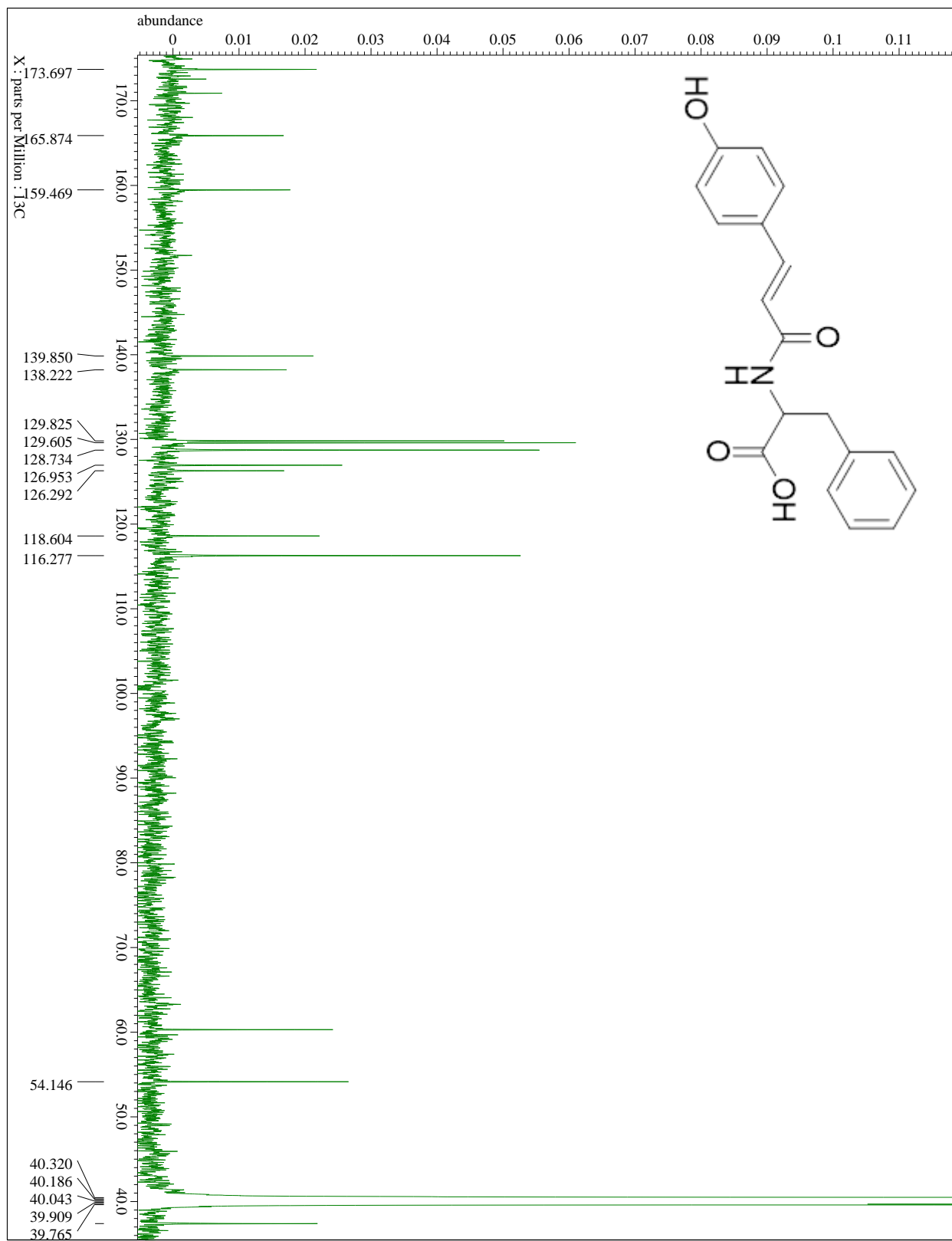


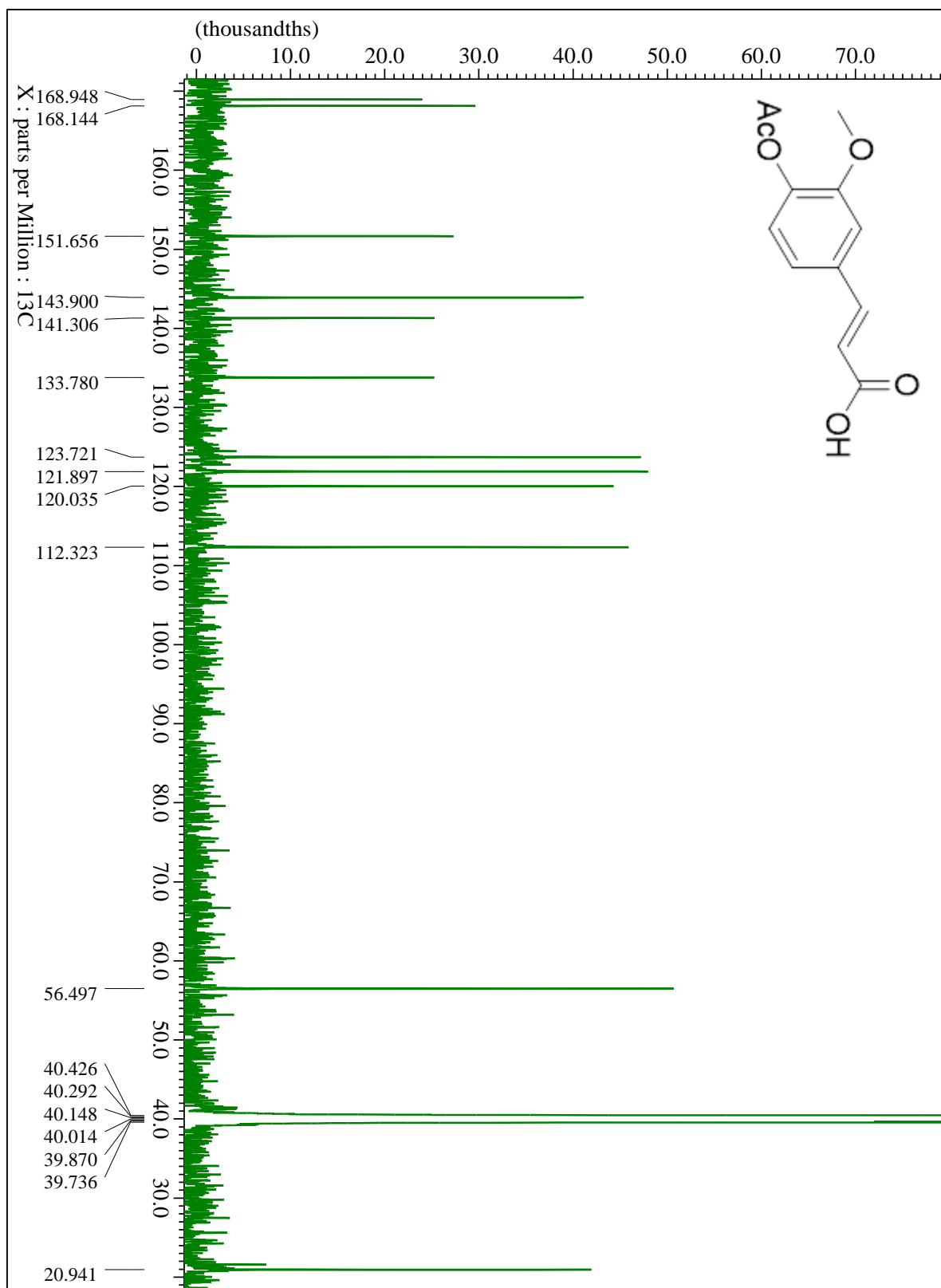


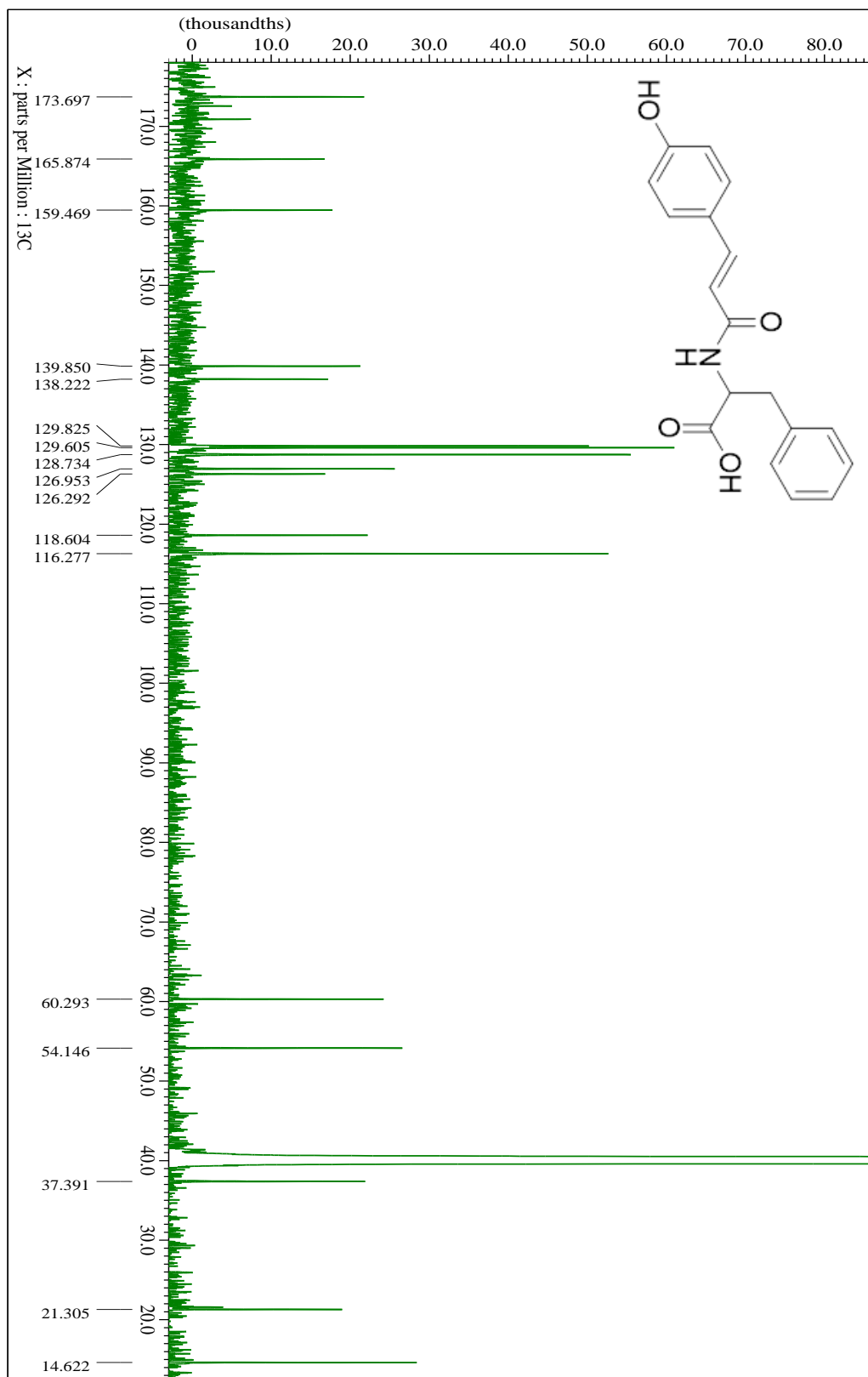


B. Selected ^{13}C -NMR Spectra

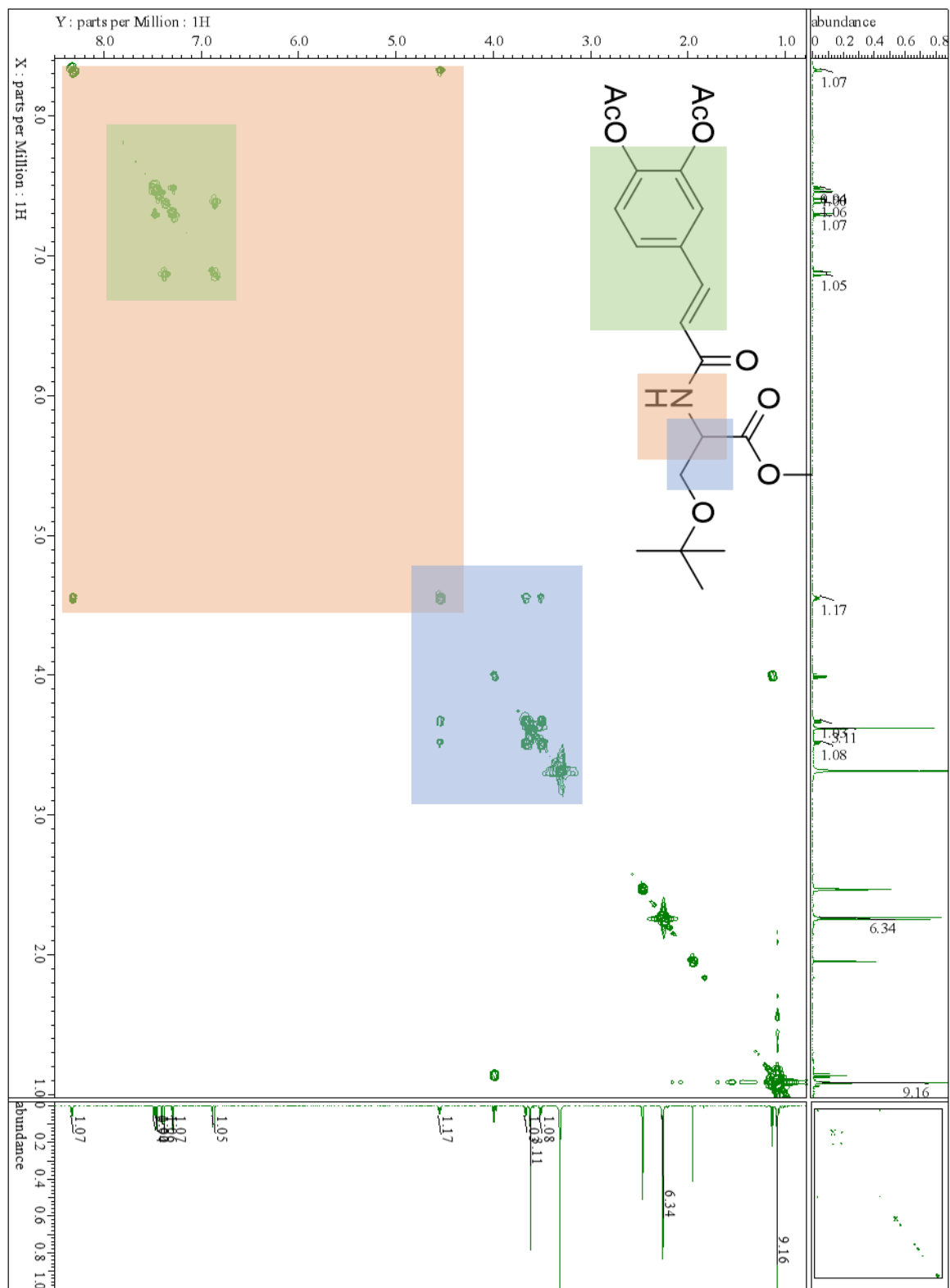




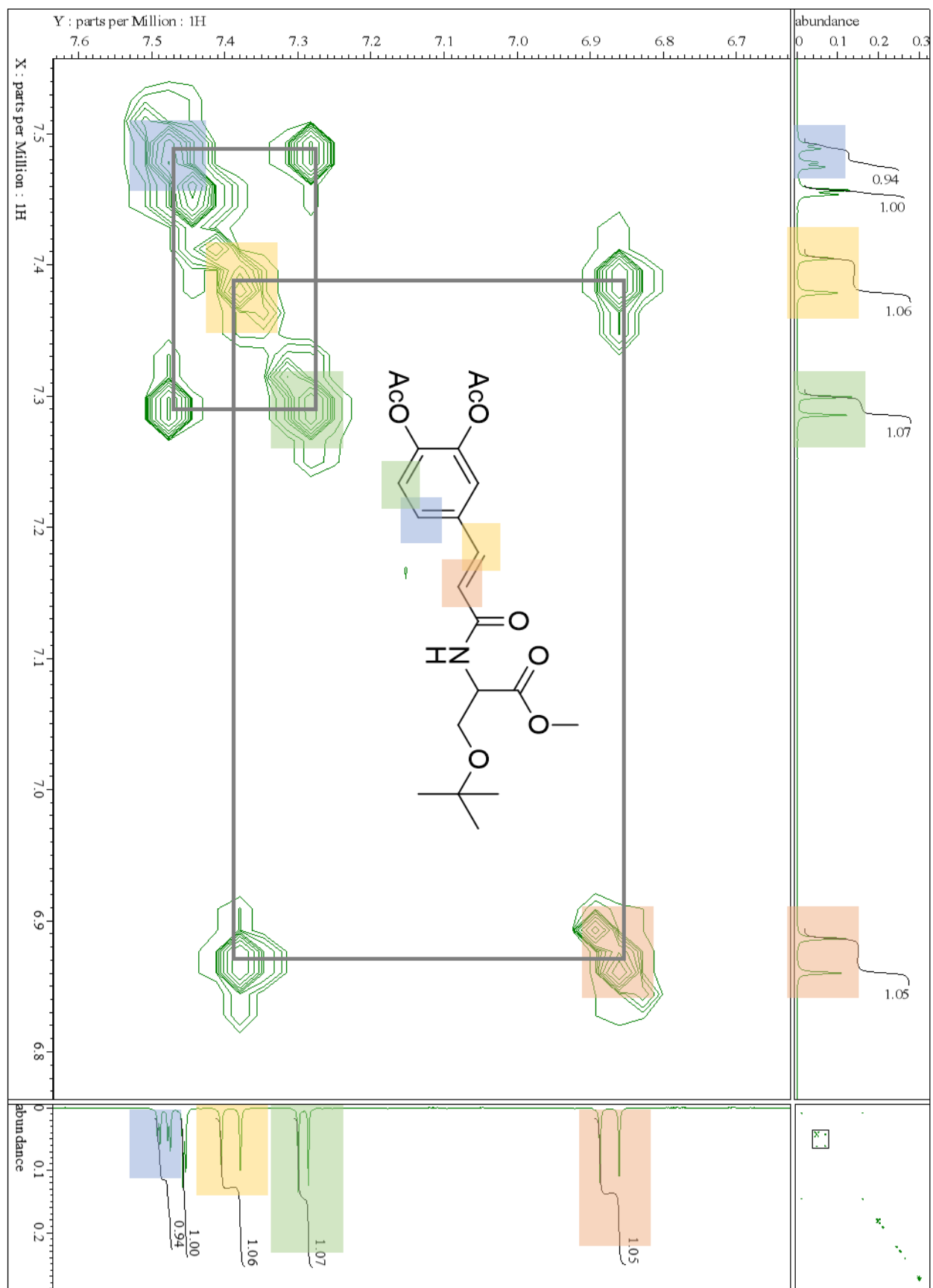


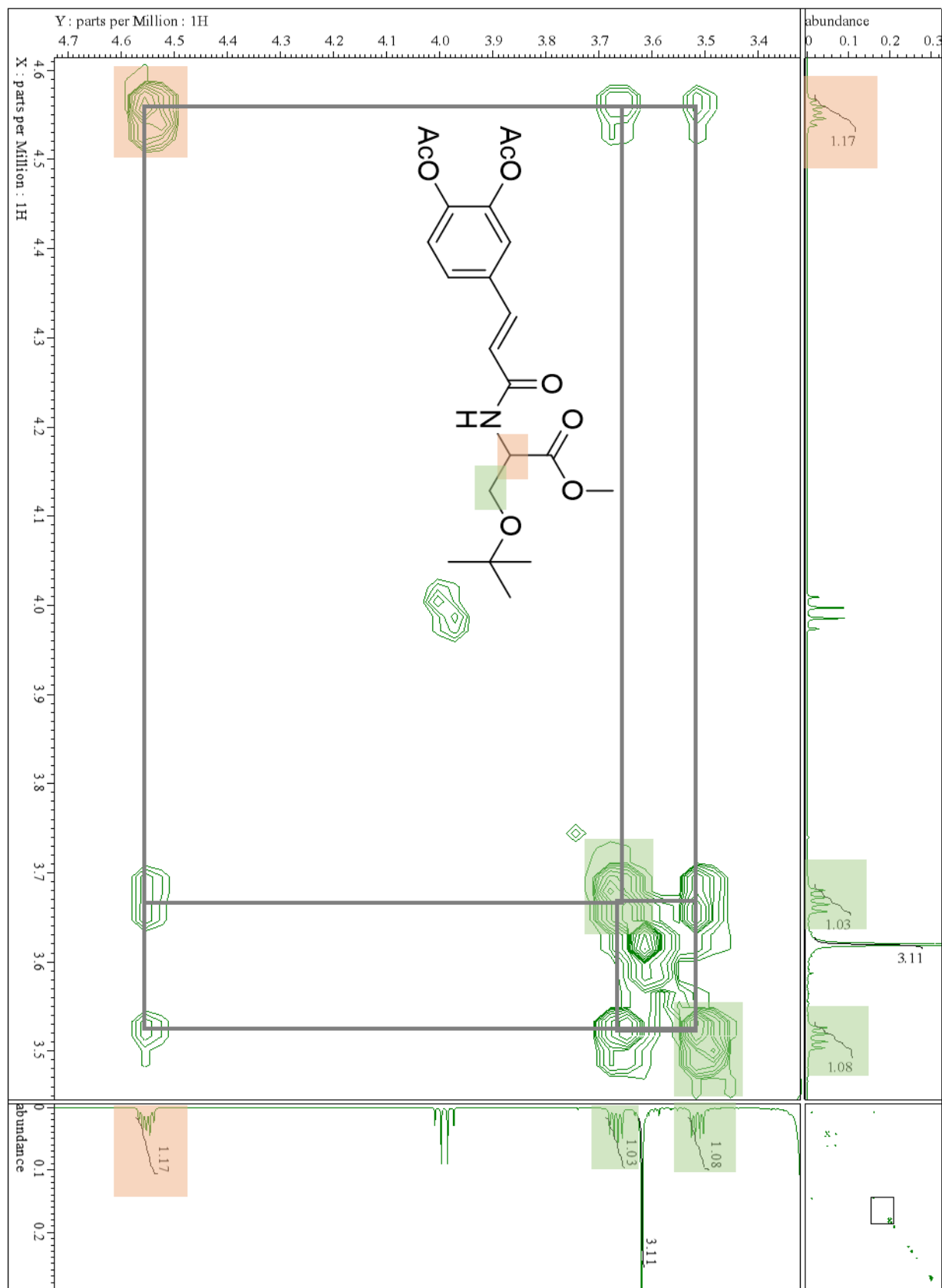


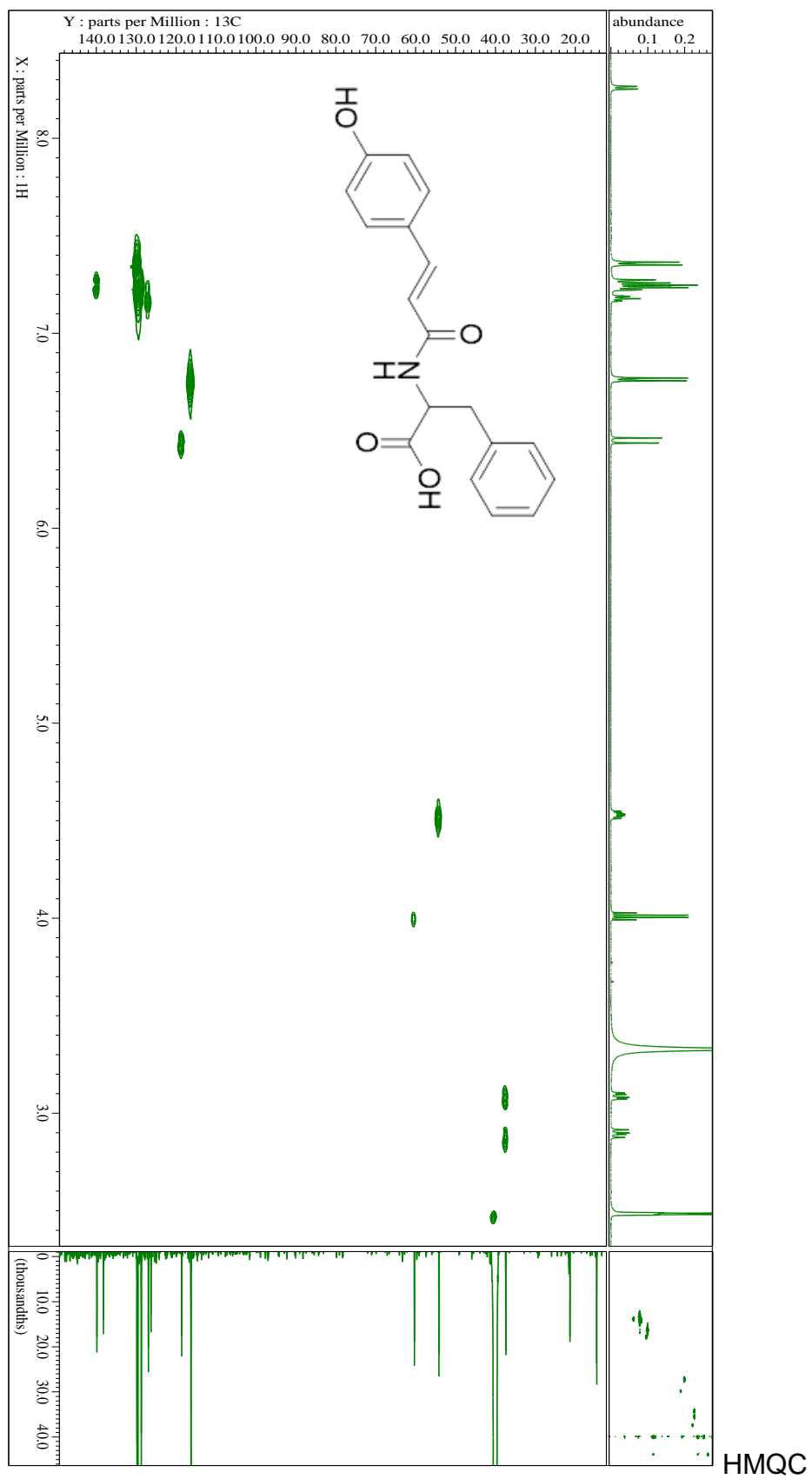
C. Selected 2D NMR Spectra



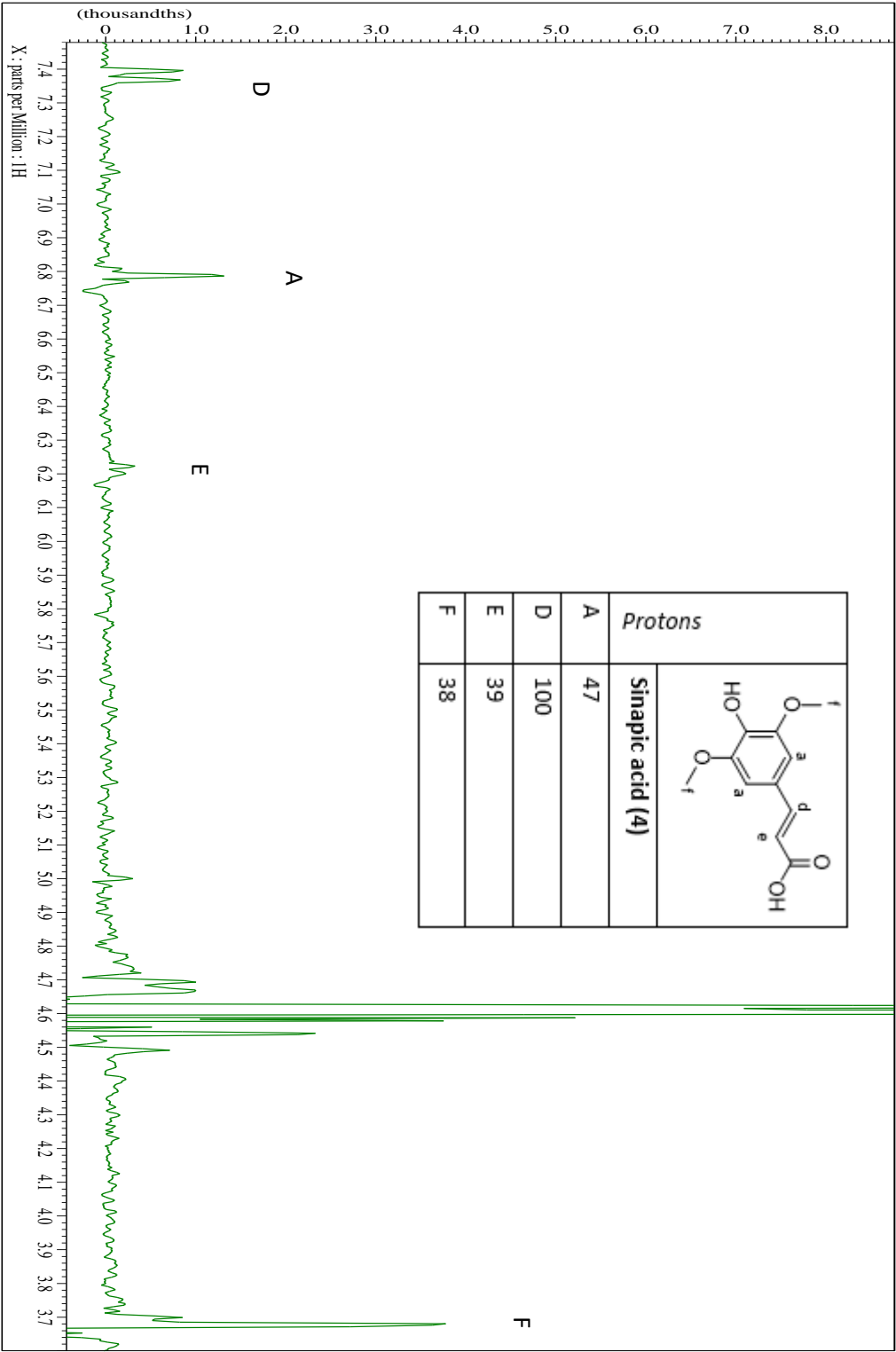
COSY



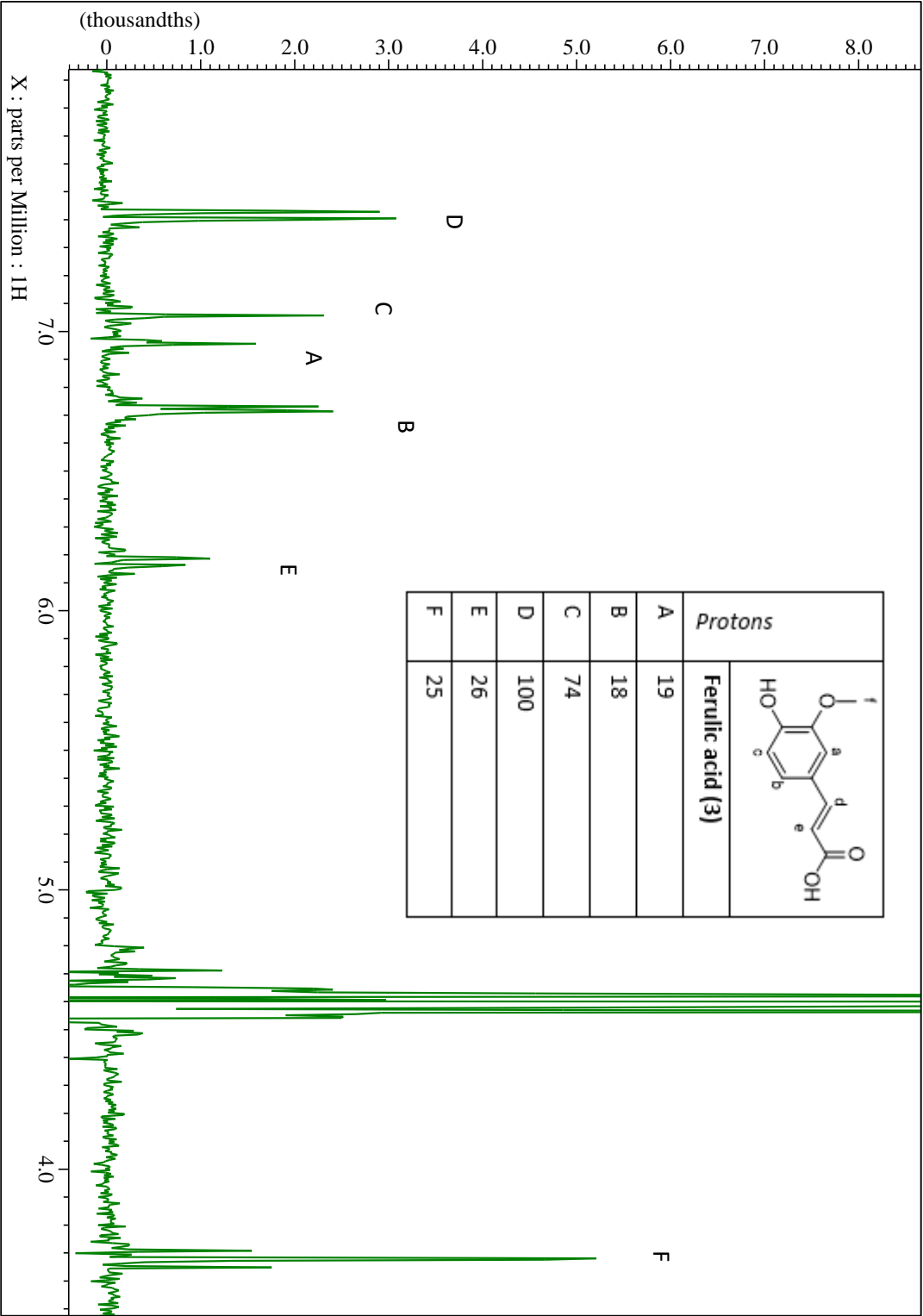




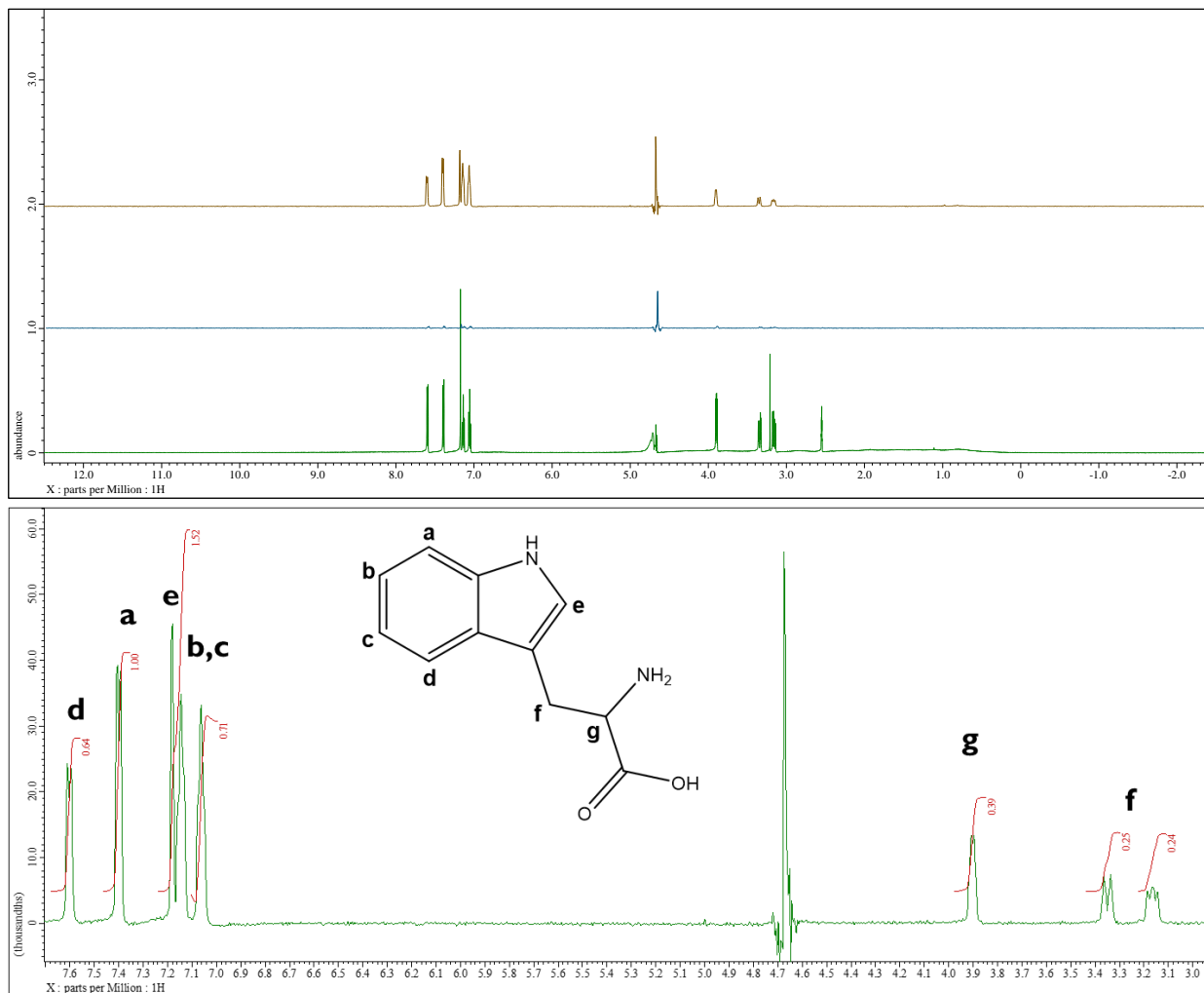
D. Selected STD-NMR Spectra



Sinapic acid and α-amylase STD-NMR



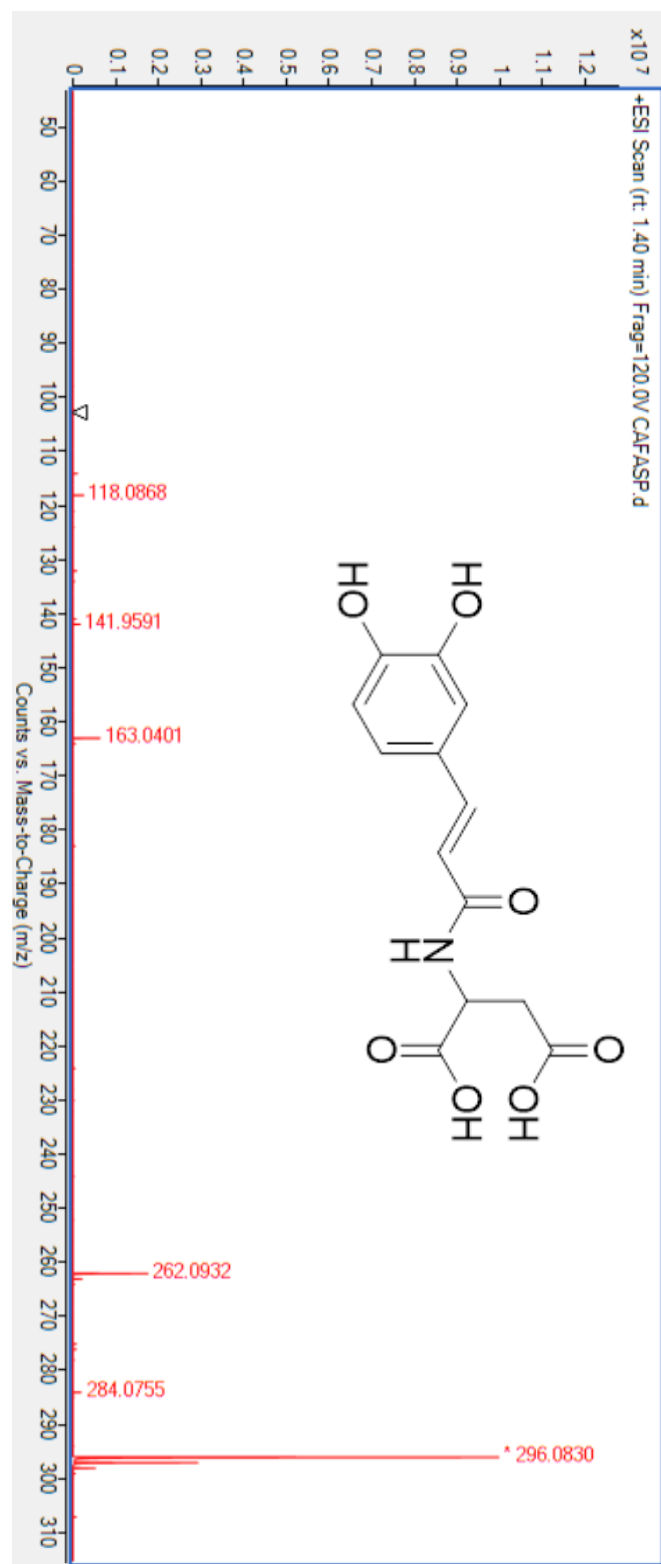
Ferulic acid and α -amylase STD-NMR results



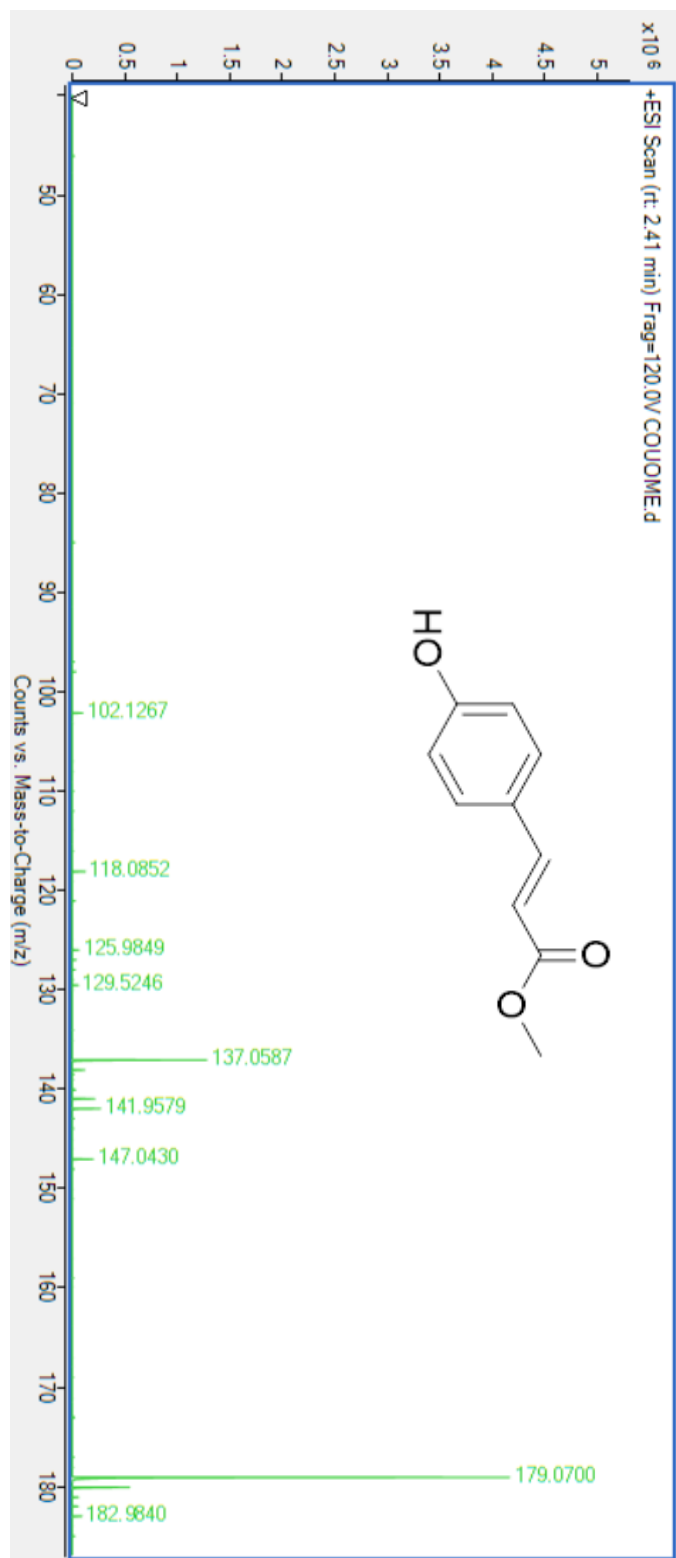
Proton	%
a	100
b	75
c	71
d	64
e	73
f	25, 24
g	39

STD-NMR: BSA and Tryptophan

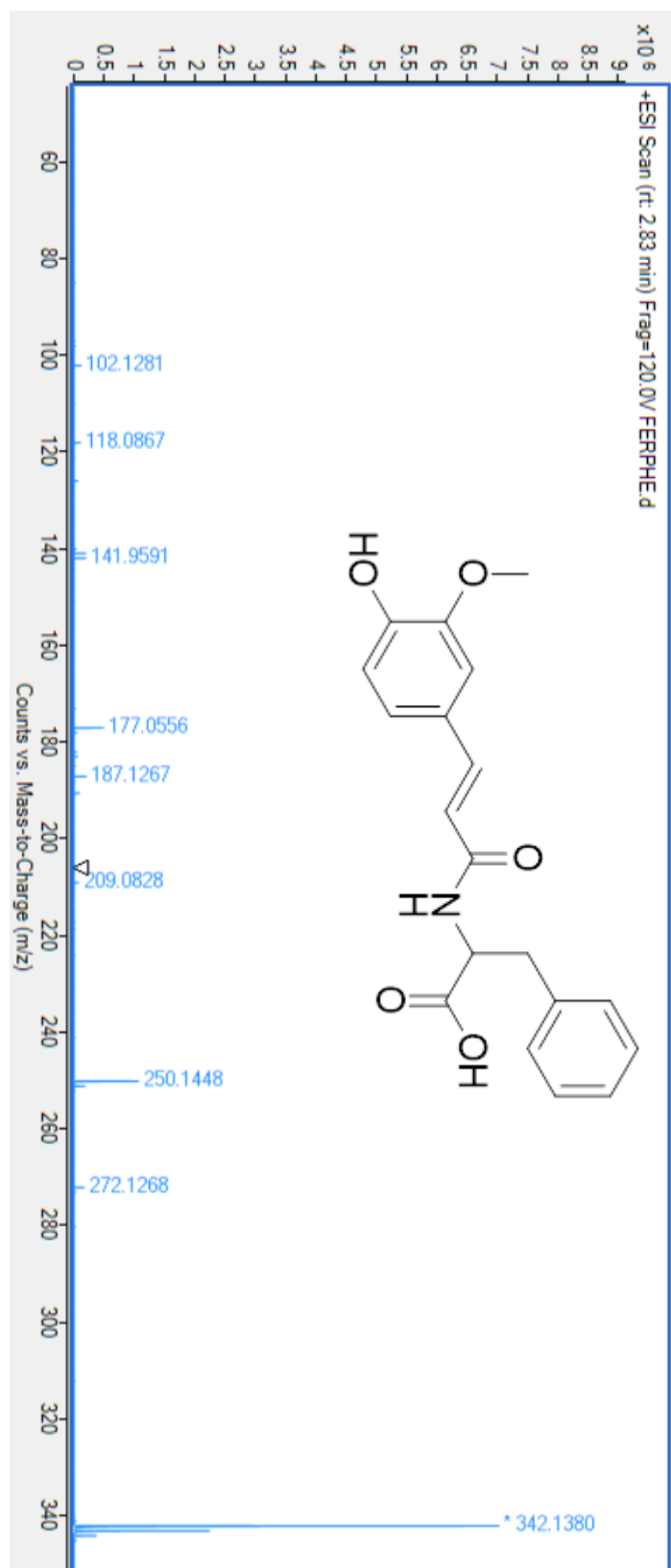
E. Selected MS Data



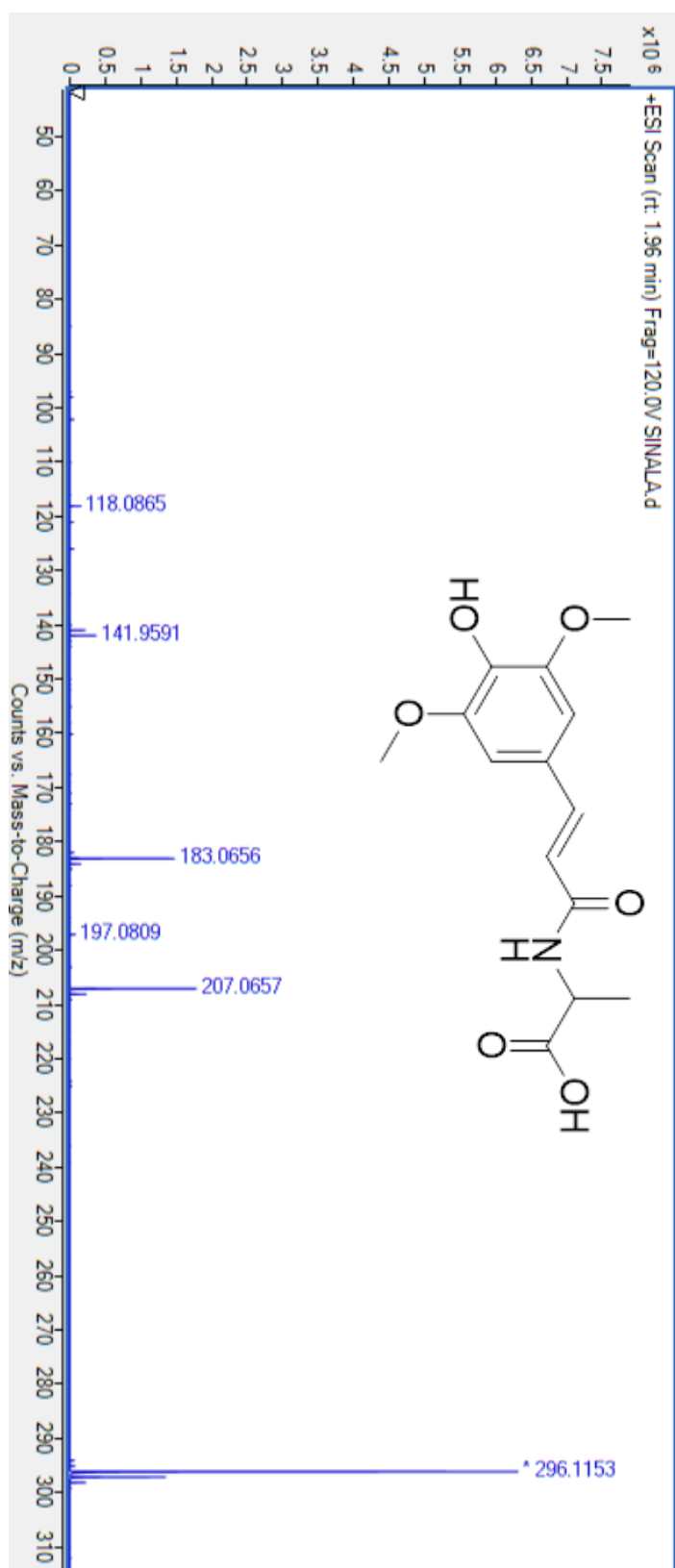
HRMS(17f)



HRMS(23)

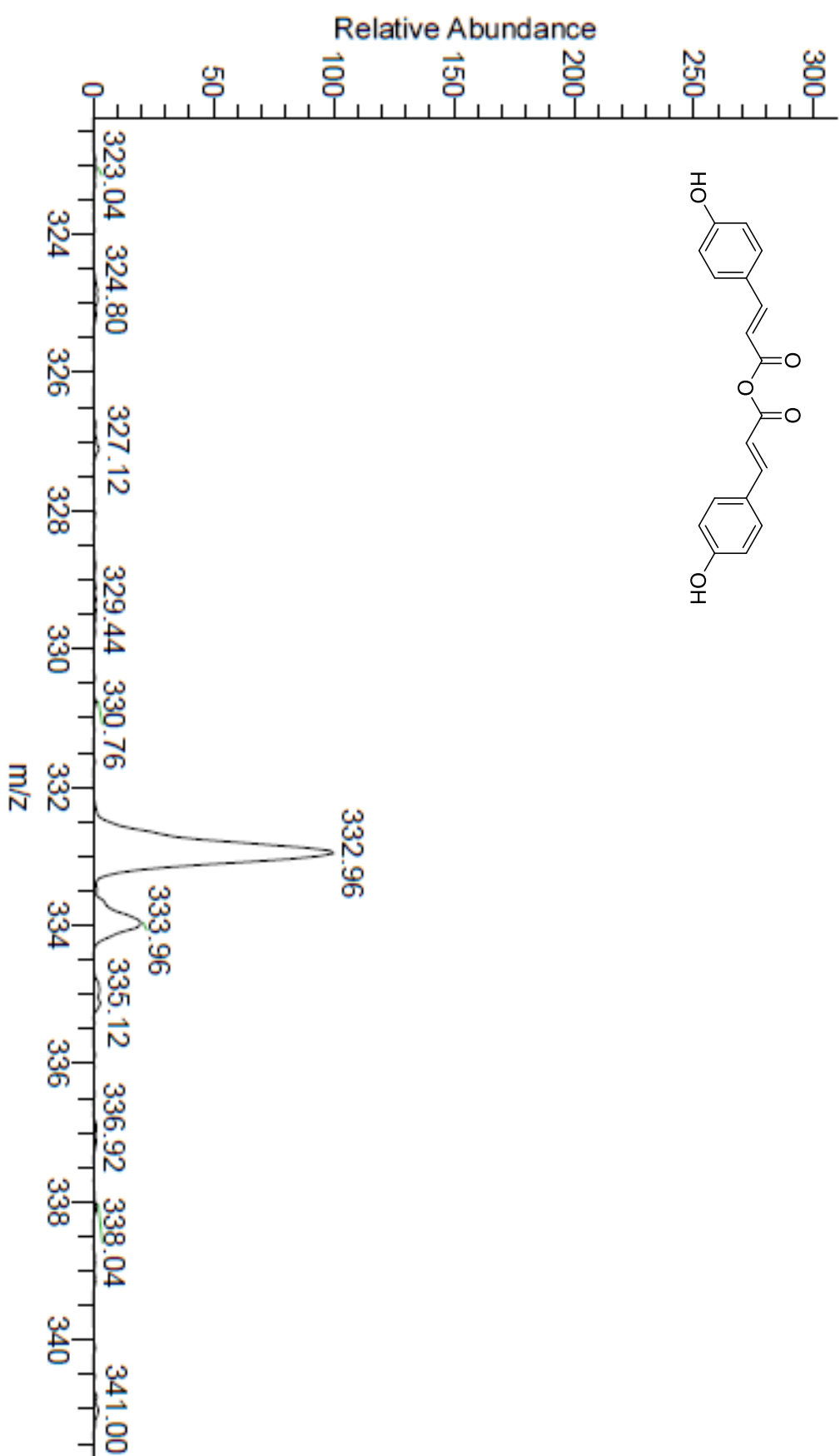


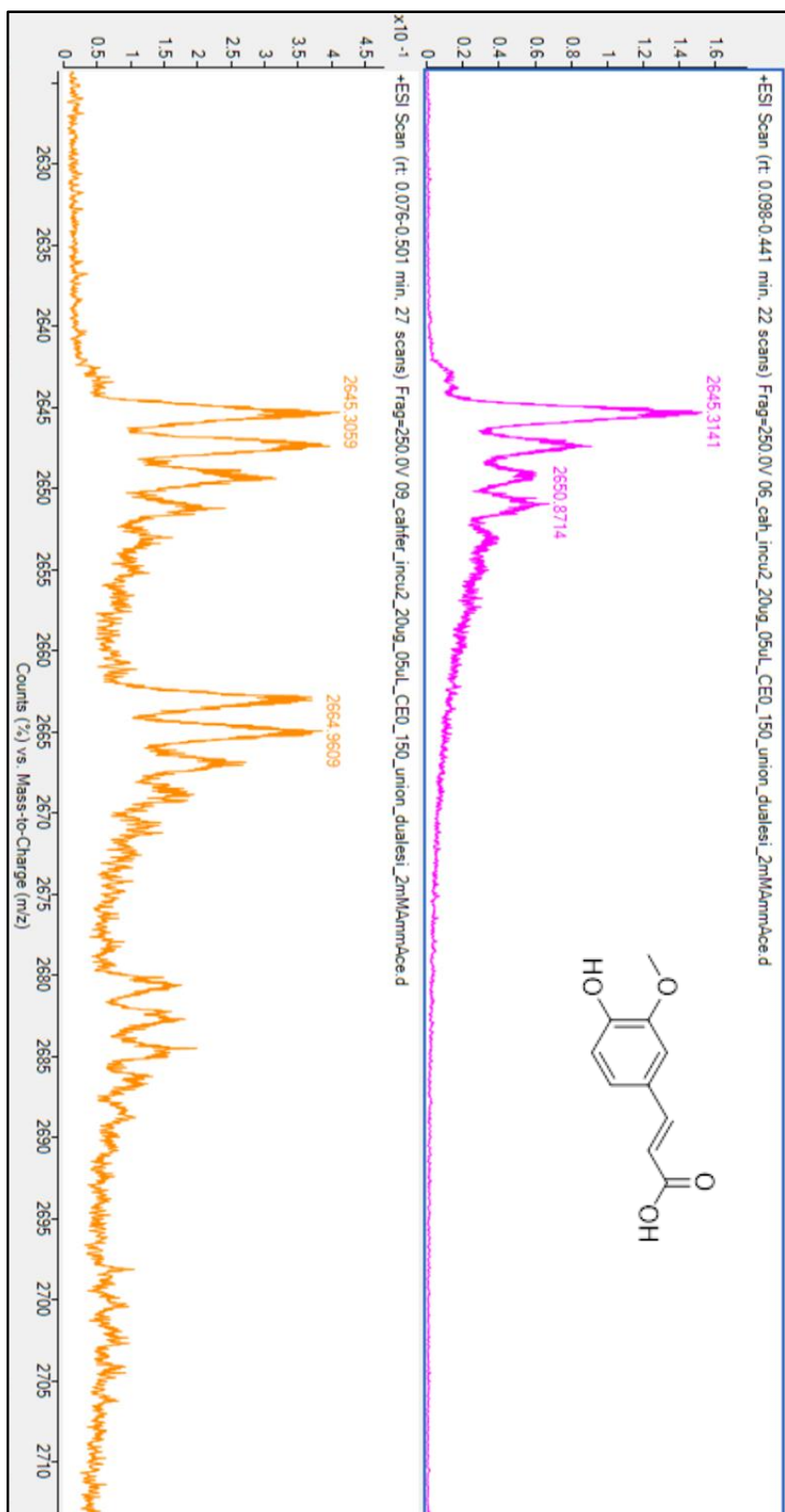
HRMS(19c)



HRMS(20b)

CS2-150_191018131334 #1367-1405 RT: 16.33-16.78 AV: 20 SB: 452 5.39-10.78 NL: 1.34E4
T: ITMS + p ESI E Full ms [90.00-1200.00]





Ferulic acid and Carbonic Anhydrase Non-Covalent Complex via ESI-MS